Energy & Environmental Science

Accepted Manuscript

This article can be cited before page numbers have been issued, to do this please use: T. M. Gur, *Energy Environ. Sci.*, 2018, DOI: 10.1039/C8EE01419A.

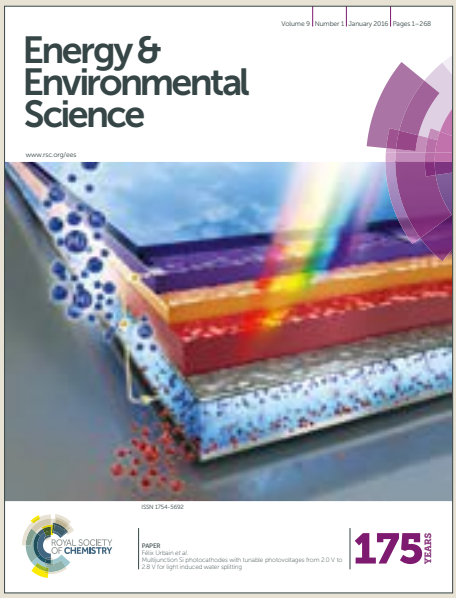

ROYAL SOCIETY OF CHEMISTRY

rsc.li/ees

View Article Online
DOI: 10.1039/C8EE01419A

Review of Electrical Energy Storage Technologies, Materials and Systems: *Challenges and Prospects for Large-Scale Grid Storage*

Turgut M. Gür

Department of Materials Science and Engineering

Stanford University

Stanford, CA 94305, USA

Abstract

Increased interest in electrical energy storage is in large part driven by the explosive growth in intermittent renewable sources such as wind and solar as well as the global drive towards decarbonizing the energy economy. However, the existing electrical grid systems in place globally are not equipped to handle mass scale integration of intermittent energy sources without serious disruptions to the grid. It is generally agreed that more than 20% penetration from intermittent renewables can greatly destabilize the grid system. Certainly, large-scale electrical energy storage systems may alleviate many of the inherent inefficiencies and deficiencies in the grid system, and help improve grid reliability, facilitate full integration of intermittent renewable sources, and effectively manage power generation. Electrical energy storage offers two other important advantages. First, it decouples electricity generation from the load or electricity user, thus making it easier to regulate supply and demand. Second, it allows distributed storage opportunities for local grids, or microgrids, which greatly improve grid security, and hence, energy security. Currently, there is nearly 170 GW of installed storage capacity around the world, but more than 96% is provided by pumped-hydro, which is site-constrained and not available widely. Hence, a broad portfolio of technologies is needed to fully address the widely varying needs for large-scale electrical storage.

The focus of this article is to provide a comprehensive review of a broad portfolio of electrical energy storage technologies, materials and systems, and present recent advances and progress as well as challenges yet to overcome. The article discusses the status of mechanical, thermal, electrochemical, and chemical storage technologies. Where appropriate, it also provides tutorial level background information on fundamental principles for the interested non-expert. It is hoped that this article is of interest to the uninitiated as well as active scientists and engineers engaged in energy storage technologies, with particular focus on large-scale electrical energy storage.

View Article Online
DOI: 10.1039/C8EE01419A

A. Background

Energy, and in particular electrical energy, is indispensable to maintain our standard of living. Globally, human activity has consumed 575 Quads (or, 575×10^{15} Btu, or 606.7×10^{18} J) of energy in 2015, and the demand is expected to grow by 28% to 736 Quads (or, 736×10^{15} Btu, or 776.5×10^{18} J) in 2040 [1]. As expected, most of this increase will be due to rapidly developing countries that fall outside of OECD (Organization for Economic Cooperation and Development) or called non-OECD, which badly need energy resources to drive their economic growth. More than 50% of this increase will be fueled by the needs of India and China.

Table.1. Global installed capacities of major power generation technologies with actual electric power produced in 2016 compared with expected production in 2040. Data compiled from ref [1].

Power Technology	Installed capacity (2016)		Realized electricity generation (2016)		Expected electricity generation (2040)	
	Capacity *(GW)*	% of World	Generation *(billion kWh)*	% of World	Generation *(billion kWh)*	% of World
World Total	**6,637.8**	**100**	**23,735.2**	**100**	**34,049.0**	**100**
Renewables	2,112.4	31.82	5,593.8	23.57	10,702.3	31.43
Hydro	*1,081.5*	*16.29*	*3,910.0*	*16.47*	*5,677.9*	*16.68*
Solar	*278.3*	*4.19*	*275.6*	*1.16*	*1,390.3*	*4.08*
Wind	*459.8*	*6.92*	*826.2*	*3.48*	*2,524.5*	*7.41*
Geothermal	*13.8*	*0.21*	*77.1*	*0.32*	*353.4*	*1.04*
Other	*279.1*	*4.20*	*504.9*	*2.12*	*756.3*	*2.22*
Nuclear	352.0	5.30	2,510.1	10.58	3,657.3	9.79
Fossil fuels	4,173.4	62.88	15,631.3	65.86	19,689.4	57.83

Furthermore, detailed analyses and reports by reputable institutions such as the US Department of Energy - Energy Information Administration (DOE-EIA), International Energy Agency (IEA), the World Energy Council and others, all indicate that fossil fuels are expected to remain as the dominant primary energy resources for many long decades to come. Currently, coal's share in power generation in the U.S. is over 35%, while it exceeds 70% in India and China. Globally, coal was responsible for 40% of electricity produced in 2016, and is expected to provide more than 30% in 2040 [1]. Table 1 provides a comparative summary of the installed capacities for electricity generation with the actual and projected production quantities of major power generation technologies in 2016 and 2040, respectively [1]. In 2040, The International Energy Outlook 2017 report by the US-DOE's Energy Information Agency [1] expects fossil fuels to provide nearly 58% of the globe's electricity need, while renewables will collectively be responsible for more than 31%. These estimates agree in general with the earlier findings of the World Energy Outlook 2015 report by the International Energy Agency that predicts 54% of the global electricity production will be by fossil fuels and 33% by renewables [2].

Ongoing domination of fossil fuels in global electricity production (nearly 2/3rd in 2016) has significantly contributed to atmospheric CO_2 concentration to recently exceed 400 ppmv. Moreover, the amount of CO_2 emissions is expected to increase monotonically between 2015 and 2040, albeit at a somewhat reduced rate of 0.1%/year [1]. Figure 1 illustrates the partitioning of CO_2 emissions among fossil fuel sources. It should be noted that burning of fossil fuels for power generation is the largest single source responsible for nearly 25% of the global greenhouse gas emissions [3]. Fossil fuel-based electricity production, and in particular coal-fired power generation that has long been indispensible for reliable and cheap base-load power, faces significant social, political and environmental

View Article Online
DOI: 10.1039/C8EE01419A

pressures to reduce carbon emissions. Increasing conversion efficiencies for fossil fuel power generation by developing advanced technologies such as fuel cells for *less-carbon* electricity holds the potential of dramatically reducing emissions and collecting CO_2 in capture ready form [4-6].

Another strategy that has already gained momentum and market interest in recent years involves shifting power generation from fossil fuels to renewable sources. Despite their impressive growth and deployment in the last decade, however, intermittent renewables still have modest capacities and collectively accounted for slightly more than only 5% of the global electricity production in 2016 (see Table 1). Moreover, the gap between the installed capacities for intermittent sources such as solar and wind, and the actual amounts of electricity they generated clearly highlights the urgent need for utility-scale storage technologies.

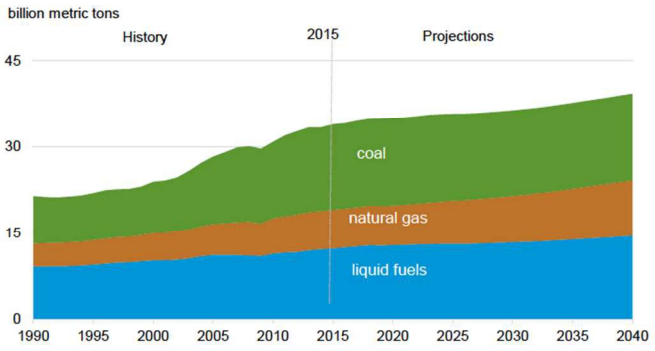

Figure 1. Energy related global CO_2 emissions in billion metric tons by fuel type (1990-2040) [1]

An added advantage for most renewables is their modular nature, which provides opportunities for distributed power generation on-location that will help reduce the economic and environmental impact of power transmission and distribution from centralized power plants. Also, major advances in wind and solar technologies brought about major reductions in the cost of electricity (COE) over the last several years. Figure 2 indicates 5-fold reduction in the cost of solar, while wind has decreased by more than 30% between 2008 and 2015, and recently they have started to compete favorably with coal-fired power in some countries. In fact, several news outlets have recently reported that solar and wind is now at a turning point, and the cost for wind at nearly $50/MWh now stands nearly one-half of the price of coal-fired power [8]. Moreover, recent auctions of solar electricity contracts in India ($64/MWh) and Chile ($29.10/MWh) have demonstrated unprecedentedly competitive prices [10]. Large-scale energy storage technologies hold the bottleneck in this respect and their rapid development and deployment is critically important in order to realize a clean and sustainable energy future.

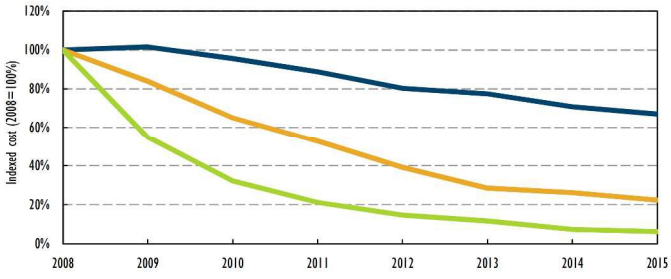

Figure 2. Dramatic cost reduction in utility scale solar PV and wind power (and Light Emitting Diodes-LEDs) between 2008 and 2015 [7]. Color legend: blue; onshore wind, orange; solar PV-utility scale, green; LED.

A recent International Energy Agency (IEA) report "World Energy Outlook 2016" (WEO 2016)

View Article Online
DOI: 10.1039/C8EE01419A

concludes that the pledges made at the 2015 Paris agreement by 195 signatory nations - minus the recent exit by US - only slows down the growth curve for CO_2 emissions but will fail to limit the total emissions to 450 ppmv CO_2 equivalents (so-called the *450 scenario*) [9]. This is illustrated in Figure 3. Indeed, the pledges by the signatory countries foresee 37% of power generation from renewables in 2040 (compared to 23% in 2016) and 150 million electric vehicles on the road by 2040 (compared to nearly 1.3 million today). WEO 2016 report also makes it clear that although the 2015 Paris agreement may indeed slow down the rise of greenhouse gas emissions, it falls far short of bending the emissions curve of Figure 3 downward towards achieving carbon-neutrality (i.e, adding no net carbon to the atmosphere) by 2100.

To limit the global temperature rise to within 2°C above pre-industrial level by 2100, the WEO 2016 report posits that we need to achieve carbon-neutral energy by the end of this century, whereby renewables need to provide more than 60% of global power generation, and among other additional measures, 715 million electric vehicles need to be deployed on the road by 2040.

Achieving these ambitious targets pose major technological, political, social and financial challenges. As an example, even meeting the Paris Agreement pledges poses political challenges, as the recent departure by the US has demonstrated. Moreover, this report estimates that more than $40 trillion in cumulative energy investments and an additional $35 trillion for improvements in energy efficiency will be required to realize the *450 scenario* [2].

Despite such major hurdles and challenges towards achieving carbon neutrality, however, one thing is quite clear. Renewable energy needs to be a major component of the roadmap towards decarbonizing the energy sector. Indeed, among the energy sources, renewables is expected to grow the fastest with an annual rate of nearly 2.3%, or from 2,112.4 GW of installed capacity in 2016, to 3,733.8 GW in 2040, and are expected to produce 10,702.3 billion kWh or nearly 31% of world's electricity by 2040 [11]. Although this increase is very significant, it should ne noted that much of this will still be provided by hydroelectric power that constitutes the lion's share of renewables, but it is restricted geographically to water-rich parts of the globe, as illustrated in Figure 4 for energy storage and renewable power generation in U.S. from sources other than wind, solar, and hydro [12].

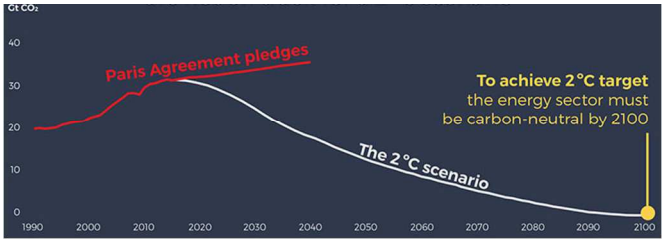

Figure 3. Global CO_2 emissions under the Paris agreement pledges and the 450 scenario for decarbonization, where the latter assumes a 50% chance of limiting the total greenhouse gases to 450 ppmv CO_{2equiv}, and the global temperature rise to less than 2°C. For this, the energy sector needs to achieve carbon-neutrality by 2100 [9].

View Article Online
DOI: 10.1039/C8EE01419A

B. Introduction

Conventional power generation and distribution infrastructure currently employed globally demands a highly delicate, low error margin, and near-instantaneous balance between electricity supply and demand on the electrical grid system. To realize balance, thousands of turbines all over the world have to be brought online instantly or taken off in order to respond to the variability in electricity demand. Usually, most of these turbines stay idle majority of the time resulting in lost generation capacity. Also, the power generated during off-peak times by these plants is often wasted due to lack of proper storage capacity.

The basic premise of energy storage involves transforming one type of energy into another type that can, when needed, deliver back the stored energy in an efficient, cost-effective, and reliable manner. In a manner similar to the wide diversity of power generation technologies, electrical energy storage technologies and systems show an equally rich diversity. Each offer a distinct set of advantages, but also disadvantages, challenges and shortcomings. As there is no single winning technology for power generation that can meet the wide range of requirements including environmental, cost, performance, availability, customer demand, portability, scalability, etc., there is also no single bullet to address our impending needs for electrical energy storage. Hence, a multi-prong portfolio strategy is best suited to develop a multitude of storage technologies and systems. Each offers its own strengths and weaknesses, as well as distinctly different technical basis governing its operating principle.

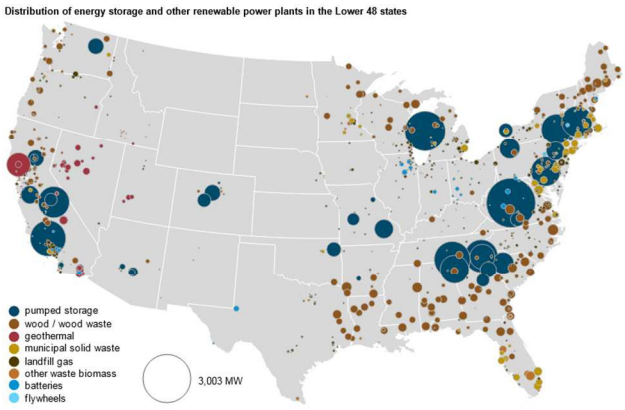

Figure 4. Geographical distribution of U.S. energy storage capacities by size (i.e., by diameter of circles scaled to 3,003 MW as shown in inset) and location. Also included is power generation by renewable sources other than solar, wind, and hydro [12].

The global excitement, momentum and vast investments in intermittent renewables to grow them as one of our primary sources for electricity production is critical to pave the way towards decorbonizing our currently fossil fuel-dependent energy economy, and in particular, electricity production. But the intermittent nature of many renewables is a major impediment to reliable electricity generation, and for their mass deployment globally. The distributed nature of renewables provides great advantage to help reduce the economic and environmental impact of power transmission from centralized power plants, as is the case currently. Renewables are also important for poor and underdeveloped parts of the world, where large populations still lack electricity and other forms of energy

View Article Online
DOI: 10.1039/C8EE01419A

even for their daily chores. In that regard, renewables can help jump-start economic growth and greatly improve quality of life in many of these societies.

However, rapid and utility-scale deployment of intermittent sources such as solar, wind, tide and wave is largely contingent on the availability of cost effective, efficient and scalable energy storage technologies. In fact, electricity storage or lack thereof may well be the "*ball-and-chain*" for intermittent renewables to break free and achieve the deployment levels foreseen by mid century [1,9]. Indeed, Bloomberg Technology News reported on July 31, 2017 that Germany had to toss out 4% of wind energy in 2015 and China has discarded 17% of its renewable energy, while California had to give up 300,000 MWh of solar and wind power in the first half of 2017, all due to lack of sufficient electricity storage capacity [13]. Without commensurate and sufficient electrical storage capability, rapid buildup of solar and wind capacity can also be an undue financial burden. Case in point is California, which in the last decade has invested heavily in solar, not only was forced often to curtail solar power production due to power glut but also had to pay exorbitant prices, up to $25/MWh, to other states just to get them to take its excess power, i.e., called 'negative pricing' [14] .

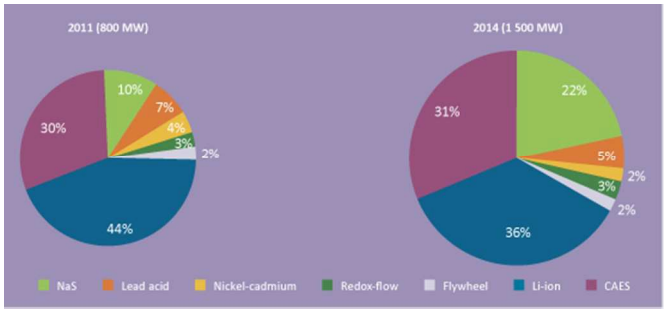

Figure 6. Comparative breakdown of global installed capacities based on electrochemical and mechanical storage technologies between 2011 and 2014 (CAES: compressed air energy storage) [18]

Investments in energy storage technologies and projects in the last decade have improved the inventory of global installed capacities. Currently, world's total installed storage capacity stands at about 169 GW (up from 132 GW in 2012), of which pumped-hydro storage provides more than 96% of the total capacity, with the remaining vested in mechanical, thermal and electrochemical storage technologies [15]. Installed storage capacities and their breakdown are summarized in Table 2, where new capacity additions for a total of 13 GW to be completed by 2018 are also presented. A 2016 report predicts that the global demand for electricity storage capacity will increase to 11.89-15.72 TWh in 2030 from 4.67 TWh in 2017 in order to double the share of renewable energy in the global mix [16].

For renewable energy to achieve its bold target of being a primary energy source by mid century, grid-compatible electricity storage technologies need to satisfy key requirements including, high capacity, rapid charge/discharge rates, high energy density, long cycle life, stable operation and performance, reliability, cost-effectiveness, and easy scale-up. For utility-scale storage of electricity, grid parity is also a critical consideration.

View Article Online
DOI: 10.1039/C8EE01419A

Table 2. Global installed energy storage capacities operational in 2016 by type of storage technology. New storage projects under construction are expected to add another 13 GW of storage capacity by 2018 [15]

Storage Technology	Installed Capacity *(GW)*	% Share
2016 World Total	**168.6**	**100**
Pumped-hydro	162.2	96.2
Electrochemical	1.6	0.95
Thermal	3.2	1.9
Electromechanical	1.6	0.95
New project capacities under construction		
2016	*2*	
2017	*5*	
2018	*6*	

Achieving grid reliability and compatibility, managing peak demand, and integration of intermittent renewable energy sources into the grid all require utility-scale electrical energy storage that delivers electricity where it is needed and when it is needed. Electrical energy storage also decouples electricity generation from the load, or electricity user, thus making it easier to regulate electricity supply and demand. Distributed electrical storage also offers important opportunities to build local grids, or microgrids, which greatly improve grid security, and hence, energy security.

However, the requirements for energy storage are widely varying and diverse, and driven primarily by the type of application. No single technology meets all the requirements and metrics for large-scale grid quality storage. Each technology may offer attributes and merits for certain applications, but not for others. Indeed in some markets, electrochemical technologies such as Na-S and Li-ion batteries have become commercially viable even though they do not satisfy all the required metrics. Considering a suitable combination of different storage systems may alleviate such shortcomings towards properly meeting the specific requirements of a particular application.

Furthermore, not all storage technologies are at the same level of development or maturity. A recent report by US Department of Energy indicated a breakdown of the groups of storage technologies either deployed or under development towards large-scale deployment [17]. Broadly, these technologies can be grouped under pumped-hydro, compressed air energy storage (CAES), a wide variety of batteries and other electrochemical systems, flywheels, and superconducting magnetic energy storage (SMES). The developmental status of storage technology groups is depicted in

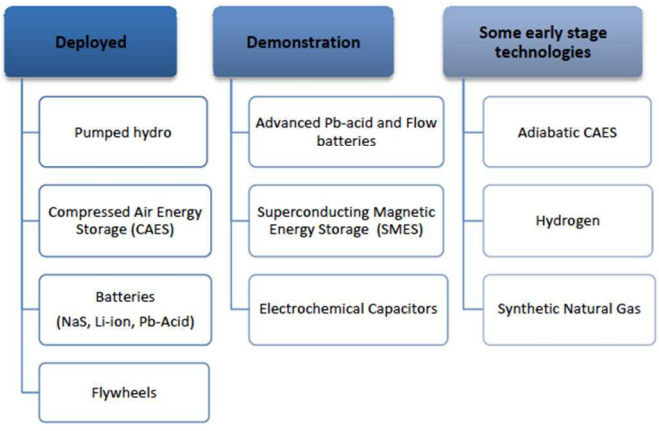

Figure 5. Developmental maturity of major electricity storage technologies towards large-scale deployment [17]

View Article Online
DOI: 10.1039/C8EE01419A

Figure 5, which categorizes their maturity levels towards full commercialization and mass scale deployment.

In the US, pumped-hydro is the most dominant technology for grid storage, which constitutes nearly 95% of the grid storage capacity [17]. A variety of other technologies including batteries, compressed air, flywheel, and thermal storage are being developed and some have already been utilized for storage operations, albeit at scales considerably smaller than the capacities that are actually needed. For example, 1.5 GW of global installed storage capacity for 2014 [18] depicted in Figure 6 of different mechanical and electrochemical storage technologies makes up only a small fraction of more than 132 GW of global pumped-hydro storage capacity available in 2012. Despite major progress and effort, the cumulative share of electrochemical, thermal and mechanical storage capacities has remained below 4% of the total global storage capacity by 2016, where pumped-hydro provided the bulk capacity of nearly 96%. These numbers, however, still fall short of the combined storage needs for wind and solar (see Table 1).

While pumped-hydro is a mature and widely used technology for utility scale commercial storage where available, CAES, which relies on storing energy as compressed air in underground caverns and formations, is not as mature and fully developed as pumped-hydro. However, both have very specific geographical requirements that render their use site specific.

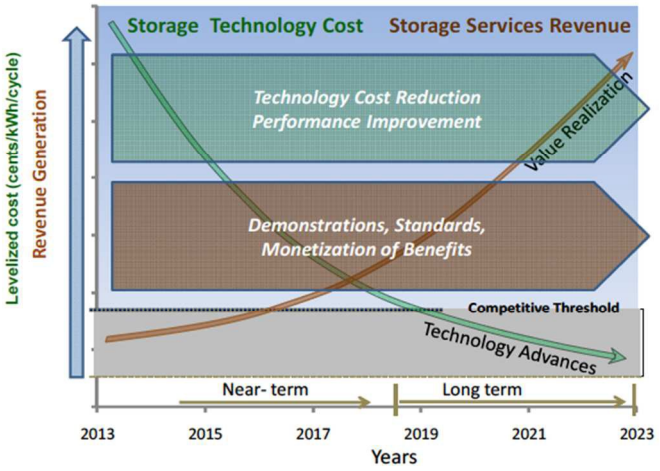

Figure 7. US DOE's expected cost reduction timeline with the evolution and market penetration of storage technologies [17].

It is expected that basic research focused on prospective technologies may expand and improve their merits and lower some of the technical barriers to better meet the required metrics for storage. This is identified as one of the strategies by US Department of Energy to drive down the cost, as investments in improving the technology and large-scale deployment will help lower costs [16]. This is depicted in Figure 7. However, cost alone does not guarantee success. Mass scale deployment of these grid-scale storage technologies also requires confidence buy-in from both the stakeholders and users such as utilities and customers as well as utility regulators for the safety, performance and reliability of these technologies.

View Article Online
DOI: 10.1039/C8EE01419A

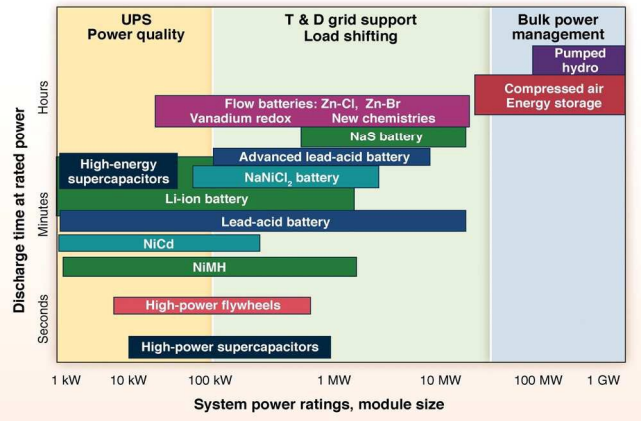

Figure 8. Comparison of power ratings and discharge time scales of various electrical energy storage systems. From [19], B. Dunn, H. Kamath, J. M. Tarascon, Electrical energy storage for the grid: A battery of choices, Science, 2011, **334**, 928-935. Reprinted with permission from AAAS.

A variety of electrical storage technologies and approaches can be organized into four general categories, namely, mechanical, chemical, electrochemical, and electrical. Many of these categories are reviewed in the next sections, and characteristic features for some of them are presented in Figure 8, which shows the power ratings and typical discharge times of many of the electrochemical and mechanical electricity storage systems under development or in practical use [19]. They exhibit a wide range of discharge characteristics and power ratings. The discharge times and system sizes may be used as helpful tools to select suitable storage systems for a particular application. For example, grid management requires frequency regulation and load levelling, which usually demand short response times of the order of seconds that are suitable for flywheel and supercapacitor storage, while bulk power management may require longer response times of the order of hours where pumped-hydro and compressed air storage offer attractive opportunities.

However, the options for large-scale storage shown at the far right column in Figure 8 are quite slim, and require augmentation of the storage portfolio by developing alternative technologies. Only pumped-hydro and CAES systems are commercially available for bulk storage at utility scale. The maturity levels of more advanced technologies, such as electrochemical storage, are still under active development and further require demonstration and deployment at utility scale. Moreover, the utility industry, which relies on low cost, scalability, and reliability, is typically averse to risk-taking. So they are understandably skeptical about many of these technologies due to cost, scale-up issues, and lack of track record on safe and reliable operation for prolonged use at industrial scale.

There have been excellent reviews of electrical energy storage technologies and materials in the literature. Some of the more recent ones are given in references [19,21-28]. The interested reader is encouraged to seek these papers to gain full appreciation of the wide scientific footprint of energy storage and to expand the scope into more specialized areas. In large part, these review articles focus primarily on a single or select few storage technologies, such as electrochemical energy storage, or a sub-division, such as Li-ion batteries.

Instead, this article distinguishes itself by taking a broad brush and presenting an in-depth review of a wide spectrum of electrical energy storage technologies, materials and

View Article Online
DOI: 10.1039/C8EE01419A

systems with an eye for large-scale electrical grid storage. The article provides a comprehensive discussion of the status of four major classes of electricity storage technologies including electrochemical, chemical, mechanical, and thermal storage systems covering a wide range of options from pumped-hydro and flywheels, to hydrogen and ammonia, to supercapacitors, batteries, regenerative fuel cells, to flow batteries, and phase change materials storage. Where appropriate, the article also offers tutorial information for the interested reader to gain better insight and appreciation of the fundamental considerations and challenges in electrical energy storage. It is hoped that this review will be of interest and benefit to the uninitiated as well as active researchers and engineers engaged in electrical energy storage technologies.

C. Fundamentals of Energy Storage

The first law of thermodynamics (or, *the law of conservation of energy*) states that in a closed system, the total energy is fixed and energy can neither be created nor destroyed. It can only be converted from one form to another. This fundamental concept serves as the foundation of nearly all forms of energy conversion and storage. Accordingly, most storage technologies fall into four generalized categories, namely, mechanical energy storage, chemical energy storage, electrochemical energy storage, and electrical energy storage.

The maximum amount of electrical work that can be extracted from a storage system is given by,

$$G = H - TS \quad (1)$$

Here, G is Gibbs free energy, H is enthalpy, T is temperature, and S is entropy. In other words, G represents the maximum energy available to do either mechanical or electrical work.

Mechanical energy storage, such as pumped-hydro, manifests itself by potential, E_{pot}, and/or kinetic, E_{kin}, energies that can be represented by,

$$E_{pot} = f\,d \quad (2)$$

$$E_{kin} = (1/2)\,mv^2 \quad (3)$$

Here, f denotes force, d is distance, m is mass, and v denotes velocity. For a rotating body such as a flywheel or a wind turbine, the kinetic energy is described in a similar expression by,

$$E_{kin} = (1/2)\,I\omega^2 \quad (4)$$

View Article Online
DOI: 10.1039/C8EE01419A

where, I denotes the moment of inertia and ω is angular velocity of rotating system. In other words, stored energy increases with the system's inertia and the square of it's angular velocity. The moment of inertia for a body of mass m, radius r, length l and density ρ can be given by

$$I = (1/2)\, mr^2, \text{ or } = (1/2)\, \rho l \pi r^4 \quad (5)$$

Accordingly, high-density materials with large radius help store more energy. For mechanical energy storage in flywheels, Eq. (5) can also be expressed as,

$$E_{kin} = \sigma_m s/\rho \quad (6)$$

Here, σ_m denotes maximum stress, s is a shape factor, and ρ is materials density. For modern flywheels made from reinforced high strength carbon fibers, it is possible to achieve storage capacities greater than 200 kJ per kilogram of flywheel mass.

Compressed air storage in salt caverns or underground aquifers relies on the gas law ($PV = nRT$), and the available work, w, is given by PdV integrated over the incremental volume change, dV.

Thermal storage relies on the amount of heat, q, one can store in a medium or material of defined volume, V, materials density, ρ, and specific heat, C_p, resulting a temperature rise of ΔT. This can be expressed by,

$$q = \rho C_p V \Delta T \quad (7)$$

In the case that the thermal energy storage medium or material undergoes a phase transformation during this process, the latent heat associated with this transformation should also be accounted for in the total energy stored.

Chemical storage relies on storing energy in the chemical bonds of fuels, which are inherently strong and thus provide very high energy densities. However, one needs to use usually electrical or thermal energy to produce the fuels for chemical storage. The governing equation for the maximum work out of chemical storage is given by Eq. (1) above.

Electrochemical storage systems are based on charge storage at the electrodes in the case of batteries, or at the electrochemical interface in the case of electrochemical capacitors or supercapacitors, or in the chemical bonds of fuels as in fuel cells. As the theoretical efficiency for electrochemical energy conversion is defined by the ration of $(\Delta G/\Delta H)$, electrochemical energy storage offers inherently high efficiencies.

Finally, electrical and magnetic energy storage can also be realized. Examples include dielectric-based capacitors, magnetic materials, and superconducting magnets. However,

View Article Online
DOI: 10.1039/C8EE01419A

these types of energy storage approaches lie outside the scope of this article, and are not covered here.

D. Electrochemical Energy Storage Systems and Materials

The underlying operating principle for electrochemical and photoelectrochemical devices (and even photovoltaic devices) involves three major process steps, namely, separation (or, ionization) of charge, transport of charged species, and recombining of charge. This basic principle governs the operation of a wide range of devices including batteries, fuel cells, supercapacitors, electrolytic capacitors, photoelectrochemical and photovoltaic devices. Their operating principles, however, involve different mechanisms where interfaces play a critical role. For example, while batteries store charge within the electrodes, in the case of fuel cells and flow batteries charge is stored in the fuel, which is fed externally on to the surface of the electrodes. Supercapacitors, on the other hand, store charge either in the electric double layer at the electrode/electrolyte interface, or as pseudocapacitance governed by surface redox reactions. Some of these electrochemical devices such as PEMFC, supercapacitors and batteries operate at room or ambient temperature, while others require elevated temperatures, e.g., sodium-sulfur batteries or molten carbonate and solid oxide fuel cells. In other words, materials requirements for each electrochemical storage system are different, and many have been reviewed in detail elsewhere [19,20,29-35]. Furthermore, the fundamentals and operating principles of batteries, fuel cells and supercapacitors have been presented as a tutorial in a recent review article [36].

The fundamental concept behind electrochemical energy storage is the reciprocity between converting the chemical energy stored in the bonds of fuels into electrical energy, and expending electrical energy to synthesize chemicals or fuels by operating in the reverse direction. The driving force for this conversion is the Gibbs free energy change, ΔG, of the electrically neutral species at the electrodes participating in the chemical reaction,

$$A + B = C \qquad \Delta G \text{ (kJ/mole)} \qquad (8)$$

This free energy change is the same if the reactants A and B were to undergo purely a chemical reaction as in Eq. (8), or an electrochemical reaction where the reaction involves the transport of ions and electrons across the cell. As these species are electrically charged, the electrostatic energy transported across by a mole of such species is given by zEF, where F is Faraday's constant, z is the charge number of the transporting species, and E is the cell voltage. Under open circuit conditions, the cell voltage is related to the Gibbs free energy change by,

$$\Delta G = - zEF \qquad (9)$$

View Article Online
DOI: 10.1039/C8EE01419A

In other words, the chemical potential difference between neutral species at the electrodes defines the underlying force driving an electrochemical cell via a chemical reaction among electrically neutral reactants, A and B, to form an electrically neutral product, C.

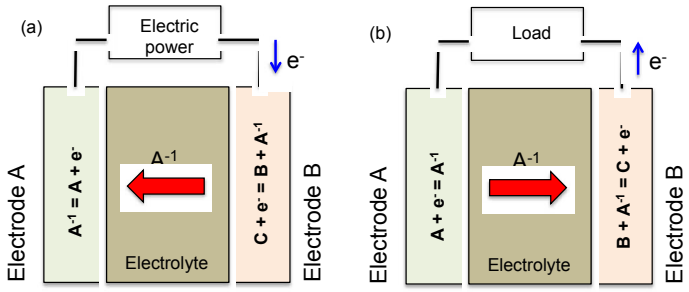

Figure 9. Basic operating principle of electrochemical energy storage, illustrating (a) electrical energy to chemical energy conversion, and (b) chemical energy back to electrical conversion for reaction A+B=C.

For electrochemical storage, the systems require basic components that have critically important roles to achieve this, namely, two specialized bodies of electrodes separated by an ionically conducting but electronically insulating "electrolyte". The electrodes are preferably chosen from abundant and cost-effective materials that exhibit good electronic conductivity, good stability, and high catalytic activity. Some applications require that the electrode material also exhibit mixed ionic electronic conductivity, where both ionic and electronic defects are mobile.

The electrode where the reduction reaction takes place is called the cathode, and where the oxidation reaction takes place is called the anode. An electrochemical energy storage and conversion system, be it a battery, a fuel cell, or an electrochemical capacitor, can schematically be illustrated in Figure 9, which shows storage of electrical energy in the form of chemical energy, and conversion of chemical energy for reaction (8) back into electrical energy that can be supplied to the grid to perform useful electrical work. Figure 9(a) represents an electrolysis cell to produce fuel B using external power (i.e., storage mode), while Figure 9(b) depicts a fuel cell that employs fuel B and oxidant A to generate electricity (i.e., power production mode). Electrolysis cells that exclusively operate for the purpose electricity storage in the form of chemical energy in fuels are discussed later under section E. Chemical Energy Storage, while regenerative solid oxide fuel cells that offer the opportunity to operate in a bi-directional manner (electricity to chemicals fuels, and chemical fuels back to electricity in the same fuel cell) are discussed here.

It should be noted that in the case of batteries, electrolytic capacitors and supercapacitors, specific energy and specific power are intimately coupled to each other by the battery chemistry and choice of battery materials. However, in fuel cells and flow batteries the energy density dictated by the choice of fuel is decoupled from power, which is dictated by the kinetic and transport properties of cell components. Such decoupling provides important advantages for many applications. Also important are the volumetric energy and power densities of electrical storage systems. Volume is especially important for transportation, space and mobile applications. Interestingly, there is an ongoing debate whether Li-ion batteries or fuel cells will eventually dominate mobile applications and in particular, which one will power the transportation sector [37].

View Article Online
DOI: 10.1039/C8EE01419A

D.1. Batteries

One of the most notable technological achievements of electrochemistry in recent years is the successful commercialization of Li-ion batteries that had a profound impact on the widespread use and deployment of portable electronic devices, and more recently, on transportation and stationary storage at the 100-200 kWh scale. In more general terms however, batteries, the first electrochemical device (i.e., the Volta pile) built more than two centuries ago, have been commercially available for more than a century. They are efficient devices to store electrical energy, and hence used extensively for a wide range of applications including transportation, portable, mobile, as well as stationary back up power. Types of commercial battery systems available today or under development employ a diverse range of battery materials [23] and chemistries both organic [38] and inorganic [21,33] in nature. Operationally, all battery systems can be grouped under primary (i.e., non-rechargeable) and secondary (or, rechargeable) batteries. Primary batteries fall outside the scope of this review article, as these are in general not suitable for storage purposes.

Comparative operational characteristics of batteries are typically represented by Ragone diagrams. This is illustrated in Figure 10, where specific power is plotted against specific energy for major rechargeable battery systems that compare various classes of batteries to those based on lithium chemistry [31,39-42]. Superior properties of Li-based batteries to other alternative chemistries presented in Figure 10 makes it easy to understand the enormous academic and commercial interest in this system.

Batteries in general offer desirable solutions for cost-effective and compact storage, pollution-free operation with no moving parts, high overall efficiency, sufficient cycle life, considerable shelf and service life. They provide opportunities for distributed storage, as well as storage and frequency regulation from intermittent renewable sources. Several battery systems including redox flow batteries, alkali metal ion-based batteries, sodium sulfur batteries are under consideration and further development for utility scale storage purposes ultimately for the 'smart grid' [19,32]. Unfortunately, many of these systems are still too expensive for commercial deployment for large-scale storage applications, and require not only cost reductions but also

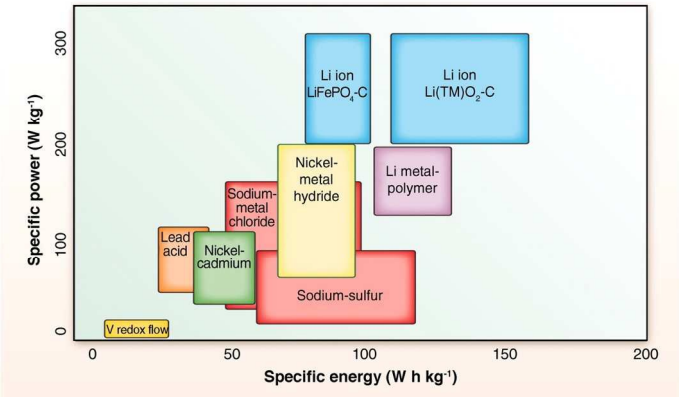

Figure 10. Ragone diagram of specific energy versus specific power for major rechargeable battery systems From [19], B. Dunn, H. Kamath, J. M. Tarascon, Electrical energy storage for the grid: A battery of choices, Science, 2011, **334**, 928-935. Reprinted with permission from AAAS.

View Article Online
DOI: 10.1039/C8EE01419A

major improvements on performance, reliability, and materials availability and stability [33,34]. However, their growing market penetration is expected to lower battery prices.

All batteries provide the convenience and portability of delivering stored chemical energy in the form of electrical energy at the point of use, with high conversion efficiency and without harmful emissions to the environment. The amount of stored electrical energy and the rate at which the energy can be extracted from a battery is indicated by its specific energy and specific power, respectively, and is a function of the cell voltage (V) and capacity (Ah/kg) of a battery. These parameters are directly governed by the thermodynamic and kinetic constraints imposed by the battery's chemistry and choice of materials for battery components. In other words, the amount of the electroactive species that can be stored in the electrode materials dictate the energy storage capacity of the battery, while the rates of interfacial charge transfer reactions and mass transport through the battery components govern its output power. It should be noted here that some of these concepts are in direct competition in terms of battery life and safety. As high storage capacity is related to cell potential, there has been a strong desire to develop electrode materials that yield a high cell potential. But this comes at the expense of battery safety, as high cell potentials are related to high activity that in turn facilitates reaction with the electrolyte and can lead to thermal runaway and fires. This is particularly true in the case of Li-ion batteries employing organic electrolytes.

The driving force for improving the properties of batteries and battery materials is to achieve low cost, rechargeability, high voltage, safety, and fast charge/discharge capability. The desired battery system not only should exhibit high energy density (i.e., specific energy) but also has high power density (i.e., specific power). Compared to others, Li-based storage systems clearly offer higher specific power and higher specific energy than others as indicated in Fig. 10 [19,43,44]. However, not all applications require high energy density simultaneously with high power density. This interplay may provide opportunities for other battery systems to offer suitable solutions for specific storage applications.

Among the systems shown in Figure 10, Li-based battery systems have deservedly attracted the biggest commercial and research interest with excellent review articles reporting on the advances and challenges [21,31,39,43,45-48]. Li-based batteries currently dominate nearly 2/3rd of the global battery market due to their high energy density, portability, acceptable cycle life, and their compact size that provides flexibility in product design, especially for portable electronics and communication devices.

D.1.1. Li-ion Batteries (LIB)

As the energy density of a battery is directly related to its working potential, or, voltage, while its power is proportional to the square of its voltage, the search for better systems and materials has often been driven by high voltage considerations. In this regard, battery

View Article Online
DOI: 10.1039/C8EE01419A

systems based on Li are attractive because Li is the most electropositive element (Li/Li^+ redox potential = -3.04 V vs SHE) in the periodic table and the lightest metal (6.94 g/mol), thus offering a high energy density. Indeed, the theoretical energy density of Li-ion batteries is about 380 Wh/kg, with commercially available Li-ion based rechargeable batteries providing 150-210 Wh/kg [44]. The power densities vary in the range 500-2000 W/kg, with efficiencies around 90%. As the Li^+ ion also has a small ionic radius (90 pm), it allows fast diffusion rates through the electrode material, offering fast charge-discharge rates. Because of these practically attractive properties, Li-based battery systems have gained strong attention in research and development as well as commercial activity. Indeed, Sony Corporation was the first to introduce the Li-ion batteries based on intercalation chemistry into the market in 1991. These commercial Li-ion batteries typically contain a graphite anode (the negative electrode), a lithium metal oxide ($LiMO_2$, where M is Co and/or Ni) cathode (positive electrode), and a Li^+ ion conducting electrolyte consisting of an organic solvent, typically ethylene carbonate, dimethyl carbonate, and their mixture, in which a soluble lithium salt such as lithium hexafluorophosphate ($LiPF_6$) is dissolved. The corresponding cell reaction provides a cell potential of around 3.7 V and is given by,

$$yC + LiMO_2 = Li_xC_y + Li_{(1-x)}MO_2 \qquad (10)$$

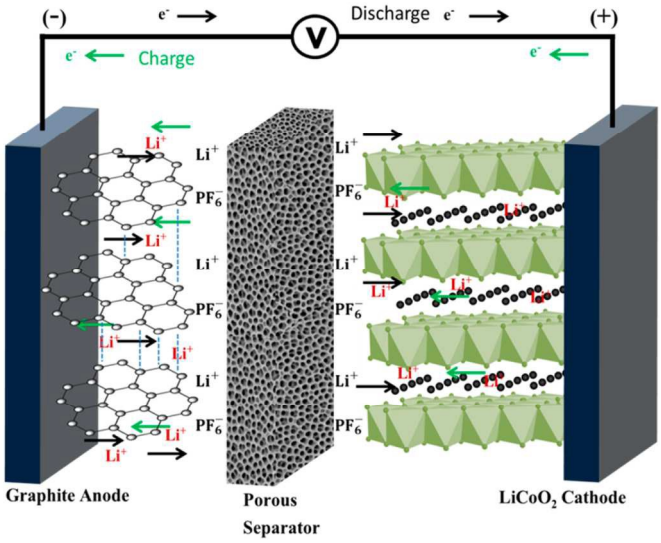

Figure 11. Schematic illustrating the operating principle of the first commercial Li-ion battery, where the Li^+ is intercalated (and, deintercalated) in the layered structures of the graphite negative electrode and the $LiCoO_2$ positive electrode [21]. Reprinted with permission from (K.M. Abraham, Prospects and limits of energy storage in batteries, J. Phys. Chem. Lett. 2015, **6**, 830-844). Copyright (2018) American Chemical Society.

Here, the typical values of x and y are 0.5 and 6, respectively. The reaction involves the insertion (i.e., lithiation) and extraction (i.e., delithiation) of lithium ions between the two electrodes, while the electrons flow through the external circuit performing useful electrical work.

Both the C_6Li anode and the $LiCoO_2$ cathode materials have layered crystal structures so involve the intercalation (or, lithiation) and deintercalation (delithiation) of Li^+ ions in between the structural layers of the anode and cathode materials. Battery operating principle and the charge and discharge cycles via transport through the electrolyte are depicted in Figure 11. During the charging process, lithium is extracted from the positive electrode, whose working potential is higher than 2 V vs Li^+/Li, and intercalated into the graphite anode, whose working

View Article Online
DOI: 10.1039/C8EE01419A

potential is lower than 3 V vs Li^+/Li. As Li is shuttled between the two electrodes, these rechargeable cells are sometimes referred to as *"rocking-chair"* batteries [48].

There have been excellent reviews of Li-based batteries and systems discussing the chemistry and electrochemistry, materials properties as well as the search for better electrode materials, performance and safety issues, and economics for large-scale storage applications [19,39,47,48,50-53]. Most Li-batteries that are commercially available employ nonaqueous electrolytes [54], although other types of electrolytes including ionic liquids [55,56], polymers [57,58], ceramics [59], and even aqueous electrolytes [60,61] have also been investigated. Much progress has been achieved in Li-battery technology in the last decades. The capacity of the first commercial Li-ion batteries, i.e., the 18650 cell, was about 900 mAh, while the same size Li-batteries today deliver a much higher practical capacity of 2,600 mAh.

D.1.1.1. Negative Electrode Materials

Although most commercial Li-ion batteries employ a graphite anode, which has a layered structure, the candidate materials under development for the negative electrode also include elemental Li, Li-alloys, or a nanostructured host material such Si-nanowire [61,62]. Each offers its own set of merits and challenges.

Elemental lithium is the ideal desired anode material as Li is the most electropositive element in the periodic table and has an exceptionally high specific capacity of 3,860 mAh/g. Unfortunately, elemental Li is quite reactive and the chemical stability of the battery electrolyte against Li poses serious concerns regarding safety, reliability and durability [64]. Also, the exothermic reactions between the Li anode and the battery electrolytes may lead to overheating and "thermal runaway". More importantly, elemental Li anodes tend to grow dendrites during charge-discharge cycling due to the nonuniformity of the Li deposition process that tend to occur at preferential sites. The dendrites eventually penetrate through the electrolyte towards the cathode and may cause electrical shorting and other serious hazard problems, even explosion.

Several approaches have been pursued to reduce the driving force for chemical stability and dendrite growth. One is based on the thermodynamic concept of lowering the activity of Li, and hence decreasing its propensity to react and also to grow dendrites, by alloying it with other metals including aluminum [65], antimony [66], bismuth [67], and especially those that alloy with lithium at low potentials such silicon [68,69], and tin [70,71]. Interestingly, the first rechargeable Li-battery was developed in 1970's by Exxon and employed a LiAl alloy negative electrode and a TiS_2 cathode [72].

Recent attention on other remedial strategies such as alloying or conversion chemistries has provided promising results. For example, Si-based alloy anodes provide a theoretical charging capacity around 4000 mAh/g, and volumetric energy densities in the range 700-972 Wh/L, which are 1.5-1.8 times higher than for commercial cells, have already been

View Article Online
DOI: 10.1039/C8EE01419A

demonstrated [73]. These and other electrode chemistries are reviewed elsewhere [43]. Although Si exhibits one of the highest capacities among others, its molar volume change during cycling can be as high as 400% depending on the microstructure, which of course can lead to rapid cell degradation and loss of capacity and performance.

It was reported that employing Si nanowires [69], and nanosize Sn anodes [71] improved mechanical durability and cycle life. Indeed, to mitigate problems associated with dendrites and improve cell performance, micro- and nanostructured negative electrodes have been widely explored and reviewed elsewhere [75-79]. However, a key challenge with nanostructured electrodes is to maintain mechanical integrity and electronic connectivity. A recent study employed electronically conducting polymer (PFFOMB) as a binder to both stabilize the Si nanoparticles mechanically and to serve as a current collector, which boost up the performance at 1 C rate to 2050 mAh/g for Si and 1360 mAh/g of the electrode [80].

Lithium alloy anodes are essentially mixed ionic-electronic conductors of both electrons and Li^+ ions. This is a desirable property for reversible electrodes. Many of these alloys also offer fast ionic transport for Li^+ chemical diffusion in the alloy reaching values up to $2x10^{-3}$ cm^2/sec as reported earlier for Li_3Sb at 360°C [67]. Alloying especially with tin or silicon also helps increase the anode capacity greatly. In fact, the theoretical specific capacities for Sn and Si are 994 mAh/g-Sn and 4200 mAh/g-Si, respectively. The latter figure is about an order of magnitude higher than that for graphite (372 mAh/g-C). Lithium forms several alloy phases with Si and the highest Li content is reported for the $Li_{22}Si_5$ phase [63,68]. In other words, 4.4 Li^+ ions can be inserted for every Si atom. This is a substantial increase in anode capacity when compared to the C_6Li stoichiometry for graphite-host anodes, which allow only 0.167 Li^+ ions for every C atom. However, this advantage comes at the cost of significantly increased volume expansion (~ 400% for Si) during Li^+ insertion or lithiation of the Sn and Si anodes, which upon cycling eventually leads to mechanical breakdown and fracturing or pulverizing of the anode structure. Using nanostructured anodes such as nanotubes instead of bulk Sn or Si greatly mitigates this problem and allows significant increase in charge-discharge cycle life [69,77]. Besides nanostructuring, studies that pursue the holly grail of using elemental Li as the anode material have also employed interface engineering. For example, coating the Li anode with a monolayer of interconnected carbon nanospheres helped avoid dendrite formation up to a practically significant current density of 1 mA/$cm^2$and maintained 99% Coulombic efficiency for more than 150 cycles [81]. Also, a thin oxide layer on the Si nanostructure is shown to help improve the mechanical integrity of the anode [82].

Although much attention is given to achieving high gravimetric capacity and long cycle life, for most battery applications, volumetric capacity is equally important, and poses one of the barriers for practical implementation of Si-based anode hosts for Li-ion batteries. Intentionally designed void spacing allowed among the nanostructured Si anode architectural features to accommodate for the large volume change during cycling adversely impacts the volumetric capacity. Depositing SiC-free multilayer (2-10) graphene on the Si anode surface resulted in a 2D layered architecture and provided volumetric energy density

View Article Online
DOI: 10.1039/C8EE01419A

of 972 Wh/L in the first cycle and 700 Wh/L at the 200th cycle [73]. These numbers represent 1.8 to 1.5 times higher values than the volumetric energy densities of currently available commercial Li-ion batteries.

Another strategy commonly practiced is to reduce the propensity for lithium dendrite growth by intercalating Li^+ ions into a suitable host structure, such as in between the graphitic sheets of a typically disordered "soft" carbon anode as depicted in Figure 11. Carbon exhibits a slightly less negative potential than Li (i.e., nominally 100 mV vs Li/Li^+). It also has a volumetric capacity of about 800 mAh/ml and hence takes up ~ 50% of the volume of commercial Li-batteries [77]. As lithium in the carbon host structure is always in ionic form, rather than in metallic form, this provides some advantage against dendrite formation and related safety and electrolyte stability issues. However, the proximity of the carbon potential to that of Li does not entirely eliminate the possibility of dendrite formation and Li plating during charging. Chemical and physical properties of carbons and carbon nanostructures as negative electrode hosts for Li-ion batteries have been reviewed elsewhere [78,79,83].

D.1.1.2. Positive Electrode Materials

Most of the strategies that aim to minimize or overcome the stability and dendrite growth problems give rise to an increase in the potential of the negative electrode with respect to Li and correspondingly cause a reduction in the net cell voltage. In order to compensate for this voltage loss, cathode materials that exhibit high half-cell potentials and high capacities for insertion or intercalation have been the subject of intense research. Accordingly, more recent developments focused on the positive electrode, which is considered as the critical component of the battery that impacts its performance the most [43,45-48].

Many oxide systems have been investigated for prospective cathode materials over the last four decades, but most of them can be grouped into three different crystal structures, namely layered, spinel and olivine structures. The layered and spinel structure cathodes have the general formulas $LiMO_2$ (M=Co, Ni, Mn) and LiM_2O_4 (M=Mn, Ni), respectively. These materials are good conductors for Li^+ ions, and also have sufficient electronic conductivity due to the electronic transitions between the oxidation states of the multi-valent transition metal cations present in the structure Furthermore, their electronic conductivities can be improved by appropriate doping [84]. For example, partial substitution of Mg^{2+} on the Co^{3+}-site that is compensated by the creation of electron holes in $LiCoO_2$ and improve the room temperature electronic conductivity by nearly two orders of magnitude to 0.5 S/cm [85]. Similarly, the conductivity of the electronically insulating (< 10^{-13} S/cm) spinel $Li_4Ti_5O_{12}$ can be improved many orders of magnitude to 10^{-2} S/cm by Mg^{2+} doping on the Li^+ site that is compensated by the reduction of Ti^{+4} to Ti^{+3} [86]. Accordingly, such advances enabled the use of these structures suitable for cathode materials.

View Article Online
DOI: 10.1039/C8EE01419A

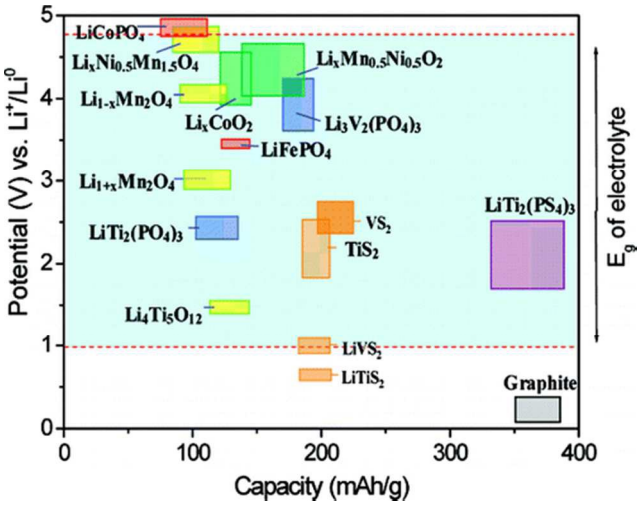

Figure 12. Comparative relation between capacity and cell potential of Li-ion batteries with various positive electrode materials (cathodes) versus the graphite anode with respect to the stability window (red dotted line) of the electrolyte (1 M $LiPF_6$ dissolved in 1:1 mixture of ethylene carbonate:diethylene carbonate) [48]. Reprinted with permission from (J. B. Goodenough, Y. Kim, Challenges for rechargeable Li batteries, Chem. Mater. 2010, **22**, 587-603). Copyright (2018)

Indeed, the first commercial Li-ion battery employed the layered structure oxide $LiCoO_2$ as the positive electrode [43]. However, $LiCoO_2$ has an inherently low capacity of about 130 mAh/g. It is also expensive and poses safety problems due to the toxicity of cobalt, which makes up only 20 ppm of the Earth's crust. Better safety, higher capacity, more abundant and lower cost cathode materials are needed for consumer electronics and energy storage applications.

In this regard, olivine structure $LiMPO_4$ where M is a transition metal such Fe offers lower cost, long cycle life, and safety [46,47]. From a safety point of view, the strong P-O covalent bond in the structure prevents the release of oxygen that can react with the electrolyte and initiate a thermal runaway. The strong P-O bond also reduces the covalency of the Fe-O bond and improves Li intercalation as well as cell voltage (3.5 V vs Li). Moreover, Fe is cheap and non-toxic, and offers a gravimetric capacity of 170 mAh/g. There has been a flurry of studies on olivine phosphates since the early results of electrochemical activity with a capacity of 100-110 mAh/g reported for $LiFePO_4$ [87]. However, the olivine structure $LiFePO_4$ is electronically insulating (10^{-10}–10^{-9} S/cm), and the Li extraction is accompanied by Fe^{+2} transition to Fe^{+3}, which results in two separate phases, namely $LiFePO_4$ and $FePO_4$, which are both poor electronic conductors. To overcome this difficulty, use of fine size $LiFePO_4$ particles or mixing it with an electronic conductor such as carbon has become necessary for cathode fabrication.

Indeed, the rates of Li insertion and extraction reactions were improved in subsequent studies by incorporating carbon-based conductive additives [88] and redox mediators [89]. Remarkably, it was shown that a small (0.5%) of Nb^{5+} doping ($Li_{1-x}M_x^{z+}FePO_4$) helps increase the electronic conductivity by eight orders of magnitude [90]. Introducing disorder in the Li-sublattice by nanosizing and nanostructuring [23], also improves reaction rates and battery performance. A recent study concluded that the desired size of battery-grade $LiFePO_4$ particles should be $\leq$ 200 nm [46]. Indeed, nanosized $LiFePO_4$ based Li-ion batteries have recently gained practical interest and commercialized originally by the US company A123 for portable applications.

View Article Online
DOI: 10.1039/C8EE01419A

The effect of doping $LiMPO_4$ on the M and/or P sites as well as the properties of other prospective materials for positive electrodes including dichalcogenides, manganese oxide spinels, and silicates are extensively reviewed elsewhere [45,47,48,91,92]. The cell potentials and storage capacities of various positive electrode materials of different crystal structures versus the graphite anode are presented in Figure 12, where the voltage stability regime of the 1 M $LiPF_6$/ethylene carbonate electrolyte is also indicated. For many of these materials, however, the useable energy density of the Li-ion battery is much smaller than the theoretically expected value. For example, in the case of electric vehicles the practically achievable energy density is approximately 25% of theoretical expected value for the active cathode material [93]. Unrealized differences between the theoretical storage capabilities and the actually achieved values are presented in Table 3 for various commercially available Li-ion cells. This gap is partly due to the dead weight of the inactive battery components. But part of this unused capacity is related to the structural properties of the cathode and the structural transformations the cathode undergoes during the lithiation and delithiation reactions during battery operation [94]. Such low utilization of the inherent capacities depicted in the table highlights the need to greatly improve the reversibility of the lithiation and delithiation reactions at the electrodes.

For large-scale energy storage, or power applications such as electric vehicles much higher capacities and energy densities, with lower cost and better safety than offered by today's Li-ion batteries are desired. Many believe that about ~300 mAh/g may approach the upper limit of the capacity for intercalation chemistry [50] due to constraints posed by the crystal structure and the limited transitions allowed in the oxidation state of the transition metal in these layered structures. A more recent review article agrees with this general assessment and estimates the ultimate limit for intercalation chemistry for Li-batteries may be 0.5 kWh/kg and 1.5 Wh/L for full cell configurations [46]. Therefore, intercalation chemistry most likely may not provide the roadmap to achieve much higher energy densities and capacities at lower cost with improved safety.

The search for improving the specific capacity of Li-ion batteries by utilizing all the accessible oxidation states of the electrode materials has lead to the concept of using conversion reactions, represented generally by the reaction,

$$M_xX_y + nyLi = yLi_nX + xM \quad (11)$$

Here, M is a 3-d transition metal such as Co, Fe, Mn, Cu, and X is N, O, S, F. Indeed, nano-sized transition metal oxide based positive electrodes for Li-ion batteries gave electrochemical capacities up to 700 mAh/g with good cycling capability retaining nearly 100% up to 100 cycles [95]. Similarly, transition metal fluorides, and in particular FeF_3, which offer high operating voltages due their highly ionic character, and large theoretical capacities (e.g., 712 mAh/g for FeF_3) gained much attention for positive electrodes [96,97]. However, metal fluorides are electronically insulating materials, thus unsuitable for use as electrodes. But carbon composites of FeF_3 overcame this problem and gave encouraging results, where reversible capacity as high as 600 mAh/g of the composite was reported [96,98]. The

View Article Online
DOI: 10.1039/C8EE01419A

reactions at the positive electrode were proposed [96,98] to proceed by the two-step sequence,

$$Fe^{+3}F_3 + Li^+ + e^- = LiFe^{2+}F_3 \qquad (4.5\text{-}2.5\ V) \qquad (12)$$

$$LiFe^{2+}F_3 + 2Li^+ + 2e^- = 3LiF + Fe \qquad (2.5\text{-}1.5\ V) \qquad (13)$$

The theoretical capacity for reaction (13), where Li is inserted into the FeF_3 structure in the potential regime of 4.5-2.5 V is 237 mAh/g, while the capacity for reaction (13) in the 2.5-1.5 V potential region is 400 mAh/g. It should be noted that the electrochemical lithiation of FeF_3 proceeds first with an intercalation step and multiple phase transitions, then followed by conversion process [97]. Binary metal fluorides FeF_2 and CuF_2 were also investigated for Li-battery positive electrode materials, and concluded that the lithiation of MF_2 occurs via a three-phase conversion process, where FeF_2 displays high reversibility for lithium via a network of Fe embedded in the insulating FeF_2 matrix, while CuF_2 shows lack of such reversibility [99].

D.1.1.3. Solid Electrolyte Interphase (SEI)

The organic carbonate-based solvent used in the nonaquesous electrolyte helps the formation of a thin solid electrolyte interface (SEI) on the anode. The SEI layer first reported nearly four decades ago, forms on the anode even after the initial charging of the fresh battery [100]. This layer contains both organic and inorganic components that are blocking to the transport of both Li^+ ions and electrons. In the case of a graphite-based anode with ethylene carbonate/$LiPF_6$ nonaqueous electrolyte, the SEI layer may contain grains of Li_2O, $LiCO_3$ and LiF. As Li_2O, Li_2CO_3, and LiF are insulators for both Li ions and electrons, they block the transport of these species, impeding the anode reaction. Indeed, probing the electrolyte/electrode interface of ethylene carbonate/metal oxide system by high resolution X-ray reflectivity, a recent study reported interfacial layering of the Li-salt and electrolyte solvent molecules on the electrode surface, which increases the interfacial transport impedance [101].

There is limited understanding of SEI formation at the cathode. Unlike the graphitic carbon anode held together by van de Waals forces that allow co-intercalation of the electrolyte solvent molecules, the ionically bonding character of the cathode crystal structure does not allow this to happen. Also, the potentials for most cathode materials with the exception ofthe emerging "5 V class" of cathodes such as $LiNi_{0.5}Mn_{1.5}O_4$ (4.6 V vs Li/Li^+) and $LiCoPO_4$ (4.8 V vs Li/Li^+) generally lie within the stability limit of the nonaqueous electrolytes avoiding the possibility of electrolyte decomposition [54]. Although the SEI at the anode may initially exhibit higher impedance, the cathode interphase over prolonged cycling builds up faster and becomes the more dominant resistive component of the two SEIs

View Article Online
DOI: 10.1039/C8EE01419A

Despite its disadvantages, the SEI layer also offers important advantages. For example, the SEI layer that forms on the bulk Li anode, in the case of Li-metal battery, provides a protective passivation layer on the Li surface that prevents violent reaction of Li with the electrolyte. In other words, the SEI layer at the anode makes it possible to operate the Li-ion battery at potentials beyond the thermodynamic stability regime of the organic electrolyte. The SEI layer also helps improve the kinetic stability of the cell by stabilizing the Li insertion and delithiation reactions during subsequent charge-discharge cycles, and provides a reversible capacity of 370 mAh/g for the graphite anode. However, it should be noted that the nature of mobile species in the SEI layer is of critical importance. If the SEI layer exhibits mixed ionic electronic conduction properties where both Li ions and electrons are mobile, then the layer will continue to grow, whereas if it is ionically conducting but electronically insulating in nature, then it will stop growing after forming a chemically protective barrier on the electrode/electrolyte interface to prevent further reaction with the electrolyte.

Table 3. Theoretical and actual storage capabilities of Li-ion batteries for various positive electrode materials [46]. Theoretical values include only the active components of the battery.

Cathode chemistry	Battery size	Theor. Wh/l	Actual Wh/l	% Realized	Theor. Wh/kg	Actual Wh/kg	% Realized
$LiFePO_4$	54 208	1980	292	14.8	587	156	26.6
$LiFePO_4$	16 650	1980	223	11.3	587	113	19.3
$LiMn_2O_4$	26 700	2060	296	14.4	500	109	21.8
$LiCoO_4$	18 650	2950	570	19.3	1000	250	25.0
Sr-$LiMO_4$ Panasonic	18 650	2950	919	31.2	1000	252	25.2

Also, the SEI layer,undergoes constant structural changes and reformation during repeated charge-discharge cycles, which leads to loss of Li to the constant repair of the SEI layer. Moreover, repeated volume changes at the anode, even in the case of bulk lithium anode as lithium is added or inserted, and extracted from the electrode lead to mechanical failure, particle fracturing and separation, and concerns about battery safety. The details of the properties, mechanisms of formation, and the structure of SEI layers have been reviewed elsewhere [54,102].

D.1.1.4. Electrolytes for Li-batteries

Other approaches to address the battery safety, stability, and dendrite problems focused on modification of the battery electrolyte or search for improvements and/or new alternatives. A wide variety of electrolytes employed in Li-based battery research and development have recently been reviewed [103,104]. The common electrolyte employed in Li-ion batteries is a non-aqueous electrolyte composed of lithium hexafluorophosphate ($LiPF_6$) dissolved in an organic solvent, typically ethylene carbonate or dimethyl carbonate. But organic-based electrolytes pose stability problems in the presence of high Li activities, i.e., high working potentials. This was a common failure of high voltage batteries with Li-metal anodes, which vigorously react with the organic components of the electrolyte irrespective of whether the electrolyte is a liquid or polymer-based. Similar reactions can also occur at the positive electrode, as the organic component usually is not stable in the

View Article Online
DOI: 10.1039/C8EE01419A

presence of high lithium activities. These exothermic reactions cause local heating in the battery that may eventually lead to thermal runaway. To avoid this problem, it is important to avoid operation at the potential where lithium at the electrode reacts with the organic component. Repeated cycling of the battery exacerbates this problem, possibly due to morphological changes that increase reaction surface area. A related problem is due to oxygen evolution building up to a flammable mixture with the highly reducing organic component in the electrolyte and causing battery fires. This is generally related to the positive electrode material that can exhibit a high oxygen activity versus Li [105], and facilitates oxygen evolution at high potentials that can lead to battery fires. Recently, several notable incidents caught the public's attention, ranging from aircraft battery fires to smartphones catching fire.

Efforts to modify liquid non-aqueous electrolytes by incorporating appropriate additives as inhibitors against dendrite growth as well as flame retardant chemicals for battery safety have provided encouraging results [106,107]. Even trace amount of water added to the nonaqueous electrolyte is reported to help eliminate dendrite formation [108]. Similarly, the use of Li^+-ion conducting polymeric membranes [39,109,110], polymer-ceramic composite electrolytes [111] or impervious Li^+-ion conducting ceramic electrolytes [112-115] provides a physical barrier layer that impedes dendrite growth between the two electrodes. Alternatively, ionic liquids [56,116,117], which are essentially room temperature molten salts, have been considered as electrolyte solvents for their high stability with a wide electrochemical window typically in excess of 4 V [118], as well as for their inherent safety due to inflammability and low vapor pressure [55]. However, they are expensive, and have limited solubility for Li-salts, high viscosity, and generally moderate ionic conductivity at ambient temperatures. Usually, ionic liquids are also susceptible to moisture, which complicates processing and battery fabrication.

Alternatively, aqueous electrolytes offer high conductivity and are highly desirable for safety and cost considerations for large-scale energy storage [119], but water has a narrow stability window of only 1.23 V. However, it is well known that several aqueous battery systems such as lead-acid (~ 2.0 V) can clearly operate outside this potential regime. This is facilitated by the formation of an electronically blocking but ionically conducting interlayers on the electrodes. In the case of Pb-acid battery, for example, the $PbSO_4$ interlayer covers both electrodes. Hence, modifying the electrolyte to promote the formation of such layers opens up opportunities for battery safety and cost. Indeed, a recent study reported a 4.0 V aqueous Li-ion battery where a fluorinated additive that is immiscible with the aqueous electrolyte provides a hydrophobic layer that minimizes the competing reaction of water reduction at the anode, and allows reversible cycling of both the graphite and Li-metal anodes [61].

Primarily for reasons of safety, stability, battery performance, and cost of manufacturing especially in thin film [120] or flexible forms [121,122], there has long been a search for high conductivity ceramic and polymeric electrolytes for solid state Li-batteries [113]. Many of the polymeric electrolytes are based on polyether or polyethylene oxide (POE) providing

View Article Online
DOI: 10.1039/C8EE01419A

the framework into which an appropriate Li salt is dissolved. Similarly, inorganic electrolytes based on various oxides, silicates, glasses and other structures have also been investigated and reviewed [103,104,114]. A more recent review provided a large compilation of comparative ionic conductivity data for a wide variety of Li-ion conducting polymer and ceramic electrolytes for Li-batteries [103,112,123]. Figure 13 presents a subset of Li-ion conducting solid polymer- and ceramic-based electrolytes from among a large collection of compositions. It is clear that most of these electrolytes are limited by their relatively poor room temperature conductivities typically in the range of 10^{-2} - 10^{-6} S/cm. This is especially true for most polymer and ceramic electrolytes whose conductivities are typically two or three orders of magnitude lower than for liquid organic electrolytes.

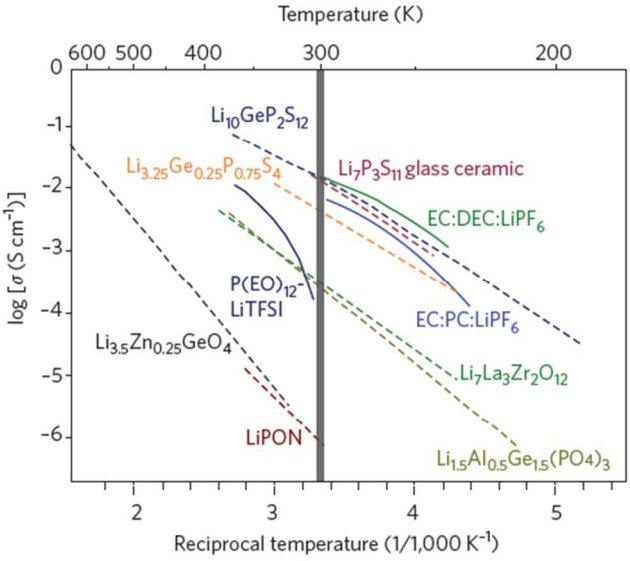

Figure 13. Comparative Li^+ ion conductivities of ceramic, polymeric, and liquid electrolytes for Li-ion batteries [123]. Reprinted by permission from Nature/Springer, J. Janek, W.G. Zeier, A solid future for battery development, Nature Energy, 2016, **1**, 16141 1-4. Copyright (2018).

There is growing interest towards an all solid-state battery architecture that employs inorganic solid electrolytes, which are expected to exhibit sufficient chemical stability against high voltage cathodes, and potentially mitigate or eliminate safety concerns [123]. Indeed, a lithium-metal anode cell employing a polymer electrolyte of lithium (bisfluorosulfonyl)imide in polyether is recently reported as a promising candidate for an all solid-state lithium-metal battery [124]. Thermodynamically, however, most solid electrolytes with few exceptions including garnets lack sufficient stability against metallic Li. This necessitates the build up of SEI protective layers at the electrode/electrolyte interfaces. Nevertheless, the presence of a Li-ion conducting inorganic impervious electrolyte membrane would eliminate the dendrite problem, and associated safety concerns of electrical shorting and thermal runaway. On the other hand, Li-batteries with organic electrolytes typically exhibit nearly twice the storage capacities (~ 0.2 mAh/cm^2) and discharge rates than batteries with solid electrolytes (~ 0.1 mAh/cm^2) due to kinetic and mass transport limitations [125].

Recent advances on sulphide-based and garnet-based solid electrolytes, have shown significant improvements in ionic conductivities. For example, $Li_{10}GeP_2S_{12}$ was shown to exhibit an ionic conductivity of 0.012 S/cm at room temperature [126], which is only an order of magnitude less than for organic electrolytes. More recently, an even higher ionic

View Article Online
DOI: 10.1039/C8EE01419A

conductivity of 0.025 S/cm was reported for $Li_{9.54}Si_{1.74}P_{1.44}$ $S_{11.7}Cl_{0.3}S_{12}$ at room temperature [127].

Garnet-based ceramics with cubic structure and the nominal composition of $Li_7La_3Zr_2O_{12}$ (LLZO) exhibit high Li-ion conductivity and also excellent stability against lithium metal, but stabilizing the cubic structure at room temperature is challenging. Room temperature conductivity of the tetragonal garnet LLZO is typically ~ 10^{-6} S/cm, nearly two orders of magnitude lower than the cubic phase. It was reported that generation of Li vacancies by extrinsic doping with aliovalent cations disrupts ordering of the Li-sublattice, and this may present opportunities to stabilize the cubic structure and improve room temperature Li-ion conductivity [128]. Incorporating ceramics into polymer electrolytes also improves ionic conductivity, expands the stability limit of the polymer electrolyte and also mitigates the dendrite problem [129]. For example, adding 15wt% of $Li_{70.33}La_{0.557}TiO_3$ nanowires to polyacrylonitrile-$LiClO_4$ electrolyte has substantially improved the room temperature Li-ion conductivity to 0.024 S/cm [130]. However, typically low transference numbers for Li ions (t_{Li} = 0.38) in composite electrolytes need significant improvement to attain higher efficiency.

The prospects of identifying highly conductive and stable electrolyte compositions in the near future require further investigation and development. However, it was recently suggested that the challenge to materials design for Li-batteries is not necessarily to find the stable materials, but instead to search for materials whose instabilities are self-limiting [94].

D.1.2. Beyond Li-ion Batteries

Although Li-ion batteries get most of the attention, their theoretical specific energy for the $LiCoO_2$/graphite and $LiFePO_4$/graphite systems is limited by the insertion chemistry to around 400 Wh/kg [42,90]. As a case in point, a battery power pack that can provide a cell-level specific energy of 350-400 Wh/kg would be required for electric vehicles to have a driving range of 300 miles on a single charge. Unfortunately, Li-ion batteries currently available today can only provide a specific energy nearly half of this value. Also, the desired life of the battery should last more than 1000 charge-discharge cycles at a rate greater than 2C capable of providing power greater than 600 W/kg [131].

D.1.2.1. Li-Sulfur Batteries

The demand for high performance batteries for transportation as well as stationary applications requires electrode materials that offer much higher specific energies, which can be achieved by increasing the cell potential and the storage capacity of the materials used for the anode and the cathode. But the stability windows of the battery electrolytes limit the cathode operating voltage to below 4.3 V [48]. Furthermore, with the capacity

View Article Online
DOI: 10.1039/C8EE01419A

limited by insertion chemistries, Li-sulfur system offers many advantages, but also challenges [132,133]. Figure 14 presents a schematic diagram for the Li-S battery system illustrating the charge and discharge processes.

The use of sulfur for the positive electrode in Li-S batteries offers low cost, low weight, high rates, low toxicity, environmental friendliness, and high theoretical capacity (2600 Wh/kg, versus ~600 Wh/kg for current Li-ion batteries), which is due to the high specific capacity of sulfur (1675 mAh/g, versus 130-200 mAh/g for current Li-ion battery cathode materials). The net cathode reaction during discharge is based on 2-electron transfer by,

$$S + 2Li^+ + 2e^- = Li_2S \qquad E = 2.2.\ V\ vs\ Li/Li^+ \qquad (14)$$

Although the cell potential of 2.2. V is about 60% of the 3.7 V for conventional Li-ion batteries, this is more than made up by the high theoretical energy densities of 2600 Wh/kg and 2200 Wh/L [43], which are 4-5 times higher than for the graphite/$LiCoO_2$ system. Potentially, Li-S batteries may be able to provide a driving range of nearly 300 miles [131]. But the Li-S battery system also poses several important challenges [134]. One is the poor electronic conductivities of sulfur (10^{-17} S/cm) and its discharge products of various polysulfides Li_2S_x (x= 1-8) deposited on the electrodes. These passivation layers increase the cell impedance and therefore require addition of an electronic conductor such as carbon or metals. Naturally, the addition of the conducting phase lowers the cell capacity, energy density, round-trip efficiency and cycle life. Another challenge is posed by the loss of sulfur from the cathode into the electrolyte due to the high solubility of the polysulfide ions (S_x^{-2}) formed on reduction of S_8 or oxidation of Li_2S. The dissolved polysulfide ions diffuse to the negative electrode and react with Li in a parasitic reaction to form lower polysulfides, which then diffuse back to the positive electrode and are re-oxidized. As expected, this internal shuttling mechanism so-called "polysulfide shuttle" lowers the Coulombic efficiency of the Li-S battery as well as the poor recyclability of the battery to achieve long cycle life. This is one of the key issues that can limit the commercial viability and prospects of the Li-S battery technology. In essence, the high order polysulfides dissolved in the electrolyte migrate toward the anode and react with the Li-metal anode and are reduced to the lower order sulfides, which migrate back to the cathode to form higher order polysulfides. Such continuous shuttling of polysulfides

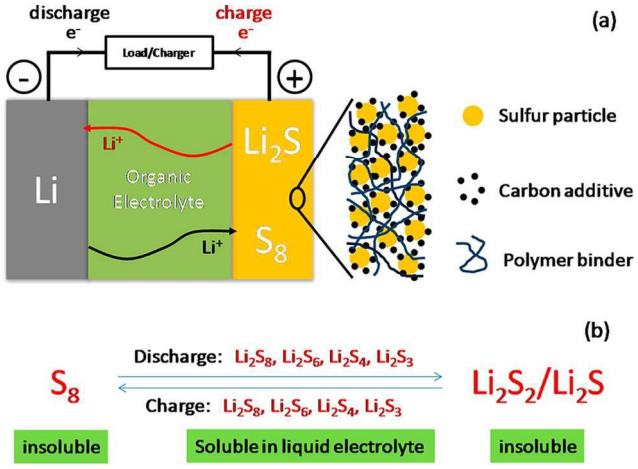

Figure 14. Schematic depiction of in the Li-S battery architecture illustrating charge and discharge processes [133]. Reprinted with permission from (A. Manthiram, Y. Fu, S.-H. Chung, Y.-S. Su, Challenges and prospects of lithium-sulfur batteries, Accnts. Chem. Res. 2013, **46**, 1125-1134). Copyright (2018) American Chemical Society.

View Article Online
DOI: 10.1039/C8EE01419A

between the two electrodes not only leads to permanent capacity fading due to loss of sulfur, but also constitutes the underlying cause of self-discharge. This self-discharge occurs even at the resting state of the Li-S battery due to the continuous dissolution of polysulfides, which gradually lower the open circuit potential and discharge capacity of the battery.

Furthermore, the multiple conversion reactions between the polysulfide species bounded by the end members S and Li_2S are accompanied by large volume changes (up to 76%), which can lead to mechanical failure or disintegration of the electrodes, and eventually to capacity loss upon cycling. Furthermore, dendrite formation and stability issues posed by the Li-metal anode and discussed in detail in the previous section are also valid for the Li-S system.

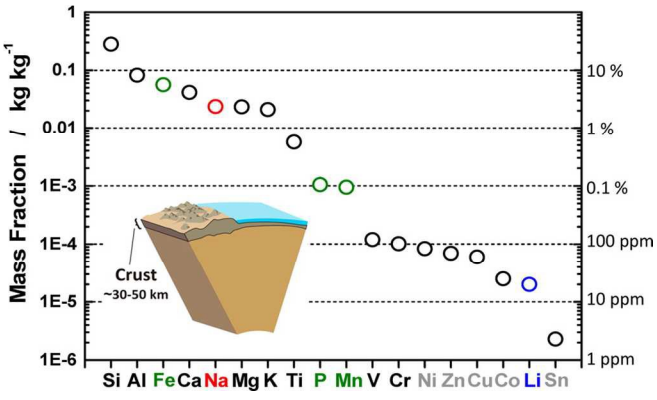

Figure 15. Relative abundance of metals in the earth's crust [138]. Reprinted with permission from (N. Yabuuchi, K. Kubota, M. Dahbi, S. Komaba, Chem. Rev. 2014, **114**, 11636-11682). Copyright (2018) American Chemical Society.

Much attention has been given to mitigate or overcome these technical challenges. Various strategies have been pursued to address and improve Coulombic efficiency, discharge capacity, cyclability, and self-discharge in Li-S batteries. Many of these strategies including carbon-composite or nanostructured electrodes [135], trapping interlayers, selective coatings or solid state electrolyte layers on the Li-metal anode, and modification of electrolytes by additives have been investigated and recently reviewed [132,133,136]. Much progress has been made. For example, nanostructured cathodes where sulfur is encapsulated inside hollow carbon nanofibers improved the cell capacity to 730 mAh/g measured at C/5 rate after 150 charge-discharge cycles [135]. Similarly, sulfur-graphene oxide nanocomposite cathode modified by cetyltrimethyl ammonium bromide provided a high specific capacity of 800 mAh/g, a long cycle (1500) life with a remarkably low decay rate of 0.039% per cycle, and allowed discharge rates as high as 6C (1C=1.675 A/g-sulfur) and charging rates as high as 3C [131]. Furthermore, the addition of $LiNO_3$ to the electrolyte facilitates passivation of the Li-anode and prevents parasitic reactions with the polysulfides. Several studies employing $LiNO_3$ additives reported Coulombic efficiencies of 96-99% even after 1500 cycles [131,135]. These advances provide encouragement for the future prospects of Li-S batteries as a potential candidate for efficient and cost effective storage system. However, for the Li-S system to compete potentially for the transportation sector, a recent techno-economic study considering a materials-to-systems approach predicted that high electrode loadings > 8 mAh/cm^2 are necessary to achieve >300 Land <$125/kWh [137]. Currently demonstrated loading levels (~2.5 mAh/cm^2) and energy densities (~100 Wh/L) indicate the major

View Article Online
DOI: 10.1039/C8EE01419A

challenges yet to be overcome for the Li-S system to vie for transportation applications.

D.1.2.2. Non-Li-based Batteries

Power modules based on Li-ion batteries have been the primary impetus for the explosive growth of portable electronic devices as well as the re-advent of electric vehicles in the last decade, albeit after a hiatus of more than one century. However, long-term sustainability of energy solutions requires a careful examination of the feasibility, cost, and availability of resources. This is especially important if Li-based batteries are to be considered for utility scale energy storage systems for the electric grid.

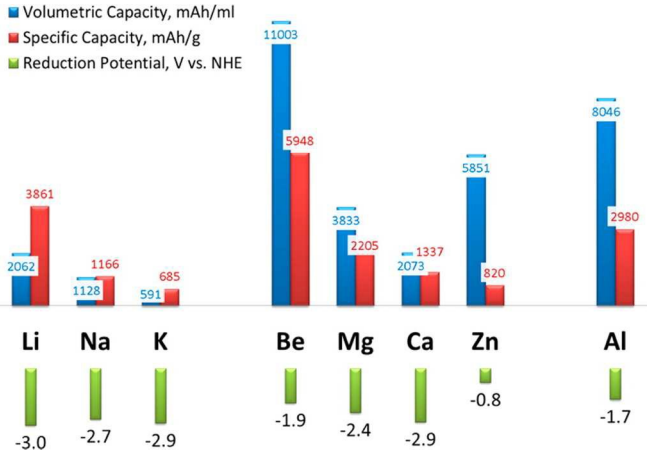

Figure 16. Comparison of specific capacities and reduction potentials of prospective metals for battery anodes [139]. Reprinted with permission from (J. Muldoon, C.B. Bucur, T. Gregory, Quest for nonaqueous multivalent secondary batteries: Magnesium and beyond, Chem. Rev. 2014, **114**, 11683-11720). Copyright (2018) American Chemical Society.

The relative abundance of lithium in the earth's crust is only 20 mg/kg (or, ppm). Furthermore, the known lithium reserves are mostly concentrated in South Africa, Chile and Australia, which create source dependency, supply reliability and price volatility for Li-based battery technologies. In fact, large fluctuations observed in the past in the price of lithium also pose economic concerns for reliability and availability when projected into the future even only for the electrification needs of the transportation sector. Recycling lithium from Li-based batteries in a cost effective manner remains an unsolved technology challenge. Moreover, the use of lithium for large-scale stationary energy storage may diminish the known lithium resources.

By contrast, other electropositive metals such as Na, K, Ca, and Mg are quite abundant in the earth's crust as indicated in Figure 15, and they are also fairly uniformly distributed geographically. In fact, Na is the fifth most abundant element. Especially oceans provide a vast and almost infinite resource for these elements. So battery systems based on Na, K, Ca, and Mg chemistries can provide cost-effective alternatives to existing Li-based batteries. Also, Na is the second lightest element next to Li in the periodic table. The reduction potentials and metal-anode-based theoretical capacities of alkali metal and alkaline earth metals are provided in Figure 16. Although the theoretical capacity for lithium is clearly superior to Na and K, the abundance and availability of these metals and others including Ca

View Article Online
DOI: 10.1039/C8EE01419A

and Mg make them attractive candidates for alternative battery systems as discussed in recent reviews [138-144].

As the active materials make up nearly 50% of the cost of most batteries, the wide availability and low cost of sodium at ~ $150/ton compared to ~ $15,000/ton for lithium presents great economic incentives for sustainability. Hence, sodium-based batteries attracted much attention. Na-ion battery architecture, chemistry and materials share many similarities with the Li-ion battery system [145]. Figure 17 illustrates the schematic depiction of the Na-ion battery. Because of such similarities in cell materials and their challenges, detailed discussion of Na-ion battery materials is not provided here. Instead, only salient features, recent progress and challenges are discussed briefly. For detailed information, the interested reader is referred to recent reviews on various aspects of Na-ion batteries [138,140,142,143,146].

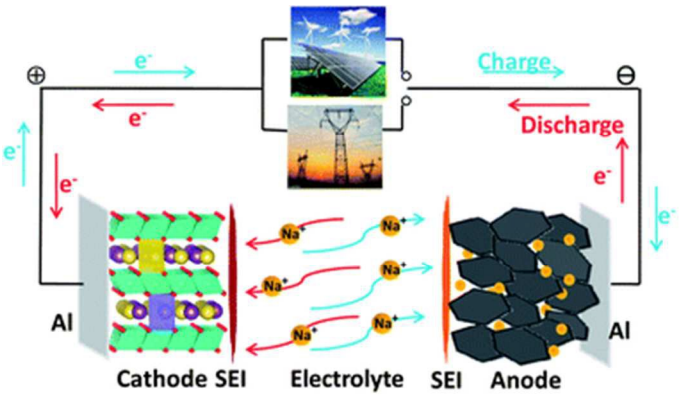

Figure 17. Schematic depicting the operating principle of the Na-ion battery. Reproduced from Ref. 142 with permission from The Royal Society of Chemistry.

Interest in the Na-ion system as a cheap and viable alternative to Li-based systems goes back to 1970's, almost concurrent with the intense research and development efforts in Li-ion batteries. Despite the similarities in most of their chemical and physical properties, however, progress has been slow for Na-ion batteries. One stumbling block (or barrier) has been the soft carbon-based anode materials such as graphite, which is commonly employed also in Li-ion batteries. Unfortunately soft carbon anodes exhibit low or no electrochemical activity when used in Na-ion batteries. Heating graphite in Na vapor seemed to be the only way to achieve intercalation. A major breakthrough came in 2000 when Na-ion cells employing hard carbon at the negative electrode were reported to provide a reversible capacity of 300 mAh/g [147]. The hard carbon anodes were prepared by the pyrolysis of glucose at 1000-1150^{o}C in an inert atmosphere to form a randomly stacked carbon layers made of small aromatic fragments that resemble a "house of cards", in between which the Na (and also Li) ions can be inserted. This high capacity, comparable to the anode capacities for the Li-ion batteries, generated great impetus and interest in Na-based storage systems research.

View Article Online
DOI: 10.1039/C8EE01419A

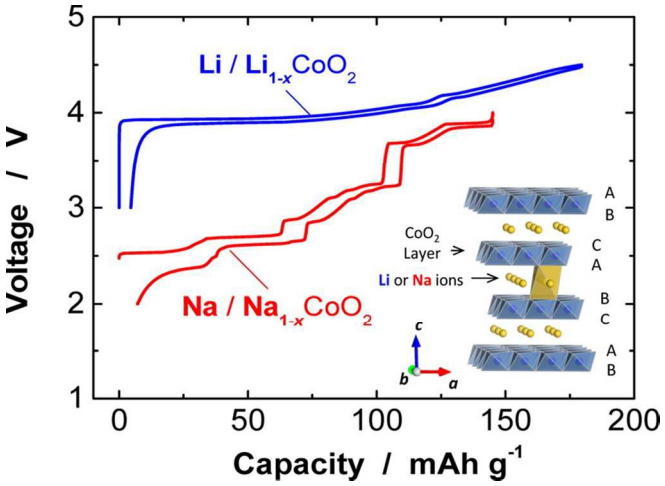

Figure 18. Comparative charge –discharge curves for $Li/LiCoO_2$ and $Na/NaCoO_2$ cells. Inset depicts Li or Na insertion into the layered crystal structure of the cathode [140]. Republished with permission of The Electrochemical Society, from [Review – Practical issues and future perspective for Na-ion batteries, K. Kubota, S. Komaba, J. Electrochem. Soc. 2015, **162**, A2538-A2550]; permission conveyed through Copyright Clearance Center, Inc. (2018).

Na exhibits a slightly less reducing potential of -2.7 V compared to the reduction potential of -3.04 V for Li, and also lower volumetric and gravimetric capacities due to the heavier Na atom (see Figure 16 above). A typical charge-discharge curve for a $Na\text{-}NaCoO_2$ cell is shown in Figure 18, which also includes a similar curve for the $Li\text{-}LiCoO_2$ couple for comparison [140]. Both cathode structures are analogs of each other and consist of layers of CoO_2 slabs in between which Na and Li ions reside as shown in the inset. The figure also compares the operating cell potential for $NaCoO_2$, which is > 1 V lower than for the $LiCoO_2$ cell. Accordingly, the Na-ion battery has a lower energy density than the Li-ion battery, marked by the stepwise potential changes for $NaCoO_2$.

As expected, many of the technical challenges facing Na-ion batteries are similar to those faced by Li-ion batteries, including better materials for electrodes with higher capacities, insufficient cycle life, capacity fading upon cycling, electrolyte stability at high voltages, etc. There has been recent progress in some of these areas, especially in seeking earth abundant, low-cost, and environmentally friendly electrode host materials for sustainability. For example, inspired by the early report [148] of high theoretical capacity (560 mAh/g) for dilithium rhodizonate ($Li_2C_6O_6$), which suffered from poor cycle life due to dissolution and exfoliation, its sodium analog disodium rhodizonate ($Na_2C_6O_6$) was recently investigated as an organic cathode material and reported achieving a four-electron redox reaction with a reversible capacity of 484 mAh/g, energy density of 726 Wh/kg of cathode material, and an energy efficiency above 87% [149]. The key to the observed long cycle life of this material was to understand and kinetically suppress the electrochemically limiting irreversible phase transformation between □-$Na_2C_6O_6$ and □-$Na_2C_6O_6$ during cycling by controlling particle size and morphology as well as using electrolyte additives. Also, this organic-based cathode material is derived from biomass, particularly from the corn extract myo-inositol, and hence, provides a sustainable and environmentally friendly synthesis route to produce the cathode material [31,148].

Similarly, a new class of non-rare-earth containing Fe-based cathode material with a composition $Na_2Fe_2(SO_4)_3$ was recently reported to provide an exceptionally high potential

View Article Online
DOI: 10.1039/C8EE01419A

of 3.8 V versus Na/Na+ with an experimentally measured capacity of 102 mAh/g, which was highly reversible over 30 cycles [150]. The measured capacity corresponds to about 85% of the theoretical capacity of 120 mAh/g based on the one electron Fe^{+3}/Fe^{+2} redox transition of the cathode material. Similarly, an all-solid-state Na-ion battery employing a Na-metal anode coated with a thin polymeric interlayer to suppress dendrite formation, a solid Na-ion conducting solid electrolyte of the composition $Na_3Zr_2Si_2PO_{12}$ (i.e., NASICON) and ionic conductivity of ~ 10^{-3} S/cm at temperatures ~ 65°C, and a $NaTi_2(PO_4)$ cathode provided 102 mAh/g after 70 cycles at 0.2C at 65°C with a Coulombic efficiency of 99.7% [151].

As the ionic size of Na (radius=97pm), compared to Li (radius=68pm), is too large to facilitate mobility in a closed packed framework of oxide ions, and needs a host structure with sufficiently large interstitial sites. A recent study reported the synthesis of a low-cost Na-Mn-hexocyanoferrate cathode composition where lowering of the activation barrier for Na-ion diffusion was achieved via weakening the Na-oxygen bonding by replacing the oxide ions by $(CN)^{-1}$ ions, whereby providing a reversible capacity of > 120 mAh/g and a high potential of 3.4 V [152]. Similarly, a family of Prussian blue structure cathode materials were reported for aqueous alkali-ion battery systems, including nanosized Cu haxacyanoferrate that showed no capacity fading after 1000 deep-discharge cycles and provided 95% round-trip efficiency when cycled at 5C [119] and Ni haxacyanoferrate that showed complete reversibility with zero capacity loss after 5,000 cycles for sodium and 1,000 cycles for potassium [153].

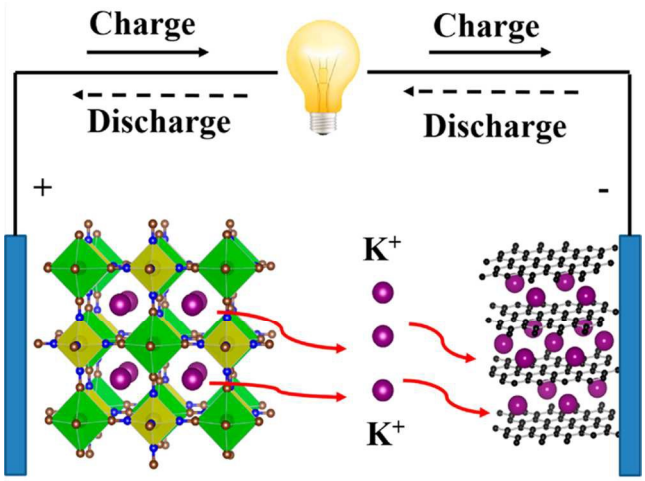

Figure 19. Schematic illustration of a K-ion cell with Prussian blue structure cathode and carbon-based anode [141]. Reprinted with permission from (A. Eftekhari, Z. Jian, X. Ji, Potassium secondary batteries, ACS Appl. Mater. Interfaces, 2016, **9**, 4404-4419). Copyright (2018) American Chemical Society.

Prussian blue (ferric hexacyanoferrate, or $Fe_4[Fe(CN)_6]_3 . xH_2O$, or $C_{18}Fe_7N_{18}$) is a low cost, effective cathode host material for the insertion and extraction of potassium over thousands of cycles, and potassium is also cheap and abundant, which makes it an ideal anode material for K-ion batteries. A schematic depiction of the K-ion battery structure with Prussian blue cathode and carbon anode is shown in Figure 19. An early demonstration of K-ion battery employed a Prussian blue-based cathode material and a potassium anode in a nonaqueous electrolyte consisting of 1 M KBF_4 dissolved in a 3:7 ratio ethylene carbonate/ethylmethyl carbonate mixture, and showed a cathode capacity of 80 mAh/g and excellent cyclability for over 500 reversible cycles [154]. With the expected carbon anode capacity of 262 mAh/g at C/10 rate and potential of 0.3 vs K+/K, a

View Article Online
DOI: 10.1039/C8EE01419A

complete K-ion cell can deliver an energy density of ~200 Wh/kg based on the mass of the electrodes, and a full battery may be able to provide ~110 Wh/kg [141]. Another advantage of K-ion batteries is the highly negative standard potential of -2.936 V vs the standard hydrogen electrode (SHE) for the K^+/K redox couple. This value compares quite well with the potential of -3.04 V vs SHE for the Li^+/Li couple for Li-ion batteries, while it is still more negative than the Na^+/Na couple at -2.714 V vs SHE, providing close to ~200 mV higher cell voltage for K-ion batteries than for Na-ion. Furthermore, transport of the "soft" K^+ ion is much faster than for the strongly solvated Li^+ ions in electrolytes, because of the smaller Stoke diameter (i.e., solvation sheath) for potassium. Again, due to many similarities in materials aspects with Li-based battery systems that were discussed previously (see section D.1.1. Li-ion Batteries), the interested reader is referred to recent review articles for more information on K-based batteries [141,145,155].

Unlike the single-electron transfer reactions in alkali metal-based battery systems, battery chemistries based on charge transfer reactions involving multivalent cations provide a great incentive to design battery materials and systems that accomplish multi-electron transfer and higher storage capacities. The theoretical capacities are presented in Figure 16. In that regard, magnesium, calcium, and even aluminum offer obvious advantages for progress beyond Li-batteries, albeit with their own challenges and shortcomings. Replacing Li^+ with multivalent Mg^{+2}, Ca^{+2}, Al^{+3} cations increases the total charge transferred per ion, which naturally increases storage capacity. For example, the theoretical volumetric capacity of 3833 mAh/ml for magnesium is nearly twice that for lithium metal (2062 mAh/ml), and it has a slightly less negative reduction potential of -2.4 V vs SHE compared to lithium (see Figure 16). Similarly, Al offers a theoretical volumetric capacity of nearly four times (i.e., 8040 mAh/ml) that of lithium and a reduction potential of only -1.67 V vs SHE, while Ca has a theoretical capacity of 2073 mAh/g and a reduction potential of -2.87 V vs SHE [139]. Moreover, Mg, Ca, and Al, are cheap and among the most abundant elements on the planet (see Figure 15). They also do not show a high propensity for dendrite formation, as is the case for metallic Li anodes. Also, these metals do not pose major safety issues and are easier to work with during processing. They do not need to be processed in glove boxes under tightly controlled and monitored inert and dry atmospheres.

Despite the great potential of these metals to be suitable battery anodes, however, progress in these systems has been slow due to multiple challenges. Major advances in the discovery of superior electrode and electrolyte materials, stability, reversible cyclability and long cycle life are needed in order to capitalize on the attractively high theoretical capacities offered by the chemistries of multivalent cations. Many of these challenges and materials issues for Mg, Ca, and Al battery systems have recently been reviewed [139,144,156-158].

There are critical barriers to designing a rechargeable battery based on these cations. For example, finding suitable high capacity cathode structures that can reversibly intercalate these multivalent cations at high potentials remains a major challenge. During charging of the battery, these metals tend to form a passive, electronically insulating oxide

View Article Online
DOI: 10.1039/C8EE01419A

layer, which also blocks cation transport. Electrolytes with sufficient stability have yet to be identified that can facilitate the formation of conductive passivation layers on the electrodes at high potentials. Intercalation of these cations into host cathode structures has been difficult and slow due to low mobility, which presents a barrier for further development. The high oxidation state of these cations slows them during mass transport due to stronger Coulombic interactions with the host electrode structures. Also, their reduction potentials are lower than that for Li, and hence provide a lower operating cell voltage for the battery.

Nevertheless, some progress has been made in some of these fronts. For example, fast Mg^{+2} ion conductivity of 0.01-0.1 mS/cm at 298K in the $MgSc_2Se_4$ spinel was recently reported with a low migration barrier of only 370 mV [156]. It should be noted that previous reports of comparably high Mg^{+2} mobility in spinel and Chevrel phases were obtained only at temperatures (400-800^{o}C), while this recent study constitutes the first report of high Mg^{+2} mobility in a closed packed chalcogenide structure at room temperature. Similarly, one of the first demonstrations of reversible Ca^{+2} intercalation was recently reported for a Prussian blue structure manganese hexacyanoferrate (MFCN) cathode in a nonaqueous electrolyte giving a capacity of 80 mAh/g, which retained 50% of its value after 35 cycles [144].

Aluminum is cheap and one of the most abundant metals on Earth (see Figure 15). As a trivalent ion, aluminum-based batteries provide a three-electron redox reaction that results in a theoretical capacity of 2.98 Ah/g [157]. This is slightly less than the theoretical capacity of 3.86 Ah/g for lithium, while its volumetric capacity of 8.04 Ah/ml is much superior to 2.06 Ah/ml for lithium, 3.83 Ah/ml for magnesium, and 5.85 Ah/ml for zinc (see Figure 16). However, early attempts to develop a rechargeable Al-based battery has faced numerous challenges including low cell discharge voltage, short cycle life (<100 cycles) in part due to disintegration of the cathode materials, and high capacity fading rate (26-85%). The first functional Al-ion rechargeable battery utilizing a Al metal anode, V_2O_5 cathode and an ionic liquid electrolyte containing $AlCl_3$ provided 305 mAh/g in the first cycle and 273 mAh/g after 20 cycles with a stable Al^{+3} insertion plateau at 0.55 V [158]. Recent progress using a Al metal anode, a graphitic foam cathode and ionic liquid electrolyte demonstrated electrochemical dissolution and deposition of aluminum at the anode, fast intercalation and de-intercalation of chloroaluminate ions in the graphite foam cathode that resulted in rapid (~ 1 min) charging times at high current densities of ~ 4,000 mA/g, and exhibited a stable discharge plateau at ~ 2.0 V, a low specific capacity of 70 mAh/g, high Coulombic efficiency of 98%, and long cycle life > 7,500 without decay [159]. Despite the remarkable progress, this Al-ion/graphite system was able to provide an energy density of only ~ 40 Wh/kg, which is comparable to Pb-acid or Ni-metal hydride batteries. On the other hand, however, it offered a high power density of ~3,000W/kg that is comparable to supercapacitors.

View Article Online
DOI: 10.1039/C8EE01419A

D.1.2.3. Na-S Batteries

The active materials of this battery system, namely, sodium and sulfur, are cheap, abundant, and readily available. Moreover the Na-S system has a cell potential of 2.1 V and high theoretical energy densities of 790 Wh/kg and 1180 Wh/L [44], high energy efficiency, and great cyclability typically in the 1000's of cycles. These attractive properties have attracted great interest in the Na-S system in the last several decades. They have been commercialized in Japan since 2002 for stationary storage in MW scale systems, and generally used in load-leveling and peak-shaving applications by the utilities. There are hundreds of Na-S battery installations around the world, most of them in Japan, that provide in excess of 300 MW of discharge capacity for energy storage.

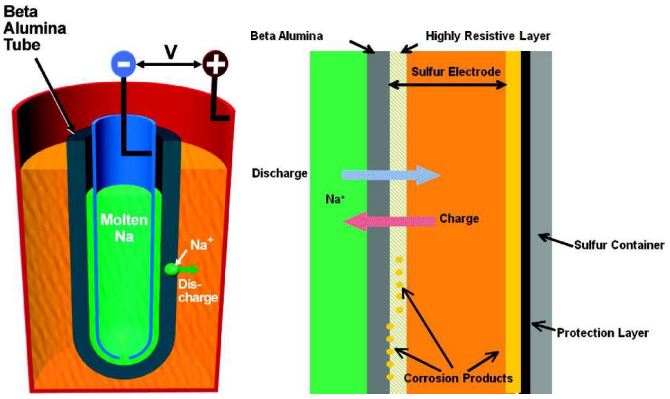

Figure 20. Schematic cell structure (left) and operating principle (right) of the Na-S battery [32]. Reprinted with permission from (Z. Yang, J. Zhang, M. C. W. Kintner-Meyer, X. Lu, D. Choi, J. P. Lemmon, J. Liu; Chem. Rev. 2011, **111**, 3577-3613). Copyright (2018) American Chemical Society.

The technical challenges for Li- and Na-sulfur battery systems posed by the high solubility of alkali metal polysulfide species in the electrolyte that are the root cause of multiple problems including passivation layers building on the electrodes, polysulfide shuttling through the electrolyte, and capacity fading as discussed in previously (see section D.1.2.1. Li-sulfur batteries) can be largely overcome by replacing the liquid electrolyte with a solid impervious membrane that selectively transports only alkali ions across and provides a physical barrier that separates the alkali metal anode from the sulfur cathode. This has been the underlying reason and the rationale for the development of the Na-S battery, which employs a Na-ion conducting solid electrolyte between the molten sodium anode and the sulfur cathode.

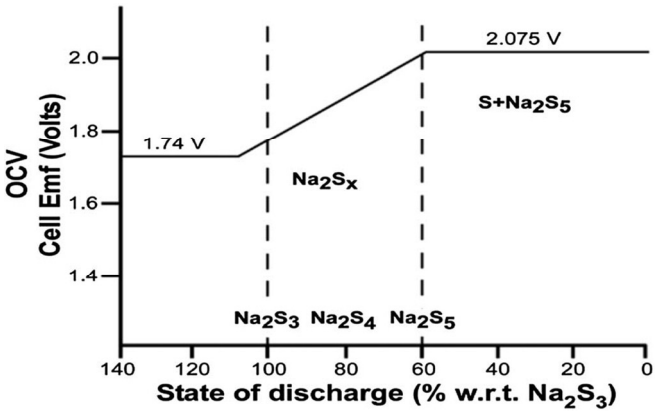

Figure 21. Voltage regimes and phase boundaries of polysulfides in the Na-S system. Reproduced from Ref. 162 with permission from The Royal Society of Chemistry.

Indeed, the discovery of fast sodium ion transport in a common refractory Na β-alumina ($Na_2O.11Al_2O_3$, or $NaAl_{11}O_{17}$) near room temperature in early 1960's

View Article Online
DOI: 10.1039/C8EE01419A

made this possible and generated great interest in Na-ion based electrochemical storage systems. At 300°C, the ionic conductivity of Na β-alumina approaches the room temperature conductivity of 10^{-1} S/cm, comparable to common aqueous electrolytes. Another member of this family is the Na β"-alumina, which exhibits an ionic conductivity of 1.3 S/cm at 500oC [160]. These highly conductive electrolyte materials opened up opportunities to explore sodium chemistries for power generation and storage applications, including Na-S and Na-metal chloride batteries [161].

Schematic depiction of the Na-S battery tubular architecture and its operating principle is shown in Figure 20. At the typical operating temperature of 300-350°C, both the Na anode and the sulfur cathode are in their molten state. Generally, a tubular sodium β"-alumina impervious electrolyte membrane houses the molten Na (negative electrode), and separates it from the molten sulfur (positive electrode). Due to its low conductivity, the sulfur electrode is mixed with carbon to improve the electronic conductivity of the positive electrode.

Elemental sulfur has a high theoretical specific capacity of 1675 mAh/g based on the 2-electron half-cell reaction at the cathode. During discharge, Na is oxidized to Na^+ and is transported across the electrolyte to react with sulfur and form sodium polysulfides (Na_2S_x). The phase boundaries of these polysulfides and the voltage regimes are presented in Figure 21. At the open circuit potential of 2.075 V, there exists a two-phase region as Na_2S_5 is insoluble in sulfur, so forms a two-phase liquid mixture at the operating temperature. As the battery discharges, sulfur combines with sodium to form a single-phase region marked by Na_2S_4 in the figure. If unchecked, the level of molten Na drops due to consumption, so process control is important. At 1.74 V, Na_2S_4 is reduced to Na_2S_3. For deeper discharge, the undesirable solid Na_2S_2 may form and increase the cell impedance. During charging, the reactions are reversed, but the re-formation of sulfur must be managed. Otherwise, it can deposit on the electrolyte and form an insulating layer, which increases cell impedance and lowers performance. The round-trip efficiency of Na-S batteries is around 80% with an estimated life of ~15 years for > 4500 cycles at 90% depth of charge [162].

The Na^+ released at the positive electrode is transported back through the Na^+ ion conducting ceramic electrolyte into the negative electrode, where it picks up an electron from the external circuit and deposits as metallic sodium. In order to facilitate sufficient rates (i.e., current) of ion transport through the solid electrolyte, the battery operates typically at 350°C. The heat produced during discharge/charge cycles is sufficient to maintain the battery temperature. Usually, no external heat input is needed.

Recent review articles provide more details into the operational, performance, and materials aspects of Na^+-based batteries and their technical challenges [142,161,163].

Although Na-S battery systems are commercially available and offer attractive advantages including inexpensive, abundant, nontoxic, and environmentally benign materials, while offering low maintenance, cycling flexibility and long cycle life, high storage capacity and efficiencies [24], they also face technical challenges still remain to overcome.

View Article Online
DOI: 10.1039/C8EE01419A

One critical problem is related to corrosion and vapor loss. High operating temperatures compared to other storage systems reviewed in earlier sections, as well as the highly reactive nature of the molten electrodes pose hot corrosion problems, related in particular, to the highly corrosive nature of the S and Na_2S_5 species at these temperatures. This places expensive demands on materials selection for the container and other cell components such as hermetic seals. High operating temperatures required for achieving sufficient ion transport through the ceramic electrolyte is also dictated by the difficulty in achieving proper wetting of the solid electrolyte by molten sodium, which is one of the most challenging issues for Na-S batteries.

The solid electrolyte, namely β- (or β"-) alumina, is a critical and expensive component of the Na-S battery. Although ionic transport of Na^+ through the electrolyte occurs anisotropically along the 2-dimensional conduction planes separated by close-packed Al-O blocks, the random positioning of the fine grains of powders that make up the finished polycrystalline electrolyte tubes mitigates the anisotropy problem greatly. Ionic conductivities of the tubular polycrystalline electrolyte are only a factor of 3-5 smaller than that for the single crystal electrolyte. However, mechanical fragility and process yields for the tubular β-alumina fabrication are major concerns and cost factors for mass production of these electrolytes.

Reducing the operating temperature of the Na-S battery is important for improving its safety, cost, and durability by slowing down degradation mechanisms. A recent study attempted to reduce the operating temperature to 150°C by employing a molten Na separated by a 600 μm thick β"-alumina electrolyte in series with a liquid catholyte of 4:1 molar ratio of S:Na_2S_4 dissolved in tetraglyme solution reported an initial discharge capacity of 473 mAh/g of which 70% was retained after 60 cycles, and cell voltages around 2 V [164]. Similarly, alloying Na with 6.7mol% of the low surface tension metal Cs markedly improves wetting of the β"-alumina solid electrolyte in the molten alloy and at the same time, helps bring down the operating temperature to 150-175oC with a capacity fading rate of < 3% over 100 cycles [165].

Others aimed at reducing the Na-S battery operation to room temperature by employing a sulfur-carbon composite cathode in nonaqueous electrolyte [166]. One critical challenge to room temperature operation is the instability of the electrolyte to form electrochemically inactive alkali metal polysulfides. Porous carbon framework doped highly with nitrogen and sulfur was suggested to help trap the sodium polysulfides and inhibit reaction with the electrolyte, and provide a long cycle of over 10,000 cycles with less than 20% capacity fading (3% after 800 cycles) at a high current density of 4.6 A/g [167]. Similarly, a more recent study that employed a Na metal anode, a metal-organic framework (MOF)-derived microporous carbon-sulfur composite cathode in a liquid carbonate electrolyte containing 1 M $NaClO_4$ and an ionic liquid (1-methyl-3-propylimidazolium-chlorate) reported a reversible storage capacity of 860 mAh/g-S at 0.1C rate (1C=1,675 mA/g) and 600 mAh/g-S at 0.5 C with a capacity fade rate of only 0.31% over 100 cycles at room temperature [168].

View Article Online
DOI: 10.1039/C8EE01419A

A different family ionically conducting solid electrolyte dubbed NASICON (for sodium-super-ionic-conductor) with the nominal composition $Na_{1+x}Zr_3P_{3-x}Si_xO_{12}$ ($0 \leq x \leq 3$) was introduced in the 1970's [169]. Unlike 2D transport of Na^+ in the layer structured β-alumina, which poses challenges in processing and ohmic losses due to misalignment of grains in the electrolyte membrane in the actual battery, transport of Na ions in the NASICON structure is 3-dimensional. This of course offers many advantages, and also, isotropic conductivity of $6x10^{-4}$ S/cm at room temperature [170], while it increases to 0.2 S/cm at 300°C with an activation energy of 0.29 eV [169], which is only 0.1 eV larger than that for □"-alumina. Despite the attractively high ionic conductivity for Na^+, however, NASICON is known to be chemically unstable in the presence of molten sodium and degrade rapidly to eventual fracture [171]. It is also unstable in water, and therefore not suitable for aqueous systems that require long service life.

Another Na-based storage system utilizing the β-alumina family of electrolytes is based on the Na-$NiCl_2$ chemistry (also called the ZEBRA cell) that also operates at moderately high temperatures of 270-300°C. The ZEBRA battery has theoretical and practical energy densities of 788 and 120 Wh/kg, respectively, theoretical capacity of 305 Ah/kg, high cell voltage (2.58 V), maintenance free operation, zero self-discharge, and long cycle life up to 5,000 cycles at 80% depth of discharge [162]. The positive electrode structure contains interconnecting porous Ni particles dispersed in the semisolid composite of the electrochemically active $NiCl_2$ and a molten secondary electrolyte $NaAlCl_4$ that conducts Na-ions. During discharge, sodium is oxidized to Na^+ and transported through the β-alumina electrolyte and then across the $NaAlCl_4$ electrolyte to the cathode, where it reacts with $NiCl_2$ to form NaCl and metallic Ni, giving a cell potential of 2.58 V. During charging, the reverse process takes place, where the Ni is oxidized and reacts with NaCl to form $NiCl_2$. Aside from conducting Na^+ ions to the cathode during discharge, the other important function of $NaAlCl_4$ is to overcome overcharging the battery, as it serves as a source for Na by the reversible reaction,

$$2NaAlCl_4 + N = 2\ Na + Ni(AlCl_4)_2 \qquad (15)$$

ZEBRA batteries offer several advantages over Na-S, including higher cell voltage, safer operation, tolerance to overcharging, and ease of assembly of the battery in the discharged state. The positive electrode primarily consists of solids, reducing corrosion and associated problems. It also eliminates the need to handle metallic Na for the negative electrode, as all Na is introduced in the form of salts using $AlCl_3$ and NaCl. However, capacity fading due to the solubility of $NiCl_2$ in the $NaAlCl_4$ and coarsening of the Ni particles pose operational challenges [162].

D.1.2.4. Metal-Air Batteries

The operating principle of metal-air systems in essence can be considered between that of traditional batteries and fuel cells. As in many battery systems, the fuel is a bulk metal

View Article Online
DOI: 10.1039/C8EE01419A

serving as the negative electrode, while the reduction reaction at the positive electrode is accomplished by the oxygen supplied through a porous electrode from the ambient air, as in fuel cells. Elimination of the bulky positive electrode of the battery and replacing it with an air electrode is key to achieving exceptionally high theoretical energy densities in metal-air systems. Obviously, such advantage that potentially offers practical prospects especially in the transportation sector has generated interest in these systems that goes back several decades [172].

Although the name "metal-air" battery is used commonly to refer to these systems as also adopted in this article, this should be considered merely as an operational label. Strictly speaking, they are metal-oxygen batteries, as they utilize oxygen from the ambient air. Although this is indeed a great advantage as air is free, it also presents operational challenges that may vary for these systems depending on the nature of the electrolyte and the metal anode they employ. Regardless, however, almost all metal-oxygen batteries require some degree of pre-treatment or removal of air impurities primarily CO_2 and moisture, but also SO_2, N_2 and possibly others depending on the metal-air system from entering the battery proper, and adversely interact with the electrolyte or battery components via parasitic reactions. For example, CO_2 is known to readily absorb in alkaline electrolyte solutions and precipitate in the porous cathode as solid carbonates, while moisture is detrimental to nonaqueous and aprotic electrolytes. In many cases, pure oxygen has preferably been employed. This is especially true for Li-air batteries, where air impurities are particularly problematic. Others employed polymeric membranes to avoid problems associated with air impurities [173]. Regardless, however, the need for such pre-treatment or clean-up processes or for oxygen separation increases the complexity of the energy storage process and adds weight to the battery that collectively reduces both the system efficiency and the energy density.

Portable electronics, transportation and other types of mobile storage applications demand high gravimetric and volumetric energy densities, low cost, long cycle life, and safe and stable operation. These requirements are difficult to meet using currently available commercial battery chemistries. For example, commercial Li-ion batteries provide close 150 to 200 Wh/kg, while the power system for an electrical vehicle with a 500 mile range would require nearly 10 times increase in the energy density of the battery [174], which is most likely an unrealistic expectation. In search for improved electrochemical systems, metal-air batteries offer many advantages particularly with respect to the amount of energy they can store. Many of the characteristic features and operational properties of metal-air battery systems are summarized in Table 4 for comparison and reviewed elsewhere [175,176]. By definition, alkaline electrolyte is an aqueous solution of a base such as NaOH. Unlike protic solvents such as water and many alcohols including methanol that contain labile protons bonded to oxygen or nitrogen, which can then be donated via hydrogen bonding, aprotic solvents such a propylene carbonate lack acidic hydrogen (i.e., O-H bonds) and hence cannot make hydrogen bonding to donate their protons. Similarly, saline electrolyte in the table refers to an aqueous solution of a soluble salt such as NaCl.

While the cell architecture of the commercially available rechargeable batteries is closed, metal-air batteries have open architecture, where oxygen from air is accessed

View Article Online
DOI: 10.1039/C8EE01419A

through the porous cathode. They have lower cost and considerably higher energy densities than other battery systems. They utilize the conversion chemistry and the high oxidation potential of the pure metal electrode with respect to oxygen. They also eliminate the need for the massive positive electrode that holds the electrochemically active species as in other battery systems, and replace it with a porous air electrode.

Table 4. Comparison of characteristic features and properties of metal-air battery systems. Adapted from ref [175].

Battery systems	Li-air	K-air	Na-air	Mg-air	Zn-air	Fe-air	Al-air
Cost of metal ($/kg)[a]	68	20	1.7	2.75	1.85	0.4	1.75
Theoretical voltage (V)	**2.96**	**2.48**	**2.27**	**3.09**	**1.65**	**1.28**	**2.71**
Practical voltage (V)	**2.6**	**2.4**	**2.2**	**1.2-1.4**	**1.0-1.2**	**1.0**	**1.1-1.4**
Theoretical energy density (Wh/kg)[b]	**3458**	**935**	**1106**	**2840**	**1086**	**763**	**2796**
Practical energy density (Wh/kg)	Not known[c]	Not known[c]	Not known[c]	**400-700**	**350-500**	**60-80**	**300-500**
Electrolyte	Aprotic	Aprotic	Aprotic	Saline	Alkaline	Alkaline	Alkaline, or saline
Primary(P), or rechargeable (R)	R	R	R	P	R	R	P
Year invented	1996	2013	2012	1966	1878	1968	1962

Notes: (a) 2014 prices, (b) includes oxygen, © Literature values are normalized to mass of catalyst

The Zn-air primary system is the only commercialized and widely used battery, most for hearing aids. Al-air and Mg-air batteries are employed in the military for underwater propulsion. The other metal-air battery systems are still under development for commercial applications. Several of these battery systems, namely, Zn-air [175,176], Al-air [157,177], and Mg-air [139], can be recharged mechanically, or refueled, by simply replacing the discharged anode and the spent electrolyte with fresh ones. This also allows the air electrode to be operational during discharge only as the cathode for oxygen reduction. Despite intense research efforts, however, achieving electrical recharging in a reversible, efficient and cost effective manner has been challenging, and presents the major obstacle for the commercialization of these high-energy density systems. Among the metal-air systems, however, Li-air and Zn-air batteries attracted the most interest partly because of their exceptionally high energy density and other advantages [176].

Cell type are labeled according to the anode material, while cell configurations can be grouped with respect to the nature of their electrolyte, namely, aqueous and non-aqueous (containing aprotic solvent). As expected, aprotic (no hydrogen bonding) electrolytes, usually employed for alkali metal-air batteries, are susceptible to moisture contamination leading to cell and performance degradation, while Fe-, Zn-, and Al-air batteries use aqueous electrolytes. Recent advances in Li-air battery materials and architecture also allow the use of aqueous electrolytes [174,178]. Many of the metal-air battery systems and their cell components, electrode

Table 5. Theoretical energy densities of Li-air batteries compared to other Li-based storage systems [43].

Battery system and net cell reaction	Cell voltage (V)	Theoretical specific energy (Wh/kg)	Theoretical energy density (Wh/L)
$Li-O_2$ battery *(nonaqueous)*	**3.0**	**3505**	**3436[a]**
$2Li + O_2 = Li_2O_2$			
$Li-O_2$ battery *(aqueous)*	**3.2**	**3582**	**2234[b]**
$2Li + ½ O_2 + H_2O = 2LiOH$			
Li-ion battery	**3.8**	**387**	**1015**
$½ C_6Li + Li_{0.5}CoO_2 = 3C + LiCoO_2$			
Li-S battery	**2.2**	**2567**	**2199[c]**
$2Li + S = Li_2S$			

Note: (a) based on the sum of initial volume of Li and the final volume of Li_2O_2 after discharge, (b) based on the sum of initial volume of ($Li+H_2O$) consumed and the final volume of LiOH after discharge, (c) based on the sum of initial volume of Li and the final volume of Li_2S after discharge,

View Article Online
DOI: 10.1039/C8EE01419A

reactions and cell performances are reviewed elsewhere [174-176,178-180].

Despite differences in their chemistries, there are many scientific and technical challenges shared by metal-air batteries regarding the anode and cathode materials and processes. Typically, poor utilization of the anode metal and slow kinetics at the air electrode are the most common problems. The anodes typically undergo corrosion in the electrolyte, which leads to self-discharge and short shelf life. It also monotonically decreases the battery's Coulombic efficiency. The non-conductive oxide and/or hydroxide layer built after the first discharge cycle due to severe passivation of the anode metal surface impedes electrolyte access to the liquid-solid-gas interface at the anode and also blocks the active anode material to participate in the oxidation/dissolution reaction, and hence, slows down the anode reaction kinetics. To mitigate these problems, one strategy is to isolate one of the active battery components, i.e., either the anode or the electrolyte, from the cell until the battery is ready for activation and use. Regardless, however, this does not solve the reversibility requirement for achieving rechargeability of the battery, as the blocking layer impedes plating of the metal on the anode during the charging cycle.

Likewise, the air electrode is arguably the most complicated and expensive component of metal-air systems. It suffers from intrinsically sluggish oxygen kinetics, high polarization losses, and poor reversibility of the oxygen electrochemistry [181]. The requirements for developing an effective air electrode also depend on the chemistry of the metal anode as well as the class or type of the electrolyte employed for the battery. These considerations are recently reviewed in detail elsewhere [180]. At the air electrode, oxygen from air accepts electrons from the metal-ion during discharge and releases them during charging. Finding a bifunctional facile catalyst that can perform both the oxygen reduction reaction (ORR) and oxygen evolution reaction (OER) reversibly and fast at or near room temperature presents many challenges. The obvious candidates, i.e., precious metal catalysts are prohibitively expensive and hence, not suitable. To cut costs and preserve performance, one study synthesized PtAu nanoparticles (6.8 nm) supported on carbon and reported bifunctional catalytic activity for both the ORR and OER with a high round trip efficiency of 77% for the Li-air system [182]. So there is a need for developing non-precious metal electrocatalysts for the air electrode. In that regard, earth abundant transition-metal oxides offer great incentives. For example, manganese oxides (MnO_x) have been shown to be effective catalyst for oxygen reduction in alkaline air electrodes, and MnOOH was identified as the bifunctional catalytic species [183]. Manganese oxide is also shown to be an effective bifunctional electrocatalyst for the oxygen evolution reaction [184,185]. Likewise, various doped transition-metal oxide compositions of the perovskite structure have also been investigated. Guided by the importance of catalyst *d*-band center as an effective descriptor for the overvoltage behavior for oxygen reduction as suggested earlier [186], a total of 15 A-site and B-site doped-perovskite compositions were explored and the results concluded that the increasing the covalency between the B-site transition metal 3*d* and oxygen 2*p* orbitals helps reduce the overvoltage for the oxygen reduction reaction on these catalysts [187].

View Article Online
DOI: 10.1039/C8EE01419A

Aside from the importance oxygen kinetics, the electrode design and structure must also consider avoiding the detrimental effects of CO_2 exposure in the case of aqueous electrolytes and moisture in the case of nonaqueous, aprotic electrolytes, which can lead to electrolyte degradation, while at the same time, provide a means for selectively introducing oxygen to the electrocatalyst surface of the air electrode.

D.1.2.4.1. Li-Air Batteries

Arguably, the Li-air battery enjoyed the most interest and most intense efforts among the other metal-air systems, mostly due to its huge potential for large-scale energy storage applications. The oxidation of 1 kg of Li releases nearly 11,700 Wh of energy, almost on par with the energy storage capacity of gasoline. On the system level, the Li-air system offers up to 10 times the theoretical energy density of the Li-ion battery. The bulky positive electrode for the intercalation or conversion reaction that is employed in Li-ion batteries is completely eliminated in the Li-air system, and is replaced by a porous oxygen-breathing cathode. The concept of the air electrode is not new, however, and has long been employed in various types of fuel cells and also in Zn-air batteries.

Table 5 summarizes the key reactions at the negative electrode, and compares the energy densities and cell potentials of Li-based battery systems. It is clear that the Li-S and Li-air cells offer significantly higher theoretical energy densities than the Li-ion chemistry. The actual cell-level energy densities depend strongly on the air cathode porosity and electrolyte. For a Li-air cell operating at 2.9-3.1 V with a cathode of 70% porosity, the maximum theoretical cell capacities are estimated to be 435 mAh/g and 509 mAh/ml (or, 1300 Wh/kg and 1520 Wh/L) for alkaline electrolyte, and 378 mAh/g and 452 mAh/ml (1400 Wh/kg and 1680 Wh/L) for acidic electrolyte, while the capacities for the same cathode in nonaqueous electrolyte are nearly two times higher at 940 mAh/g and 950 mAh/ml (or, 2790 Wh/kg and 2800 Wh/L) [188]. This is due to the fact that excess electrolyte is needed to counter the consumption of the aqueous electrolyte during cell operation. However, a practical Li-air battery employing nonaqueous electrolyte has not been developed yet [189]. So, it is not clear if the estimated capacities reported above for Li-air batteries with nonaqueous electrolytes may or may not be realistic. Nevertheless, the potential for achieving exceptionally high energy density batteries offered by the Li-oxygen chemistry is the underlying reason for the intense interest in this system.

Although the concept of Li-air goes back nearly two decades, the first rechargeable Li-air battery was reported in 2006 using a Li metal anode, MnO_2/C cathode, and 1 M $LiPF_6$ dissolved in propylene carbonate nonaqueous electrolyte, and showed that Li_2O_2 is key to reversibility of the battery, and forms on discharge and decomposes back to Li and O_2 during charging [190]. Since then, a variety of Li-air battery designs and materials have been reported, and the progress has been reviewed elsewhere [174,176,189,191-196]. The

View Article Online
DOI: 10.1039/C8EE01419A

cell designs that are currently being pursued are illustrated in Figure 22 and can be grouped under four general classes of electrolytes, namely, aprotic liquids, aqueous electrolytes, solid electrolytes, and the hybrid, or mixed, electrolyte design concept where the cathode is immersed in an aqueous electrolyte while the anode resides in an aprotic electrolyte. Examples of aprotic electrolytes used in these studies include organic carbonates such as ethylene carbonate, propylene carbonate, and dimethyl carbonate, ethers such as tetrahydrofuran (THF) and dioxolane, and esters such as γ-butyrolactone, where soluble Li-salts such as $LiAsF_6$, $LiPF_6$, $LiSO_3CF_3$, or $LiN(SO_2CF_3)_2$ are dissolved.

Both in the aprotic electrolyte and hybrid designs, where the Li-metal anode resides in the aprotic electrolyte compartment, the carbonates employed in the electrolyte reacts with the lithium to form a solid electrolyte interphase (SEI) layer that protects the electrolyte from reacting further with the Li anode. It should be noted, however, that organic carbonate-based nonaqueous electrolytes are later shown to decompose irreversibly at the cathode on discharge into several parasitic products. The microstructural aspects of the SEI layer are discussed earlier (see section D.1.1.3. Solid Electrolyte Interphase). Alternatively, a selectively Li^+-ion conducting but electronically insulating solid state electrolyte membrane either of ceramic or polymer in nature may be coated over the Li anode and serves as the artificial SEI. The natural and artificial SEI concepts are illustrated in Figure 23. A similar SEI layer is also formed naturally on the positive electrode, demonstrating the

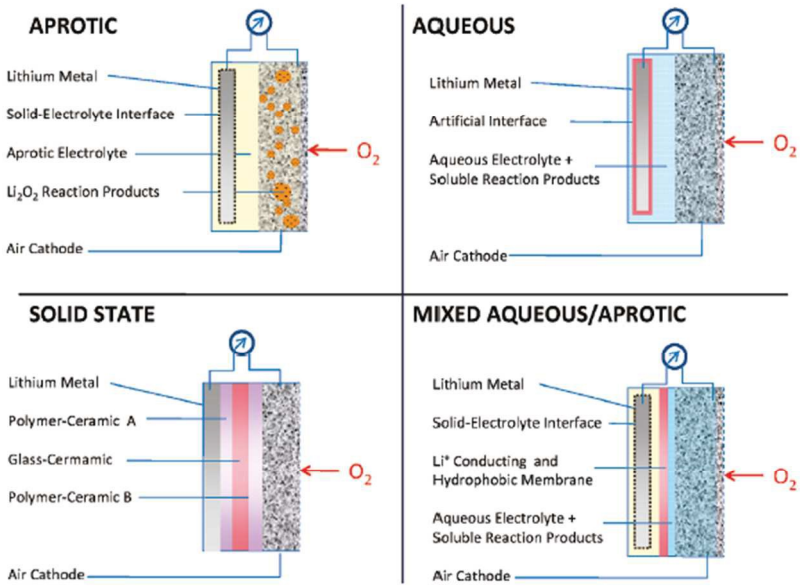

Figure 22. Li-air battery architectures using four different nonaqueous, aqueous, solid state and mixed (or, hybrid) electrolytes. Dashed boundaries indicate the spontaneously formed SEI layers, while artificial SEI layers are indicated by solid lines [174]. Reprinted with permission from (G. Girishkumar, B. McCloskey, A. C. Luntz, S. Swanson, W. Wilcke, Lithium-air battery: Promise and challenges, J. Phys. Chem. Lett. 2010, **1**, 2193-2203). Copyright (2018) American Chemical

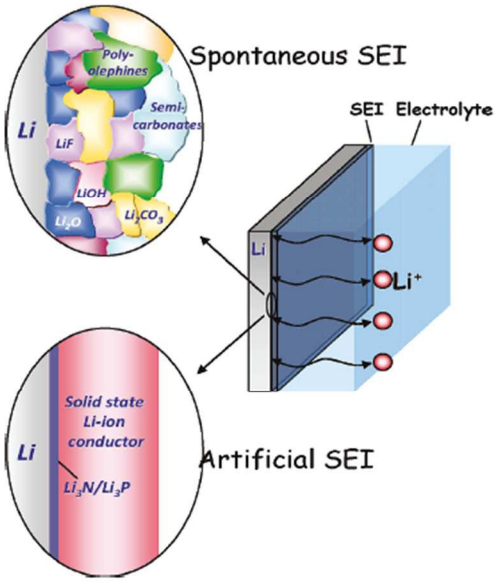

Figure 23. Schematic depiction of the spontaneous and artificial SEI layer on the Li anode of the Li-air battery [174]. Reprinted with permission from (G. Girishkumar, B. McCloskey, A. C. Luntz, S. Swanson, W. Wilcke, Lithium-air battery: Promise and challenges, J. Phys. Chem. Lett. 2010, **1**, 2193-2203). Copyright (2018) American Chemical Society.

View Article Online
DOI: 10.1039/C8EE01419A

importance of understanding and control of the electrode/electrolyte interface.

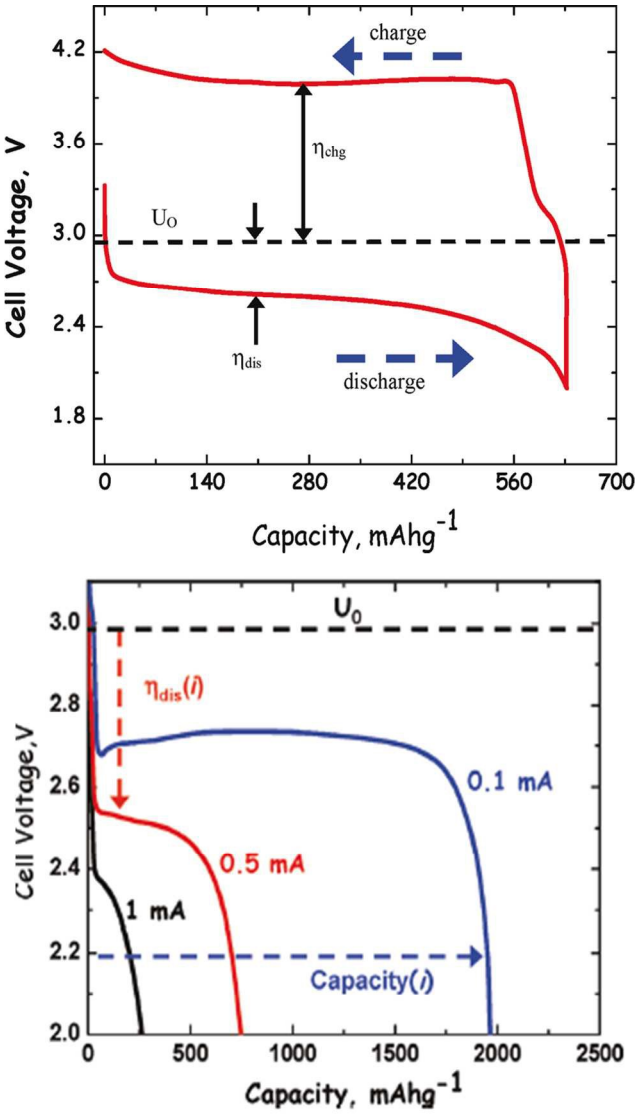

Figure 24. Capacity and cell charge-discharge overvoltages for a rechargeable Li-air battery with active electrode areas of 1.2 cm² in aprotic electrolyte having a theoretical OCV of 2.96 V shown by the dashed line. (Left) Single discharge-charge cycle at a current density of 0.1 mA/cm² with dashed arrows indicating the charge and discharge directions. (Right) Capacity loss as a function of cell current during discharge (per gram of carbon in the cathode) [174]. Reprinted with permission from (G. Girishkumar, B. McCloskey, A. C. Luntz, S. Swanson, W. Wilcke, Lithium-air battery: Promise and challenges, J. Phys. Chem. Lett. 2010, **1**, 2193-2203). Copyright (2018) American Chemical Society.

In the aprotic electrolyte cells, the reaction at the anode during discharge involves oxidization of metallic Li to Li^+ to form Li_2O_2 at the cathode, and also possibly Li_2O, yielding a cell potential of 2.96 V, although the practical discharge potential is typically around 2.7 V, while that for charging is over 4 V as depicted in Figure 24. The large difference between the charge and discharge potentials leads to low round-trip efficiencies around 65%. As Li_2O_2, which is electronically and ionically insulating, builds up and clogs up the pores of the porous positive electrode, it increases polarization losses and is believed to be the controlling factor in governing the end point of discharge. The formation of Li_2O_2 as well as the reduction of oxygen at the cathode requires the presence of a catalyst for activating these reactions. Even though several transition metal oxides including Fe_2O_3, CuO, Co_3O_4 and, in particular MnO_2, are found to be effective catalysts for this purpose [197] discharge overpotentials of 0.3-0.4 V below the theoretical value as well as total cell overpotentials around 1.5 V are typically observed in practical cells between charge and discharge curves (see Figure 24). The status and advances in cathode materials and processes are extensively reviewed elsewhere [198].

The blocking of catalytic sites by the solid Li_2O_2 is a major problem not only on discharge but during the

View Article Online
DOI: 10.1039/C8EE01419A

charging cycle as well, leading to nucleating the reaction products and high polarization losses. Moving to aqueous electrolytes would provide partial solution to the blocking problem at the cathode by producing the soluble LiOH species, but aqueous cells exhibit significantly lower cell voltage and reduced capacity. Indeed, a protective Li-ion conducting solid electrolyte such as LISICON (for "lithium super ion conductor", e.g., $Li_{1+x+y}Al_xTi_{2-x}Si_yP_{3-y}O_{12}$) layer coated on the Li anode is needed to physically separate the water-reactive Li metal anode from the aqueous electrolyte. This innovation opened up attractive opportunities towards realizing aqueous Li-air batteries [199,200]. Similarly, a garnet-type of Li-ion conducting ceramic $Li_{6.4}La_3Zr_{1.4}Ta_{0.6}O_{12}$ (LLZTO) was employed for a Li-air battery, where it was reported to provide a specific capacity of 20,300 mAh/g-C at 80°C and at 20 □A/cm² [201]. The all solid-state Li-air battery concept [115,123] based on ceramic electrolytes eliminates some of the issues related to other battery designs such as safety and fire hazards related to flammable organic based electrolytes, overcharging, and electrical shorting by dendrite formation, and offers compact battery design, but brings along its own technical challenges including insufficient ionic conductivity and narrow stability window of the electrolyte against Li, interfacial charge transfer resistance, mechanical integrity due to volume changes in the electrodes, and poor cycling life. By contrast, use of solid polymer electrolytes provide flexibility to accommodate for volume change in the battery electrodes, but they have narrow windows for electrochemical stability and poor ionic conductivities that usually allow anion transport also. Their polymer matrix is also sensitive to the presence peroxide and superoxide species and deteriorates in the battery environment [202]. Extensive reviews of published work exist on the variety of liquid electrolytes as well as Li-ion conducting ceramic and polymer electrolytes [114,115,195,202].

Although there has been immense interest and activity in Li-air battery research and development, there still remains much work before these systems can offer their inherent potential for commercial applications. Of utmost importance is the lack of mechanistic details of the electrode reactions and battery processes, which are highly impacted by the sensitivity of the Li-O_2 electrochemistry to the nature of the battery electrolyte [196,203-206]. This makes it difficult to compare and rationalize experimental findings on a common platform. In fact, a recent review felt the need to caution discretion in interpreting claims of cycle life and efficiency, and battery performance [189]. Moreover, the results are complicated and affected by parasitic reactions both due to the electrolyte solvent and the impurities in the ambient air that may occur in parallel to the Li-O_2 electrochemistry [196]. For example, the parasitic decomposition reaction of the electrolyte solvent dimethoxyethane is identified as the dominant reaction that is catalyzed by carbon, Pt and MnO_x especially above 3.5 V, while the onset of OER starts slightly above OCV indicating that the evolution reaction did not necessitate electrocatalytic promotion [205]. It is generally assumed that the parasitic reactions in the electrolyte involve the highly reactive intermediates LiO_2, or O_2^- such that most strategies for down-selecting a suitable electrolyte have been based on the electrolyte's stability against these species. Recently, singlet oxygen ($^1O_2$) was detected in the electrolyte above 3.5 V [206]. This highly reactive species forms on the cathode upon Li_2CO_3 oxidation in aprotic electrolytes [207], and has been shown to account for parasitic reaction products of electrolyte decomposition [208]. Superoxide and

View Article Online
DOI: 10.1039/C8EE01419A

peroxide are found to play a role in the formation of the singlet oxygen, which is also promoted by presence of traces of water in the electrolyte. These important findings must be taken into consideration in the design and interpretation of Li-air battery studies to avoid reaching erroneous conclusions regarding the oxidation of Li_2O_2. If indeed the singlet oxygen holds the key to the reversibility of the Li-O_2 electrochemistry, this will require a shift from electrolyte-focused strategies to finding suitable electrolyte additives that can effectively trap or quench singlet oxygen formation [209].

Significant gains have been made in the last few years regarding the mechanistic understanding of electrode processes [194]. The fate of Li_2O_2 during oxygen reduction upon discharge has always been a critical issue. It was shown that whether Li_2O_2 deposits on the cathode as a blocking film or remains in solution as particulates inside the electrolyte is controlled primarily by the solubility of the single electron reaction intermediate LiO_2, which governs the mechanism of cell discharge [210]. As the solubility of cations in aprotic solvents depends on the solvation of the cation by the solvent molecules defined largely by the Gutmann donor number (DN) [211], aprotic solvents with high donor number exhibit stronger solvation. Thus, for electrolytes with high donor number that strongly solvate Li^+, the oxygen reduction reaction to form Li_2O_2 occurs inside the electrolyte, while for electrolytes with low donor numbers, Li_2O_2 forms an electronically blocking film on the cathode, passivating the electrode surface and giving rise to low rates, high polarization losses and poor performance. On the other hand, aprotic solvents with low donor numbers are generally more stable, and hence desirable. This conflict is mitigated by adding a soluble redox mediator to the electrolyte that altered the pathway for the oxygen reduction reaction and allowed the use of a low donor number aprotic solvent such as ether [212].

Despite the potential of achieving extremely high energy densities and improved specific power [213], most Li-air cell designs still suffer from poor specific capacity and power due to their slow kinetics and high polarization losses that result in low current densities. During charging, the large overpotential is reported to be associated with deposition of the solid discharge products of electrolyte decomposition at the oxygen evolving surface or the Li_2O_2/electrolyte interface [214]. They also have stability and materials issues that require further optimization for cost and performance. For example, H_2O contamination in the aprotic electrolyte cells and CO_2 contamination in aqueous cells can lead to parasitic reactions with the Li metal anode or Li_2O_2. Interestingly, addition of trace amounts (500-400 ppm) of water to ethereal electrolytes helped increase discharge capacity by inducing a solution mechanism for the growth of Li_2O_2, while also enhancing parasitic reactions as expected [215]. Li-air batteries also exhibit high charge-discharge overvoltages that result in modest round trip efficiencies around 65% [174]. Moreover, these cells are generally not 100% reversible, as the amount of oxygen consumed during discharge is considerably more than the oxygen evolved during charging [209]. On the high side, 95% retention of capacity after 100 cycles was reported for Au-C nanoparticle cathode with dimethyl sulfoxide electrolyte, providing a capacity of 3,000 mAh/g-C (or 300 mAh/g for carbon-gold combined) [213]. However, most studies report much lower values.

View Article Online
DOI: 10.1039/C8EE01419A

So at the present state of art, they are not particularly suitable for transportation applications for electric vehicles yet, but can be considered for low load stationary storage applications. However, further understanding and advances in battery electrode materials, catalysts and SEI materials can improve kinetics by, for example, nanostructuring, doping, interface engineering, and other strategies. Similarly, exploring ionic liquid electrolytes [55], which offer high ionic conductivity and a wide thermodynamic stability regime up to 5 V, offers exciting possibilities to improve cell stability and kinetics. A recent study using an ionic liquid electrolyte reported a highly reversible charge-discharge cycle, low overvoltage for the charging reaction, and an energy efficiency of 83% for the Li-oxygen battery [216]. Similar advances were made using nonaqueous electrolytes with high stability. Using tetra(ethylene) glycol dimethyl ether-lithium triflate (TEGDME-$LiCF_3SO_3$) electrolyte in a Li-oxygen cell, exceptionally high capacities of up to 5,000 mAh/g-C and rates of 3 A/g-C were reported without the use of a catalyst [217]. At the average discharge voltage of 2.7 V, this capacity value corresponds to a exceptionally high theoretical energy density of 13,500 Wh/kg.

Although much progress has been made, the jury is out on the commercial prospects of the Li-air battery. The technical challenges are far from being resolved completely. The short cycle life of these systems is still a major problem. Optimistically, even a 500 Wh/kg Li-air battery is only 2-3 times better than the commercial Li-ion battery technology. A recent review article discusses the prospects of the Li-air battery in light of the technical challenges and suggests pursuing instead a holistic rather than an issue or problem-based approach as had been the case so far, to address and resolve these problems [193].

D.1.2.4.2. Zn-Air Batteries

Primary Zn-air batteries have been commercially available for more than half a century, and this relatively mature technology has widely been employed in hearing aids, medical devices, telecommunications and other applications. The rechargeable Zn-air battery system, however, is a more recent development, and is considered as one of the contenders for electric vehicle applications provided that the technical challenges related to the Zn-anode and air catalyst can be resolved effectively. Recent reviews provide extensive discussions on the details of this battery system [175,176,218,219].

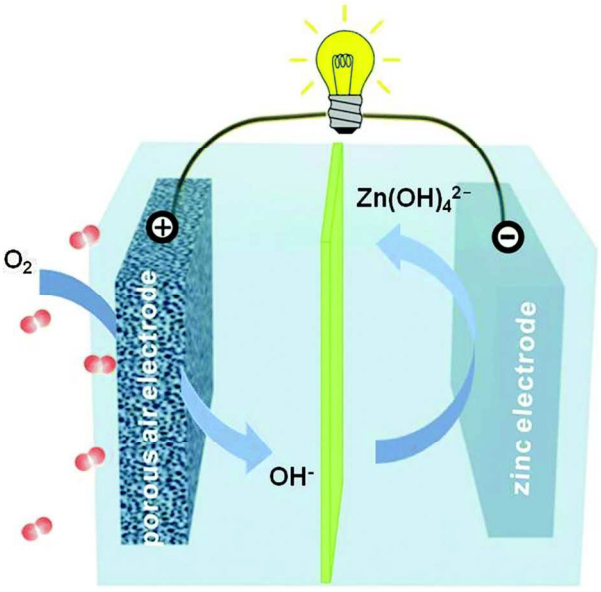

Figure 25. Schematic cell design of the Zn-air battery, indicating the porous air cathode, Zn anode, and the separator. Reproduced from Ref. 175 with permission from The Royal Society of Chemistry.

View Article Online
DOI: 10.1039/C8EE01419A

Zinc is a non-toxic, earth-abundant, and relatively cheap material, and is relatively stable to corrosion in aqueous and alkaline solutions. The Zn-air batteries are light weight and low cost at <$10/kW (> 10 times cheaper than Li-ion batteries), and have high theoretical energy density of 1086 Wh/kg, which is more than 5 times higher than currently available Li-ion batteries on the market. Zn-air system provides the highest energy density among all primary batteries, and as a rechargeable battery offers a competitive, safe and cost-effective alternative to Li-ion batteries. Recently, flexible Zn-air battery architectures have been reported that may provide innovative and attractive opportunities as portable power for mobile and wearable electronics [220,221].

Typical cell design of the Zn-air battery is schematically illustrated in Figure 25. It consists of three major components, a Zn metal negative electrode, the air cathode and an electrochemically inactive but ionically permeable membrane separator to transport the hydroxyl (i.e., OH^-) ions. The Zn anode is generally made of fine powdered Zn metal bound by the aid of binders and other additives to make a porous body. Such Zn foam anode structures can provide high energy densities in the range of 300-500 Wh/kg. Other micro- or nanostructured Zn anodes have also been developed in many different forms including nanospheres, nanofibers, flakes, rods, or sheets in order to increase surface area and battery performance [222]. Indeed, these attempts resulted in increasing the capacity by 40%, energy by 50% and Zn utilization by 30% [172]. The air-breathing electrode, especially for rechargeable Zn-air batteries, is arguably the most critical component of the battery as it greatly impacts battery performance and reversibility. The air electrode for the Zn-air battery typically contains a porous carbon matrix with a gas diffusion layer to provide access for oxygen, and a catalyst deposited on the carbon matrix to promote the oxygen reduction (during discharge) for the primary battery, or a bifunctional catalyst that also promotes the oxygen evolution (during charging) reaction for rechargeability. Finally, the aqueous electrolyte is typically KOH, although other alkaline solutions such as NaOH and LiOH are also employed.

The net electrode reactions during cell discharge can be summarized in the following sequence.

Negative electrode:

$$Zn + 4OH^- = Zn(OH)_4^{-2} + 2e^- \qquad (E^o = -1.25 \text{ V vs NHE}) \qquad (16)$$

$$Zn(OH)_4^{-2} = ZnO + H_2O + 2OH^- \qquad (17)$$

Positive electrode:

$$O_2 + 4e^- + 2H_2O = 4OH^- \qquad (E^o = 0.4 \text{ V vs NHE}) \qquad (18)$$

Overall cell reaction:

$$2Zn + O_2 = 2ZnO \qquad (E^o = 1.65 \text{ V vs NHE}) \qquad (19)$$

Parasitic corrosion reaction at the negative electrode:

View Article Online
DOI: 10.1039/C8EE01419A

$$2Zn + 2H_2O = Zn(OH)_2 + H_2 \quad (20)$$

During discharge, oxygen from air is reduced to hydroxyl ions by reaction (18) and zinc is oxidized in accordance with reaction (16) to the soluble zincate ions (i.e., $Zn(OH)_4^{-2}$) until supersaturation in the alkaline electrolyte is reached, after which the zincate ions decompose to form the insoluble product ZnO via reaction (17). Zincate ions can also cross over through the semipermeable separator membrane to the positive electrode compartment. This migration decreases the capacity of the Zn-air battery. At the same time, the parasitic reaction (20) between Zn and water takes place on the anode to give off hydrogen gas. This corrosion reaction leads to self-discharge and gradual loss of Zn metal resulting in decreased utilization, efficiency and shelf life. Attempts to minimize the impact of self-discharge by the parasitic reaction (20) and slow down the corrosion include alloying Zn with other metals such as Bi, Sn, Pb, Cd, In, Mg, Ni, and Al to stabilize it [223], adding surfactants [224] or organic-based corrosion inhibitors to the electrolyte [225], and using surfaced modification techniques such as coating the Zn surface with conductive polymers (PMMA, polypyrrole, polyaniline) or inorganic films such as lithium boron oxide (i.e., Li_2O-$2B_2O_3$) and Al_2O_3 [226], all of which are aimed to modify and improve the electrochemical behavior of the negative electrode and suppress hydrogen evolution.

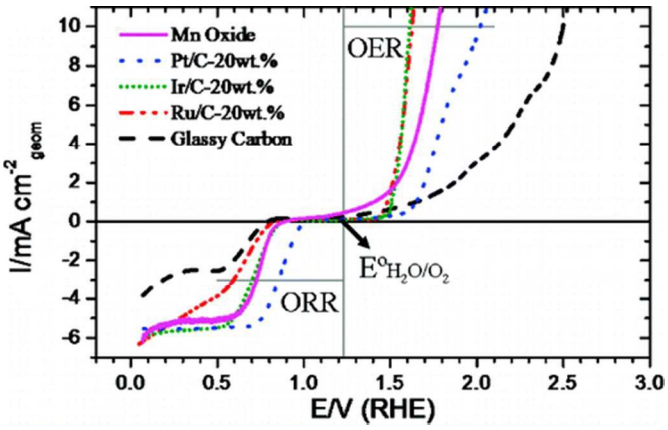

Figure 26. Comparison of the ORR and OER activities of nanostructured MnO_x with the best precious metal catalysts [184]. Reprinted with permission from (Y. Gorlin, T.F. Jaramillo, A bifunctional nonprecious metal catalyst for oxygen reduction and water oxidation, J. Am. Chem. Soc. 2010, **132**, 13612-13614). Copyright (2018) American Chemical Society

The alkaline electrolyte employed in Zn-air batteries is susceptible to CO_2 contamination from the air supply, resulting in the formation of insoluble carbonates at the air electrode and parasitic consumption of the electrolyte, which in turn lowers the electrolyte conductivity and clogs up the pores of the gas diffusion layer on the cathode. Naturally, carbonate formation adversely impacts the performance and service life of the battery. Generally, aqueous NaOH or KOH solutions are employed for Zn-air battery electrolytes. Typically, 7M (or, 30wt%) KOH solution is the electrolyte of choice due to its higher ionic conductivity, higher oxygen diffusion coefficient and lower viscosity, but suffers from higher solubility for CO_2 than NaOH solutions. Recent interest in aprotic electrolytes, especially highly conductive and stable ionic liquids, may provide new opportunities to suppress these parasitic reactions. It should be noted, however, that the air electrode structure has been specifically optimized for aqueous electrolytes, and hence, switching to aprotic electrolytes may require a design change.

View Article Online
DOI: 10.1039/C8EE01419A

The theoretical OCV for the Zn-air battery is 1.65 V vs NHE, as given by the overall cell reaction (19). In practice, however, working cell potentials are typically less than 1.2 V due to activation, ohmic, and concentration polarization losses. In particular, the activation loss at the cathode for ORR largely dominates the overall cell losses, as is also the case for PEM and other types of fuel cells. The ORR reaction occurs at the triple phase boundaries (*tpb*) where the electrolyte, catalyst impregnated carbon current collector and the gas phase (i.e., air) meet. Wettability of the cathode structure is as important as the access of the gas phase to the *tpb* sites. In attempts to improve the activation losses for ORR, both unifunctional (e.g., Pt, Ag, γ-MnO_2, doped-perovskites) and bifunctional (e.g., MnO_2-Co_3O_4, $NiCo_2O_4$, La_2NiO_4) catalysts have been reported [175].

As discussed in some detail (under section D.1.4. Metal-air batteries) above, the air electrode is the most critical component of the Zn-air battery, as reviewed recently elsewhere [219]. Specifically, bifunctionality poses a major challenge to achieving rechargeability of the Zn-air battery. It requires facile catalysis of the ORR during discharge, and fast promotion of the OER during charging. For example, Pt is known to be the best ORR catalyst, but even then, it exhibits significant overpotential due to surface coverage by strongly adsorbed O and OH species, which are found to be stable [186]. Pt also shows poor activity as an OER catalyst due to the coverage of its surface with an oxide layer at the charging potentials in alkaline media. Moreover, Pt is cost-prohibitive to employ widely as a bifunctional electrocatalyst in practical systems. Hence, there has been an intense search for earth-abundant, inexpensive, and high activity bifunctional catalysts for air-breathing electrodes for many electrochemical devices and applications, including all types of metal-air batteries.

Among many electrocatalyst compositions reported in the literature, nanostructured MnO_2, an inexpensive, nonprecious and abundant material, shows promise and its activity was shown to approach to that of precious metal-based catalysts [184]. Figure 26 compares the ORR and OER performance of various precious metal electrocatalysts with manganese oxide. As a bifunctional electrocatalyst for ORR and OER, MnO_x clearly performs favorably with precious metal electrocatalysts Pt, Ir and Ru. Other transition metal electrocatalysts have been investigated also. A carbon-free, mesoporous Ni-Fe nitride (Ni_3FeN) bifunctional electrocatalyst was reported to show excellent activity with low overpotential of 0.355 V measured at 10 mA/cm_2 for OER, and a more positive half-wave potential ($E_{1/2}$) of 0.78 V (vs RHE) for ORR compared to RuO_2 (0.54 V), but smaller than Pt (0.84 V) [227]. Moreover, the Ni_3FeN electrocatalyst showed excellent cycling stability for 310 cycles over 100 hours, with a low voltage-gap of 0.7 V between discharge-charge cycles, and only 3.9% decrease in the round-trip efficiency after 90 cycles. Similarly, 3D carbon- and binder-free air electrodes made of Co_3O_4 nanotubes nominally 300 nm in outside diameter (50 nm inside) and 15 μm in average length were deposited on a stainless steel (SS) mesh current collector and exhibited stable charge and discharge potentials of 2.0 V and 0.98 V, respectively, that remained unchanged after 100 cycles, and retained 94% of the discharge potential and 97% of the charging potential after 600 hours [228]. A similar study employed carbon nanotube-supported CoO and carbon-free NiFe nanoplates as electrocatalytic air-electrodes and

View Article Online
DOI: 10.1039/C8EE01419A

reported a high discharge power density of 265 mW/cm^2 and energy density > 700 Wh/kg for the former composition under primary battery mode, while the combination of the two electrocatalysts in the rechargeable battery mode gave a small charge-discharge polarization of only 0.7 V and good cycling stability during 4- to 20-h long charge-discharge cycles at 20-50 mA/cm^2 [229]. Doped-perovskites are potential candidates but so far, redox stability of these bifunctional catalysts during repeated cycling has not been satisfactory. More work is needed to develop nonprecious metal-based bifunctional ORR-OER catalysts, not only for achieving the full potential of Zn-air batteries, but also for most fuel cell systems.

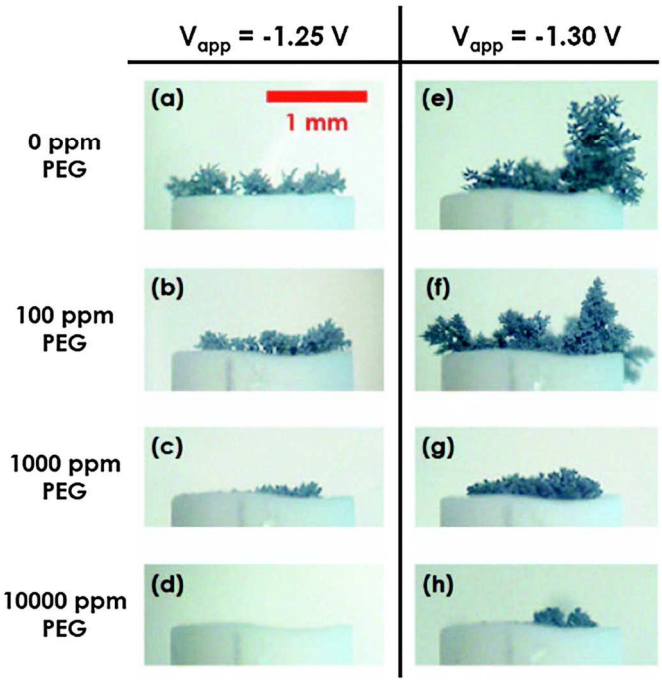

Figure 27. Optical images of dendritic growth of Zn during electrodeposition at two different potentials (vs Ag/AgCl) on a Zn wire from a 0.1 M $ZnCl_2$ electrolyte solution with various concentrations of the additive polyethylene glycol (PEG). Reproduced from Ref. 175 with permission from The Royal Society of Chemistry.

Indeed for the Zn-air battery, the overpotential at the Zn anode is relatively small, while the cathode overpotential for the ORR reaction to form hydroxyl ions via reaction (16) makes up the major portion of the cell polarization losses. During charging, an external potential significantly larger than the OCV needs to be applied to reverse the cell reactions. Typical voltages required for the charging process are 2 V or higher. Because of such losses during charging and discharging, typical round trip efficiencies of Zn-air batteries are less than 60% [175].

Designing an electrically rechargeable Zn-air battery pose many challenges. For long and stable cycle life of Zn-air batteries between charge-discharge cycles, it is imperative to avoid irreversible and morphological changes in all battery components. It is well known, however, the Zn metal in the negative electrode undergoes shape changes and dendritic growth during the dissolution/electrodeposition cycles while discharging and charging, respectively. This is shown in Figure 27, which illustrates the growth of dendrites during electrodeposition of Zn from a $ZnCl_2$ solution.

Dendrite growth is driven by the inherent instability of the solid/liquid interface during electrodeposition. When the current density is sufficiently high to cause depletion of the solute in the electrolyte near the electrode surface, the local gradient of the solute's chemical potential near the surface becomes positive and drives any microscopic surface

View Article Online
DOI: 10.1039/C8EE01419A

feature to grow at a much faster rate than the solid/liquid interface. The roughened surface eventually leads to the formation of dendrites and/or filaments.

The poor cyclability of the Zn-air battery is largely due to the highly soluble zincate ion that is formed via reaction (16) during discharge, and not returning to the same surface site to electrodeposit Zn metal during the charging process. Needless to say, this process is very difficult to control. It causes shape change, and eventually leads to the formation of dendrites. As expected, it degrades cell performance and, in extreme cases, may even lead to electrical shorting of the battery as the dendrites cross over to the positive electrode.

One of the practical solutions to get around the electrical rechargeability problem for Zn-air batteries is mechanical charging. This approach may particularly be attractive for automotive or other transportation applications. Mechanical charging employs the primary Zn-air battery concept and simply involves replacing the Zn-anode assembly mechanically. This simplifies or eliminates many of the technical and materials challenges posed by electrical rechargeability, including using simple unifunctional ORR catalysts, avoiding dendrite and other shape change problems at the negative Zn electrode, and improve battery efficiency. The spent Zn anodes can be recycled in centralized regeneration facilities back to Zn anodes. For transportation applications, this provides attractive opportunities, but require both the distribution of Zn-fuel anodes and collection of spent anodes for regeneration. The vast network of gasoline service stations in place already may be appropriate to serve as Zn anode replacement stations. However, a collection system for spent Zn, and centralized regeneration facilities to recover and regenerate the Zn anodes are required.

D.1.3. Flow Batteries

Flow batteries offer many advantages for electrical energy storage including ease of scaleability, fast response, high power density that can respond to rapid changes in the load, high round-trip efficiency, and long service life for repeated charge-discharge cycles. Arguably, however, the major advantage of redox flow batteries is their ability to decouple rated power from energy storage capacity, unlike batteries where the two are intimately linked. This advantage provides a considerable latitude and flexibility for designing flow battery systems with respect to the specific requirements of particular applications. In flow batteries, while the power output is controlled by the size of the cell stack, the size of the storage tanks that hold the electrolyte solutions for the redox couple defines its energy capacity. These attributes make flow batteries attractive for grid scale stationary energy storage applications for electricity generation and transmission industries. Although there are a large number of flow battery configurations and chemistries, flow batteries can be grouped in two general types of chemistries from a mechanistic point of view, namely, redox flow batteries (RFB) and hybrid flow batteries (HFB). Prominent members of each group are discussed in the next two sections.

View Article Online
DOI: 10.1039/C8EE01419A

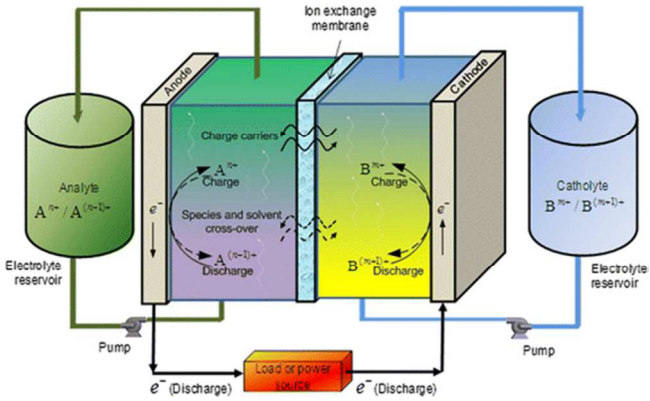

Figure 28. Basic cell design and operating principle of a redox flow battery based on the generalized redox couples A and B [230]. Republished with permission of The Electrochemical Society, from [Advanced redox-flow batteries: A perspective, M. L. Perry, A. Z. Weber, J. Electrochem. Soc. 2016, **163**, A5064-5067]; permission conveyed through Copyright Clearance Center, Inc. (2018).

Typical schematic design and operating principle of RFBs is given in Figure 28, which also illustrates the operating principle of the battery with respect to the generalized redox couples A and B dissolved in appropriate aqueous or organic liquid electrolytes. The electrolytes for the redox couples A and B need not be the same, and in general are different. The anode and cathode compartments (or, anolyte and catholyte, respectively) of the cell is partitioned by an ionically-conducting membrane or a separator that prevents the two electrolytes from mixing with each other, while providing selective transport for the charge carrying ions. The electrochemical process involves pumping of the stored electrolyte from the tank to the flow-through electrodes in the cell stack. During discharge, the chemical energy of the reversible redox couple is converted into electricity, while during charging the reaction is reversed and the redox couple is regenerated from an external power source such as off-peak power from the grid, or preferably from a renewable source. For this reason, RFBs operate like rechargeable batteries in many ways. As the redox couple can be considered as the fuel, however, RFBs also resemble very much the operation of a fuel cell, and hence, are sometimes referred to as "regenerative fuel cells".

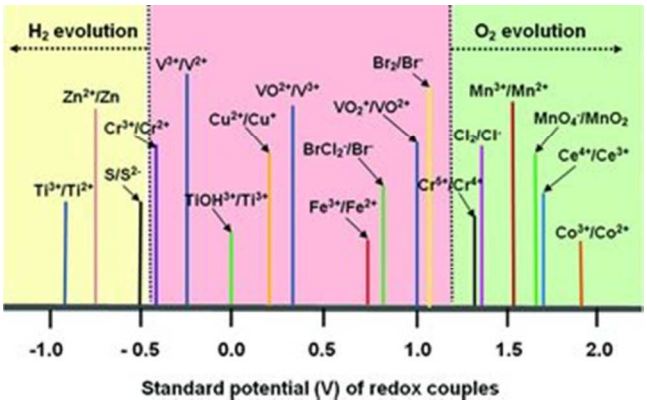

Figure 29. Standard potentials vs SHE of selective redox couples in aqueous electrolytes, also indicating the boundaries for H_2 and O_2 evolution on carbon electrodes [231]. Reprinted from Advanced Functional Materials, vol. 23, W. Wang, Q. Luo, B.Li, X. Wei, L. Li, Z. Yang, Recent progress in redox flow battery research and development, pp. 970-986 (2013), with permission from John Wiley and Sons.

There has been a wide range of organic and inorganic redox chemistries that were explored and reported in the literature since the advent of RFBs in the early 1970's. Most of this work has been reviewed recently [230-235]. More recently, a special focus issue of the Journal of The Electrochemical Society was entirely dedicated to most recent progress in RFBs [236]. Among the multitude of redox couples that were studied or developed for RFBs, the standard potentials for some of the more common ones are provided in

View Article Online
DOI: 10.1039/C8EE01419A

Figure 29 that also indicates the electrolyte stability boundaries, including the overpotentials for hydrogen and oxygen evolution on carbon electrodes. It is clear that the choices for the appropriate redox couples within this window are not unlimited. Also important is the consideration for the solubility of the redox couples in the electrolytes.

Among the various chemistries, the Fe-Cr redox chemistry with an OCV of 1.18 V was the first truly RFB system that was developed for the space program by NASA in the 1970's. Since then, a diverse range of organic- [237] and inorganic-based [230-234,236,238] and even organic-inorganic-based [235,239] RFB chemistries have been reported. The redox cycles, electrochemically active species, and cell potentials of some of the RFB systems are illustrated in Figure 30. The working potentials of RFBs employing non-aqueous electrolytes are nearly twice higher than those with aqueous electrolytes. Among the multitude of inorganic redox chemistries, the all-vanadium-based RFB system has arguably received the most attention. There has also been renewed interest in Zn-Br_2 RFBs, although other interesting chemistries have also been investigated. Recently, an exceptionally high power density was reported for a quinone-bromine flow battery that exhibited 1 W/cm^2 at peak power [239], which is more than 75% higher that the best power reported for the vanadium-based RFBs.

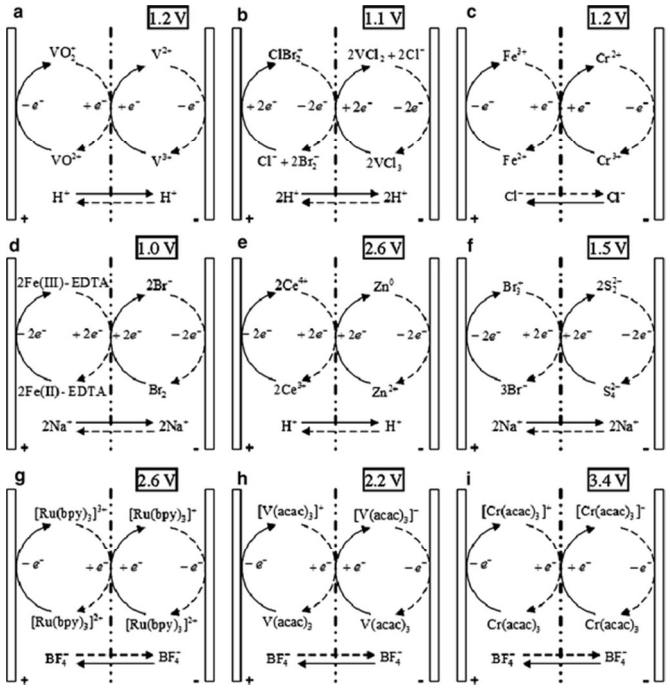

Figure 30. Redox chemistries, transport pathways and working potentials of select RFBs: (a) all vanadium, (b) vanadium/bromine, (c) iron/chromium, (d) Fe-EDTA/bromine, (e) zinc/cerium, (f) bromine/polysulfide, (g) non-aqueous ruthenium/bypyridine, (h) non-aqueous vanadium/acetylacetonate, (i) non-aqueous chromium/acetylacotonate [232]. Reprinted by permission from Springer Nature, A. Z. Weber, M. M. Mench, J. P. Meyers, P. N. Ross, J. T. Gostick, Q.Liu, Redox flow batteries: A review, J. Appl. Electrochem. 2011, **41**, 1137-1164. Copyright (2018).

However, it is important to note that unlike batteries that store energy in its electrodes, whose mass defines its energy capacity while its kinetic and transport properties in turn govern the battery's power output, RFBs store energy in the form of chemical energy of the soluble redox couple held in storage tanks that can easily be scaled up to demand size. As the tank sizes are necessarily large, the volumetric energy densities for RFBs are usually less than 25 Wh/L [231].

Again in contrast to batteries whose electrodes usually undergo morphological, compositional, structural and molar volume changes, and even sometimes phase transformations during each discharge-charge cycle, which place a heavy toll on the mechanical

View Article Online
DOI: 10.1039/C8EE01419A

integrity, stability and useful lifetime of the electrodes, RFB electrodes merely provide an electrochemically active surface for the redox reactions without the burden of physical or chemical changes. This simplifies the operation, and provides high stability, long cycle and service life, low cost, and scaleability for RFBs. Using cell performance criteria as well as cell components and materials costs, a techno-economic study of various electrochemical storage technologies suggested that it may be possible to achieve system level energy storage costs in the range $106-148/kWh for non-specific aqueous RFBs and $114-156/kWh for non-specific nonaqueous RFBs with the right combination of cell and system attributes [227249]. For comparison, this study also suggested the future cost of storage for V^{+2}/V^{+3} RFBs (or, VRB) at $118-207/kWh and Zn/Br_2 RFB at $103-160/kWh, which compare favorably with $193-254/kWh estimated in a similar manner for Li-ion batteries. It should be noted however, that by comparison, the cost target by the U.S. Department of Energy (DOE) is $100/kWh [241], while the system level cost estimates for current VBRs are reported to be around $500-600/kWh [242]. Obviously, there remains much catching up to meet these cost and performance targets for RFB storage.

D.1.3.1. Vanadium Redox Flow Battery

The vanadium redox flow battery (VRB) is arguably the most extensively studied RFB and is a promising technology that was pioneered in the early 1980's. Materials issues and technological challenges for VRBs have been reviewed extensively elsewhere [242-245]. The all-vanadium redox battery was originally proposed as an attempt to minimize or overcome the chemical cross talk across the separator of the different redox species employed in earlier RFB chemistries. By exploiting vanadium's four oxidation states, the same element (i.e., vanadium) can be employed in both the anolyte and the catholyte, which provides major improvements in reducing cross contamination and extending battery life. The anolyte and the catholyte employed in the VRB consist of soluble V^{+2}/V^{+3} and V^{+4}/V^{+5} (in the form of VO^{+2}/VO_2^{+}), respectively. Both electrolytes are made of aqueous 5M H_2SO_4 solution separated by an ionically conducting membrane. The half-cell reactions are given by,

Negative electrode:

$$V^{+3} + e^{-} = V^{+2} \quad (21)$$

Positive electrode:

$$VO^{+2} + H_2O = VO_2^{+} + 2H^{+} + e^{-} \quad (22)$$

Overall cell reaction:

$$VO_2^{+} + V^{+2} + 2H^{+} = VO^{+2} + V^{+3} + H_2O \quad (23)$$

The overall cell reaction (23) proceeds to the right during discharge, and to the left during charging. The standard cell potential corresponding to the overall cell reaction is 1.26 V at room temperature, but the OCV for VRB can be as high as 1.6 V when the anolyte and catholyte contain of ~ 2 M V^{+2} and V^{+5}, respectively. The four different oxidation states

View Article Online
DOI: 10.1039/C8EE01419A

can easily be identified by the color of the solution, such a that the color of the V^{+2}, V^{+3},V^{+4}, and V^{+5} states correspond to violet, green, blue and light yellow, respectively. For these vanadium electrolytes, an energy density of 25 Wh/L was reported [233]. However, the VBR performance is severely impacted by the limited solubility (~ 2 mol/l) and stability of vanadium ions in sulfuric acid solutions. This in turn constrains the operating temperature regime between 10 and 40^{o}C, and requires active heat management, which lowers efficiency. The low fuel utilization due to solubility limitation also impacts performance adversely. When VRB is over-charged, hydrogen and oxygen gas evolution may be observed at the negative and positive electrodes, respectively. But such gas evolution can impact the pH, increase cell resistance by disruption of the liquid electrolyte flow, and oxidation of the carbon at the positive electrode.

Moreover, the highly corrosive nature of V^{+5} makes it necessary to employ more expensive membranes or separators, and containers as well as cell components. Accordingly, the volumetric energy density remains modestly low and does not exceed 25-35 Wh/L, while the round trip efficiencies are around 60-65%. Similarly, the current densities are usually in the 50-80 mA/cm^2 corresponding to a power density below 100 mW/cm^2 [234], which is much lower than provided typically by PEM fuel cells. High cost and price fluctuations of vanadium and its salts makes it difficult to reliably do economic forecasting, which poses challenges for commercial development of VRBs. For these reasons, a multitude of different redox chemistries based on vanadium and others has been reported in aqueous as well as in non-aqueous electrolytes, but many pose challenges [231,233,243,244,246]. For example, the cell membrane (typically Nafion) makes up more than 40% of the total cost of the VRB stack [242]. Advanced hydrocarbon-based cost-effective membranes that display adequate stability and selectivity may have a major impact on stack costs. Vanadium is expensive so another major cost item is the vanadium-based electrolytes. More cost-effective redox chemistries, including organic redox couples, may help improve both VRB economics as well as increasing the cell operating voltage and hence, the energy density. On the other hand, developing nonaqueous electrolytes with sufficient solubility and stability for the redox couple is challenging. Redox chemistries that can undergo multiple-electron transfer reactions and yield high discharge potentials are highly desirable for advancing RFB technology. Achieving high utilization and effective use of large electrode areas in large-scale storage applications, chemical stability, low cell impedance, and long term recycling capability will significantly improve overall performance.

Commercially, VRB units in the kW to MW scale have been developed for nearly two decades for local grid load-levelling and other storage applications in countries like Japan, Australia, and South Africa. Although they have fast cycling properties, the capital cost of $3000-3310/kW for VRBs are still high, which limits their use for specialized applications and niche markets [19]. A recent study estimated the energy storage cost for a 2 kW (30 kWh) all-vanadium RFB unit to be ~ $100/kWh, corresponding to $0.10/kWh for the cost of stored electricity [245]. It should cautioned, however, this estimate is far too optimistic

View Article Online
DOI: 10.1039/C8EE01419A

than more recent estimates of $500-600/kWh for current VRB systems [242], and the projected estimates of $118-207/kWh for the future cost of storage for VRB [240].

D.1.3.2. Zn-Br_2 Flow Battery

The Zn-Br_2 flow battery is actually a hybrid flow battery (HFB), different from the true definition of a redox flow battery system. As in the case of the Zn-air battery, the Zn-Br_2 flow battery also employs Zn metal as the negative electrode, where Zn is dissolved and electrodeposited during discharge and charge cycles, while the Br_2 gas soluble in the electrolyte rather than the ionized redox couple is at the positive electrode, where Br^-/Br_2 conversion takes place. This is schematically illustrated in Figure 31. The half-cell reactions are given below, and provide an open circuit potential of 1.85 V.

Positive electrode:

$$Br_{2(aq)} + 2e^- = 2\ Br^- \quad (24)$$

Negative electrode:

$$Zn = Zn^{+2} + 2e^- \quad (25)$$

Overall cell reaction:

$$Zn + Br_{2(aq)} = Zn^{+2} + 2\ Br^- \quad (26)$$

Although the Zn-Br_2 battery concept was originally proposed more than century ago, research on this battery system was revived by commercial interest in the 1970's and 1980's. More recently, there has been renewed interest propelled in large part by the urgent need for developing large-scale energy storage systems.

Generally, Zn-Br_2 flow batteries offer higher energy densities (65-75 Wh/kg) than traditional redox flow batteries [233]. This is in part due to the use of Zn metal anode that eliminates the need for large volumes of anolyte, otherwise required in RFBs. Also, the OCV for Zn-Br_2 flow batteries is relatively higher than those for RFBs. They have storage efficiencies 70% or higher, with high Coulombic and voltage efficiencies of 90% and 85%, respectively [233]. However, B_2 gas is highly corrosive and hazardous, and leakage of this gas presents public health and environmental problems. It also has the propensity to cross over the membrane separator due to the unsatisfactory selectivity of the membrane for Br^- ions that lowers the working cell potential, contributes to polarization losses, and reduces reactant utilization.

View Article Online
DOI: 10.1039/C8EE01419A

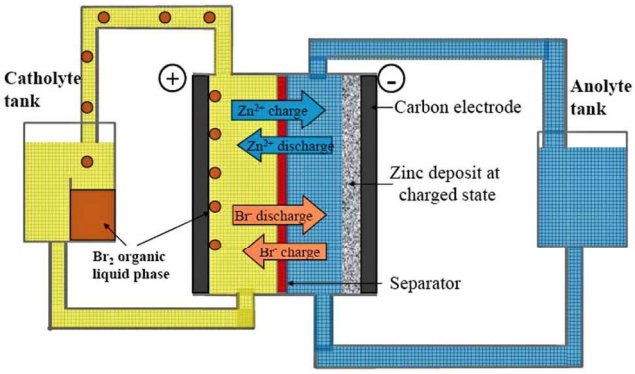

Figure 31. Schematic flow diagram of the Zn-Br_2 flow battery [233]. Republished with permission of The Electrochemical Society, from [Progress in flow battery research and development, M. Skyllas-Kazacos, M. H. Chakrabarti, S. A. Hajimolana, F. S. Mjalli, M. Saleem, J. Electrochem. Soc. 2011, **158**, R55-R79]; permission conveyed through Copyright Clearance Center, Inc. (2018).

Repetitious dissolution and electrodeposition of Zn on the anode during discharge and charge cycles leads to irreversible shape or morphological changes, surface roughening, and dendrite formation (see Figure 27). The latter can eventually lead to electrical shorting. At the same time, a parasitic reaction (20) between Zn and the aqueous electrolyte takes place according to reaction (20) above to give off hydrogen gas. This corrosion reaction leads to gradual loss of Zn metal resulting in decreased cycle life and in particular, zinc utilization, which can be as low as 40% [247].

Furthermore, the slow reduction reaction (24) kinetics of bromine gives rise to polarization losses at the positive electrode, leading to lower voltage efficiency and useful cell potential. High surface area carbon is usually employed to mitigate this loss, but due to gradual consumption of carbon by oxidation, it is difficult to preserve this high surface area over long service life.

Due to these challenging problems, the highly negative reduction potential of the Zn^{+2}/Zn couple makes this half-cell reaction attractive for flow batteries. the performance of Zn-Br_2 flow batteries does not compare favorably with the VRB system, which generally offers better performance. A new single-chamber, membrane-free design concept that eliminates many of the expensive components in the traditional Zn-Br_2 HFB system reported to operate at > 60% energy efficiency for over 1000 cycles, and achieved > 90% Coulombic efficiency with a volumetric energy density of 9 Wh/L at a projected cost of < $100/kWh [248]. The latter figure meets the U.S. DOE cost target for electrical storage systems [241]. Nevertheless, Zn-Br_2 flow batteries are generally limited to small scale storage applications up to 500 kWh [233]. However, the economics of Zn-B_2 batteries are more favorable than VRBs. The average capital cost of $3000-3310/kW for VRBs is significantly more expensive than the capital cost of $1650-2015/kW for Zn-$B_2$ batteries, which competes favorably well with other electric storage and even generation systems [19].

View Article Online
DOI: 10.1039/C8EE01419A

D.2. Supercapacitors

Supercapacitors are in essence electrochemical capacitors that lie between dielectric capacitors and batteries, and store large amounts of charge. Similar to batteries, their design architecture involves two electrodes separated by an electrolyte and a separator to keep the electrodes from shorting. They offer exceptionally high capacitances ranging from several 100s of farads per gram up to 1700 F/g [249], depending on the storage mechanism, choice and microstructure of the electrode materials, and the electrolyte. Although they store charge orders of magnitude more than dielectric capacitors, their relatively low energy density limits their practical use as stand-alone storage systems. However, they can be useful for many high-power but low energy applications. Recent review articles extensively discuss the fundamental aspects of this technology, and report progress in advanced materials for electrodes and electrolytes [249-255].

Power densities of supercapacitors are generally around 10,000 W/kg, which is 2-3 orders of magnitude higher than batteries, but on the other hand, they have much lower energy densities, typically < 5 Wh/kg [252,256]. Most electrochemical storage systems exhibit low power densities, partly due to the long diffusion distances and slow mobility of charge carrying ionic species either in the electrolyte and/or in the electrode material as they rely on bulk diffusion for mass transport. In supercapacitors, however, diffusion lengths are significantly shorter (of the order of nanometers) due to the nature of charge storage mechanism occurring at interfaces or surfaces. Hence, they usually have small time constants, or short response times, that allow them to store and release charge at fast rates. Accordingly, they are suitable for fast power drain applications as they can be discharged and charged in a manner of seconds to minutes, as opposed to batteries that typically take several hours to recharge.

Another important feature of supercapacitors is their exceptionally long cycle life, up to several 100,000 cycles [250,255]. Typically batteries store charge by insertion or chemical reactions at the electrodes, which result in induced strain due to structural or volume changes that limit the battery's cycle life. In supercapacitors, however, charge is stored at interfaces or surfaces and does not involve changes in the microstructure or volume of the electrodes during discharge-charge cycles. Without such strain on the electrodes, these devices have long service and cycle life. These attractive attributes make supercapacitors highly efficient (85-98%) electrical energy storage devices that fill the gap between batteries and conventional capacitors.

Operationally, supercapacitors behave differently from batteries. The cell voltage of an ideal battery remains constant during the charging and discharging operations, while the ratio of the discharge-to-charge potential is a measure of battery's efficiency. In supercapacitors, however, the cell voltage linearly decreases during discharge, and increases linearly during recharging. This is illustrated in Figure 32. As the voltage of the supercapacitor during charge/discharge cycles varies linearly, it is quite easy to assess the state of charge or discharge of the device as indicated by the dashed line in Figure 32, while the flat cell voltage makes this assessment significantly more difficult in the case for

View Article Online
DOI: 10.1039/C8EE01419A

batteries. Moreover, the energy of a battery is proportional to its cell voltage and defined by the area under the flat discharge potential, while the energy of a supercapacitor is proportional to the square of the cell voltage and defined by the area triangular area in Figure 32, which makes it clear why batteries pack more energy. Recently, an interesting question was raised regarding where batteries end and supercapacitors begin especially for nanostructured devices, where the distinction may sometimes be blurred between the discharge behavior of a nanostructured Li-ion battery from an EDL capacitor [257], and suggested cyclic (i.e., sweep) voltammetry to determine characteristic charge-discharge behavior and device identity.

High power-low energy density property of supercapacitors can complement the low power-high energy density characteristics of batteries. In fact, batteries and supercapacitors are considered as power trains for electric vehicles, where useful life and cost are the most critical factors for implementation [257,258]. In addition, suitable combinations of these systems may open up new design opportunities to build battery-supercapacitor hybrid storage systems for high-power – high-energy applications.

There are generally two major classes of supercapacitors, those that rely on charge storage at the electrochemical double layer and those that rely on surface redox reactions, or pseudocapacitance. In both cases, capacitance is proportional to the active surface area. Hence, synthesis routes for producing ultrafine particle size, and nanostructuring methods to fabricate 0D, 1D, 2D, and 3D active materials as well as composite structures have been explored for supercapacitor electrodes [249,251,254].

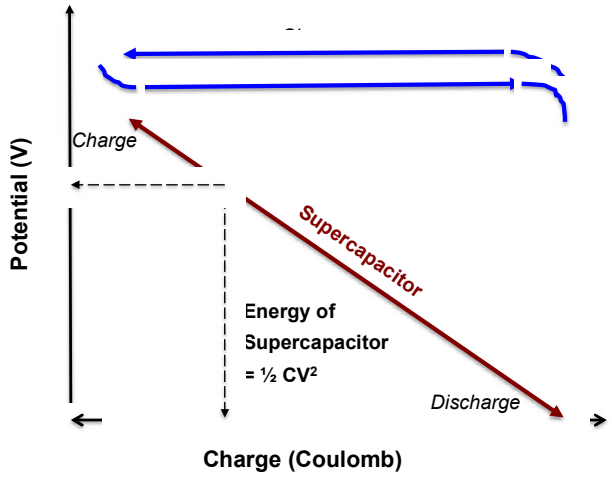

Figure 32. Schematic comparing the characteristic performance of ideal batteries with supercapacitors. Batteries ideally charge and discharge at constant potential plateaus providing energy at fixed voltage, while the potential of supercapacitors decrease with discharge, which makes it easy to assess the state of charge by simply by measuring its voltage, as indicated by the dotted arrows. The energy for the battery is defined by the rectangular shaded area under the discharge plateau, while the striped triangular area defines the energy of the supercapacitor.

Electrochemical double layer (EDL) supercapacitors (also called, ultracapacitors [256]) have been commercially available for more than three decades, first introduced in Japan by Nippon Electric Corporation in early 1980's, and later by others like Panasonic. However, supercapacitors are expensive systems with an estimated cost of $10,000-$20,000/kWh [24,255], which is more than one order of magnitude more expensive than Li-ion batteries. Although cost is a major impediment for large-scale industrial deployment of this technology, supercapacitors are

View Article Online
DOI: 10.1039/C8EE01419A

employed in select military applications or in niche markets such as power supplies for Airbus A380 aircraft emergency doors.

Supercapacitors that are based on the principle of electrochemical double layer capacitance (also called electrostatic supercapacitors) usually involve high surface area activated or nanostructured carbon electrodes connected to metal current collectors. The charge is stored electrostatically in the electrochemical double layer by adsorbed ions at the carbon/electrolyte interface, and the resulting capacitance is usually in the 5-25 $\mu F/cm^2$ range [259]. This type of charge storage does not involve a chemical reaction, and involves only atomic scale distances. Hence, double layer supercapacitors can be charged and discharged in a matter of seconds and have very long cycle lives up to 500,000 cycles with 100% depth of discharge, but suffer from self-discharge with rates up to 14% loss of capacity per month, which limits shelf life [24]. Naturally, the higher the surface area, higher is the total cell capacitance. In this regard, work has been focused on nanostructured carbons with increased surface area such as nanospheres, , nanofibers and nanorods, nanotubes and mesoporous carbons, foams and aerogels that can offer up to 3,000 m^2/g of active surface area. Electronically conducting 2D materials such as graphene and graphene-oxide offer high surface area (up to 2675 m^2/g), high electronic conductivity of $\sim 10^5$ S/cm and high thermal conductivity that make them ideal electrode materials for electrochemical energy storage applications [260]. Indeed, these graphene-based 2D materials provide high specific capacitance up to 528 F/g (at 0.3A/g) for EDL superconductors, and a high energy density of 12.5 Wh/kg and 110 kW/kg power density in graphene-MnO_2 composite pseudocapacitive asymmetric supercapacitor cells [248].

A typical activated carbon-based supercapacitor has a smooth and near-rectangular shaped cyclic voltammetry curve, reminiscent of conventional capacitors. The capacitance, C, of the double layer is adequately defined by Helmholtz as,

$$C = \varepsilon_r \varepsilon_o A/d \quad (27)$$

Here, A is surface area, d is the thickness of the double layer (or, charge separation distance), ε_r and ε_o are the dielectric constants of the electrolyte and of free space, respectively. The energy storage capacity varies with the square of cell potential, V, and is given by,

$$E = \tfrac{1}{2} CV^2 \quad (28)$$

The second category of supercapacitors operates on the principle of pseudocapacitance, which is a Faradaic charge storage mechanism that relies on fast and highly reversible surface or near-surface redox reactions. Many electronically conducting transition metal oxides such as RuO_2, NiO, MnO_2, Fe_2O_3 as well as electronically conducting polymers such as polypyrrole and polyaniline exhibit pseudocapacitive behavior and have been developed for supercapacitor applications [23,249,252]. Capacitances of transition metal oxides are significantly higher than for carbon-based EDL supercapacitors, as they offer multi-electron transfer during the redox reaction. Among these, hydrated RuO_2 is the most studied,

View Article Online
DOI: 10.1039/C8EE01419A

because it has three oxidation states that are accessible within 1.2 V, and offers an energy storage capacity of 240-440 Wh/kg, or a theoretical capacitance of 1200-2200 F/g [254], although others reported much smaller capacitance values ranging from 600 F/g [252], to 750 F/g [33], and 900-1300 F/g [249], highlighting the importance of the thermal history, synthesis method and processing conditions, particle size, and surface area of RuO_2 on its pseudocapacitive behavior.

The charge storage reaction for RuO_2 in acidic electrolytes involves proton insertion (and de-insertion) and can be expressed by,

$$RuO_2 + xH^+ + xe^- = RuO_{2-x}(OH)_x \qquad (0 < x < 2) \qquad (29)$$

Key to the storage mechanism is fast and reversible electron transfer step concurrent with electrosorption of protons on the RuO_2 surface [262]. The continuous change of x between the limits 0 and 2 during proton insertion and extraction processes occurring within the 1.2 V window, provides a capacitive storage mechanism operating within the few nanometers of the surface.

Due to the prohibitively high cost of RuO_2, however, there have been efforts to develop less expensive and abundant materials for surface redox active components for supercapacitor. Among cheaper materials, earth abundant transition metal oxides and other materials ranging from nitrides, carbides, and oxynitrides to polymers have also been reported [249-252], including composite electrodes made by mixing high surface area carbon- or graphene-based materials with redox-active pseudocapacitive materials [254,261]. Inspired by battery design, supercapacitor devices with asymmetric electrode architecture that marry a carbon-based EDL electrode with a redox-based electrode have been reported. A wide range of materials properties and active components, fundamental mechanisms as well as device architectures and performance of such devices have been reviewed elsewhere [23,249,251,252,255,263].

In a similar manner reminiscent of Li-ion batteries, the concept of lithium intercalation chemistry has recently gained interest for pseudocapacitive behavior. These hybrid devices with asymmetric cell design typically employ a high surface area activated or nanostructured carbon as the positive electrode and nanostructured transition metal oxide Li^+ intercalation negative electrode materials such as $Li_4Ti_5O_{12}$, $MnFe_2O_4$, $LiMn_2O_4$ [249,264,265], and mesoporous orthorhombic Nb_2O_5 [266]. This type of asymmetric device architecture exhibits attributes derived both from batteries and supercapacitors and is capable of storing 5-10 times more energy than the all-carbon based EDL type supercapacitors. Furthermore, as the nanostructured negative electrodes experience no strain during discharge/charge cycling, these hybrid asymmetric supercapacitor devices exhibits not only fast rate capability, e.g., charging in 1 minute at 60C rate for Nb_2O_5 [266], but also excellent cycling capability for long service life. Indeed, the $C/Li_4Ti_5O_{12}$ hybrid supercapacitor architecture has maintained more than 95% of its charge after more than 4000 cycles and performed at nearly the same level as a carbon-based EDL supercapacitor [30].

View Article Online
DOI: 10.1039/C8EE01419A

As energy stored in supercapacitors is proportional to square of the potential, electrolytes that offer a wide potential stability window are desirable. In that respect, organic electrolytes and ionic liquids provide a significant advantage. They usually increase the cell potential to exceed 3.5 V, and also significantly widen the typical operating temperature window from -30 – 80°C range to -50 – 100°C in the case of ionic liquid electrolytes [255]. Although most of the early double layer supercapacitors were based on alkaline or acidic aqueous electrolytes, and operated around 1 V, more recent ones employ nonaqueous electrolytes. However, this comes at a price. For example, the typical capacitance of carbon-based materials is 100-300 F/g in aqueous electrolytes, while this value drops to < 150 F/g for organic electrolytes [251], and 20-70 F/g for ionic liquids [23]. There is usually a trade off between operating potential of the supercapacitor and the ionic conductivity of its electrolyte. Organic electrolytes and ionic liquids generally have ionic conductivities that are at least one order of magnitude lower than that for aqueous electrolytes, which results in high equivalent series resistance (ESR) indicative of the large ohmic losses that limit the power and energy densities.

With advances in cost reduction and materials improvements, the exceptional ability of supercapacitors for high power at fast charge-discharge rates is expected to open up wide range of applications that may include short duration peak power boost on the grid, peak backup for uninterrupted power sources (UPS), or for storing energy during regenerative braking in transportation vehicles. They can also be combined with batteries to complement the strengths of the two storage systems for improved electrical storage. Such hybrid systems offer the collective advantages of the two systems, increasing cycle life especially when used with Li-ion batteries. However, the costs of both Li-ion batteries (> $270/kWh) and supercapacitors ($10,000-$20,000/kWh) are currently too high for large-scale deployment for utility grid storage applications.

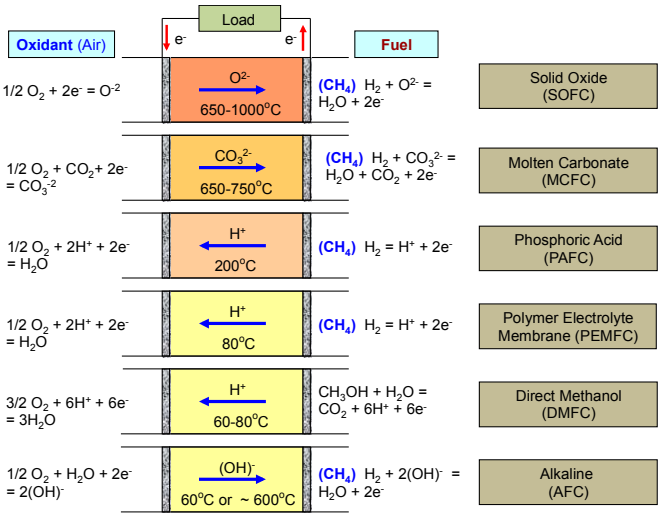

Figure 33. Schematic depiction of the operating details such as net electrode reactions, transporting ions, and temperature regimes of major types of fuels cells [6]. Reprinted with permission from (T.M. Gür, Comprehensive Review of Methane Conversion in Solid Oxide Fuel Cells: Prospects for Efficient Electricity Generation from Natural Gas, Progress in Energy and Combustion Science, 2016, **54**, 1-64). Copyright (2018) American Chemical Society.

View Article Online
DOI: 10.1039/C8EE01419A

D.3. Regenerative fuel cells

Fuel cells are essentially electrochemical engines that provide inherently efficient conversion of the chemical energy of fuels directly into electrical energy. They are environmentally friendly and operate under isothermal conditions without generating noise.

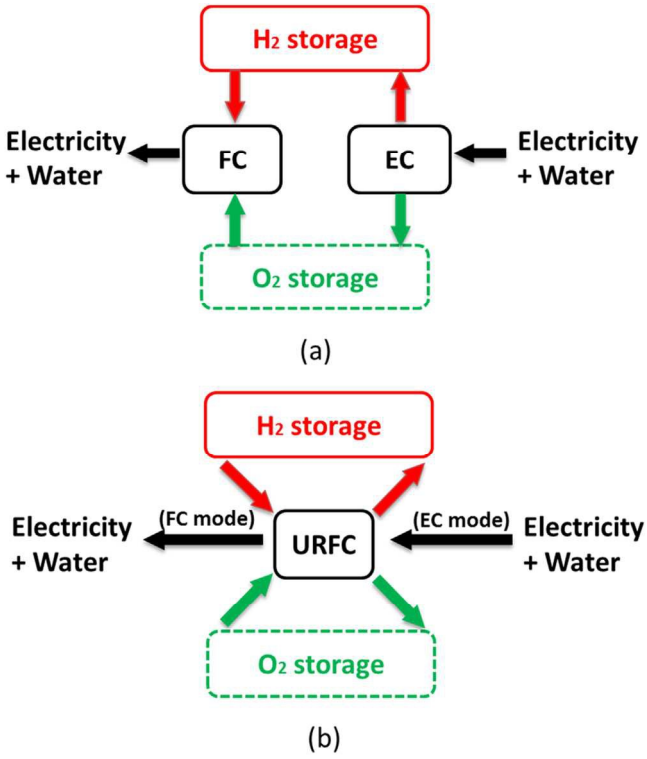

Figure 34. Electrochemical energy storage systems (a) electrolyzer-fuel cell combination, and (b) regenerative fuel cell (also called, unitize regenerative fuel cell (URFC) in the PEMFC community) [291]. Reprinted from Renewable and Sustainable Energy Reviews, vol. 65, Y. Wang, D.Y.C. Leung, J. Xuan, H. Wang, A review of unitized regenerative fuel cell technologies, part A: Unitized regenerative proton exchange membrane fuel cells, pp. 961-977 (2016), with permission from Elsevier.

There are many types of fuel cells operating at different temperature regimes, and employing different types of liquid or solid electrolytes. They employ different sets of cell components including electrolytes or separators, electrocatalyst and/or electrodes, current collectors, and seals. Figure 33 illustrates some of the more prominent types of fuel cells and indicates the corresponding net electrode reactions, ionic species transported across the electrolytes, and their operating temperature regimes. The fuel cell types in the figure are arranged from low to high with respect to their typical operating temperatures. Low temperature fuel cells including aqueous alkaline (AFC) and polymer exchange membrane fuel cell (PEMFC) generally employ hydrogen as fuel. Bulk of the global hydrogen production is based on steam reforming of methane, which yields a hydrogen stream with small quantities of CO even after extensive separation and purification. Unfortunately, the Pt catalyst at the PEMFC anode is susceptible to CO poisoning leading to degradation of cell performance even at trace levels around several ppm. Also, only precious metals such as Pt are the only catalysts that have sufficient activity, but add considerable cost to PEMFCs.

Due to its high operating temperature, by contrast, solid oxide fuel cells (SOFC) employ non-precious metal and/or earth-abundant oxide electrocatalysts and offer other important advantages [29,267] including fuel flexibility [268]. Indeed, SOFC configurations can

View Article Online
DOI: 10.1039/C8EE01419A

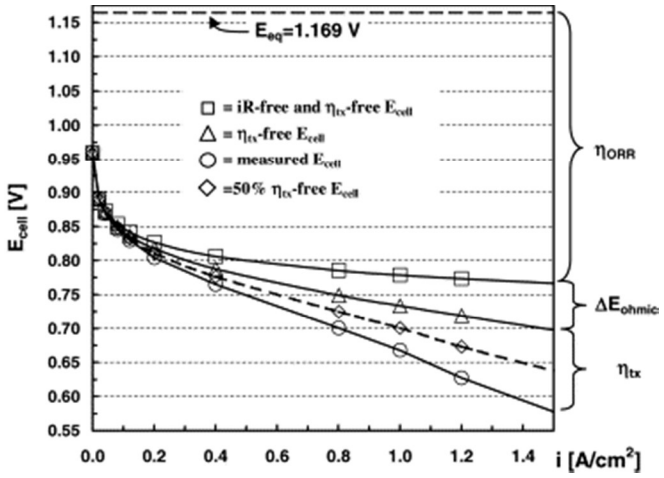

Figure 35. Electrochemical performance of a H_2/O_2 PEMFC at 80°C with 50wt%Pt/C (04/0.4 mgPt/cm^2) catalyst-loading and stoichiometric flows of H_2 and O_2. The figure shows the partitioning of individual voltage losses η_{tx} for mass transport, and η_{ORR} for the oxygen reduction reaction, which makes up more than half of the total voltage losses of the cell [286]. Reprinted from Applied Catalysis B: Environment, vol. 56, H.A. Gasteiger, S.S. Kocha, B. Sompalli, F.T. Wagner, Activity benchmarks and requirements for Pt, Pt-alloy, and non-Pt oxygen reduction catalysts for PEMFCs, pp. 9035 (2005), with permission from Elsevier.

successfully utilize and convert gaseous [269-272] and liquid hydrocarbons [273-275], as well as solid fuels [5] including carbon [276-278], biomass, [279], and coal [280] into electricity. Furthermore, CO, which is an undesirable impurity for PEMFCs is in fact a viable fuel for power generation in SOFCs as recently demonstrated in a 1 kW planar stack [281]. However, not all fuel cell systems depicted in Figure 33 can be employed in the electrolysis mode with relative ease or without major cell modification. Only aqueous alkaline (AFC), aqueous polymer exchange membrane (PEMFC), and solid oxide fuel cells (SOFC) have been investigated for regenerative operation for storage purposes [282,283].

There is lack of unanimous agreement in the literature on a common terminology to describe the fuel cell systems that can switch their operating mode from electrolyzer to fuel cell and back in the same cell, without modifications. The term “reversible fuel cells” seems to be used more than others especially in the SOFC literature, but the term “regenerative” has also been employed. Yet others especially in the PEMFC community use the terminology in quite a different context such that the regenerative fuel cell refers to a pair of discrete electrolyzer and fuel cell units, where the fuel, e.g., H_2, and the oxidant O_2 are first produced in the electrolyzer, stored in tanks, and then recombined in a fuel cell to generate electricity when needed, while calling the single cell configuration that can switch without modification between electrolyzer and fuel cell modes a “unitized” regenerative fuel cell [283-285]. The latter two concepts are schematically illustrated in Figure 34. However, labelling separate electrolyzer-fuel cell configurations as “regenerative” may be misleading. More appropriately, this is merely a coupled electrolyzer-fuel cell configuration, and in the view of this author, is unfitting to describe the intended functionality of a bimodal electrolyzer/fuel cell operation. As for the terminology “reversible fuel cells”, reversibility implies well-defined connotations in both kinetics and thermodynamics, and hence, it too may be unsuitable to describe this system. Hence, the term “regenerative fuel cells” is preferred in this article and is used in the context of operating the very same cell sequentially in electrolyzer or fuel cell modes without modifications, as indicated in Figure 34(b).

View Article Online
DOI: 10.1039/C8EE01419A

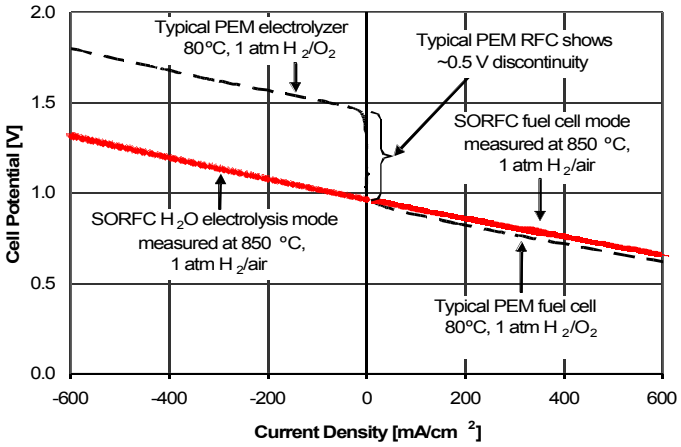

Figure 36. Comparative performance of regenerative SOFC versus PEMFC, where the latter exhibits a large activation loss around OCV [292]. Republished with permission of The Electrochemical Society, from [Applications and markets for solid oxide regenerative fuel cells, K.R. Sridhar, J. McElroy, F. Mitlitsky, V. Venkataraman, M.C. Williams, Electrochem. Soc. Proceedings, vol. 2005-07, pp. 295-305 (2005)]; permission conveyed through Copyright Clearance Center, Inc. (2018).

Low temperature aqueous fuel cell configurations such as alkaline and PEMFC have been successfully transformed into electrolyzer configurations for distributed production of hydrogen via splitting of water, their kinetic reversibility for regenerative operation mode is poor due to large activation overvoltage and scarcity of cost-effective dual action catalysts for the oxygen and hydrogen electrodes. In the acidic environment of the PEMFC, the catalytic electrodes have to perform the difficult tasks of both the water oxidation and oxygen reduction reactions (ORR) at the oxygen electrode, and hydrogen reduction and hydrogen evolution reactions (HER) at the hydrogen electrode. To activate these reactions selectively and at sufficiently fast rates, highly selective specialized bifunctional catalysts are needed. Only precious metals and their oxides such as Pt, RuO_2, $PtIrO_2$, $PtRuO_2$ have shown satisfactory rates, but still exhibit appreciable overvoltages for these reactions that result in considerable irreversibility. For example, Pt is the preferred electrocatalyst for ORR even though the relatively sluggish ORR kinetics on Pt accounts for nearly 50% of the total cell voltage loss in PEMFCs [286]. This is shown in Figure 35. Furthermore, Pt also lacks sufficient activity for OER [287]. The oxides of Ir and Ru exhibit the lowest overvoltages for OER among other electrocatalysts, but they are not suitable for ORR. Similarly for the hydrogen electrode, Pt is the preferred catalysts and economically not suitable for large-scale applications. Nevertheless, no cheaper alternatives have been found yet to compete with the performance of precious metal-based catalysts for regenerative PEMFC electrodes. The prohibitively expensive cost of these catalysts presents a barrier for large-scale energy storage applications.

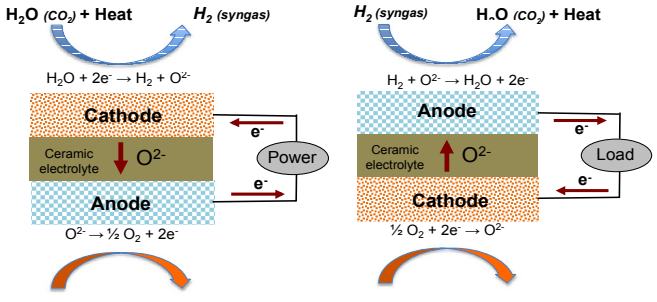

Figure 37. Schematic depiction of the general concept of a regenerative, or, "reversible" oxide-ion conducting solid oxide fuel cell operating on the H_2/H_2O couple.

In alkaline fuel cells, the bifunctional catalyst need to effectively drive the ORR and OER at the oxygen electrode, and hydrogen oxidation (HOR) and water reduction (i.e., hydrogen evolution (HER)) reactions at the hydrogen electrode. Unlike PEMFC, the alkaline environment of AFCs offer catalyst

View Article Online
DOI: 10.1039/C8EE01419A

alternatives other than Pt, which is nearly two orders of magnitude less active as hydrogen electrocatalyst in alkaline than in acidic environments [288,289]. Various metal hydride compositions have been investigated for hydrogen electrodes in alkaline fuel cells, where they serve not only as the catalyst to promote HOR and HER, but also function as medium for hydrogen storage [290]. For the oxygen electrode, various transition metal oxides including perovskites, spinels and MnO_x have been reported. The detailed reviews of electrode materials and cell performance of low temperature regenerative cells are provided elsewhere [282,283,285,291].

The importance of operating temperature is highlighted in Figure 36, which compares the nearly reversible SOFC-based regenerative operation at 850°C with the large irreversibility of PEM-based regenerative fuel cell operation at 80°C, where the predominant activation loss around the open circuit voltage (OCV) for the PEM fuel cell/electrolyzer operation is evident with a discontinuous drop of nearly 0.5 V. In the case for solid oxide based electrolyzer (SOEC), however, the polarization behavior of the solid oxide-based regenerative cell is continuous and smooth across the OCV indicating sufficiently high kinetic reversibility for steam reduction and hydrogen oxidation reactions at elevated temperatures [292,293].

Accordingly, solid oxide fuel cells (SOFC) are offer attractive opportunities for regenerative operation, where off-peak electricity can be employed to store the excess energy for electrolytic production of useful fuels, e.g., hydrogen, which can then be oxidized in the fuel cell mode to generate electricity when demand increases. Many of the regenerative SOFC systems and related materials have been reviewed recently [294-296]. It should be noted that kinetic reversibility has been limited to the H_2O-H_2 couple only. Compared to liquid fuels such as ethanol (21,200 MJ/m^3) and gasoline (34,560 MJ/m^3) [297], hydrogen has quite a low volumetric energy density of 11 MJ/m^3. Hence, it is highly desirable to achieve reversible cell operation cycling between a liquid hydrocarbon fuel and its oxidation products CO_2 and H_2O in the same regenerative SOFC. But this is yet to be demonstrated. Thermodynamic constraints imposed by the high operating temperatures of regenerative SOFCs, and the technical challenges posed by kinetics and selectivity issues have hampered progress to achieve electrosynthesis of high value added liquid fuels.

The general concept of regenerative SOFCs has been around for several decades [298] and is schematically illustrated in Figure 37, which shows how the symmetrical SOFC can both store electrical energy in the form of hydrogen fuel by splitting steam, and then re-utilize the hydrogen to generate electricity by oxidizing it back to steam. The details of this high temperature steam electrolysis process have been extensively studied and reported recently, using oxide-ion conducting SOFC configurations [294,295,299-302], and also using protonically conducting SOFC configurations [303-305].

As expected, this scheme demands stringent requirements for the catalytic electrodes, which must serve both the dual function of anode and cathode depending on whether it is the storage or generation cycle. For example, the electrode in the storage cycle serves a cathode to reduce steam into hydrogen, while in the generation cycle it serves as the anode

View Article Online
DOI: 10.1039/C8EE01419A

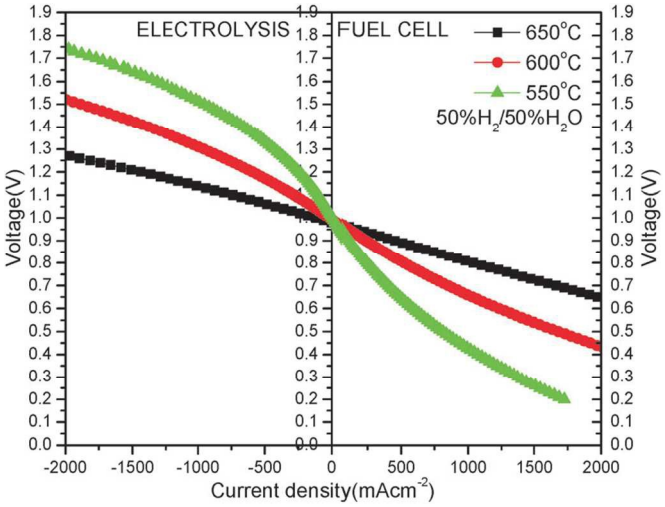

Figure 38. Performance of a regenerative SOFC operating between 550 and 650°C. Reproduced from Ref. 307 with permission from The Royal Society of Chemistry.

to oxidize hydrogen back to steam. As expected, this requires that the electrode material possess high catalytic activity for both steam reduction and hydrogen oxidation reactions. Moreover, it has to exhibit exceptional redox stability over a wide range from reducing to oxidizing environments at these elevated temperatures. So there have been intense efforts to achieve high redox stability in catalytic electrodes for regenerative SOFCs, such as the composition $La_{0.75}Sr_{0.25}Cr_{0.5}Mn_{0.5}O_3$ (LSCM) [293,306]. Indeed, kinetically highly reversible fuel cell behavior that remains stable over several cycles and 120 hours has been reported for (LSCM) [293]. Other perovskite-based electrodes for reversible operation have been explored for regenerative SOFCs, and reviewed elsewhere [295,307]. There have also been attempts to both lower the operating temperature of these systems [308-310]. The performance of a reduced temperature regenerative SOFC cell shown in Figure 38 features a doped-perovskite ($La_{0.9}Sr_{0.1}Ga_{0.8}Mg_{0.2}O_3$ (LSGM)) electrolyte with Gd-doped ceria (GDC) modified catalytic electrodes, and exhibits a smooth and continuous transition between the power generation (fuel cell) and electrolysis (storage) modes across the OCV and a low value of area specific resistance (ASR) of 0.18 ohm.cm^2 at 650°C [307].

Various storage systems based on regenerative SOFCs have been proposed [296,299,307]. These storage schemes involve H_2O, CH_4, or CO_2 chemistries, and explore combining a regenerative SOFC with solar, wind or other renewable sources. One of these storage concepts involves integration of a 250 MW SOFC stack with underground storage of CO_2 and CH_4 having a total capacity equivalent to 500 GWh of storage. The modeling study of this system concept predicted 70% round-trip system efficiency and electricity storage costs of $0.03/kWh [307].

A similar concept was proposed for a 100 kW regenerative SOFC with 800 kWh of storage capacity in the form of fuels [296]. Assuming 600°C and 1 atm pressure, 0.2 A/cm^2 current density, a H/C ratio of 9.9, and a fuel utilization of 65%, this modeling study predicted round-trip conversion efficiency of 74% and storage density of 90 kWh/m^3 (or, 324 MJ/m^3), resulting in a capital cost of $2.33-3.17/kWh for storage. The encouraging results may warrant exploring further into similar storage schemes that incorporate regenerative fuel cells with intermittent renewable energy sources.

View Article Online
DOI: 10.1039/C8EE01419A

However, despite their immense potential for large-scale energy storage, major progress in regenerative SOFCs has been slow due to degradation issues largely related to materials instability, kinetic reversibility, and microstructural and architectural integrity of the cells [311]. Delamination is the most common problem observed at the oxygen electrode/electrolyte interface at high current densities due to build up of high internal pressures during oxygen discharge. Also, oxygen evolution at this interface may often lead to chemical changes to form secondary phases increasing ohmic losses. Hence interface engineering and control is important for stable cell operation, and several different approaches to improve stability and cell performance have been suggested including impregnation, exsolution, and impurity control [312]. Interestingly, it was recently reported that microstructural degradation at the oxygen electrode, which is dominant during electrolysis in particular, could be eliminated by reversibly cycling regenerative SOFCs between fuel cell and electrolysis modes [301]. Reversible cycling seems to slow down microstructural changes and mitigate the build up of high internal pressures at the interface and restore sintering. However, detailed mechanisms of degradation (and recovery) processes in these systems are not well understood. Accordingly, the mechanical integrity, chemical stability and microstructure of regenerative SOFC interfaces are important considerations that require further research for development.

E. Chemical Energy Storage

Our addiction to fossil fuels is no accident, because energy storage in chemical fuels offers the highest energy density, most convenient, cost-effective, scalable, flexible, and highly portable way to store and transport large amounts of energy in the chemical bonds of fuels. The comparative numbers for the gravimetric and volumetric energy densities of fuels provided in Table 6 clearly demonstrate the superiority of chemical storage over electrochemical storage. In this regard, converting excess electrical output or renewable electricity into chemical fuels, which can then be converted efficiently back to electricity naturally holds much merit. However, many fuels as such including hydrogen and ammonia as such do not exist in nature in large quantities, so need to be synthesized. This is of course a thermodynamically uphill process and is quite energy intensive.

The starting chemicals to synthesize most fuels are typically hydrogen- and carbon-containing species, and more commonly H_2 (H_2O) and CO. There are multiple synthesis routes to produce high energy density chemical fuels. Examples include electro-reduction of CO_2 to fuels, photoelectrochemical reduction of CO_2 to fuels, solar thermochemical reduction of CO_2 to fuels, and partial oxidation of methane to syngas or coal gasification to syngas, which can then be converted to higher hydrocarbon fuels via Fischer-Tropsch (F-T) process. Some of these routes e.g., gasification to F-T, are mature technologies that have been in use commercially for decades, while others like photoelectrochemical and

View Article Online
DOI: 10.1039/C8EE01419A

electrochemical reduction of CO_2 to fuels are under development. Regardless, however, all these process schemes involve carbon-containing species that contribute to global carbon emissions, and fail to provide carbon-free solutions for the electrical energy enterprise. Accordingly, carbon-containing synthesis schemes are left outside the scope of this article. Also, photocatalytic splitting of water to produce hydrogen is also not reviewed here.

Table 6. Gravimetric and volumetric energy densities of liquid fuels compared with select storage systems. Most values are taken from ref. # 297.

Fuel	Gravimetric Energy Density (Wh/kg)	Volumetric Energy Density (Wh/L)
Gasoline	12,330	9.060
Diesel	12,700	10,700
Propane	12,870	7,490
Butane	12,700	7,190
Ethanol	7,490	5,890
Methanol	5,620	4,470
Liq. Hydrogen	33,570	2,200
Liq. Ammonia	5,170	3,750
Batteries:		
*Li-ion battery**	*150-210*	*450*
*Ni-metal hydride**	*70*	*220*
*Zn-air battery**	*300*	*240*
* Practical values		

Chemical storage topics covered in this section focuses on converting excess or off-peak electrical energy preferably from renewable resources such as solar and wind into environmentally benign, carbon-free, high energy density transportable fuels via electrosynthesis. In this regard, electrochemical production of hydrogen and ammonia are presented and reviewed below. It is important to note that chemical energy storage in hydrogen and ammonia also offers environmentally benign solutions towards decarbonization of the global energy systems. The proponents of hydrogen see this energy carrier on which to build a carbon-free energy economy [313,314], while opponents of hydrogen-based economy have long argued that the heavy energy and carbon emission penalties paid during hydrogen production, the difficulties in handling and transporting hydrogen, and lack of earth-abundant cost-effective materials that can provide >6.5wt% H_2 for long term storage are major barriers for practical adoption and implementation at a wider scale. Ammonia as an environmentally benign energy carrier has recently gained interest as a viable option for chemical storage, but electrosynthesis of this chemical faces similar obstacles to be overcome.

E.1. Chemical Storage in Hydrogen

Exceptionally high gravimetric energy density of hydrogen makes it an ideal candidate for chemical storage and a carbon-free energy carrier. As hydrogen does not occur naturally, it is produced largely from natural gas. More than 75% of the industrial hydrogen production in the world is via steam reforming of methane, which is a highly efficient (60-85%) and mature technology but is cost effective only when it is produced centrally and at large scale. This process is also highly energy intensive and consumes nearly 2% of the world's energy output. Most of the industrially produced hydrogen is utilized on-site (i.e.,

View Article Online
DOI: 10.1039/C8EE01419A

captive hydrogen) for chemical, catalytic and petrochemical processes. A small fraction is supplied to the market (i.e., merchant hydrogen) for other industrial processes or uses.

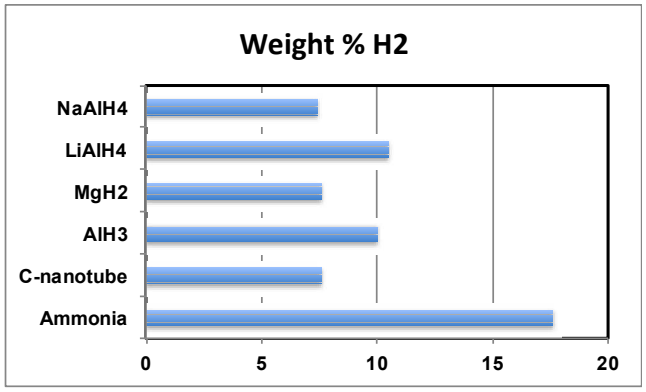

Figure 39. Gravimetric storage capacities of various materials given in weight percent hydrogen.

Hydrogen is an environmentally benign energy carrier with the highest gravimetric energy density of 142 MJ (HHV)/kg among the common liquid fuels (see Table 6), but it has also one of the lowest volumetric energy densities of about 10 MJ/l in its gaseous form at atmospheric pressure and room temperature. The latter property poses challenges in wider utilization of hydrogen for portable or mobile power generation applications, including transportation. Although there have been intense research activity in the last two decades to develop effective storage medium or materials, cost effective solutions for extended use capacity has been elusive. Among the options, mechanical storage via cryogenic liquefaction as well as compression are mature technologies but both have practical challenges including safety, cost, and energy penalties [315]. For example, a pressurized hydrogen tank offers a system energy density of less than 2 MJ/l at 350 bar and 3.4 MJ/l at 700 bar. Compared to other fuels listed in Table 6, the energy density of pressurized tank storage is quite limited.

Storing hydrogen in solids via chemical or physical routes has many advantages, but also often have low gravimetric capacities that add extra weight to the mobile application. Many also have either undesirable thermodynamics that limit reversibility of storing and releasing hydrogen and/or slow kinetics that lead to long charge and/or discharge times. Many storage materials or methods have been under development but none has reached commercial maturity.

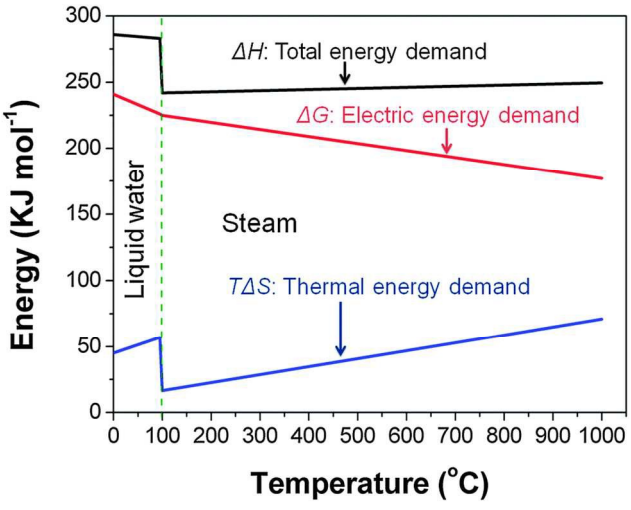

Figure 40. Energy demands for water electrolysis as a function of temperature. Reproduced from Ref. 303 with permission from The Royal Society of Chemistry.

Many materials can store hydrogen by absorption or hydride formation (e.g., Pd and its alloys), adsorption (e.g., carbon nanostructures), or chemical reactions (e.g., MgH_2, $NaBH_4$, alanates). An in-depth review of hydrogen storage materials and technologies fall outside the scope of the present article. The

View Article Online
DOI: 10.1039/C8EE01419A

interested reader is referred to in-depth reviews published in the literature [316-318]. Gravimetric capacities of various materials for hydrogen storage are provided in Figure 39 for comparison purposes.

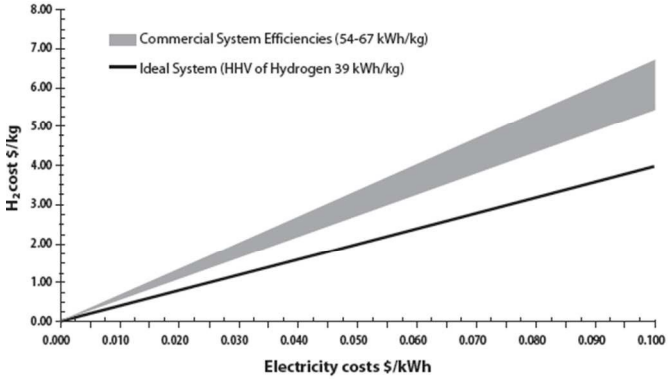

Figure 41. Cost of hydrogen via electrolysis varies linearly with cost of electricity, according to a 2004 NREL study [319].

Storage and transportation of hydrogen is costly and inefficient. That is why distributed generation may be critically important for an effective carbon-free energy economy for the future. In this regard, water electrolysis driven by renewable electricity presents attractive opportunities for local production of hydrogen.

Currently, low temperature electrolysis of water is the only commercial technology available for distributed generation of hydrogen. Thermodynamically, water splitting is an uphill process and hence, is high energy intensive. It needs to overcome the thermodynamic barrier as presented in Figure 40, which indicates the thermal ($T\Delta S$), electrical (ΔG), and total energy (ΔH) demands to water (and steam) electrolysis as a function of temperature. For this, an external bias that opposes and is greater than the theroetical open circuit voltage (1.23 V at 298K) must be applied to the cell in order to break the O-H bonds in water, permitting the formation of the H-H bond. A large fraction of the electricity used in conventional water electrolyzers is consumed merely to overcome this potential barrier, which reduces efficiency. Dissociation of water to hydrogen is also an endothermic reaction with ΔH = + 286 kJ/mol at room tempearture, which corresponds to the thermoneutral potential of 1.48 V. Clearly, this is greater than the theoretical cell potential of 1.23 V. So if no external heat source is employed, the applied potential required to split water has to be greater than 1.48 V. In practice the externally imposed potential is much higher, up to 2.0 V or above, depending on the type of water electrolyzer and the electrolyte used.

The rate of hydrogen production is linearly related to the amount of current supplied to the electrolytic cell, as electrolysis generally occurs under nearly Faradaic conditions with close to 100% Coulombic efficiency. Hence, the cost of electricity is an important consideration in assessing the economics of electrolytic hydrogen production. The strong dependence of the production cost for electrolytic hydrogen on the cost of electricity is shown in Figure 41. The high sensitivity to the cost of electricity renders electrolysis a costly process for distributed hydrogen production. An earlier study concluded that the electricity costs must be below the \$0.045-0.055/kWh range in order to produce hydrogen using current commercial electrolyzers at a cost of \$3/kg of H_2 to stay competitive with gasoline [319]. Although the cost of electricity cost is a major contributor to electrolytic hydrogen production, the origin of electricity for electrolysis is another important consideration. Most of the electricity from the grid is derived from fossil fuels, and hence

View Article Online
DOI: 10.1039/C8EE01419A

yield greenhouse gas emissions. So hydrogen production by electrolysis is best suited for renewable power such as wind and solar in order to avoid upstream carbon emissions.

The appeal of hydrogen as a viable and sustainable energy carrier drives commercial interest in these high temperature electrolyzers and several development efforts are being pursued, but the technology is far from being ready for commercialization. Besides the technical challenges, the economics of hydrogen production in SOECs is very likely to be considerably more expensive than the average cost target for wind-based low temperature water electrolysis of $3.10/kg of hydrogen for central and $3.70/kg for distributed production recently set forth in 2015 by the U.S. Department of Energy (DOE) [320] based on the 2011 NREL analysis [321]. It should be noted that the cost estimates for high temperature SOECs may be necessarily inaccurate as the cost models are largely based on laboratory scale results. In fact, U.S. DOE Office of EERE possibly refrained from providing a cost target for hydrogen production in SOECs [322] most likely for the reason that the reported cost estimates may be somewhat premature.

E.1.1. Hydrogen Production by Water or Steam Electrolysis

Combining water or steam electrolysis with renewable energy provides an integrated distributed storage system whereby hydrogen produced can be either utilized for end use in a fuel cell or for chemical energy storage. Unlike steam electrolysis still under development, hydrogen produced via the electrolysis of water is a mature technology and has been available commercially for many decades. Water electrolyzers serve relatively a small market, where access to merchant hydrogen is limited by geography or other reasons. The operational parameters, cell performance and materials, and economics of water electrolyzers for hydrogen production have been reviewed recently [319,323-326]. These commercial electrolyzers typically operate at 70-80^{o}C with an imposed potential of 1.75-2.0 V and have electrical conversion efficiencies in the range of 60-70%. But unless this electricity for electrolysis is derived from renewable sources, the primary efficiencies commercial electrolyzers drop to around 20-25% when electricity from conventional power is used. Also, the cost of hydrogen production using electrolyzers cannot compete with the large-scale centralized production of hydrogen via steam reforming of natural gas, which provides more than 75% of the world's industrial hydrogen production. Capital costs for

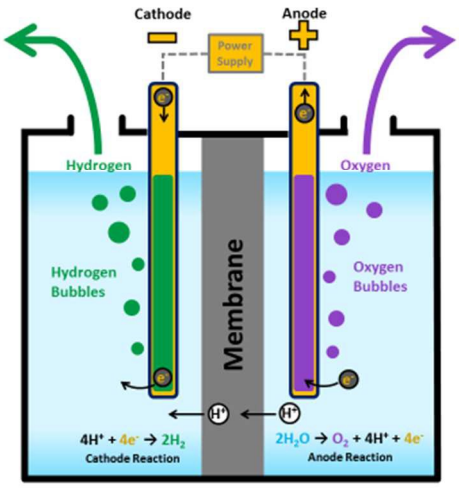

Figure 42. Hydrogen production via water electrolysis [329].

View Article Online
DOI: 10.1039/C8EE01419A

commercial water electrolyzers reported in the literature range from >$3000/kW for small (<50kW) alkaline electrolyzers to $400-$700/kW for larger plants with life times from 5 to 10 years [326]. A more recent review estimates the capital costs for commercial alkaline electrolyzers in the range of $1200-1500/kW and polymer electrolyte-based electrolyzers in the $1300-$2000/kW range [327]. Driven in large part by cost concerns, water electrolyzers have been generally employed for niche markets, for specialized applications in remote locations or confined spaces, or where abundant hydroelectric power or other renewables are readily available.

Electrolysis cells are usually named after their electrolytes. Typical materials, operating temperatures, advantages and disadvantages of the four major classes of water or steam electrolysis technologies are summarized in Table 7. The simplicity and modular design of electrolytic cells provide many advantages including ease in scaling up simply by adding units, and suitability for distributed chemical storage, which is particularly attractive for intermittent renewable sources that usually generate electricity at remote locations far from the populated areas or points-of-use. Electricity generated from intermittent renewable energy sources makes water (or, steam) electrolysis an attractive way to store high quality energy in a clean and environmentally benign fuel such as hydrogen. Indeed, hydrogen storage has gained renewed interest for distributed energy storage driven by the recent and rapid expansion of solar and wind energy [328].

Table 7. Typical structure and operational characteristics of the four major classes of electrolyzers for hydrogen production named after their electrolytes, where PEM stands for polymer exchange membrane, and SOEC denotes solid oxide electrolysis cell. (YSZ: yttria-stabilized zirconia, BYZ: yttria-doped barium zirconate)

	Alkaline	Acid	PEM	SOEC
Electrolyte	NaOH KOH	H_2SO_4 H_3PO_3	Polymer (Nafion™)	Ceramic (YSZ, BYZ)
Carrier ion	OH^-	H^+	H^+	O^{2-} (YSZ) H^+ (BYZ)
Electrodes	Ni	Pt/C, IrO_2	Pt/C, IrO_2	Ni, ceramic
Operating temperature	80°C	150°C	80°C	600-900°C
Strengths	Cheap materials Commercial technology	High activity electrodes	High activity electrodes Commercial technology	Cheap materials Lower barrier to split H2O Higher efficiency
Short-comings	High barrier to split H2O Lower efficiency	High barrier to split H2O Expensive electrodes Cell durability Developing technology	High barrier to split H2O Expensive electrodes Hydrogen crossover Cell durability	High operating temperature Materials stability Fabrication costs Developing technology

Commercial electrolyzers for water electrolysis are similar in design to fuel cells, and compose of an anode and a cathode immersed in an electrolyte and separated by an inert separator, diaphragm, or an ionically conducting polymer exchange membrane (PEM) such as Nafion®. Most commercial electrolyzers operate at temperatures < 80°C and generally employ alkaline electrolytes such as NaOH and KOH solutions, which allows the use of inexpensive catalysts such as Ni in contrast to electrolysis in acidic electrolytes that would necessitate the use of precious metal catalysts such as Pt. However, they are slightly less efficient (60-70%) when compared to efficiencies of PEM-based acidic electrolyzers in the 65-82% range [325]. PEM-based acid electrolyzers can sustain high current densities and high production rates, high voltage efficiencies, and also higher purity of product gases H_2 and O_2 due to minimal crossover across the solid polymer electrolyte membrane. Unlike alkaline

View Article Online
DOI: 10.1039/C8EE01419A

electrolytes that provide better stability and longer service life, however, acidic electrolytes also cause severe corrosion problems that require more expensive materials for cell components. On the other hand, alkaline electrolyte-based electrolyzers suffer from low current densities leading to low hydrogen production rates, large ohmic losses up to 25% of total cell loss across the electrolyte and the separator, low ionic conductivity of the electrolyte, crossover of product gases across the porous separator or diaphragm that yields impure products, and unwanted transport of hydrogen gas into the anode chamber, which can accumulate beyond the explosion limit of > 4% H_2 in O_2 to cause safety concerns. Despite these disadvantages, commercial alkaline electrolyzers seem to be the preferred product compared to acid electrolyzers, due mostly to the cost of the precious metal catalysts used at the electrodes, cell stability and service life concerns.

In order to improve upon the low current densities of alkaline electrolyzers, high temperature alkaline electrolzyers that typically operate at temperatures 150-200^{o}C have gained interest [299]. As expected, these cells need to operate under pressure in order to minimize evaporation losses and accommodate the high operating temperatures of the aqueous electrolyte. High temperature operation lowers cell voltage from the typical $\geq$ 2.0 V to < 1.5 V, which improves efficiency, and reduces ohmic losses due to improved electrolyte conductivity. High pressure operation on the other hand, reduces size of gas bubbles evolving at the gas diffusion electrodes that result in less disruptions to current stability and distribution, but at the same time may cause bubbles to block the micropores of the electrodes and render those sites ineffective and inactive. Hence, the operating cell pressure should be kept lower than for steam condensation, but high enough to avoid evaporation losses from the electrolyte. In an alkaline electrolyzer using aqueous KOH immobilized in mesoporous $SrTiO_3$ and operating at 250^{o}C under 42 bar pressure, high current densities of 1,000 mA/cm^2 at 1.5 V and 2,000 mA/cm^2 at 1.75 V were achieved using Ni foam gas diffusion electrodes [330].

Conceptual cell design and half-cell reactions for water electrolysis are shown in Figure 42. The thermodynamic potential corresponding to the half-cell reactions is 1.23 V, but cell polarization losses require significantly higher voltages around 1.8-2.2 V to be applied externally to drive the water splitting reaction. The half-cell reactions in alkaline electrolyte are,

Cathode: $2H_2O_{(l)} + 2e^- = H_{2(g)} + 2OH^-_{(aq)}$ (30)

Anode: $2OH^-_{(aq)} = (1/2)\ O_2 + 2e^-$ (31)

while in acidic electrolytes, the corresponding reactions are,

Cathode: $2H^+_{(aq)} + 2e^- = H_{2(gas)}$ (32)

Anode: $H_2O_{(l)} = (1/2)\ O_{2(g)} + 2H^+_{(aq)} + 2e^-$ (33)

Regardless of the type of electrolysis cell, splitting of water requires highly active electrocatalytic electrodes for the hydrogen evolution reactions (HER) (30) and (32), and

View Article Online
DOI: 10.1039/C8EE01419A

the oxygen evolution reactions (OER) (31) and (33). HER is a 2-electron proton-coupled reaction while OER involves 4 electrons. Naturally, the activation barrier or overpotential for OER is significantly higher than for HER. Lowering the barriers require the use of effective catalysts. High efficiency, low cost and long durability or lifetime considerations are important criteria for the desirable catalyst. Platinum is an excellent catalyst for both HER and OER but is prohibitively expensive, but still serves as the benchmark for HER when comparing the performance of other electrocatalysts. For OER, IrO_2 and RuO_2 are the best electrocatalysts with the lowest overpotentials in both acidic and alkaline electrolytes compared to others. They are also excellent electronic conductors and can serve as their current collectors as well. Under high anodic potentials, however, both RuO_2 and to a lesser extent IrO_2 suffer from stability problems in both electrolytes because they oxidize to RuO_4 and IrO_3, respectively, and form soluble product that dissolve in the electrolytes. So besides cost, these precious metal catalysts have durability or lifetime problems.

There has been an intense search for efficient and cheap catalysts for HER and OER that are made of non-precious metals, as well as the oxides, sulfides, phosphides and carbides of earth abundant materials [331,332]. Many strategies for catalyst development have been employed including advanced processing techniques such as nanostructuring to fabricate metastable structures, core-shell structures, and engineered surfaces and interfaces [333], atomic layer deposition for atomic scale control of nanostructure, doping and morphology of the catalyst [334-336], as well as theoretical simulations and computational tools coupled to experimentation for rational design [332,337]. One of the key parameters that can guide catalyst design efforts is the adsorption free energy of the electroactive species on the catalyst surface. In accordance with the Sabatier principle, the surface binding energy of the species should be moderate for a good catalyst, and neither too weak (then adsorption becomes rate limiting) nor too strong (then desorption becomes rate limiting). When the free energy of adsorption of the electroactive species is plotted against a performance parameter such as overpotential or exchange current density on various electrolytic surfaces, the resulting "volcano" plots present a descriptive tool to observe the trends and select the electrocatalyst candidates exhibiting the best performance criteria, e.g., the lowest overpotential, or the highest exchange current density. Insights for the selection process of several catalyst systems for various electrochemical reactions have been presented recently [337]. For example, guided by the results of an earlier theoretical study [338], nanoparticles of earth-abundant MoS_2 prepared in a double gyroid morphology with 3-dimensional mesoporous microstructure in order to maximize the edge-site density have shown great promise for HER with overpotentials only 150-200 mV away from Pt [339]. Similarly, nanostructured MnO_2 has shown great promise as an earth abundant effective catalyst for OER [184]. The OER activity of MnO_2 is already presented in Figure 26, which compares MnO_2 quite favorably with the precious metal OER catalysts Ir, Pt and Ru. A detailed review of many classes of prospective OER catalyst materials is provided elsewhere [331].

It is also possible to achieve water splitting using steam in high temperature solid oxide electrolysis cells (SOEC) operating at 600-800^{o}C and employing a ceramic membranes that

View Article Online
DOI: 10.1039/C8EE01419A

exhibit selective ion transport for either O^{2-} such as yttria-stabilized zirconia (YSZ) and gadolinia doped ceria (GDC), or for H^+ as in proton-conducting perovskites such as yttria-doped barium zirconate (BYZ) and yttria-doped barium cerate (BYC), as also indicated in Table 7. In the case of steam electrolysis using an oxide-ion-conducting ceramic electrolytic cell, steam is fed on the cathode side and air is in the anode compartment. By the use of an external power, oxygen is abstracted from steam at the cathode and transported across the solid electrolyte and discharged at the anode as molecular oxygen into the air compartment. In the meantime, hydrogen is produced at the cathode. In the case of steam electrolysis using a proton-conducting ceramic electrolyte, steam is fed on the anode side and the hydrogen evolves at the cathode. But the steam decomposition reaction is thermodynamically uphill and requires an external power source and the associated cost of electricity.

Operating the SOEC at elevated temperatures lowers the electrical energy requirement (see Figure 40). It also increases the kinetic and transport rates significantly. Accordingly, non-precious metal or oxide catalytic electrodes can be employed at high temperature SOECs. Furthermore, a thermodynamic modeling study showed that the difference between the energy and exergy efficiencies for SOECs operating at elevated temperatures is quite small, unlike electrolyzers running at low temperatures, due to the fact that at high temperatures, the energy quality is high and also the thermal energy input constitutes a relatively small portion of the total energy requirement [340].

Steam electrolysis at elevated temperatures can be achieved either by using an oxide-ion conducting solid oxide electrolyte [299,300] such as yttria-stabilized zirconia, or by a proton-conducting solid oxide electrolyte [300,303,341] such as yttria-doped barium zirconate ($Y:BaZrO_2$, or BYZ) or cerate ($Y:BaCeO_2$, or BYC). These electrolytes are made dense and impervious to block chemical shorting, and allow only mobile ionic species O^{2-} and H^+ to transport selectively through the crystal lattice of the ceramic membrane. Steam electrolysis schemes for the two types of ceramic electrolytes are illustrated in Figure 43, which also indicate the direction of ionic transport through the solid oxide electrolytes.

The impervious ceramic electrolyte membrane physically separates the anode and cathode compartments and eliminates chemical shorting or mixing of the product gases. This results in high purity hydrogen production. The electrolyte transport mechanisms are respectively, lattice diffusion via oxygen vacancies in the oxide-ion conducting fluorite structure solid oxide electrolytes, and Grotthuss mechanism for proton transport in the perovskite-type protonically conducting solid oxide electrolytes. As the activation energy for proton transport in perovskites is considerably smaller than that for oxide ion transport in fluorites, protonic SOECs can be operated a lower temperatures (< 600^{o}C) than the oxide ion-based SOECs, which typically operate at 700-1000^{o}C. The major elements of cell voltage loss in SOECs are ohmic losses due to finite ionic conductivity of the electrolyte and activation losses at the electrodes due to slow kinetics and transport. To overcome these difficulties, progress has been made at the laboratory scale in advanced catalytic electrodes and cell architectures, which have been reviewed in detail elsewhere [299,300,303].

View Article Online
DOI: 10.1039/C8EE01419A

E.1.2. Spontaneous Hydrogen and Electricity Co-Generation

As emphasized in Figure 41, it is desirable to minimize or preferably avoid the electrical costs for electrolysis. Indeed, the nascent steam-carbon fuel cell (SCFC) concept proposed earlier [315] aims to accomplish hydrogen production from steam without the need for external power, and in fact, spontaneously generates electricity and hydrogen at the same time. Essentially, the SCFC concept represents the steam gasification reaction of carbon carried out electrochemically. This is accomplished by replacing the more expensive electrical energy requirement for electrolysis (see Figure 41) with much cheaper chemical energy, which provides a sufficiently low oxygen activity to reverse the sign of the activation barrier and drive the steam decomposition reaction downhill. As the equilibrium (chemical) potential for oxygen in the carbon-oxygen system is significantly lower than that for the H_2-H_2O system, the uphill barrier disappears and the gradient becomes downhill, allowing the generation of carbon-free hydrogen and electricity simultaneously. This concept is illustrated in Figure 44, and shows the uphill barrier of about - 0.9 V for steam electrolysis at elevated temperatures of 800-1000°C, which reverses its sign by the presence of solid carbon at the anode and becoming instead a downhill potential gradient with a driving force of about + 0.5 V that allows the cell to operate in a fuel cell mode, while co-producing hydrogen and electricity spontaneously [343,344]. The driving force is governed by the prevalent H_2/H_20 and CO/CO_2 ratios at the cathode and anode compartments, respectively. The SCFC concept utilizes a typical solid oxide fuel cell design and materials, where the only difference is that air is replaced with carbon fuel at the anode. The impervious solid oxide electrolyte membrane serving as a physical barrier between the anode and cathode gas environments allows the production of carbon-free hydrogen, which is critically useful for PEMFC applications. Moreover at high fuel utilization, the anode product gas is highly concentrated in CO_2 with only a small amount unreacted CO in the balance, and hence, nearly ready for capture.

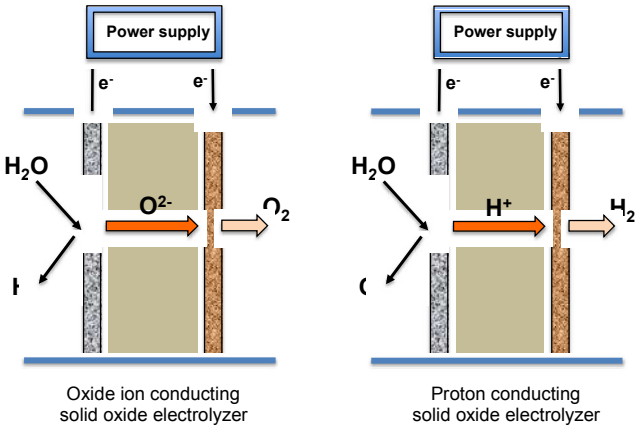

Figure 43. Schematic cell configurations for steam electrolysis and directions of ionic transport in solid oxide electrolyzers featuring (a) oxide ion conducting solid electrolyte, and (b) proton conducting solid electrolyte.

View Article Online
DOI: 10.1039/C8EE01419A

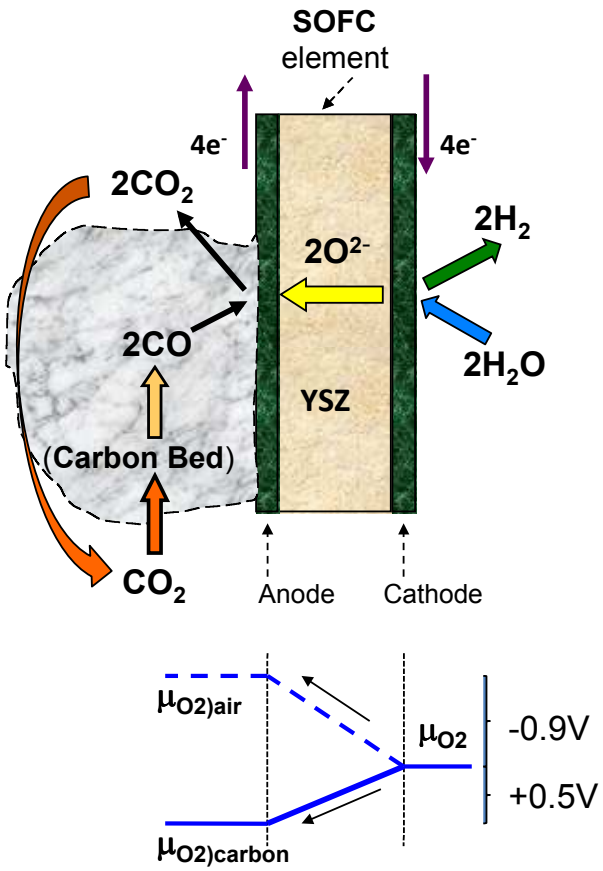

Figure 44. Schematic of the steam-carbon fuel cell concept, indicating its operating principle, and the chemical potential gradients for steam electrolysis [5]. While steam electrolysis in SOEC is uphill by about -0.9 V at operating temperatures above 800°C, replacing air with carbon at the anode compartment lowers the oxygen activity such that the oxygen chemical potential gradient reverses sign and provides SCFC a downhill potential of about +0.5 V. Reprinted with permission from (T. M. Gür, Critical Review of Carbon Conversion "Carbon Fuel Cells", Chemical Reviews, 2013, **113**, 6179-6206). Copyright (2018) American Chemical Society.

The SCFC concept accomplishes the steam gasification reaction of carbon inside a fuel cell with discrete anode and cathode reaction gas streams, producing power and carbon-free hydrogen in the process. Figure 45 presents the experimental results for simultaneous and spontaneous co-generation of hydrogen and electrical energy in a button-type SCFC employing a yttria-stabilized zirconia (YSZ) solid electrolyte at 850°C with activated carbon at the anode and steam at the cathode, which provided a downhill driving force of 0.56 V open circuit potential that enabled achieving steam electrolysis in a fuel cell mode.

A similar concept, this time using reducing gases such as methane and CO at the anode, was also proposed [346]. As expected, the placement of these gaseous fuels at the anode greatly reduces the energy barrier. However, the open circuit potentials reported in this study were less than 90 mV, not sufficiently large enough to spontaneously drive the steam electrolysis reaction. Hence, electricity from an external power, albeit less than otherwise needed for conventional steam electrolysis cells, is still required to drive the electrolysis reaction and produce hydrogen using this configuration.

E.2. Chemical Storage in Ammonia

Ammonia is an effective energy carrier with a high-energy density. For comparison, liquid ammonia provides 13.7 MJ/L (or 3,800 Wh/L) versus 8 MJ/l (or, 2,200 Wh/L) for liquid hydrogen. It is an environmentally benign, carbon-free liquid fuel that when combusted in a turbine or converted in a fuel cell back to electricity, it's reaction products are only nitrogen and water vapor. Hence, ammonia is ideally suited for environmentally

View Article Online
DOI: 10.1039/C8EE01419A

benign chemical storage. Although 79% of the earth's atmosphere is made up by nitrogen, it is difficult to utilize this abundant resource to make ammonia or other nitrogen chemicals, as molecular N_2 is difficult to activate due to the unusual strength (940 kJ/mol) of the N-N triple bond. Actually, this is a kinetic hindrance because thermodynamically the reaction between H_2 and N_2 to make ammonia is favorable and spontaneous below 175°C and at 1 bar pressure.

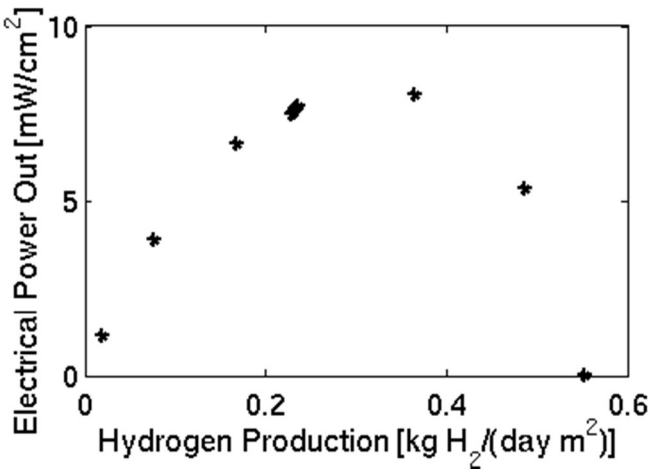

Figure 45. Experimentally measured electrical power output and co-production of hydrogen in SCFC operating at 850°C illustrating the tuneable nature of SCFC output between the two products. The SCFC button cell used in this experiment consisted of 300-μm thick YSZ disk with Pt electrodes, and steam at the cathode and activated carbon placed on the anode surface [345].

Fixation of nitrogen to make fertilizers was made possible by the Haber-Bosch process invented in 1904 that catalytically achieved reduction of nitrogen to produce ammonia at practical production rates in the presence of a Fe-based catalyst using high temperatures (~500°C) and high pressures (150-300 bar). High pressures are needed to shift the synthesis reaction equilibrium to the right due to the Le Chatelier principle, and high temperatures are required to achieve practically high reaction rates, despite the fact that the synthesis reaction between nitrogen and hydrogen is actually exothermic in nature. Accordingly, the Haber-Bosch is an energy intensive process and consumes nearly 2% of the world's energy production. As the hydrogen for ammonia synthesis is derived from natural gas, it also consumes 3-5% of the global natural gas supply while emitting large quantities of CO_2. Hence for both energy and environmental reasons, it is desirable to synthesize ammonia near ambient pressures and at lower temperatures, as ammonia tends to decompose above 175°C into N_2 and H_2, and thermodynamically is not stable at high temperatures. Progress made in new catalytic routes for ammonia synthesis at low temperatures and ambient pressures has recently been reviewed elsewhere [347].

E.2.1. Electrochemical Synthesis of Ammonia

Unlike the case for the reaction between H_2 and N_2, however, thermodynamics of ammonia synthesis using H_2O as the reactant is unfavorable. But this can be overcome, in principle, by applying externally a sufficiently large potential to overcome the thermodynamic barrier and drive the synthesis reaction towards ammonia formation. Indeed, using water as the hydrogen source and nitrogen from air, previous work has demonstrated ammonia synthesis in electrochemical reactors running at atmospheric pressure. The operating temperature of these reactors varied from near room temperature

View Article Online
DOI: 10.1039/C8EE01419A

using liquid [348] or polymer electrolytes [349] such as Nafion^R [350], to temperatures up to 570^{o}C using proton-conducting solid oxide electrolytes such ytterbium-doped strontium cerate (Yb:$SrCeO_2$) [351,352]. Most of the electrochemical studies for ammonia synthesis on precious metal and oxide catalysts utilizing both solid-state and liquid electrolytes have recently been reviewed elsewhere [353].

Electrochemical synthesis of ammonia from N_2/H_2 and N_2/steam mixtures at production rates of 10^{-10} mol/cm^2.s and 10^{-11} mol/cm^2.s, respectively, was demonstrated under atmospheric pressure at 220^{o}C on carbon paper cathodes containing Ru and Ag-Pd alloy catalysts in a solid-state cell that featured a protonically conducting CsH_2PO_4/SiP_2O_7 composite electrolyte [354]. Ammonia synthesis at atmospheric pressure and at 450-700^{o}C was demonstrated at an electrochemical production rate of $2.9x10^{-9}$ mol/cm^2.s at 550^{o}C in a solid-state dual chamber reactor featuring a protonically conducting $BaZr_{0.7}Ce_{0.2}Y_{0.1}O_{2.9}$ (BZCY) ceramic electrolyte and Ni/BZCY cermet catalytic cathode [355], where it was suggested that the protons stored in the Ni/BZCY in the form of highly reactive hydride reacts with adsorbed nitrogen to promote the formation of ammonia [356]. Ammonia synthesis by electrolysis of steam and N_2 on nanoscale Fe_2O_3 catalyst particles suspended in a 0.5NaOH/0.5KOH molten electrolyte at 200^{o}C was reported to achieve 35% Coulombic efficiency [357]. A similar study employing Fe_3O_4 nanoscale catalysts in a NaOH/KOH molten electrolyte has recently demonstrated ammonia synthesis from N_2 and H_2 at a rate of $6.53x10^{-10}$ mol/cm^2.s at 2 mA/cm^2 at 210^{o}C with a Faradaic efficiency of 9.3% [358]. More recently, ammonia was synthesized at a high rate of $5.3x10^{-8}$ mol/cm^2.s with a Faradaic efficiency of 10.2% at room temperature in an electrochemical cell featuring a metal-organic framework-derived nitrogen-doped highly disordered carbon electrocatalytic cathode and 0.1 M KOH alkaline electrolyte [359].

In all studies, however, production rates for ammonia have generally been low (typically 10^{-9}-10^{-10} mol/cm^2.s) due to low kinetic rates resulting from large polarization losses at the cathode. Also, with few exceptions, the Faradaic efficiencies for ammonia were fairly low below 1% largely due to the competition between the hydrogen evolution and ammonia synthesis reactions at the cathode, as the protons do not only react with nitrogen to form ammonia, but may also receive electrons from the cathode to form H_2 gas. Such competition highlights the importance of selective electrocatalysis with high activity for nitrogen reduction towards ammonia synthesis, but with low activity (i.e., high overvoltage) for the hydrogen evolution reaction at the cathode.

Indeed, theoretical studies also suggest that electrosynthesis of ammonia is limited by the competitive processes of nitrogen reduction reaction (NRR) and hydrogen evolution reaction (HER) on the electrocatalytic sites at the cathode, where the HER usually has a smaller overpotential than for NRR [360]. Din search of new catalysts, density functional theory (DFT) investigation of the energetics of electro-reduction of nitrogen on □-Mo_2N electrocatalyst indicated that among other Mo_2N surfaces, the (111) surface shows the highest reactivity and requires the least cell potential (-0.7 V) to activate the N-N bond of the adsorbed N_2 for nitrogen reduction [361]. Similar theoretical studies of electrochemical

View Article Online
DOI: 10.1039/C8EE01419A

ammonia synthesis reported a thermodynamic limiting-potential of -0.71 V for nitrogen reduction on Ru electrocatalysts, but also indicated the competitive evolution of hydrogen that limits the efficiency of conversion to ammonia [360]. More recently, DFT studies of nitrogen electro-reduction to ammonia and the hydrogen evolution reaction on cubic MoC surfaces suggested that the MoC (111) surface is capable of both adsorbing nitrogen at low overpotentials (-0.3 V vs SHE) and suppress hydrogen evolution [335], while a lower potential of -0.53 V for nitrogen activation on a MoS_2 nanosheet was predicted for the single Mo atom on the sheet identified as the active site [363].

It is generally accepted that the associative mechanisms among surface intermediates favor the undesirable HER over the desired NRR on the cathode surface, resulting in low Faradic efficiencies reported often for the electrochemical synthesis of ammonia. A detailed density functional theory (DFT) investigation of the energetics of nitrogen electro-reduction to ammonia on more than one dozen precious and transition metal catalysts identified that the potential-limiting step for nitrogen activation on most of these catalyst surfaces is the reductive adsorption of $*N_2$ to form $*N_2H$ adsorbate requiring a theoretical overpotential of at least - 0.5 V [364]. The study also proposed strategies such as stabilizing the adsorbed $*N_2H$ while destabilizing the $*NH_2$ adsorbate by designing new catalyst that can bind $*N_2H$ more strongly on the surface, but without affecting or strengthening the binding energy of $*NH_2$. As the binding energies of these two species require individual optimization for selective electro-reduction of nitrogen, designing bifunctional catalysts that can bind the two species on different surface sites may be effective pathway to address this difficult problem of nitrogen activation. In this regard, designing catalysts for experimental verification should be guided by theoretical simulations and finding to identify opportunities and gain better insight into the mechanistic aspects of surface processes.

E.3. Other Chemical Options for Storage

Compounds of hydrogen and/or nitrogen offer chemical storage options that release carbon-free environmentally benign products when oxidized for electricity generation. Among such energy carriers, and excepting the rocket fuel hydrazine (N_2H_4) which is toxic and dangerously unstable, energy storage in hydrogen peroxide has recently gained interest as a potential energy storage chemical [365-367]. Hydrogen peroxide is produced commercially and mostly via the hydroquinone process. Alternatively, power from renewable resources can also be employed for cathodic reduction of oxygen in air on an electrocatalyst (typically Co-based) to produce hydrogen peroxide [367,368]. Hydrogen peroxide can be converted directly into electricity in a fuel cell [366,369].. Alternatively, electrolysis of hydrogen peroxide can produce H_2 and O_2, which can be electrochemically converted back into electricity in a fuel cell. Hydrogen peroxide stores 5.88wt% H_2 and 94.12wt% O_2, so it can be used as an oxidant or a fuel in fuel cell [370]. However, its theoretical energy density is only 1.72 MJ/kg of a 50wt% aqueous H_2O_2 solution (or, 478 Wh/kg) with respect to its decomposition products of water and oxygen. This is not an

View Article Online
DOI: 10.1039/C8EE01419A

attractively high energy density for large scale mobile storage applications, and is several orders of magnitude lower than the energy density of 142 MJ/kg of gaseous hydrogen, and 33,570 MJ/kg for liquid hydrogen (see Table 6). Also, hydrogen peroxide is corrosive and reactive with metal surfaces, so it must be stored and transported only in plastic tanks and containers. It also is unstable against alkaline medium. In its dilute form, hydrogen peroxide solutions are safely employed in household cleaners and disinfectants. However, it is not stable above 52wt% in water and this may place additional constraints on hydrogen peroxide as a practical energy carrier.

At the carbon end of the chemical storage spectrum, there is obvious incentive to recycle CO_2 emissions for reutilization by converting to chemical fuels. However, the most obvious source, which is the atmosphere, is too dilute in CO_2 (~400 ppmv), so finding pure sources for CO_2 may pose challenges. Nevertheless, multiple avenues for CO_2-to-fuels conversion have been explored, including low temperature [371-373] and high temperature electrochemical reduction of CO_2 to hydrocarbon fuels [374,375], or to CO [376], or a mixture of $CO+H_2$ (i.e., syngas) [377]. Reduction products CO and/or syngas can further be converted catalytically into fuels via the Fischer-Tropsch synthesis process [378]. Power from renewable sources can be employed to accomplish CO_2-to-fuels conversion without adding new CO_2 emissions to the environment. Alternatively, solar energy can be employed directly for CO_2 conversion using photoelectrochemical reduction [379], and solar fuel production via photocatalytic conversion [380,381] or solar-thermal splitting [382].

Conversion of CO_2 to fuels in electrochemical, photoelectrochemical or photocatalytic cells can offer incentives for carbon-neutral re-utilization and repurposing of carbon-emissions [383]. However, conversion of CO_2 to fuels is challenging, as it requires both the reduction of CO_2 and the oxidation of water. Reduction potential of CO_2 (-1.06 to -1.40 V vs SHE) is not vastly different from the H_2O splitting reaction (-1.23 V vs SHE), but CO_2 reduction over various metal catalysts usually exhibits high overpotentials due to multiple electron transfer steps as well as the poisoning and deactivation of the catalytic surface by the reaction products. Moreover, the reduction reaction over most catalytic surfaces yields a wide product distribution that may include hydrocarbons and oxygenates as well as CO and H_2, making product separation challenging [384]. Hence, selectivity is an important consideration.

Search for earth abundant, high activity, efficient and selective catalysts for the multi-electron reduction reaction have been elusive. After the earlier reports that Cu is an active electrocatalyst for CO_2 reduction [385], many transition metal catalysts have been investigated. Recent progress has shown that nanostructured catalysts [371,386,387] and reticular processing of metal-organic framework catalysts with atomic level chemical and structural control may offer promising results [388]. However, reduction of CO_2 in low temperature aqueous cells is greatly limited by its low solubility (typically 0.03 mol/l), pressurization is required to improve solubility. Reduction in non-aqueous electrolytes such as propylene carbonate improves CO_2 solubility. Low product yields and catalyst selectivity

View Article Online
DOI: 10.1039/C8EE01419A

need significant improvement too, where the formation of formic acid is often favoured as the primary product of the CO_2 reduction reaction.

High temperature (i.e., 600-800^{o}C) electrolytic reduction of CO_2 to synthetic methane first reported several decades ago [374,389] overcomes some of these difficulties in converting CO_2 to useful fuels, but pose other challenges including product stability and high reduction overpotentials that require search for non-noble metal electrocatalyst with low overpotentials for CO_2 reduction. Often, carbon deposition is observed during reduction on transition metal catalytic anodes including Ni, a commonly employed employed anode catalyst in high temperature solid oxide electrolyzers (SOE). Moreover, most hydrocarbons are unstable above 300-400^{o}C and undergo thermal cracking. Hence, high temperature electrolysis of CO_2 poses limitations on the viability of this approach, so lowering the electrolysis temperature is desirable. Many of these difficulties can be minimized by adding steam to SOE for the concurrent reduction of CO_2 and H_2O into hydrocarbon fuels [390]. On the other hand, if employed for the production of CO and/or syngas only, high SOE operating temperatures should not pose an issue for product stability [391].

[a] F. Mechanical Energy Storage

In mechanical storage systems, inexpensive electrical energy is converted into mechanical energy during off-peak times. Mechanically stored energy is converted back into electricity when the supply of electricity falls short of demand. It should be noted that the stored mechanical energy can easily be converted to heat also, but this is outside the scope of this article. Similarly, mechanical energy storage systems and materials such as springs, pendulums, piezoelectrics that do not lend the potential to store utility scale electrical energy are left outside the scope of this review. Accordingly, only pumped-hydro, flywheels and compressed air energy storage systems are reviewed here.

F.1. Flywheels

Mechanical energy storage in flywheels generally offers high reliability, rapid charge/discharge rates, high power density and storage efficiency, low maintenance costs, long cycle life, and environmentally friendly clean operation [392-395]. Flywheels offer effective and efficient storage for applications where fast charge/discharge rates, long cycle life (up to hundreds of thousands), and medium to high power (kW to MW) are needed. For these attractive attributes, flywheels are increasingly finding applications in the areas of electric power storage, telecommunications, automotive, marine and aeronautics. Especially for storing energy from variable speed wind generators, they can improve the quality of power delivered to the grid [396].

The amount of kinetic energy that can be stored in a flywheel is related linearly to the mass of the flywheel and the square of its angular velocity (see Eqs. (4-6)). Hence, its energy

View Article Online
DOI: 10.1039/C8EE01419A

Table 8. Comparative properties of composite materials considered for flywheel rotors [395].

Material	Density	Tensile Strength	Max. Energy Density		Cost
	(kg/m^3)	(Mpa)	(MJ/kg)	(kWh/kg)	($/kg)
4340 Stainless Steel	7700	1520	0.19	0.05	1
Composites:					
E-glass	2000	100	0.05	0.014	11.0
S2-glass	1920	1470	0.76	0.21	24.6
Carbon T1000	1520	1950	1.28	0.35	101.8
Carbon AS4C	1510	1650	1.1	0.30	31.3

density is largely dependent on the mass and type of the material used for the manufacturing of the flywheel. Moreover, monitoring the angular velocity of the flywheel allows a simple but accurate way of determining its state-of-charge.

The flywheel can be designed to operate either at moderately low speeds (up to 6,000 rpm) or at high speeds reaching up to 50,000 rpm. Low speed flywheels are usually constructed of steel, and because of their weight can achieve typical energy densities of around 5 Wh/kg (or 18 kJ/kg). Since achieving high angular velocities requires the use of high strength materials, carbon fiber reinforced composite materials are typically being used in most high-speed flywheel construction. Rotors made from such lightweight high strength materials greatly improve the energy density of high-speed flywheels up to 100 Wh/kg (or, 360 kJ/kg). A further advantage of such lightweight flywheels is that they can come up to speed in a matter of minutes rather than hours, and can provide 1 kW/kg of power. It is also worth noting, however, that nanomaterials such as carbon nanotubes exhibit greater tensile strength and Young's modulus than carbon fibers, and hence offer opportunities to further improve the energy density of flywheels. Table 8 illustrates some of the pertinent properties of composite materials explored for flywheel rotors [395], where storage capacities in excess of 1 MJ/kg may be achievable.

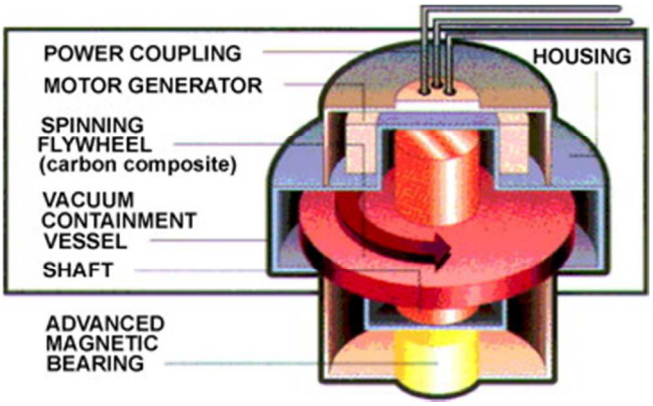

Figure 46. Schematic cross-section illustrating the basic design and operation of a flywheel energy storage system [24]. Reprinted from Renewable and Sustainable Energy Reviews, vol. 13, I. Hadjipaschalis, A. Poullikkas, V. Efthimiou, Overview of current and future energy storage technologies for electric power applications, pp. 1513-1522 (2009), with permission from Elsevier.

The general design of a flywheel shown in Figure 46 consists of a massive rotating drum, i.e., the spinning wheel in the figure, an electromotor generator, and a magnetic suspension bracket, or magnetic bearing that supports the massive rotating drum. In more advanced flywheel designs, superconducting bearings are explored to reduce frictional losses [397]. These components are housed in a physical enclosure generally maintained in low-pressure helium gas or vacuum to minimize frictional and self-discharge loses. The interface with the power system includes a motor/generator, and a

View Article Online
DOI: 10.1039/C8EE01419A

variable speed power converter and controller. The motor/generator usually consists of a permanent magnet integrated to a rotor serving as a synchronous generator.

When cheap electricity is available during off-peak times, the electromotor drives the flywheel to high angular velocities where the electrical energy is stored as kinetic energy in the flywheel. When there is demand for electricity, the kinetic energy stored in the flywheel is converted to electricity in the generator as the flywheel slows down. This process is generally efficient, with round-trip storage efficiencies as high as 90%. They also have good cycling capability that range from 10^4 to 10^6 cycles. By virtue of converting mechanical to electrical and back, flywheel can essentially be considered as a mechanical battery.

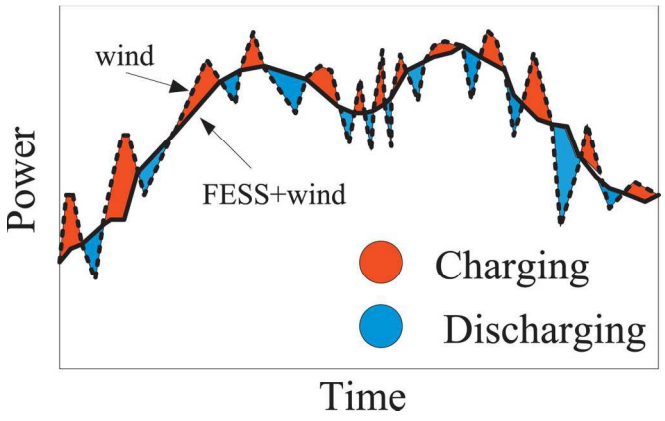

Figure 47. Power conditioning and peak shaving by the use of flywheel energy storage system (FESS) coupled to a wind turbine [394]. Reprinted from Renewable and Sustainable Energy Reviews, vol. 69, A.A.K. Arani, H. Karami, G.B. Gharehpetian, M.S.A. Hejazi, Review of flywheel energy storage systems structures and applications in power systems and microgrids, pp. 9-18 (2017), with permission from Elsevier.

The typical shortcomings of flywheels include low energy density suitable only for short-term storage, inability to directly produce high output voltage (typically > 36 kV) [395], self-discharge during idling, and high capital cost ($5000/kWh) [394]. Storing large amounts of electricity from the power grid requires high capacity, and hence massive size flywheels. However, frictional losses, which scales with size, reduces rotational speed and are the primary cause of self-discharge that lower the flywheel efficiency. For example, the frictional losses in a 200-ton flywheel are estimated to be about 200 kW, which lowers the efficiency of the flywheel to 78% after 5 hours of operation, and down to 45% after 24 hours [22]. In others, self-discharge rates as high as 20% per hour have been reported [24]. Such dramatic impact of frictional forces, even in vacuum environment, renders flywheels unsuitable for long-duration storage. However, this handicap may not pose a major barrier for short periods. In the case of integration with intermittent renewable sources, whose electricity output fluctuates by the hour, flywheels offer attractive advantages due to their fast response times. This is illustrated in Figure 47, where a flywheel coupled to a wind turbine successfully smoothens the fluctuating and intermittent nature of power generation by peak shaving [394]. Even with conventional power generation, where there is a mismatch between the electricity demand (or, load) and the electricity supply, flywheels can rapidly supply stored energy back to the grid and also provide power conditioning.

View Article Online
DOI: 10.1039/C8EE01419A

F.2. Compressed Air Energy Storage (CAES)

The idea of storing energy in the form of compressed air pumped into large underground cavities goes back many decades [398], but early progress has been somewhat slow in large part due to the lack of need or interest for grid storage until recently, where rapid growth and deployment of intermittent renewable sources has generated renewed interest in compressed air energy storage (CAES) [399,400].

Unlike flywheels, the typical discharge times for compressed air energy storage (CAES) are long and measured in hours up to days. Their start-up times are also relatively longer than flywheels, measured in minutes [399]. Furthermore, CAES requires ready availability and proximity to large underground cavities, aquifers, and caverns that exhibit impervious rock formations to ensure gas tight containment of compressed air. Hence, it's availability and feasibility is necessarily restricted by geological constraints. This is one of the major shortcomings of this technology. On the other hand, it eliminates large and costly installations for building a storage facility. Where geological conditions are favorable, CAES offers an attractive and cost-effective technological option to store off-peak power from the grid in the form of compressed air that is kept underground reservoirs during low demand. When make-up power is needed, the high-pressure compressed air is converted back to electricity with an estimated efficiency up to 70% [22]. This process is schematically depicted in Figure 48.

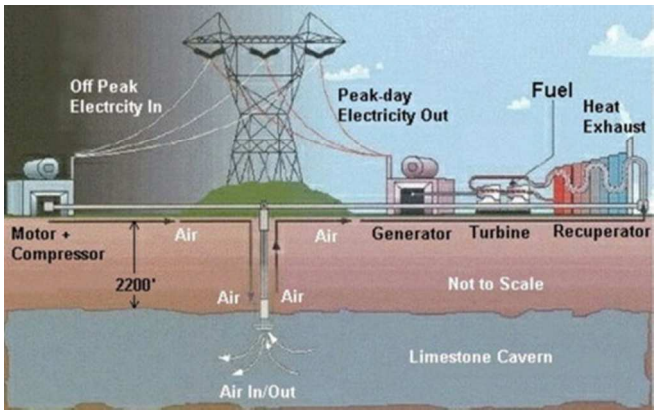

Figure 48. Schematic illustration of compressed air energy storage [22]. Reprinted from Renewable and Sustainable Energy Reviews, vol. 12, H. Ibrahim, A. Ilinca, J. Perron, Energy storage systems – characteristics and comparisons, pp. 1221-1259 (2008), with permission from Elsevier.

The typical charging cycle of CAES starts with compressing air to high pressures in several stages by electrically drive compressors during low electricity demand, usually with cooling in between successive compressions before injecting into the underground storage cavity, which is maintained at air pressures up to 100 bar. Temperature of the injected air is typically kept at or below 40°C to avoid thermal stress in the underground cavity. During high electricity demand, i.e., discharge cycle, compressed air from the underground cavity is preheated in a recuperator or heat exchanger, and mixed with fuel in a combustor. The hot combustion gases are expanded in a turbine to generate electricity.

There are a variety of CAES processes being considered or developed for different applications, but all of them can be grouped under three categories differentiated by how the heat is managed during charging and discharging cycles, namely, adiabatic CAES,

View Article Online
DOI: 10.1039/C8EE01419A

diabatic CAES and isothermal CAES. In the adiabatic CAES process, the heat of compression during the charging cycle is fully captured into a thermal energy storage system, and re-used to preheat the compressed air prior to expansion during the discharge cycle. In the diabatic CAES process, by contrast, the heat of compression is lost to the surrounding atmosphere during the charging cycle by cooling the compressed air, which then necessitates an external heat source to reheat the compressed air during the discharge cycle. Unlike in diabatic and adiabatic CAES processes, heat of compression needs to be minimized or eliminated completely during isothermal CAES to keep the air temperature near ambient at all times. Consequently, performance parameters such cycle efficiencies, energy densities, and start-up times widely vary among the three process groups.

There are a number of installations of CAES systems around the world. The first CAES system, namely the Huntorf facility, was installed near Bremen, Germany in 1978. It had a charging time of 8 hours, discharge time of 2 hours, and maximum charging and discharging power of 60 MW and 290 MW, respectively, with a power plant efficiency of 42% [4000]. In 1991, another CAES system built over a 700-meter deep 2.55×10^6 m^3 cavern in McIntosh, Alabama, USA, and operated at 54% efficiency but with significantly longer charge/discharge times of 40/26 hours, respectively, had provided 110 MW of power for a duration of 226 hours, and has been in use for 1770 hours per year [22]. In the last decade, several CAED projects with storage capacities in the 175-315 MW range have been initiated in the U.S. [399].

It is estimated that 0.7-0.8 kWh of off-peak electricity is required to compress the air into the underground formations in order to supply 1 kWh of peak-demand electricity back into the grid [22]. As more than 2/3rd of the available power in a power plant is consumed in compressing the combustion air for the gas turbines, it makes sense to separate this process in time and use the off-peak power to compress the air, and use it to convert to electricity when peak demand increases.

Due largely to their geological requirements and constraints, CAES can be used only at large scales. In fact among all other storage technologies and systems, CAES is currently the only technology other than pumped-hydro that has the ability to provide large-scale energy storage capacity, typically, less than 300 MW. CAES also offers the longest storage duration of the order of 20-40 years without significant losses, and long cycle life reaching more than 13,000 charge/discharge cycles. However, the volumetric energy density for CAES is low, typically 2-12 kWh/m^3 (or, 7.2-43.2 MJ/m^3). By comparison, the typical volumetric energy densities of liquid fuels are nearly 3 orders of magnitude larger than these values. A recent economic analysis of the Danish electric system that produces a significant portion (42% in 2015) of its electricity from offshore wind has concluded that investments in CAES carry risks and do not offer more cost-effective options than other storage alternatives [401]. Thermodynamic analysis and modeling of CAES systems using first and second law (i.e., exergy) efficiencies predicted more optimistic results regarding the viability of CAES for large scale storage with efficiencies as high as 86% when combined with thermal storage,

View Article Online
DOI: 10.1039/C8EE01419A

but these studies still caution on the technical challenges that still remain to overcome by this technology [399,400,402].

F.3. Pumped Hydro Storage

Hydropower constitutes the major segment among the renewable energy sources with a global share of more than 16% of the global electricity production in 2016, and is a mature commercially proven technology. It has been used at industrial scale since the turn of the 20th century. Globally, more than 25 countries depend heavily on hydropower to supply a large fraction of their electricity production [403]. Figure 49 indicates the geographical distribution for the global potential of hydropower with respect to the continents and highlights the fact that significant potential remains unexploited. Likewise, Table 9 provides information about the world top ten countries with the largest installed and generation capacities of hydropower.

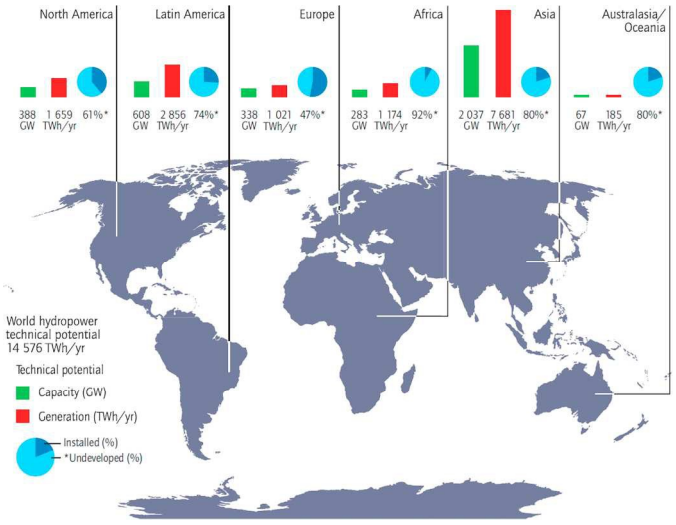

Figure 49. Continental potential of hydropower generation, also indicating the percentage of undeveloped hydropower potential as of 2009 [404].

When and where geographical conditions are satisfied, hydropower plants can be employed for pumped hydro energy storage (PHES). Indeed, pumped hydro constitutes by far the largest segment of the electricity storage technologies globally. Extensive reviews of PHES technology addressing the various aspects of the technical challenges [406], technology trends [407,408], coupling to other renewable sources [406,409], and international PHES projects [407,410] are provided elsewhere.

However, the availability and cost of this mature technology is site-dependent and only feasible where geographic conditions are favorable for its implementation. PHES provides more than 96% of the global installed storage capacity [411] (see also Table 2). It provides cost effective solutions to load-leveling and peak-shaving in the grid and during peak demand, eliminates the need for generating make-up power by gas turbine plants using natural gas. Thus, pumped-hydro displaces the use of fossil fuels and thus helps reduce carbon emissions.

View Article Online
DOI: 10.1039/C8EE01419A

Table 9. Top-ten countries in the world with the largest installed and generation capacities of hydropower in 2010. Data compiled from refs. # 404 and 405.

Country	Installed Capacity (GW)	Hydro Electricity Production (TWh)	Share of Electricity Generation (%)
China	210	694	14.8
Brazil	84	403	80.2
Canada	74	379	62.0
United States	79	328	7.6
Russia	50	165	15.7
India	38	132	13.1
Norway	30	122	95.3
Japan	28	85	7.8
Venezuela		84	68
Sweden		67	42.2
World Total	**936**	**3300**	**16**

In principle, PHES employs the potential and kinetic energy of vast quantities of water stored between two water reservoirs with sufficiently large volumes and separated by a significant difference in altitude. Some of the pumped-hydro facilities employ abandoned mines or artificial formations as reservoirs, but most employ natural reservoirs such as lakes.

During off-peak times where the electricity demand is low, excess generation capacity is used to pump water from a lower reservoir to a higher one, such as a volcanic lake. When electricity demand is increased beyond generation capacity, water is released from the upper reservoir to turn a turbine to generate make-up electricity. The general layout of the key features of a PHES plant is schematically shown in Figure 50. The turbine serves dual purposes, both to pump water to the upper reservoir and also to generate electricity when water is released from the upper into the lower reservoir.

PHES generally provides large storage capacities with power ratings in some places ranging up to 1000's of MW (or, 100's of GWh of energy). However, the storage capacity depends strongly on the separation height between the two reservoirs and the volume of water transferred between the two. For example, 1 ton of water released from 100 meters can potentially generate 0.27 kWh of electricity. Figure 51 illustrates the relation between the volume of water and the vertical separation height between the two reservoirs required to store about 6 MWh of electrical energy [22].

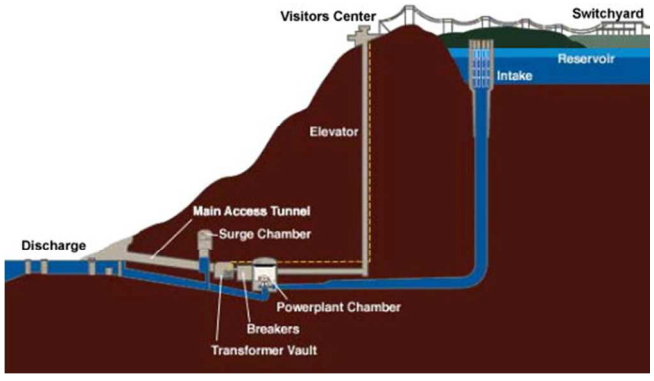

Figure 50. A typical layout of pumped-hydro storage plant operating between two water reservoirs [412]. Reprinted from Renewable and Sustainable Energy Reviews, vol. 13, I. Hadjipaschalis, A. Poullikkas, V. Efthimiou, Overview of current and future energy storage technologies for electric power applications, pp. 1513-1522 (2009), with permission from Elsevier.

One of the major shortcomings of pumped-hydro is its strong reliance

View Article Online
DOI: 10.1039/C8EE01419A

on both the availability and suitability of two large bodies of water located in reasonable physical proximity of each other and separated by a sufficient vertical distance. As Figure 51 shows clearly, relatively low energy density of this technology requires both large volumes of water and large differences in altitude. The capital costs for plant construction may vary widely from 470 Euro/kW to 2170 Euro/kW (in 2009 Euros) [410] and strongly depends on geographic constraints. A more recent report estimated the average capital cost for a 500 MW green field hydropower generation plant in the USA to be about $3500 (+35%) in 2012 with capacity factors ranging between 25 and 90% and a levelized cost of electricity between $20/MWh and 190/MWh for large plant operations [403].

Sometimes, conventional hydroelectric power generation plants can operate also for storage purposes provided that another large body of water at a lower, or higher, altitude is conveniently available nearby, which is more an exception than a norm. When available, such combined hydropower generation-storage plants provide the opportunity for peak-leveling and shaving in an environmentally friendly manner.

An unavoidable problem with pumped hydro storage is evaporation losses from the large surface areas of the two large bodies of water, especially the ones at high altitudes, where such losses can be significant. This leads to lost work from pumped water due to natural causes, and reduces the efficiency for storage.

Nevertheless, PHES offers high conversion efficiencies, where 70-85% of the energy used to pump water to the upper reservoir can be recovered during the generation cycle. Pumped-hydro storage offers response times that may range between minutes to hours, which allows it smooth out changes in load or demand conditions on the grid. This is critical for power management and frequency regulation on the network. By contrast, thermoelectric power requires relatively longer start up times, which can lead to frequency and voltage instabilities in the grid.

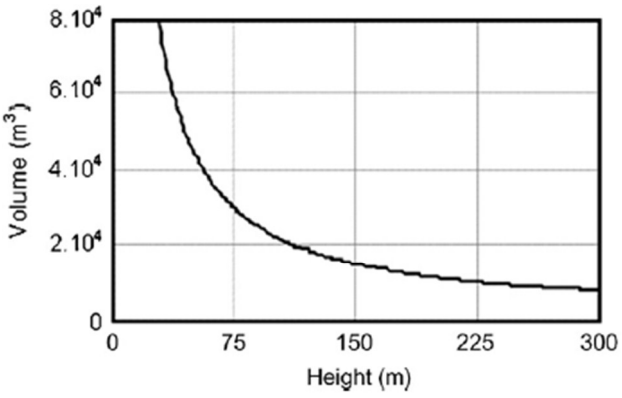

Figure 51. Volume of water needed to store 6 MWh of electrical energy as a function of separation height between reservoirs [22]. Reprinted from Renewable and Sustainable Energy Reviews, vol. 12, H. Ibrahim, A. Ilinca, J. Perron, Energy storage systems – characteristics and comparisons, pp. 1221-1259 (2008), with permission from Elsevier.

With significant cost reductions in wind and solar, there is growing interest in hybrid storage systems that explore various combinations of wind, solar and PHES technologies for consideration for large-scale energy storage as well as autonomous or isolated electric grids [407,408,413]. Mostly, these studies employ system modeling to simulate widely varying conditions for optimum performance, cost and efficiency. Although the outcomes are impacted by site-specific constraints, it is suggested

View Article Online
DOI: 10.1039/C8EE01419A

nevertheless that coupling PHES to intermittent renewable power sources help increase the penetration level of these renewable sources into the power mix.

As inland PHES is limited by geographical conditions, seawater presents a nearly unexplored potential for PHES. Currently, there is only one seawater-based PHES facility in the world operating since 1999 in Okinawa, Japan with a design a capacity of 30 MW and a head of 136 meters. There are few others in conceptual or design stage, including the Dead Sea Power project located on the Red Sea with a design capacity of 1500-2500 MW, and one proposed seawater PHES project in Ireland to provide 480 MW of storage capacity [406].

G. Thermal Energy Storage

Central to the storage of electricity is to close the gap between generation and consumption, and thermal energy storage is a fundamentally sound approach that can provide attractive opportunities to achieve storage at large scale. Already, thermal energy storage is ubiquitous in our daily lives including hot water heaters and residential heating and cooling. But converting thermal energy back to electricity is generally not a highly efficient process. Moreover, the "energy quality", which sometimes is also referred to as the quality of heat, may be a design consideration for many applications. For thermal storage, the temperature, T, at which the energy, or heat, is delivered, is an important factor. As Gibbs free energy, G, defined in Eq. (1) represents the maximum amount of work that can be extracted from a system, the energy quality can be defined as the ratio of the Gibbs free energy to enthalpy by,

$$G/H = \Delta T/T = 1 - (T_o/T) \quad (34)$$

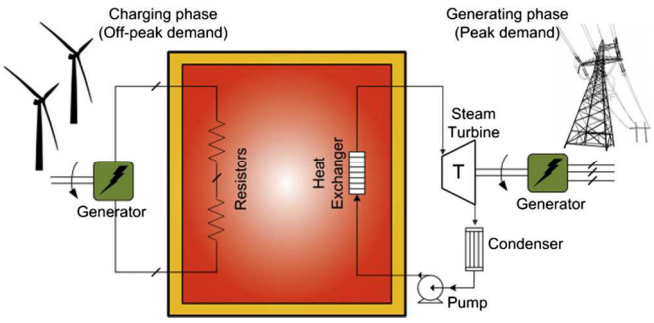

Figure 52. Schematic process flow diagram for sensible heat thermal storage from wind power. Reprinted from ref # 414 (Luo X, Wang J, Dooner M, Clarke J. (2015), Overview of current development in electrical energy storage technologies and the application potential in power system operation, Appl. Energy, 137, 511-536).

Here, T_o denotes the ambient temperature. It is clear from Eq. (34) that higher the delivery temperature, T, higher will be the energy quality, or the quality of the heat delivered.

There have been renewed interest in thermal energy storage materials and technologies, and several excellent reviews are available in this topical area [415-419]. Most thermal energy storage systems can be grouped under two general categories, namely sensible heat storage and latent heat storage.

View Article Online
DOI: 10.1039/C8EE01419A

The latter employs the latent heat that often accompanies a phase change such as fusion or melting, or a structural transformation. Those that utilize the sensible heat given in Eq. (7) rely on the specific heat and mass of a material. The schematic of thermal storage using sensible heat is illustrated in Figure 52, where electricity from a wind farm is used to heat up a thermal mass of desirable heat capacity. The heated mass may be in liquid or solid form, which is then employed to make steam and generate electricity when the demand is high. Many of these systems consider molten salts or their eutectic mixtures for thermal storage, which brings about potential problems related to hot corrosion, and thermal and chemical stability issues for the container materials in the highly corrosive environment of the molten salt. To mitigate such undesirable stability problem, the use of costly construction materials is often required. So cost and stability, and hence useful service life, are important considerations in the proper evaluation and selection of the appropriate thermal storage medium, materials and system design.

G.1. Sensible Heat Storage in Molten Salts and Other Materials

Thermal storage via sensible heat typically involves heating up a mass of a material in liquid or solid from and raising its temperature by ΔT without undergoing a phase change or structural transformation. The process of converting the stored thermal energy back to electricity typically involves using the sensible heat to make steam that drives a turbine, and finally the generator. Excess electricity during low demand, electricity from renewable sources, or thermal solar energy can all be employed as viable sources to heat up the storage material or medium. As the required mass or volume of the storage medium is typically large in order to store sufficient energy, the economics of this scheme favor relatively abundant and inexpensive materials with sufficiently high heat capacities. For that reason, solids are mostly preferred but molten salts are also being employed as well. Representative physical properties of select solids, liquids and molten salts are provided in Table 10.

Some of the materials listed in the table offer attractive properties for thermal energy storage applications but some have disadvantages or shortcomings such as low energy density, thermal conductivity or specific heat. Most are cheap and abundantly available, and several such as iron and water offer high volumetric energy densities around 4 MJ/m^3. Particularly, water possesses nearly two times larger specific heat than most other materials, and offers an energy density of 4.19 MJ/m^3, but it is only operable below 100^oC. So the energy quality of water as a storage medium for large-scale storage applications is necessarily low. Environmental impact should also be taken into consideration. For example, underground energy storage using hot water may cause irreparable damage to the ground or the geological structure. However, water is a suitable energy storage medium for heating and cooling for residential buildings and workplaces where low quality heat is acceptable. Similarly, water-ethylene glycol mixtures are also limited by their operating

View Article Online
DOI: 10.1039/C8EE01419A

window for storage, but are suitable for heating and cooling applications that do not require high quality heat.

On the other hand, most inexpensive solids offer a wide window of operating temperatures that can extend close to their melting points. Thus the quality of energy for these materials can be quite high, and makes them attractive for large-scale storage applications. Furthermore, their high densities nearly twice that for liquid and molten medium helps render the storage medium to be compact. Unlike water, other liquids, or molten salts, low vapor pressure of solids makes containment easy and inexpensive, while reducing materials loss to the surroundings. Indeed, solar energy can be stored up to 36 kJ/kg (or, 10^5 kJ/m^3) in rocks or concrete for space heating applications [418].

There is, however, another important consideration that has to do with how fast energy is transferred to or retrieved from the storage medium. In this respect, thermal conductivity is an important material parameter for system design purposes. As shown in Table 10, metals possess significantly higher thermal conductivity than many of the refractory solids, as well as liquids. For molten salts, thermal conductivity information is rather scarce, but for several fluoride-, carbonate- and nitrate-based molten salt eutectics, thermal conductivity values between 1.09 and 1.21 W/m.K have been reported [420]. Clearly, nearly two orders of magnitude difference between the thermal conductivities of metals and refractory solids, liquids, or molten salts can be an important factor in the selection of the proper storage material and system design for a specific application.

Needless to say, heat loss to the surrounding in the forms of radiation, convection and/or conduction is another important consideration in energy storage, because it directly impacts overall system efficiency. Such losses are dependent not only on the temperature difference between the storage medium and its surrounding, but also on other factors including exposed surface area, emissivity, and thermal conductivity. Hence, proper design, materials selection, and effective thermal insulation of the storage system are important considerations.

G.2. Latent Heat Storage in Phase Change Materials

This approach utilizes the enthalpy change during phase transitions without a change in composition, i.e., congruent phase transitions, where typically the first derivative of Gibbs free energy during the phase change is discontinuous. This type of energy storage may involve either the enthalpy of fusion, typically during melting, or the enthalpy change during a solid-state crystal structure transformation below the melting point of the material. As in the case of sensible heat, energy is stored in the material either for inducing melting or a structural phase change, and retrieved back in the reverse process. Since most congruent phase changes occur at sufficiently elevated temperatures, the energy quality of energy storage using latent heat is typically high. Also, the entropies of solid materials are considerably smaller than those of liquids or melts. So the entropy change during melting

View Article Online
DOI: 10.1039/C8EE01419A

can be considerable. Hence, the enthalpy change across the phase transformation is relatively larger for fusion rather than for solid-state phase transformations. On the other hand, congruent melting and solidification usually involves considerable molar volume changes in the storage material, which makes containment and system design more complicated, while molar volume changes during solid-state phase transformation are typically much smaller. Table 11 lists a number of cheap and readily available materials that can be considered for thermal energy storage via phase change. However, it also illustrates that the amount of storable energy may be quite limited, as the energy densities of 0.3 - 0.5 MJ/kg of many phase change materials are several orders of magnitude lower than those for chemical fuels such as hydrogen (142 MJ/kg), gasoline (44 MJ/kg), or methanol (20 MJ/kg).

Nevertheless, phase change materials can store 5-14 times more energy per unit volume than sensible storage materials such as water, most rocks and many other solids. Unlike sensible heat storage materials, they store and release heat at nearly constant temperature, which is an advantage. Most phase change materials can be grouped in two major categories, namely, organic and inorganic materials, and their eutectics. The inorganic group exhibits early twice the volumetric capacity of 250-400 kg/dm^3 for storage compared to 128-200 kg/dm^3 for organic phase change materials [416].

Table 10: Comparison of materials properties for thermal storage.

Materials	Melting Point (°C)	Thermal Conductivity (W/m.K)	Density (kg/m^3)	Specific Heat, Cp (J/kg.K)	Vol. Energy Density (kJ/m^3)
Solids					
Aluminum	660	205	2700	920	2484
Iron (cast)	1150	58	7200	540	3890
Glass	N/A		2710	837	2272
Brick	>1500	1.3	1970	921	1813
Concrete	N/A	1.0-1.8	2000	880	1760
Granite	1215-1260	1.7-4.0	2400	790	1896
Liquids					
Water	100	0.58	1000	4190	4190
Molten sodium	98		750	1260	945
50:50 ethylene glycol -water mix			1075	3480	3740
Molten salts					
50 wt% KNO_3 -40% $NaNO_2$ - 7% $NaNO_3$	149		1680	1560	2620
$LiNO_3$-$NaNO_3$-KNO_3	117		1710	1540	1056
$NaNO_3$-KNO_3	222		1750	1530	756

The most common organic phase change material is the paraffin group of hydrocarbons with melting points slightly higher than room temperature and moderate enthalpies of fusion. The latter increase with chain length. They possess many desirable properties including low vapor pressure, chemical stability in some cases up to 500°C, low toxicity and corrosivity, commercial availability at large quantities and at low cost, and negligible supercooling. On the hand, they undergo considerable volume change during solid-liquid phase transition and exhibit low thermal conductivities that greatly limit the rate at which heat is stored and released.

View Article Online
DOI: 10.1039/C8EE01419A

Table 11. Latent heats of fusion of phase change materials. Compiled from refs. # 416 and 421.

Material	Transition Temperature (°C)	Enthalpy of Fusion (MJ/kg)
Water	0	0.335
Paraffin	20-60	0.14 – 0.28
$LiNO_3$	250	0.37
NH_4NO_3	170	0.12
$NaNO_3$	307	0.13
NaOH	318	0.15
$Ca(NO_3)_2$	561	0.12
LiCl	614	0.31
$FeCl_2$	670	0.34
$MgCl_2$	708	0.45
KCl	776	0.34
NaCl	801	0.50
$LiNO_3.2H_2O$	30	0.296
$FeCl_3.6H_2O$	37	0.223
$Na_2PHO_4.12H_2O$	40	0.279

An important group among inorganic phase change materials is salt hydrates (see last three rows in Table 11), which break up at the melting temperature to water and an anhydrous salt (or, water and the lower hydrate). They offer attractive properties such as high volumetric latent heat of fusion, significant thermal conductivity nearly twice that of paraffins, small volume change during phase transition, and mostly non-corrosive and non-toxic and low cost. However, many inorganic salt hydrates melt incongruently, i.e., the water released during the phase transition is not sufficient to dissolve all the solid salt phase(s). Another important disadvantage of salt hydrates is supercooling. As the rate of nucleation at the phase transition temperature is rather slow, the solution requires supercooling to lower temperatures to achieve a reasonable nucleation. Hence, the energy stored in the material can only be released at a temperature lower than the fusion point. The undesirable effect of supercooling naturally renders inefficiency in the storage cycle.

Most studies concluded that low thermal conductivities of phase change materials pose a major limitation for their implementation for large scale energy storage applications. Therefore, recent attention has turned to designing microstructures and methodologies such as adding dispersions of metals, graphite and other high thermal conductivity materials, microtubes, fins, and encapsulation, all intended for enhancing the rate of heat transfer in these materials [360].

H. Grid Storage

The electrical grid depicted in Figure 53 is a critical component of the vital connection between the point of use and power generation. In many parts of the world, the existing grid infrastructure is insufficient, old or obsolete. In the U.S., the Department of Energy estimates that 70% of the transmission lines and 70% of power transformers are 25 years or older, and 60% of the circuit breakers are more than 30 years old [17]. The expected growth of 43% in the global electricity production (see Table 1) urgently requires major upgrading of the grid system to make the grid more secure, reliable, and responsive. Certainly, large-scale deployment of distributed storage capacity will help improve grid resilience and security,

View Article Online
DOI: 10.1039/C8EE01419A

reduce line congestion and line loss, lower the need for generation during peak demand times, and also extend the capability of the transmission grid, for example, by positioning the storage system downstream on the load side. A White House 2013 report from the Executive Office of the President also concluded that energy storage is important for emergency preparedness during natural disasters and also in increasing grid resilience and robustness to weather outages [367].

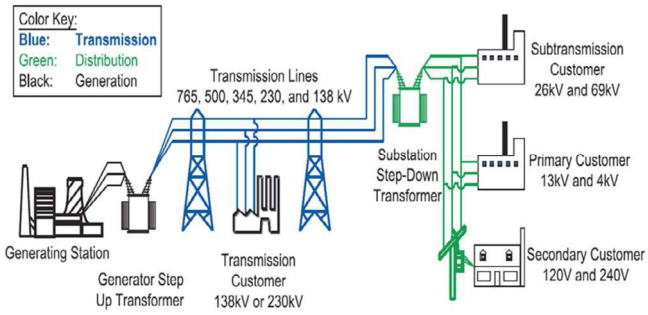

Figure 53. Basic structure and lay out of the U.S. electric grid system [422].

Rapid deployment of intermittent renewables such as wind and solar has highlighted the difficulties in fully integrating these renewable sources into the grid. A recent report by the U.S. National Renewable Energy Laboratory (NREL) has suggested that more than 20% penetration of intermittent renewables such as solar into the electric grid can cause operational challenges that can adversely affect grid reliability [423]. Although the scope of this study was rather limited to the grid systems in the islands of Oahu and Maui in Hawaii, it strongly underscores the importance of storage technologies to cope with dynamic loads. Assuming 20% penetration by renewable sources by 2020, a recent report by Pacific Northwest National Laboratory (PNNL) [424] estimated that the U.S. would need a total of 37.67 GW for intra-hour balancing capacity, and an energy storage capacity of 14.3 GWh that can provide power at rated capacity for 20 minutes. By comparison, the U.S. has 24.6 GW of storage capacity (~ 2.3% of total electricity production capacity), including announced projects [17]. Unfortunately, 95% of this storage capacity is by pumped-hydro, whose availability is site-specific and constrained by location, and only 1.2 GW of this capacity is provided collectively by CAES, flywheel, thermal, and battery storage. The situation is not much different elsewhere. For example, Europe and Japan have considerably higher fractions of grid storage than U.S., but it is largely dominated by pumped-hydro also. The global energy storage capacity has now grown to 168.6 GW (see Table 2), where pumped-hydro makes up more than 96% of the total capacity. It is clear that distributed storage can help remove or mitigate the logistic mismatch problem between the siting of storage availability and demand.

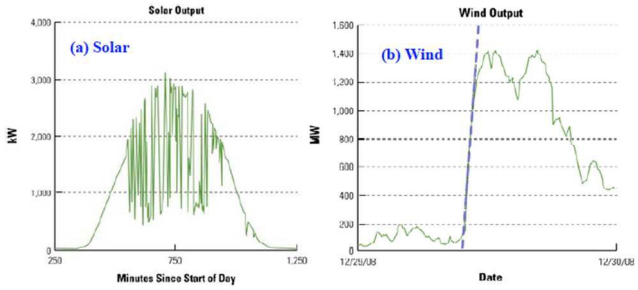

Figure 54 Time-dependent intermittency of solar and wind power varying > 80% within time scales of minutes to hours in a single day. The high rate of change of power (i.e., ramp rate) of the order of MW/min is illustrated for wind power. [241].

View Article Online
DOI: 10.1039/C8EE01419A

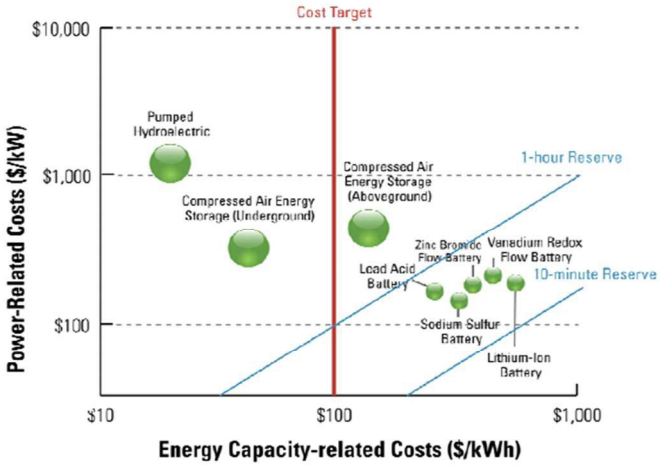

Figure 55. Cost of energy storage for various technologies, showing cost targets and minimum required response times. Small circles denote response times of seconds, large circles indicate time scale in minutes [241].

To appreciate the need for storage, one needs to look no further than intermittent sources such as solar and wind, whose power generation show large variability up to 80% during time scales of minutes to hours, as depicted in Figure 54 The ramp rates, especially for wind power which can be of the order of MW/min of higher, requires energy storage with characteristic time constants and capacities compatible with power production. U.S. Department of Energy recommends [241] three time scales to accommodate variability of intermittent power sources; (a) seconds-to-minutes, with storage capacity of 5-7% of generated power for frequency and voltage support – for U.S. this is about 20-50 GW of storage capacity for the domestic generation capacity of more than 1,100 GW of power; (b) minutes-to-hours of capacity for up to one hour of storing 20% of power from renewable sources for smoothing intermittency – or, nearly 220 billion kWh of storage capacity in order to accommodate more than 1100 billion kWh of solar and wind power generated globally in 2016 (see Table 1); and (c) hours-to-days of power storage capacity for peak shaving and 20% integration of renewables into the grid, which requires a power capacity on the order of 200 GW and 1,000 GWh for 20% integration of renewable energy . These estimates were based on the assumption that 200 GW generation from renewable resources would be required to meet 40% of daily load with 100% load shifting for 5 hours [241].

The need for cost-effective storage is highlighted in Figure 55, which shows the 2010 costs of power and energy for various storage technologies, as well as the cost targets set by U.S. DOE ARPA-E [241]. The figure also marks the required response times for 10-minute and 1-hour reserve storage capacity. Pumped-hydro and CAES with time scales from hours to days provide cost-effective storage where available, but rapid development and deployment of a portfolio of diverse storage technologies with the required characteristic response times and energy capacities are needed for broader siting of storage facilities, especially for intermittent renewable sources. Clearly, the figure indicates that major cost reductions are needed for electrochemical technologies to meet the cost target.

View Article Online
DOI: 10.1039/C8EE01419A

Sizing of a storage system for grid applications requires several operational parameters to be specified, including the power rating (in MW) to meet the target load, the energy rating (in MWh) that the storage unit is required to deliver to the grid or absorb form it at any given cycle, and the characteristic response time. Large variations between on and off-peak electricity demand and generation can effectively be balanced and smoothed out using large-scale electrical storage to provide peak-leveling and shaving options, as shown schematically in Figure 56. Real time regulation of the grid to control and respond to momentary fluctuations caused by the imbalance between load and generation is also a critically important need that can be achieved when combined with proper storage technology. Currently, grid regulation is in large part accomplished by placing generator units that are ready to go online or offline, or increase or decrease their power as needed. Besides lost generation capacity when off-line, such variable power and on/off fluctuations cause their wear and tear on the generation equipment and plants, especially for thermal base-load generators. Another consideration is frequency response, which is similar to regulation but responds to sudden fluctuations, usually in time periods of seconds. Figure 57 illustrates the effects of using grid regulation and frequency response. Electrical storage not only provides time-shift duty, i.e., buying electricity off-peak times or when prices are low, but also prevents wasting of excess generation.

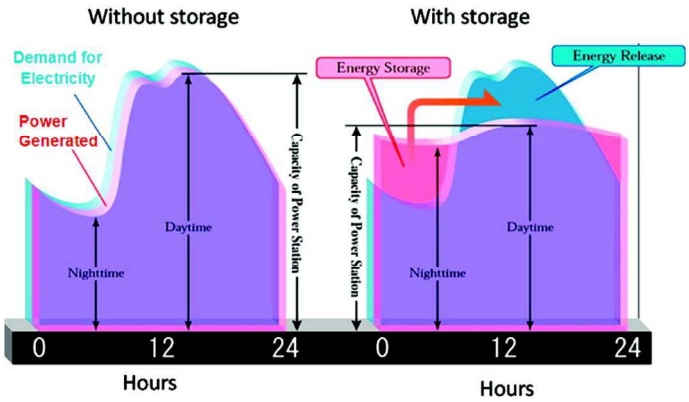

Figure 56. Schematic illustration of balancing the demand and generation by load-leveling via storage [32]. Reprinted with permission from (Z. Yang, J. Zhang, M.C.W. Kintner-Meyer, X. Lu, D. Choi, J.P. Lemmon, J. Liu, Electrochemical energy storage for green grid, Chemical Reviews, 2011, **111**, 3577-3613). Copyright (2018) American Chemical Society.

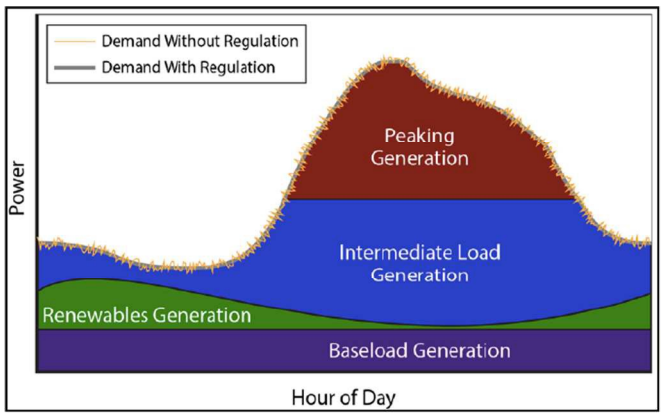

Figure 57. Variation of the load on the grid with and without regulation and frequency response [17].

Load-following, depicted in Figure 57, is characterized by power output that changes frequently within minutes in response to the changing balance between demand and electricity generation and to maintain the scheduled system frequency and establish the interchange with other generation areas. This is particularly important for intermittent and constantly varying renewable power sources such as wind and solar. Storage can

View Article Online
DOI: 10.1039/C8EE01419A

alleviate some of these problems. However, large scale deployment of electrical energy storage technologies and systems for grid applications require that these widely diverse technologies need to overcome several barriers before they can be fully adopted and deployed by the utility industry. Namely, these storage technologies need to demonstrate [17]:

Cost competitiveness: This includes bringing down the cost not just of the storage component (e.g., flywheel, battery, etc), where most of the present focus and attention is concentrated, but also of the balance of plant that makes up the entire storage system, where the storage component makes up roughly 30-40% of the entire system cost. Based on published techno-economic analyses by others, an independent study suggested a target cost for energy storage at < $100/kWh (and power at < $600/kW) [425]. Also important is to quantify the value of storage in terms of the services provided to the grid, such that a single storage unit may capture several revenue streams and achieve economic viability. It is likely that the early deployment for storage systems will happen in high value applications. Hence, it is important to focus on key factors such as life-cycle cost, and performance parameters such as round-trip efficiency, energy density, cycle life, and capacity fading.

Validated performance and safety: Performance and safety evaluation of the storage system should be verified in accordance with the accepted industry codes and standards. For example, the true lifetime of the storage system and the time its takes to generate revenue is important for industry stakeholders and decision makers. Hence, validation of safety, reliability, and performance of the storage system is critically important for gaining the confidence of the user, investor and the insurer.

Equitable regulatory environment: Incentive to invest and install electrical energy storage requires a reliable revenue generation model or roadmap for storage operators. This is largely lacking due partly to inconsistent pricing and market plans, and also to uncertainty in the use-case economics, all of which deter investment. Hence, the value proposition for adopting storage systems for the grid relies on lowering the regulatory barriers.

Industry acceptance: This arguably poses the highest barrier among all. Due to uncertainties about how well these systems perform in practice and over time, system operators many of whom have no or only limited experience with them, are skeptical about adopting storage technologies. Equally important is the inability of today's utility planning, transmission and distribution tools to analyze energy storage as an integral part of their portfolio. Naturally, integration of storage options into industry's planning tools helps build confidence in storage technologies. Acceptance and adoption of grid storage by the industry requires verified confidence that the storage system will deliver and perform as predicted and expected.

A recent US DOE workshop has identified several near- and long-term cost and performance targets for grid applications in order to aid and guide storage technology

View Article Online
DOI: 10.1039/C8EE01419A

researchers and developers of [17]. In the near term, the workshop report recommended demonstration of AC energy storage systems involving redox flow batteries, sodium-based batteries, lead-carbon batteries, lithium-ion batteries and other technologies to meet the following electric grid performance and cost targets; system capital cost - under $250/kWh, levelized cost - under 20 ¢/kWh/cycle, system efficiency - over 75%, and cycle life - more than 4,000 cycles, with system capital cost targets under $1,750/kW. For the long term, the workshop's recommendations included research and development for new technologies based on advanced materials and chemistries to meet the following AC energy storage system targets; system capital cost - under $150/kWh, levelized cost - under 10 ¢/kWh/cycle, system efficiency - over 80%, cycle life - more than 5,000 cycles, with system capital cost targets under $1,250/kW. It also recommended system capital cost of < $15/kWh, system efficiency of 95%, cycle life of 10,000 cycles for concentrated solar power (CSP) storage systems.

These targets, especially for emerging storage technologies are ambitious to meet, and to gain commercial interest storage systems need to add value and be competitive with existing storage technologies. Also, to make progress, it is important to understand the inherent limitations and factors that govern the technical and economical viability of these storage technologies. As a case in point, the global incentive for electric vehicles is driven largely by the commercial availability of Li-ion batteries. But it is estimated that replacing the gasoline engines in transportation vehicles with 15 kWh Li-ion batteries would use up more than 30% of the world's lithium reserves [31]. This may pose a serious limitation. The cost of storage is also a major concern. Although the cost, for example, of the Li-ion battery pack for a 240-mile driving range was estimated several years ago to be nearly $30,000 at $400-800/kWh, this has steadily decreased to $273/kWh in 2016 [426]. However, this is still too expensive, compared to the cost target of < $100/kWh [241,425]. Certainly, source, cost and performance limitations of storage systems need to be overcome. Basic research that can address the challenges and meet the required cost and performance targets for these and other applications will help move practical storage technologies forward.

I. Concluding Remarks and Summary

The 2003 blackout in the U.S. northeast that immersed New York City and the surrounding states into darkness, and the 2011 power failure in southern California and Arizona are recent examples of how critical is the availability of cost-effective, reliable electrical power for our living standards, security, economy, and technology.. Clearly, effective energy storage systems would have helped mitigate such major disruptions. But more so, it is widely agreed that electrical energy storage will help catalyze rapid transformation of the global energy infrastructure towards clean energy technologies, achieve efficient load-leveling and regulation, accelerate mass penetration of renewables, realize distributed generation and local grids, and improve energy security.

View Article Online
DOI: 10.1039/C8EE01419A

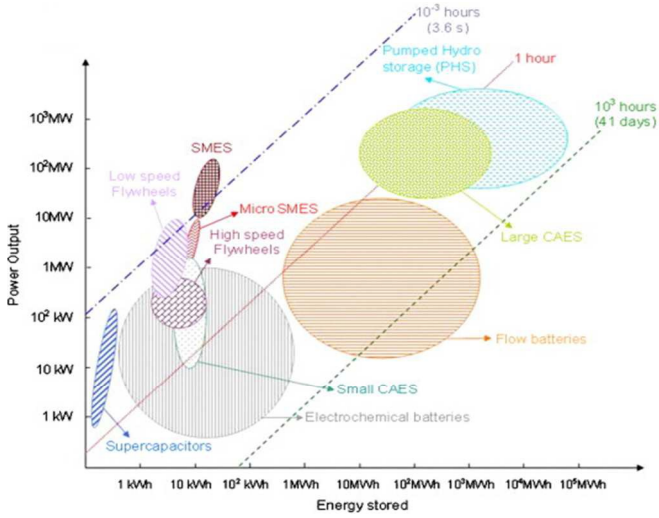

Figure 58. Distribution of storage technologies according to their energy stored and power output, and typical discharge time windows [22]. Reprinted from Renewable and Sustainable Energy Reviews, vol. 12, H. Ibrahim, A. Ilinca, J. Perron, Energy storage systems – characteristics and comparisons, pp. 1221-1259 (2008), with permission from Elsevier.

A case in point is the explosive growth of wind and solar as well as electric vehicles, which in large part is enabled by storage. Deployment and integration of intermittent renewables into the grid without effective storage capabilities poses major challenges, and compromises the stability and integrity of the aging grid systems. Storage can serve as a buffer between electricity supply and demand, and provide flexibility of the grid to allow greater integration of variable renewable resources. Storage also allows power generation, when needed, at or near load centers, thereby augmenting the electricity infrastructure with distributed generation. Technology advances to date provided significant cost reductions. However, full adoption and deployment of storage technologies still requires that the user benefit from multiple potential benefit streams.

Table 12. Characteristic performance requirements for electrical (e) and thermal (t) storage technology applications [427].

Application	Output (electricity, thermal)	Size (MW)	Discharge duration	Cycles (typical)	Response time
Seasonal storage	e,t	500 to 2 000	Days to months	1 to 5 per year	day
Arbitrage	e	100 to 2 000	8 hours to 24 hours	0.25 to 1 per day	>1 hour
Frequency regulation	e	1 to 2 000	1 minute to 15 minutes	20 to 40 per day	1min
Load following	e,t	1 to 2 000	15 minutes to 1 day	1 to 29 per day	<15min
Voltage support	e	1 to 40	1 second to 1 minute	10 to 100 per day	millisecond to second
Black start	e	0.1 to 400	1 hour to 4 hours	< 1 per year	<1 hour
Transmission and Distribution (T&D) congestion relief	e,t	10 to 500	2 hours to 4 hours	0.14 to 1.25 per day	>1hour
T&D infrastructure investment deferral	e,t	1 to 500	2 hours to 5 hours	0.75 to 1.25 per day	>1hour
Demand shifting and peak reduction	e,t	0.001 to 1	Minutes to hours	1 to 29 per day	<15 min
Off-grid	e,t	0.001 to 0.01	3 hours to 5 hours	0.75 to 1.5 per day	<1hour
Variable supply resource integration	e,t	1 to 400	1 minute to hours	0.5 to 2 per day	<15 min
Waste heat utilisation	t	1 to 10	1 hour to 1 day	1 to 20 per day	< 10 min
Combined heat and power	t	1 to 5	Minutes to hours	1 to 10 per day	< 15 min
Spinning reserve	e	10 to 2 000	15 minutes to 2 hours	0.5 to 2 per day	<15 min
Non-spinning reserve	e	10 to 2 000	15 minutes to 2 hours	0.5 to 2 per day	<15 min

Several extensive techno-economic analyses recently claimed that it is possible to realize low-cost grid reliability with 100% penetration of renewables [428], and further proposed an electrification roadmap to achieve 100% renewables (wind, water, solar) for 139 countries in the world [429]. However, the methodology and assumptions employed in these analyses as well as their assessments and conclusions came under question and were challenged by others [430]. It is generally agreed that transition towards a decarbonized energy economy will require the development of a multitude of clean electricity generation and

View Article Online
DOI: 10.1039/C8EE01419A

storage technologies. Indeed, as much diversity as there is in power generation, a broad portfolio of electrical energy storage technologies and systems is needed to respond appropriately and cost-effectively to the wide spectrum of specific requirements of divergent electricity production systems. Each electrical storage technology offers its unique set of advantages and challenges, as well as operational characteristics such as discharge times that may be best suited for a particular application. This is depicted in Figure 7 above, and also in Figure 58. For example, flywheels and supercapacitors can provide high power with fast response times in a matter of seconds to respond to fluctuations in demand but have low energy densities, whereas metal-air and flow batteries offer high energy densities. In other words, the choice for the right system requires matching the system performance characteristics and cost, with the requirements of the desired application. Many of these electricity storage applications and their characteristic system and storage requirements are summarized in Table 12, where the terminology "arbitrage" refers to the trade practice in the energy business whereby electricity that was bought (and stored) at low price during low demand is sold back to the market during high-priced demand, "voltage support" refers to injection and absorption of reactive power to the system to maintain the desired voltage levels in the distribution and transmission systems, and "black start" refers to restarting the electrical supply system after catastrophic power failure without pulling power from the grid. Likewise, "spinning reserve" refers to the response time of less than 15 minutes for the stored reserve electricity capacity to kick in in order to compensate for the loss of generation capacity elsewhere in the system, and "non-spinning" reserve relates to response times longer than 15 minutes.

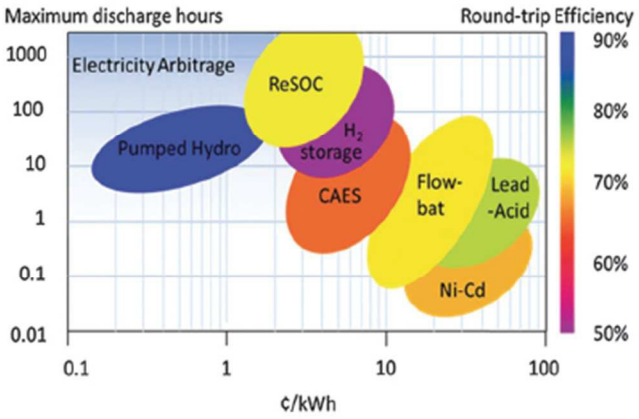

Figure 59. Comparison of cost of electricity storage, round-trip efficiencies and discharge times of various storage systems [32]. Reprinted with permission from (Z. Yang, J. Zhang, M.C.W. Kintner-Meyer, X. Lu, D. Choi, J.P. Lemmon, J. Liu, Electrochemical energy storage for green grid, Chemical Reviews, 2011, **111**, 3577-3613). Copyright (2018) American Chemical Society.

For comparison and compatibility purposes, Table 13 presents typical performance characteristics of various energy storage systems and technologies, which show widely varying ranges of performance parameters. As also discussed in section H. Grid Storage, the storage times and capacities vary widely depending on the application. Comparing Tables 12 and 13 makes it clear that no single storage system or technology can alone meet these requirements fully. This necessitates the development of multiple storage technologies to fully meet the varying needs of grid electricity storage.

View Article Online
DOI: 10.1039/C8EE01419A

Distributed storage offers many advantages, although not all storage systems reviewed in this article are suitable for this purpose. Pumped-hydro and CAES require specific geographic conditions and may not be a viable option available widely. On the other hand, systems such as batteries, regenerative fuel cells, flywheels, and chemical storage may be available regardless of location to couple into renewable energy sources or into the local grid. For example, instead of building a centralized power plant of 1 GW, placing 100 of 10 kW battery storage capacity in utility service areas would help reduce the loads, but more importantly, eliminate expensive "spinning reserves", i.e., supplementary power generated typically by gas turbines that fire up to respond to daily spikes in electric demand. Moreover, such distributed storage also helps improve energy security greatly.

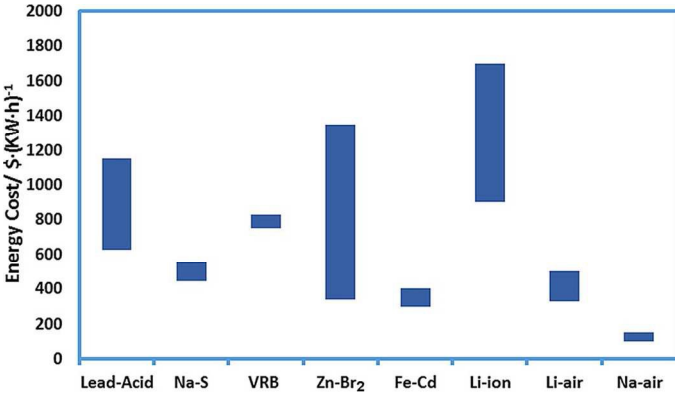

Figure 60. Energy costs ($/kWh) of various battery systems [432]. Reprinted from ChemCatChem, vol. 9, W.-W. Yin, Z.-W. Fu, The potential of Na-air batteries, pp. 1545-1553 (2017), with permission from John Wiley and Sons.

The infrastructure for power transmission and distribution in the US as well as in many other parts of the world is old and even antiquated. For political, legal, environmental and social reasons, replacing or upgrading the existing grid system is challenging and expensive. Distributed storage may alter this paradigm, and shift power generation from centralized stations that require a vast network of expensive and lossy transmission and distribution systems, to having local control and energy security. Naturally, such distributed mode is easier to manage than a vast national grid, which requires a network of computers working in tandem to control the flow of electricity and are vulnerable to hacking and other malicious attacks.

Table 13. Typical performance characteristics of various energy storage systems and technologies [431].

	Power Rating (MW)	Discharge Time	Cycles or Lifetime	Self-discharge (%)	Energy Density (Wh/l)	Power Density (W/l)	Efficiency (%)	Response Time
Pumped-hydro	100-2,500	4 -16 h	30 - 60 yr	~ 0	0.2 - 2	0.1 – 0.2	70 - 85	10 s - min
Compressed Air	100-1,000	2 - 30 h	20 - 40 yr	~ 0	2 - 6	0.2 – 0.6	40 - 70	min
Flywheel	0.001-20	sec - min	20,000 – 100,000	1.3 - 100	20 - 80	5,000	70 - 95	< sec
Li-ion Battery	0.05-100	1 min - 8 h		0.1 – 0.3	200 - 400	1,300 – 10,000	85 - 95	< sec
Lead-acid Battery	0.001-100	1 min - 8 h	6 – 40 yr	0.1 – 0.3	50 80	90 - 700	80 - 90	< sec
Na-S Battery	10-100	1 min – 8 h	2,500 – 4,500	0.05 - 20	150 - 300	120 - 160	70 - 90	< sec
Flow Battery	0.1-100	hours	12,000 – 14,000	0.2	20 - 70	0.5 - 2	60 - 85	< sec
Supercon. Magnet	0.1-1	ms - sec	100,000	10 - 15	~ 6	~ 2,600	80 - 95	< sec
Super-capacitor	0.01-1	ms - min	10,000 – 100,000	20 - 40	10 - 20	40,000 – 120,000	80 - 95	< sec
Hydrogen	0.01-100	min - week	5 - 30 yr	0 - 4	600 (200 bar)	0.2 - 20	25 - 45	sec - min
Synthetic Natural Gas	1-100	hour - week	30 yr	~ 0	1800 (200 bar)	0.2 - 2	25 - 50	sec - min
Molten Salt (Latent thermal)	1-150	hours	30 yr	N/A	70 - 210	N/A	80 - 90	min

As economics of storage is as important as performance, the corresponding cost of electricity storage of various electrical storage systems are

View Article Online
DOI: 10.1039/C8EE01419A

compared with respect to their round-trip efficiencies and discharge times in Figure 59. The data suggests that regenerative SOFCs with their high round-trip efficiency, long discharge times, and low storage cost can compete favorably with pumped-hydro and CAES technologies, albeit their maturity is far from being deployed on a commercial scale. Similarly, cost of electricity storage for various rechargeable battery systems are presented in Figure 60. Although there is considerable uncertainty in the estimated cost figures, Na-S and Li-air batteries show favorable economics, while cost reductions in others, such as VRB and Li-ion batteries, are needed for wide scale implementation of these systems. Unfortunately, none of the battery systems singly satisfies the full set of performance, size and economic requirements for effective electrical storage. Instead, each storage technology reviewed here offers characteristic properties and specific benefits as well as shortcomings and challenges. In other words, there is no silver bullet for electrical energy storage. One size does not fit all. Therefore, a multi-prong technology approach is desirable to adequately address the global needs for electrical energy storage in a comprehensive manner.

For example, there may be merit in considering smaller size batteries in the 5-10 kW range for energy storage for the grid. One prevailing view for megawatt-scale storage batteries is to place them on the high voltage (>10 kV) side of the utility transformer, which would then require multiple step-down transformers and other controls that would complicate the hook-up process. On the other hand, smaller batteries in the 10 kW range can be placed instead on the 100 V side of the transformer, which would render a simple hook up process and enable to achieve switching using inexpensive solid-state relays.

In assessing storage systems, source availability and access also need to be considered in the life cycle analysis. For example, Li-based batteries may be vulnerable to the cost and availability of lithium, which is largely mined and produced in select countries in the world. Other active chemicals, such as cobalt that are currently used in commercial Li-ion batteries pose also concerns regarding cost, scarcity, and availability. Other battery systems employ toxic elements in their electrodes such as lead, cadmium, and mercury, which are of great health and environmental concern. Precious metal catalysts used in other electrochemical storage systems such as low temperature aqueous electrolyzers are also expensive and source-dependent elements. So recycling battery components may supplement availability, and is definitely of practical, environmental and economic interest. For example, it takes 250 tons mineral ore and 750 tons of brine to produce 1 ton of lithium, compared to only 28 tons of used Li-batteries [433]. There have been recycling efforts to collect and re-process used batteries to recover active elements. However, for wide scale and cost-effective recovery of these spent resources, we need to develop more efficient, higher yield and inexpensive recycling processes, and also implement global environmental policies that mobilize a concerted recycling effort.

In a manner similar to cost of storage, another important consideration should be given to the amount of emissions produced during the life of storage systems. For example, based on life cycle analysis results it was estimated that to make a 1 kWh Li-ion battery, nearly

View Article Online
DOI: 10.1039/C8EE01419A

400 kWh of energy is consumed [433], resulting in 75 kg of CO_2 emissions during its production. Simple arithmetic suggests that the service life of the Li-ion battery needs to be >400 cycles to pay pack the energy in terms of storage. By comparison, a coal-fired power plant emits only 1 kg of CO_2 for every 1 kWh of electrical energy it produces. Accordingly, these comparative examples highlight the importance of long service life for the storage system before its benefits can have a positive impact on the environment.

It should be noted that theoretical energy densities for electrochemical storage systems are usually calculated based on the weight and volume of the active materials, which constitute only a portion of the final packaged product. Hence, real energy densities are necessarily lower than those calculated theoretically. This is illustrated in Table 14, where average efficiencies for major systems are in range of 10s of %. Only, Li-ion batteries seem to reach a relatively high energy utilization level between 42 and 58%. Surely, there is room for major improvements in active materials for electrochemical storage technologies that will help increase storage efficiencies of these systems. Better sealing and packaging processes and cost-effective materials will also help reduce this discrepancy between calculated and actual utilization capacities. So more work and innovation is needed to improve existing technologies and expand the storage options. For example, in most electrochemical storage systems such as batteries, only single-electron transfer reactions have been utilized. In today's Li-ion batteries, for example, less than only one Li^+ ion is intercalated per transition metal redox center in the cathode material. Obviously, this limits the ultimate capacity of the battery. A recent article challenges this paradigm and suggests that for next generation batteries, it may be worth exploring multi-electron transfer chemistries, by either intercalating multivalent cations per redox site or intercalating multiple monovalent cations [434]. Certainly, accomplishing this goal will greatly improve the practically realizable capacity for electrochemical storage. Similarly, development of earth-abundant materials with superior catalytic properties for regenerative fuel cells, electrolyzers for hydrogen production, electrochemical reactors for ammonia synthesis, highly conductive, stable and selective membranes used in most electrochemical storage systems, and cost-effective EDL and pseudocapacitive electrode materials for supercapacitors will help expand the materials space, improve device performance, and bring down systems costs. In that regard, two additional tools, namely theoretical and computational simulations guiding experimentation and rational design of materials, as well as nanostructuring to control and enhance desirable properties will help shorten the pathway to innovation and discovery. Moreover, nanostructured materials may

Table 14. Theoretical and actual energy densities and actual utilization percentages for select electrochemical storage with various battery systems compared with the H_2/O_2 fuel cell [44].

System	Calculated energy density (Wh/kg)	Real energy density (Wh/kg)	Utilization (%)
Pb-acid	171	25-55	15-32
Na-S	792	80-150	10-19
Ni-MH	240	50-70	20-29
Li-ion	360	150-210	42-58
Li-S	2654	250-350	9-13
Li-O_2	5217	-	-
Zn-O_2	1094	150-200	14-18
H_2-O_2	3525	120-800	3-23

View Article Online
DOI: 10.1039/C8EE01419A

form highly active metastable structures and exhibit properties different from bulk, and offer attractive opportunities in overcoming some of the kinetic and mass transport limitations observed in energy storage systems.

Certainly, storage is an essential component of the global energy systems of the future, especially if renewables were to take on 80% of the global need [16]. The maturities, or technology readiness levels (TRL), of storage technologies vary widely as illustrated in Figure 5. Similarly, the U.S. DOE's view of the evolution, cost reduction and market penetration of storage technologies is expected to follow the trends depicted in Figure 7, i.e., there will be both short term and long term milestones and goals that need to be achieved.

In recent years, there has been an increasing drive to build more storage capacity. Some of the projects around the world that are based on electrochemical energy storage are summarized in Table 15 and categorized according to the storage system and country [16]. It is clear that the installed capacities provided in Tables 2 and 14 are quite low compared to the storage needs for solar and wind (see Table 1) that may require durations between hours to days, and in some remote applications, even weeks.

The variability of the storage technologies, systems and materials make it hard to predict which technologies will excel, but successful commercialization of any one or more of the different systems will likely depend on the confluence of several important factors. Certainly, the technical challenges discussed and reviewed in this article must be overcome to achieve reliable, robust, long service and cycle life, efficient, and scalable technology options. Likewise, materials and fabrication costs must be reduced further for many these systems and technologies to become truly competitive. Large investments both public and private are required to achieve these goals. Market forces of supply and demand fueled by the rapid expansion and growth in renewables such as solar and wind, will also drive the need for large-scale storage. But this may still not be sufficient to achieve complete decarbonization of the electricity infrastructure, which we urgently need to make happen. Without globally accepted policies to implement an agreeable price on carbon emissions, storage may not receive the attention or the investment it deserves, and we may not achieve complete decarbonization of the global energy system, risking undesired consequences.

Table 15. Major electrochemical storage projects that are announced, contracted or under construction by technology and country [16].

Country	Electro-chemical (unspecified)	Electro-chemical Capacitor	Lithium-ion Battery	Flow Battery	Vanadium Redox Flow Battery	Lead-acid Battery	Metal-Air Battery	Sodium-based Battery	Total (kW)
United States	500 398		61 959	3 030	20 250	21 500	14 250		621 397
Australia	122 010		9 400						131 410
Germany	30 000		92 000	210					122 210
India	110 000		125						110 125
Republic of Korea			48 500						48 500
Canada	12 150		12 010	4 000	5 000				33 160
Egypt			30 000						30 000
Italy		1 920	20 000	1 950				4 000	27 870
Kazakhstan				25 000					25 000
United Kingdom	1 000		20 300	140					21 440
Top 10	775 558	1 920	294 304	34 330	25 250	21 500	14 250	4 000	1 171 112
World	784 258	2 920	333 404	34 965	25 250	21 500	5 650	4 800	1 212 747

View Article Online
DOI: 10.1039/C8EE01419A

In summary, as much as we need a broad range of electric power technologies to meet our needs, we need an equally diverse portfolio of energy storage technologies with matching operational characteristics and properties. The urgent need for large-scale cost effective storage has become increasingly pronounced by the rapid growth and deployment of renewable power generation sources. It is difficult to predict which of the energy storage technologies will dominate the future, but most likely, a broad range of storage systems will be needed to accommodate the specific but diverse requirements of the equally diverse power generation technologies we employ today, and in the future. Meeting the requirements of such a rich diversity of individual system characteristics certainly poses technical challenges as discussed in this article, but it also provides a wide range of options and prospects for storage applications, especially when these technologies may be employed in synergistic combinations that complement each other's strengths and compensate for their deficiencies. It also offers opportunities for innovation and advancements in storage technologies, materials and processes, where the scientific community has an important role to play.

b. **Conflicts of interest**

The author has no conflicts to declare.

c. **Acknowledgements**

The author gratefully acknowledges partial support from the Stanford Energy 3.0 Program, and many helpful discussions with Prof. Friedrich B. Prinz of Stanford University.

d.

e.

f. **References**

1. DOE-EIA International Energy Outlook 2017 (Sept. 2017) report No: DOE/EIA-0484(2017) https://www.eia.gov/outlooks/ieo/ieo_tables.php, (accessed Nov. 2, 2017)
2. World Energy Outlook 2015, International Energy Agency, London, Nov. 10, 2015, see http://www.worldenergyoutlook.org/weo2015/

View Article Online
DOI: 10.1039/C8EE01419A

3. Global Greenhouse Gas Emissions Data (2017), U.S. Environmental Protection Agency, https://www.epa.gov/ghgemissions/global-greenhouse-gas-emissions-data, (accessed Nov 10, 2017)

4. T.M. Gür, Low-carbon electricity is great. What about "less-carbon"?, J. Electrochem. Soc. 2017, **164**, F1587-F1590

5. T.M. Gür, Critical Review of Carbon Conversion in "Carbon Fuel Cells", Chemical Reviews, 2013, **113**, 6179-6206

6. T.M. Gür, Comprehensive Review of Methane Conversion in Solid Oxide Fuel Cells: Prospects for Efficient Electricity Generation from Natural Gas, Progress in Energy and Combustion Science, 2016, **54**, 1-64

7. Next Generation Wind and Solar Power: From cost to value. IEA 2016 report, https://www.iea.org/publications/freepublications/publication/Next_Generation_Wind and_Solar_PowerFrom_Cost_to_ValueFull_Report.pdf

8. www.independent.co.uk/environment/solar-and-wind-power-cheaper-than-fossil-fuels-for-the-first-time-a7509251.html, (accessed Nov 10, 2017)

9. International Energy Agency, World Energy Outlook 2016 (Nov. 2016), also see http://www.iea.org/newsroom/news/2016/november/world-energy-outlook-2016.html

10. www.bloomberg.com/news/articles/2016-12-15/world-energy-hits-a-turning-point-solar-that-s-cheaper-than wind, (accessed Nov 10, 2017)

11. DOE-EIA International Energy Outlook 2017 (Sept. 2017) report No: DOE/EIA-0484(2017) https://www.eia.gov/outlooks/ieo/ieo_tables.php, (accessed Nov. 2, 2017)

12. U.S.-DOE Energy Information Administration, Today in Energy, https://www.eia.gov/todayinenergy/detail.php?id=31372, (accessed Nov. 19, 2017)

13. Bloomberg Technology News, July 31, 2017, https://www.bloomberg.com/news/articles/2017-07-31/alphabet-wants-to-fix-renewable-energy-s-storage-problem-with-salt

14. www.latimes.com/projects/la-fi-electricity-solar/

15. DOE Global Energy Storage Database, Office of Electricity Delivery and Energy Reliability, http://www.energystorageexchange.org/projects/data_visualization (accessed Nov. 9, 2017)

16. Electricity Storage and Renewables: Costs and Markets to 2030, International Renewable Energy Agency (IRENA 2017), available at http://www.irena.org/-/media/Files/IRENA/Agency/Publication/2017/Oct/IRENA_Electricity_Storage_Costs_2017.pdf (accessed July 6, 2018)

View Article Online
DOI: 10.1039/C8EE01419A

17. Grid Energy Storage, US Department of Energy, Dec. 2013, http://www.energy.gov/sites/prod/files/2014/09/f18/Grid%20Energy%20Storage%20December%202013.pdf

18. Energy Technology Perspectives 2015, International Energy Agency, www.iea.org/newsroomandevents/graphics/2015-06-30-installed-global-capacity-for-grid-connected-storage.html

19. B. Dunn, H. Kamath, J. M. Tarascon, Electrical energy storage for the grid: A battery of choices, Science, 2011, **334**, 928-935

20. Electrical Energy Storage Technology Options report #1020676, Dec. 2010, Electric Power Research Institute, Palo Alto, CA

21. K.M. Abraham, Prospects and limits of energy storage in batteries, J. Phys. Chem. Lett. 2015, **6**, 830-844

22. H. Ibrahim, A. Ilinca, J. Perron, Energy storage systems – characteristics and comparisons, Renew. Sustain. Energy Rev., 2008, **12**, 1221-1259

23. C. Liu, F. Li, L.-P. Ma, H.-M. Cheng, Advanced materials for energy storage, Adv. Energy Mater. 2010, **22**, E28-E62

24. I. Hadjipaschalis, A. Poullikkas, V. Efthimiou, Overview of current and future energy storage technologies for electric power applications, Renew. Sustain. Energy Rev., 2009, **13**, 1513-1522

25. P. J. Hall, E. J. Bain, Energy-storage technologies and electricity generation, Energy Policy, 2008, **36**, 4352-4355

26. H. B. Radousky, H. Liang, Energy harvesting: an integrated view of materials, devices, and applications, Nanotechnology, 2012, **23**, 502001 1-35

27. A. Evans, V. Strezov, T.J. Evans, Assessment of utility energy storage options for increased renewable energy penetration, Renew. Sustain. Energy Rev., 2012, **16**, 4144-4147

28. X. Luo, J. Wang, M. Dooner, J. Clarke, Overview of current development in electrical energy storage technologies and the application potential in power system operations, Appl. Energy, 2015, **137**, 511-536

29. E.D. Wachsman, C.A. Marlowe, K.T. Lee, Role of solid oxide fuel cells in a balanced energy strategy, Energy Environ. Sci. 2012, **5**, 5498-5509

30. A.S. Arico, P. Bruce, B. Scrosati, J.-M. Tarascon, W.V. Schalkwijk, Nanostructured materials for advanced energy conversion and storage devices, Nature Mater. 2005, **4**, 366-377

31. M. Armand, J.-M. Tarascon, Building better batteries, Nature, 2008, **451**, 652-657

View Article Online
DOI: 10.1039/C8EE01419A

32. Z. Yang, J. Zhang, M.C.W. Kintner-Meyer, X. Lu, D. Choi, J.P. Lemmon, J. Liu, Electrochemical energy storage for green grid, Chemical Reviews, 2011, **111**, 3577-3613

33. M.S. Whittingham, Materials challenges facing electrical energy storage, MRS Bull. 2008, **33**, 411-419

34. C.J. Barnhart, S.M. Benson, On the importance of reducing the energetic and material demands of electrical energy storage, Energy Environ. Sci. 2013, **6**, 1083-1092

35. D.A.J. Rand, A journey on the electrochemical road to sustainability, J. Solid State Electrochem. 2011, **15**, 1579-1622

36. M. Winter, R.J. Brodd, What are batteries, fuel cells, and supercapacitors?, Chem. Rev. 2004, **104**, 4245-4269

37. O. Groger, H.A. Gesteiger, J.-P. Suchsland, Review-Electromobility: Batteries or fuel cells?, J. Electrochem. Soc. 2015, **162**, A2605-A2622

38. S. Muench, A. Wild, C. Friebe, B. Haupoler, T. Janoschka, U.S. Schubert, Polymer-based organic batteries, Chem. Rev. 2016, **116**, 9438-9484

39. J.M. Tarascon, M. Armand, Issues and challenges facing rechargeable lithium batteries, Nature, 2001, **414**, 359-367

40. P. G. Bruce, Energy storage beyond the horizon: Rechargeable lithium batteries, Solid State Ionics, 2008, **179**, 752-760

41. W. Wakihara, O. Yamamoto (eds.), Lithium Ion Batteries: Fundamentals and Performance, published jointly by Kodansha Ltd. Tokyo (Japan), and Wiley-VCH Verlag GmbH, Weinheim (Germany), Tokyo (1998),

42. B. Kang, G. Ceder, Battery materials for ultrafast charging and discharging, Nature Lett. 2009, **458**, 190-193

43. N.-S. Choi, Z. Chen, S. A. Freunberger, X. Li, Y.-K. Sun, K. Amine, G. Yushin, L. F. Nazar, J. Cho, P. G. Bruce, Challenges facing lithium batteries and electrical double layer capacitors, Angew. Chem. Int. Ed. 2012, **51**, 9994-1124

44. C.X. Zu, H. Li, Thermodynamic analysis on energy densities of batteries, Energy Environ. Sci. 2011, **4**, 2614-2624

45. M.S. Whittingham, Lithium batteries and cathode materials, Chem. Rev., 2004, **104**, 4271-4301

46. M.S. Whittingham, Ultimate limits of intercalation reactions for lithium batteries, Chem. Rev. 2014, **114**, 11414-11443

47. B.L. Ellis, K. T. Lee, L. F. Nazar, Positive electrode materials for Li-ion and Li-batteries, Chem. Mater. 2010, **22**, 691-714

48. J.B. Goodenough, Y. Kim, Challenges for rechargeable Li batteries, Chem. Mater. 2010, **22**, 587-603

View Article Online
DOI: 10.1039/C8EE01419A

49. B. Scrosati, Lithium rocking chair batteries: An old concept?, J. Electrochem. Soc. 1992, **139**, 2776-2781

50. J.B. Goodenough, K.-S. Park, The Li-ion rechargeable battery: A perspective, J. Am. Chem. Soc. 2013, **135**, 1167-1176

51. B. Scrosati, J. Garche, Lithium batteries: Status, prospects and future, J. Power Sources, 2010, **195**, 2419- 2430

52. V. Etacheri, R. Marom, R. Elazari, G. Salitra, D. Aurbach, Challenges in the development of advanced Li-ion batteries: A review, Energy Environ. Sci. 2011, **4**, 3243-3262

53. J.W. Choi, D. Aurbach, Promise and reality of post-lithium-ion batteries with high energy densities, Nature Review Materials, 2016, **1**, 1-16

54. K. Xu, Nonaqueous liquid electrolytes for lithium-based rechargeable batteries, Chem. Rev. 2004, **104**, 4303-4418

55. M. Armand, F. Endres, D.R. MacFarlane, H. Ohno, B. Scrosati, Ionic-liquid materials for the electrochemical challenges of the future, Nature Mater. 2009, **8**, 621-629

56. C.A. Angell, Y. Ansari, Z. Zhao, Ionic liquids: Past, present and future, Faraday Discuss. 2012, **154**, 9-27

57. F. Croce, L. Persi, F. Ronci, B. Scrosati, Nanocomposite polymer electrolytes and their impact on the lithium battery technology, Solid State Ionics, 2000, **135**, 47-52

58. P.V. Wright, Developments in polymer electrolytes for lithium batteries, MRS Bull. 2002, **27**, 597-602

59. V. Thangadurai, S. Narayanan, D. Pinzaru, Garnet-type solid-state fast Li ion conductors for Li batteries: Critical review, Chem. Soc. Rev. 2014, **43**, 4714-4727

60. W. Li, J.R. Dahn, D.S. Wainwright, Rechargeable lithium batteries with aquesous electrolytes, Science, 1994, **264**, 1115-1118

61. C. Yang, J. Chen, T. Qing, X. Fan, W. Sun, A. von Cresce, M.S. Ding, O. Borodin, J. Vatamanu, M.A. Schroeder, N. Eidson, C. Wang, K. Xu, 4.0 V Aqueous Li-ion batteries, Joule, 2017, **1**, 122-132

62. M.N. Obrovac, V.L. Chevrier, Alloy Negative electrodes for Li-ion batteries, Chem. Revs. 2014, **114**, 11444-11502

63. U. Kasavajjula, C.S. Wang, A.J. Appleby, Nano- and bulk-silicon-based anodes for lithium-ion secondary cells, J. Power Sources, 2007, **163**, 1003-1039

64. X.-B. Cheng, R. Zhang, C.-Z. Zhao, Q. Zhang, Toward safe lithium anode in rechargeable batteries: A review, Chem. Rev. 2017, **117**, 10403-10473

65. C.J. Wen, B.A. Boukamp, R.A. Huggins, W. Weppner, Thermodynamics and mass transport properties of "LiAl", J. Electrochem. Soc. 1979, **126**, 2258-2266

View Article Online
DOI: 10.1039/C8EE01419A

66. W. Weppner, R.A. Huggins, Determination of the kinetic parameters of mixed-conducting electrodes and application to the system Li_3Sb, J. Electrochem. Soc. 1977, **124**, 1569-1578

67. W. Weppner, R.A. Huggins, Electrochemical investigation of the chemical diffusion, partial ionic conductivities, and other kinetic parameters in Li_3Sb and Li_3Bi, J. Solid State Chem. 1977, **22**, 297-308

68. B.A. Boukamp, G.C. Lesh, R.A. Huggins, All-solid lithium electrodes with mixed-conducting matrix, J. Electrochem. Soc. 1981, **128**, 725-729

69. C.K. Chan, H. Peng, G. Liu, K.McIlwrath, X.F. Zhang, R.A. Huggins, Y. Cui, High-performance lithium battery anodes using silicon nanowires, Nature Nanothechnol. 2008, **3**, 31-35

70. C.J. Wen, R.A. Huggins, Thermodynamic study of the lithium tin system, J. Electrochem. Soc. 1981, **128**, 1181-1187

71. J.E. Trevey, A.F. Gross, J. Wang, P. Liu, J.J. Vajo, Stable cycling and excess capacity of a nanostructured Sn electrode based on $Sn(CH_3COO)_2$ confined within a nanoporous carbon scaffold, Nanotechnol. 2013, **24**, 424001-1-6

72. M.S. Whittingham, Electrical energy storage and intercalation chemistry, Science, 1976, **192**, 1126-1127

73. I.H. Son, J. H. Park, S. Kwon, S. Park, M. H. Rummeli, A. Bachmatiuk, H. J. Song, J. Ku, J. W. Choi, J.-M. Choi, S.-G. Doo, H. Chang, Silicon carbide-free graphene growth on silicon for lithium-ion battery with high volumetric energy density, Nature Comm. 2015, **6**, 7393

74. C. K. Chan, H. Peng, G. Liu, K. McIlwrath, X. F. Zhang, R. A. Huggins, Y. Cui, High-performance lithium battery anodes using silicon nanowires, Nature Nanotechnol. 2008, **3**, 31-35

75. H. Wu, Y. Cui, Designing nanostructured Si anodes for high energy lithium batteries, NanoToday, 2012, **7**, 414-429

76. Y.-M. Chiang, Building a better battery, Science, 2010, **330**, 1485-1486

77. T. Jiang, R. Zhang, Q. Yin, W. Zhou, Z. Dong, N.A. Chernova, Q. Wang, F. Omenya, M.S. Whittingham, Morphology, composition and electrochemistry of a nano-porous silicon versus bulk silicon anode for lithium-ion batteries, J. Mater. Sci. 2017, **52**, 3670-3677

78. S. Goriparti, E. Miele, F. De Anglesi, E. Di Fabrizio, R.P. Zaccaria, C. Capiglia, Review on recent progress of nanostructured anode materials for Li-ion batteries, J. Power Sources, 2014, **257**, 421-443

79. N.A. Kaskhedikar, J. Maier, Lithium storage in carbon nanostructures, Adv. Mater. 2009, **21**, 2664-280

View Article Online
DOI: 10.1039/C8EE01419A

80. G. Liu, S. Xun, N. Vukmirovic, X. Song, P. Ollade-Velasco, H. Zheng, V.S. Battaglia, L. Wang, W. Yang, Polymers with tailored electronic structure of high capacity lithium battery electrodes, Adv. Mater. 2011, **23**, 4679-4683

81. G. Zheng, S.W. Lee, Z. Liang, H.-W. Lee, K. Yan, H. Yao, H. Wang, W. Li, S. Chu, Y. Cui, Interconnected hollow carbon nanospheres for stable lithium metal anodes, Nature Nanotechnol. 2014, **9**, 618-623

82. M.T. McDowell, S.W. Lee, I. Ryu, H. Wu, W.D. Nix, J.W. Choi, Y. Cui, Novel size and surface oxide effects in silicon nanowires as lithium battery anodes, Nano Lett. 2011, **11**, 4018-4025

83. Y.P. Wu, E. Rahm, R. Holze, Carbon anode materials for lithium ion batteries, J. Power Sources, 2003, **114**, 228-236

84. M. Thackeray, Lithium-ion batteries: An unexpected conductor, Nature Mater. 2002, **1**, 81-82

85. H. Tukamoto, A.R. West, Electronic conductivity of $LiCoO_2$ and its enhancement by magnesium doping, J. Electrochem. Soc. 1997, **144**, 3164-3168

86. C.H. Chen, J.T. Vaughey, A.N. Jansen, D.W. Dees, A.J. Kahaian, T. Goacher, M.M. Thackeray, Studies of Mg-substituted $Li_{4-x}Mg_xTi_5O_{12}$ spinel electrodes ($0 \leq x \leq 1$) for lithium batteries, J. Electrochem. Soc. 2001, **148**, A102-A104

87. A.K. Padhi, K.S. Nanjundaswamy, J.B. Goodenough, Phospho-olivines as positive-electrode materials for rechargeable lithium batteries, J. Electrochem. Soc. 1997, **144**, 1198-1194

88. N. Ravet, Y. Chouinard, J.F. Magnan, S. Besner, M. Gauthier, M. Armand, Electroactivity of natural and synthetic triphylite, J. Power Sources, 2001, **97-98**, 503-507

89. Q. Wang, S.M. Zakeerudin, D. Wang, I. Exnar, M. Graetzel, Redox targeting of insulating electrode materials: A new approach to high-energy density batteries, Angew. Chem. 2006, **45**, 8197-8200

90. S.-Y. Chung, J.T. Bloking, Y.-M. Chiang, Electronically conductive phosphor-olivines as lithium storage electrodes, Nature Mater. 2002, **1**, 123-128

91. J.-M. Tarascon, N. Recham, M. Armand, J.-N. Chotard, P. Barpanda, W. Walker, L. Dupont, Hunting for better Li-based electrode materials via low temperature inorganic synthesis, Chem. Mater. 2010, **22**, 724-739

92. G. Amatucci, J.-M. Tarascon, Optimization of insertion compounds such as $LiMn_2O_4$ for Li-ion batteries, J. Electrochem. Soc. 2002, **149**, K31-K46

93. K.G. Gallagher, S. Goebel, T. Greszler, M. Mathias, W. Oelerich, D. Eroglu, V. Srinivasan, Quantifying the promise of lithium-air batteries for electric vehicles, Energy Environ. Sci. 2014, **7**, 1555-1563

94. M.D. Radin, S. Hy, M. Sina, C. Fang, H. Liu, J. Vinckeviciute, M. Zhang, M.S. Whittingham, Y.S. Meng, A.V. der Ven, Narrowing the gap between theoretical and practical

View Article Online
DOI: 10.1039/C8EE01419A

capacities in Li-ion layered oxide cathode materials, Adv. Energy Mater. 2017, **7**, 1602888 -1-33

95. P. Poizot, S. Laruelle, S. Grugeon, L. Dupont, J.-M. Tarascon, Nano-sized transition-metal oxides as negative-electrode materials for lithium-ion batteries, Nature, 2000, **407**, 496-499

96. F. Badway, N. Pereira, F. Cosandey, G. G. Amatucci, Carbon metal fluoride nanocomposites: Structure and electrochemistry of FeF_3:C, J. Electrochem. Soc. 2003, **150**, A1209-1218

97. N. Yamakawa, M. Jiang, B. Key, C. P. Grey, Identifying the local structures formed during lithiation of the conversion material, iron fluoride, in a Li ion battery: A solid-state NMR, X-ray diffraction, and pair distribution function analysis study, J. Am. Chem. Soc. 2009, **131**, 10525-10536

98. F. Badway, F. Cosandey, N. Pereira, G. G. Amatucci, Carbon metal fluoride nanocomposites: High capacity reversible metal fluoride conversion materials as rechargeable positive electrodes for Li batteries, J. Electrochem. Soc. 2003, **150**, A1318-1327

99. F. Wang, R. Robert, N.A. Chernova, N. Pereira, F. Omenya, F. Badway, X. Hua, M. Ruotolo, R. Zhang, L. Wu, V. Volkov, D. Su, B. Key, M.S. Whittingham, C.P. Grey, G.G. Amatucci, Y. Zhu, J. Graetz, Conversion reaction mechanisms in lithium ion batteries: Study of the binary metal fluoride electrodes, J. Am. Chem. Soc. 2011, **133**, 18828-18836

100. E. Peled, The electrochemical behavior of alkali and alkaline earth metals in nonaqueous battery systems – the Solid Electrolyte Interphase model, J. Electrochem. Soc. 1979, **126**, 2047-2051

101. H.-G. Steinruck, C. Cao, Y. Tsao, C.J. Takacs, O. Konovalov, J. Vatamanu, O. Borodin, M.F. Toney, The nanoscale structure of the electrolyte-metal oxide interface, Energy Environ. Sci. 2018, DOI: 10.1039/c7ee0272a

102. D. Aurbach, B. Markovsky, G. Salitra, E. Markevich, Y. Talyossef, M. Koltypin, L. Nazar, B. Ellis, D. Kavacheva, Review on electrode-electrolyte solution interactions, related to cathode materials for Li-ion batteries, J. Power Sources, 2007, **165**, 491-499

103. K. Xu, Electrolytes and interphases in Li-ion batteries and beyond, Chem. Rev. 2014, **114**, 11503-11618

104. R. Chen R, W. Qu W, X. Guo X, L. Li L, F. Wu, The pursuit of solid-state electrolytes for lithium batteries: from comprehensive insight to emerging horizons, Mater. Horiz. 2016, **3**, 487-516

105. R.A. Huggins, Do you really want an unsafe battery?, J. Electrochem. Soc. 2013, **160**, A3001-A3005

View Article Online
DOI: 10.1039/C8EE01419A

106. R. Tao, X. Bi, S. Li, Y. Yao, F. Wu, Q. Wang, C. Zhang, J. Lu, Kinetic tuning the electrochemistry of lithium dendrites formation in lithium batteries through electrolytes, ACS Appl. Mater. Interfaces, 2017, **9**, 7003-7008

107. M. Ishikawa, H. Kawasaki, N. Yoshimoto, M. Morita, Pretreatment of Li metal anodes with electrolyte additive for enhancing Li cycleability, J. Power Sources, 2005, **146**, 199-203

108. J. Qian, W. Xu, P. Bhattacharya, M. Englehard, W.A. Henderson, Y. Zhang, J.-G. Zhang, Dendrite-free Li deposition using trace amounts of water as an electrolyte additive, Nano Energy, 2015, **15**, 135-144

109. H. Zhang, C. Li, M. Piszcz, E. Coya, T. Rojo, L.M. Rodriguez-Martinez, M. Armand, Z. Zhou, Single lithium-ion conducting solid polymer electrolytes: advances and perspectives, Chem. Soc. Rev. 2017, **46**, 797-815

110. T.F. Miller III., Z.-G. Wang, G.W. Coates, N.P. Balsara, Designing polymer electrolytes for safe and high capacity rechargeable lithium batteries, Acc. Chem Res. 2016, **50**, 590-593

111. W. Liu, N. Liu, J. Sun, P.-C. Hsu, Y. Li, H.-W. Lee, Y. Cui Y, Ionic conductivity enhancement of polymer electrolytes with ceramic nanowire fillers, Nano Lett. 2015, **15**, 2740-2745

112. J. W. Fergus, Ceramic and polymeric solid electrolytes for lithium-ion batteries, J. Power Sources, 2010, **195**, 4554-4569

113. J.G. Kim, B. Son, S. Mukherjee, N. Schuppert, A. Bates, O. Kwon, M.J. Choi, H.Y. Chung, S. Park, A review of lithium and non-lithium based solid state batteries, J. Power Sources, 2015, **282**, 299-322

114. P. Knauth, Inorganic solid Li ion conductors: An overview, Solid State Ionics, 2009, **180**, 911-916

115. A. Manthiram, X. Yu, S. Wang, Lithium battery chemistries enabled by solid-state electrolytes, Nature Reviews Mater. 2017, **2**, 16103 -1-16

116. I. Osada, H. de Vries, B. Scrosati, S. Passerini, Ionic-liquid-based polymer electrolytes for battery applications, Angew. Chem. Int. Ed. 2016, **55**, 500-513

117. M. Watanabe, M.L. Thomas, S. Zhang, K. Ueno, T. Yasuda, K. Dokko, Application of ionic liquids to energy storage and conversion materials and devices, Chem. Rev. 2017, **117**, 7190-7239

118. S. Zhang, N. Sun, X. He, X. Lu, X. Zhang, Physical properties of ionic liquids: Database and Evaluation, J. Phys. Chem. Ref. Data, 2006, **35**, 1475-1516

119. M. Pasta, C.D. Wessells, R.A. Huggins, Y. Cui, A high-rate and long cycle life aquesous electrolyte battery for grid-scale energy storage, Nature Communications, 2012, **3**, 1149 -1-7

View Article Online
DOI: 10.1039/C8EE01419A

120. M. Liu, S.J. Visco, L.C. De Jonghe, Novel solid redox polymerization electrodes: All-solid-state, thin-film, rechargeable lithium batteries, J. Electrochem. Soc. 1991, **138**, 1891-1895

121. J.-M. Tarascon, A.S. Gozdz, C. Schmutz, F. Shokoohi, P.C. Warren, Performance of Bellcore's plastic rechargeable Li-ion batteries, Solid State Ionics, 1996, **86-88**, 49-54

122. A.J. Blake, R.R. Kohlmeyer, J.O. Hardin, E.A. Carmona, B. Maruyama, J.D. Berrigan, H. Huang, M.F. Durstock, 3D printable ceramic-polymer electrolytes for flexible high-performance Li-ion batteries with enhanced thermal stability, Adv, Energy Mater. 2017, **7**, 1602920 1-10

123. J. Janek, W.G. Zeier, A solid future for battery development, Nature Energy, 2016, **1**, 16141 1-4

124. I. Aldalur, M. Martinez-Ibanez, M. Piszcz, L.M. Rodriguez-Martinez, H. Zhang, M. Armand, Lowering the operational temperature of all-solid-state lithium polymer cell with highly conductive and interfacially robust solid polymer electrolyte, J. Power Sources, 2018, **383**, 144-149

125. J. Kasemchainan, P.G. Bruce, All-solid-state batteries and their remaining challenges, Johnson Matthey Technol. Rev. 2018, **62**, 177-180

126. N. Kamaya, K. Homma, Y. Yamakawa, M. Hirayama, R. Kanno, M. Yonemura, T. Kamiyama, Y. Kato, S. Hama, K. Kawamoto, A. Mitsui, A lithium superionic conductor, Nature Mater. 2011, **10**, 682-686

127. Y. Kato, S. Hori, T. Saito, K. Suzuki, M. Hirayama, A. Mitsui, M. Yonemura, H. Iba, R. Kanno, High-power all solid-state batteries using sulphide superionic conductors, Nature Energy, 2016, **1**, 1-7

128. L.J. Miara, W.D. Richards, Y.E. Wang, G. Ceder, First-principles studies on cation dopants and electrolyte/cathode interphases for lithium garnets, Chem. Mater. 2015, **27**, 4040-4047

129. C.-Z. Zhao, X.-Q. Zhang, X.-B. Cheng, R. Zhang, R. Xu, P.-Y. Chen, H.-J. Peng, J.-Q. Huang, Q. Zhang, An anion-immobilized composite electrolyte for dendrite-free lithium metal anodes, Proceed. Nat. Acad. Sci. 2017, **114**, 11069-11074

130. W. Liu, N. Liu, J. Sun, P.-C. Hsu, Y. Li, H.-W. Lee, Y. Cui, Ionic conductivity enhancement of polymer electrolytes with ceramic nanowire fillers, Nano Lett. 2015, **15**, 2740-2745

131. M.-K. Song, Y. XZhang, E.J. Cairns, A long-life, high-rate lithium/sulfur cell: A multifaceted approach to enhancing cell performance, Nano Lett. 2013, **13**, 5891-5899

132. A. Manthiram, Y. Fu, S.-H. Chung, C. Xu, Y.-S. Su, Rechargeable lithium-sulfur batteries, Chem. Rev. 2014, **114**, 11751-11787

133. A. Manthiram, Y. Fu, S.-H. Chung, Y.-S. Su, Challenges and prospects of lithium-sulfur batteries, Accnts. Chem. Res. 2013, **46**, 1125-1134

View Article Online
DOI: 10.1039/C8EE01419A

134. M.-K. Song, E.J. Cairns, Y. Zhang, Lithium/sulfur batteries with high specific energy: Old challenges and new opportunities, Nanoscale, 2013, **5**, 2186-2204

135. G. Zheng, Y. Yang, J.J. Cha, S.S. Hong, Y. Cui, Hollow carbon nanofiber-encapsulated sulfur cathodes for high specific capacity rechargeable lithium batteries, Nano Lett. 2011, **11**, 4462-4467

136. M. Wild, L. O'Neill, T. Zhang, R. Purkayastha, G. Minton, M. Marinescu, G. Offer, Lithium Sulfur Batteries, a Mechanistic Review. Energy Environ. Sci. 2015, **8**, 3477–3494

137. D. Eroglu, K.R. Zavadil, K.G. Gallagher, Critical link between materials chemistry and cell-level design for high energy density and low cost lithium-sulfur transportation battery, J. Electrochem. Soc. 2015, **162**, A982-A990

138. N. Yabuuchi, K. Kubota, M. Dahbi, S. Komaba, Chem. Rev. 2014, **114**, 11636-11682

139. J. Muldoon, C.B. Bucur, T. Gregory, Quest for nonaqueous multivalent secondary batteries: Magnesium and beyond, Chem. Rev. 2014, **114**, 11683-11720

140. K. Kubota, S. Komaba, Review – Practical issues and future perspective for Na-ion batteries, J. Electrochem. Soc. 2015, **162**, A2538-A2550

141. A. Eftekhari, Z. Jian, X. Ji, Potassium secondary batteries, ACS Appl. Mater. Interfaces, 2016, **9**, 4404-4419

142. H. Pan, Y.-S. Hu, L. Chen, Room-temperature stationary sodium-ion batteries for large-scale electric energy storage, Energy Environ. Sci. 2013, **6**, 2338-2360

143. M.D. Slater, D. Kim, E. Lee, C.S. Johnson, Sodium-ion batteries, Adv. Funct. Mater. 2013, **23**, 947-958

144. A.L. Lipson, B. Pan, S.H. Lapidus, C. Liao, J.T. Vaughey, B.J. Ingram, Rechargeable Ca-ion batteries: A new energy storage system, Chem. Mater. 2015, **27**, 8442-8447

145. K. Kubota, M. Dahbi, T. Hosaka, S. Kumakura, S. Kobama, Towards K-ion and Na-ion batteries as "beyond Li-ion", Chem. Rec. 2018, **18**, 1-22

146. M. Dahbi, N. Yabuuchi, K. Kubota, K. Tokiwa, S. Komaba, Negative electrodes for Na-ion batteries, Phys. Chem. Chem. Phys. 2014, **16**, 15007-15028

147. D.A. Stevens, J.R. Dahn, High capacity anode materials for rechargeable sodium-ion batteries, J. Electrochem. Soc. 2000, **147**, 1271-1273

148. H. Chen, M. Armand, G. Demailly, F. Dolhem, P. Poizot, J.-M. Tarascon, From biomass to a renewable $Li_xC_6O_6$ organic electrode for sustainable Li-ion batteries, ChemSusChem. 2008, **1**, 348-355

149. M. Lee, J. Hong, J. Lopez, Y. Sun, D. Feng, K. Lim, W.C. Chueh, M.F. Toney, Y. Cui, Z. Bao, High-performance sodium-organic battery by realizing four-sodium storage in disodium rhdizonate, Nature Energy, 2017, **2**, 861-868

150. P. Barpanda, G. Oyama, S.-I. Nishimura, S.-C. Chung, A. Yamada, A 3.8 V earth-abundant sodium battery electrode, Nature Comm. 2014, **5**, 4358 -1-8

View Article Online
DOI: 10.1039/C8EE01419A

151. W. Zhou, Y. Li, S. Xin, J.B. Goodenough, Rechargeable sodium all-solid-state battery, ACS Central Sci. 2017, **3**, 52-57

152. L. Wang, Y. Lu, J. Liu, M. Xu, J. Cheng, D. Zhang, J.B. Goodenough, A superior low-cost cathode for Na-ion battery, Angew. Chem. Int.Ed. 2013, **52**, 1964-1967

153. C.D. Wessells, S.V. Peddada, R.A. Huggins, Y. Cui, Nickel hexacyanoferrate nanoparticle electrodes for aqueous] sodium and potassium ion batteries, Nano Lett. 2011, **11**, 5421-5425

154. A. Eftekhari, Potassium secondary cell based on Prussian blue cathode, J. Power Sources, 2004, **126**, 221-228

155. J.C. Pramudita, D. Sehrawat, D. Goonetilleke, N. Sharma, An initial review of the status of electrode materiuals for potassium-ion batteries, Adv. Energy Mater. 2017, **7**, 1602911 -1-21

156. P. Canepa, S.-H. Bo, G.S. Gautam, B. Key, W.D. Richards, T. Shi, Y. Tian, Y. Wang, J.Li, G. Ceder, High magnesium mobility in ternary spinel chalcogenides, Nature Comm. 2017, **8**, 1759 -1-8

157. Q. Li, N.J. Bjerrum, Aluminum as anode for energy storage and conversion: A review, J. Power Sources, 2002, **110**, 1-10

158. N. Jayaprakash, S.K. Das, L.A. Archer, The rechargeable aluminum-ion battery, Chem. Commun. 2011, **47**, 12610-12612

159. M.-C. Lin, M. Gong, B. Lu, Y. Wu, D.-Y. Wang, M. Guan, M. Angell, C. Chen, J. Yang, B.-J. Hwang, H. Dai, An ultrafast rechargeable aluminum-ion battery, Nature, 2015, **520**, 324-328

160. H. Engstrom, J.B. Bates, W.E. Brundage, J.C. Wang, Ionic conductivity of sodium beta"-alumina, Solid State Ionics, 1981, **2**, 265-276

161. X. Lu, G. Xia, J.P. Lemmon, Z. Yang, Advanced materials for sodium-beta alumina batteries: Status, challenges, and perspectives, J. Power Sources, 2010, **195**, 2431-2442

162. K.B. Hueso, M. Armand, T. Rojo, T. High Temperature Sodium Batteries: Status, Challenges and Future Trends. Energy Environ. Sci. 2013, **6**, 734–749

163. B.L. Ellis, L. F. Nazar, Sodium and sodium-ion energy storage batteries, Current Opinion Solid State Mater. Sci. 2012, **16**, 168-177

164. X. Lu, B.W. Kirby, W. Xu, G. Li, J.Y. Kim, J.P. Lemmon, V.L. Sprenkle, Z. Yang, Advanced intermediate-temperature Na-S battery, Energy & Environ. Sci. 2013, **6**, 299-306

165. X. Lu, G. Li, J.Y. Kim, D. Mei, J.P. Lemmon, V.L. Sprenkle, J. Liu, Liquid-metal electrode to enable ultra-low temperature sodium-beta alumina batteries for renewable energy storage, Nature Comm. 2014, **5**, 4578 -1-8

View Article Online
DOI: 10.1039/C8EE01419A

166. J. Wang, J. Yang, Y. Nuli, R. Holze, Room temperature Na/S batteries with sulfur composite cathode materials, Electrochem. Comm. 2007**, 9**, 31-34

167. Z. Qiang, Y.-M. Chen, Y. Xia, W. Liang, Y. Zhu, B.D. Vogt, Ultra-long cycle life, low-cost room temperature sodium-sulfur batteries enabled by highly doped (N,S) nanoporous carbons, Nano Energy, 2017, **32**, 59-66

168. S. Wei, S. Xu, A. Agrawral, S. Choudhury, Y. Lu, Z. Tu, L. Ma, L.A. Archer, A stable room temperature sodium-sulfur battery, Nature Comm.2016, **7**, 11722 -1-10

169. J.B. Goodenough, H.Y.P. Hong, J.A. Kafalas, Fast Na^{+}-ion transport in skeleton structures, Mater. Res. Bull. 1976, **11**, 203-220

170. O. Bohnke, S. Ronchetti, D. Mazza, Conductivity measurements on nasicon and nasicon-modified materials, Solid State Ionics, 1999, **122**, 127-136

171. H. Schmid, L.C. De Jonghe, C. Cameron, Chemical stability of Nasicon, Solid State Ionics, 1982, **6**, 57-63

172. K.F. Blurton, A.F. Sammells, Metal/air batteries: Their status and potential – A review, J. Power Sources, 1979, **4**, 263-279

173. D. Zhang, R. Li, T. Huang, A. Yu, A novel composite polymer electrolyte for lithium-air batteries, J. Power Sources, 2010, **195**, 1202-1206

174. G. Girishkumar, B. McCloskey, A. C. Luntz, S. Swanson, W. Wilcke, Lithium-air battery: Promise and challenges, J. Phys. Chem. Lett. 2010, **1**, 2193-2203

175. Y. Li, H. Dai, Recent advances in zinc-air batteries, Chem. Soc. Rev. 2014, **43**, 5257-5275

176. J.-S. Lee, S.T. Kim, R. Cao, N.-S. Choi, M. Liu, K.T. Lee, J. Cho, Metal-air batteries with high energy density: Li-air versus Zn-air, Adv. Energy Mater. 2011, **1**, 34-50

177. E.J. Rudd, D.W. Gibbons, High energy density aluminum/oxygen cell, J. Power Sources, 1994, **47**, 329-340

178. C.D. Wessels, S.V. Peddada, M.T. McDowell, R.A. Huggins, Y. Cui, The effect of insertion species on nanostructured open framework hexacyanoferrate battery electrodes, J. Electrochem. Soc. 2011, **159**, A1-A6

179. X. Zhang, X.-G. Wang, Z. Xie, Z. Zhao, Recent progress in rechargeable alkali metal-air batteries, Green Energy Environment, 2016, **1**, 4-17

180. F. Cheng, J. Chen, Metal-air batteries: From oxygen reduction electrochemistry to cathode catalysts, Chem. Soc. Rev. 2012, **41**, 2172-2192

181. K. Kinoshita, Electrochemical oxygen technology, J. Wiley, New York (1992)].

182. Y.C. Lu, Z. Xu, H.A. Gastieger, S. Chen, K. Hamad-Schifferli, Y. Shao-Horn, Platinum-gold nanoparticles: A highly active bifunctional electrocatalyst for the rechargeable lithium-air batteries, J. Am. Chem. Soc. 2010, **132**, 12170-12171

View Article Online
DOI: 10.1039/C8EE01419A

183. L. Mao, D. Zhang, T. Sotomura, K. Nakatsu, N. Koshiba, T. Ohsaka, Mechanistic study of the reduction of oxygen in air electrode with manganese oxides as electrocatalysts, Electrochim. Acta, 2003, **48**, 1015-1021

184. Y. Gorlin, T.F. Jaramillo, A bifunctional nonprecious metal catalyst for oxygen reduction and water oxidation, J. Am. Chem. Soc. 2010, **132**, 13612-13614

185. J.W.D. Ng, M. Tang, T.F. Jaramillo, A carbon-free, precious-metal-free, high performance O_2 electrode for regenerative fuel cells and metal-air batteries, Energy & Environ. Sci. 2014, **7**, 2017-2024

186. J.K. Norskov, J. Rossmeisl, A. Logadottir, L. Lindqvist, J.R. Kitchin, T.B. Pederson, H. Jonsson, Origin of the overpotential for oxygen reduction at a fuel cell catode, J. Phys. Chem. B. 2004, **108**, 17886-17892

187. J. Suntivich,H.A. Gesteiger, N. Yabuuchi, H. Nakanishi, J.B. Goodenough, Y. Shao-Horn, Design principles for oxygen-reduction activity on perovskite oxide catalysts for fuel cells and metal-air batteries, Nature Chem. 2011, **3**, 546-550

188. J.P. Zheng, R.Y. Liang, M. Hendrickson, E.J. Plichta, Theoretical energy density of Li-air batteries, J. Electrochem. Soc. 2008, **155**, A432-A437

189. A.C. Luntz, B.D. McCloskey, Nonaqueous Li-air batteries: A status report. Chem. Rev. 2014, **114**, 11721-11750

190. T. Ogasawara, A. Debart, M. Holzapfel, P. Novak, P. G. Bruce, Rechargeable Li_2O_2 Electrode for lithium batteries, J. Am. Chem. Soc. 2006, **128**, 1390-1393

191. A. Kraytsberg, Y. Ein-Eli, Review on Li-air batteries: Opportunities, limitations and perspective, J. Power Sources, 2011, **196**, 886-893

192. J. Christensen, P. Albertus, R.S. Sanchez-Carrera, T. Lohmann, B. Kozinsky, R. Liedtke, J. Ahmed, A. Kojic, A critical review of Ai/air batteries, J. Electrochem. Soc. 2012, **159**, R1-R30

193. L. Grande, E. Paillard, J. Hassoun, J.-B. Park, Y.-J. Lee, Y.-K. Sun, S. Posserini, B. Scrosati, The lithium/air battery: Still an emerging system or a practical reality?, Adv. Mater. 2015, **27**, 784-800

194. D. Aurbach, B.D. McCloskey, L. Nazar, P.G. Bruce, Advances in understanding mechanisms underpinning lithium-air batteries, Nature Energy, 2016, **1**, 161281 1-11

195. M. Balaish, A. Kraytsberg, Y. Ein-Eli, A critical review on lithium-air battery electrolytes, Phys. Chem. Chem. Phys. 16, 2801-2822 (2014),

196. Y.-C. Lu, B.M. Gallant, D.G. Kwabi, J.R. Harding, R.R. Mitchell, M.S. Whittingham, Y. Shao-Horn, Lithium-oxygen batteries: Bridging mechanistic understanding and battery performance, Energy Environ. Sci. 2013, **6**, 750-768

197. A. Debart, J. Bao, G. Armstrong, P. G. Bruce, An O_2 cathode for rechargeable lithium batteries: The effect of a catalyst, J. Power Sources, 2007, **174**, 1177-1182

View Article Online
DOI: 10.1039/C8EE01419A

198. Z. Ma, X. Yuan, L. Li, Z.-F. Ma, D.P. Wilkinson, L. Zhang, J. Zhang, A review of cathode materials and structures for rechargeable lithium-air batteries, Energy Environ. Sci. 2015, **8**, 2144-2198

199. S.J. Visco, M.-Y. Chu, Protective coatings for negative electrodes, US Patent 6,025,094 (Feb. 15, 2000)

200. S.J. Visco, B.D. Katz, Y.S. Nimon, L.C. De Jonghe, Protected active metal electrode and battery cell structure with non-aqueous interlayer architecture, US Patent 7,282,295 (Oct. 16, 2007)

201. J. Sun, N. Zhao, Y. Li, X. Guo, X. Feng, X. Liu, Z. Liu, G. Cui, H. Zheng, L. Gu, H. Li, A rechargeable Li-air fuel cell battery based on garnet solid electrolytes, Sci. Reports, 2017, **7**, 41217 -1-8

202. J. Yi, S. Gao, P. He, H. Zhou, Status and prospects of polymer electrolytes for solid-state Li-O_2 (air) batteries, Energy Environ. Sci. 2017, **10**, 860-894

203. W. Xu, J. Xiao, D. Wang, J. Zhang, J.-G. Zhang, Effects of nonaqueous electrolytes on the performance of lithium/air batteries, J. Electrochem. Soc. 2010, **157**, A219-A224

204. T. Kuboki, T. Okuyama, T. Ohsaki, N. Takami, Lithium-air batteries using hydrophobic room temperature ionic liquid electrolyte, J. Power Sources, 2005, **146**, 766-769

205. B.D. McCloskey, R. Scheffler, A. Speidel, D.S. Bethune, R.M. Shelby, A.C. Luntz, On the efficacy of electrocatalysis in nonaqueous Li-O_2 batteries, J. Am. Chem. Soc. 2011, **133**, 18038-18041

206. J. Wandt, P. Jakes, J. Granwehr, H.A. Gasteiger, R.-A. Eichel, Singlet oxygen formation during the charging process of an aprotic lithium-oxygen battery, Angew. Chem. 2016, **128**, 7006-7009

207. N. Mahne, S.E. Renfrew, B.D. McCloskey, S.A. Freunberger, Electrochemical oxidation of lithium carbonate generates singlet oxygen, Angew. Chem. Int. Ed. 2018, DOI: 10.1002/anie.201802277

208. N. Mahne, B. Schafzahl, C. Leypold, M. Leypold, S. Grumm, A. Leigeb, G.A. Strohmeier, M. Wilkening, O. Fonatine, D. Kramer, C. Slugovc, S.M. Borisov, S.A. Freunberger, Singlet oxygen generation as a major cause for parasitic reactions during cycling of aprotic lithium-oxygen batteries, Nature Energy, 2017, **2**, 17036 -1-9

209. A.C. Luntz, B.D. McCloskey, Importance of singlet oxygen, Nature Energy, 2017, **2**, 17056 -1-2

210. L. Johnson, C. Li, Z. Liu, Y. Chen, S.A. Freunberger, P.C. Ashok, B.B. Praveen, K. Dholakia, J.-M. Tarascon, P.G. Bruce, The role of LiO_2 solubility in O_2 reduction in aprotic solvents and its consequences for Li-O_2 batteries, Nature Chem. 2014, **6**, 1091-1099

211. V. Gutmann, Solvent effects on reactivity of organometallic compounds. Coordin. Chem. Rev. 1976, **18**, 225-255

View Article Online
DOI: 10.1039/C8EE01419A

212. Y. Chen, S.A. Freunberger, Z. Peng, O. Fontaine.G. Bruce, Charging a Li-O_2 battery using a redox mediator, Nature Chem. 2013, **5**, 489-494

213. Z. Peng, S. A. Freunberger, Y. Chen, P. G. Bruce, A reversible and higher-rate Li-O_2 battery, Science, 2012, **337**, 563-566

214. B.D. McCloskey, A. Speidel, R. Scheffler, D.C. Miller, V. Viswanathan, J.S. Hummelshoj, J.K. Norskov, A.C. Luntz, Twin problems of Interfacial carbonate formation in nonaquesous Li-O2 batteries, J. Phys. Chem. Lett. 2012, **3**, 997-1001

215. N.B. Aetukuri, B.D. McCloskey, J.M. Garcia, L.E. Krupp, V. Viswanathan, A.C. Luntz, Solvating additives drive solution-mediated electrochemistry and enhance toroid groth in non-aqueous Li_O2 batteries, Nature Chem. 2014, **7**, 50-56

216. G.A. Elia, J. Hassoun, W.-J. Kwak, Y.-K. Sun, B. Scrosati, F. Mueller, D. Bresser, S. Passerini, P. Oberhumer, N. Tsiouvaras, J. Reiter, An advanced lithium-air battery exploiting and ionic liquid-based electrolyte, Nano Lett. 2014, **14**, 6572-6577

217. H.-G. Jung, J. Hassoun, J.-B. Park, Y.-K. Sun, Bruno Scrosati, An improved high-performance lithium-air battery, Nature Chem. 2010, **4**, 579-585

218. P. Gu, M. Zheng, Q. Zhao, H. Xue, H. Pang, Rechargeable zinc-air batteries: A promising way to green energy, J. Mater. Chem A, 2017, **5**, 7651-7666

219. J. Pan, Y.Y. Xu, H. Yang, Z. Dong, H. Liu, B.Y. Xia, Advanced architectures and relatives of air electrodes in Zn-air batteries, Adv. Sci. 2018, 1700691 -1-30

220. Y. Xu, Y. Zhang, Z. Guo, J. Ren, Y. Wang, H. Peng, Flexible, stretchable, and rechargeable fiber-shaped zinc-air battery based on cross-stacked carbon nanotube sheets, Angew. Chem. Int. Ed. 2015, **54**, 15390-15394

221. J. Fu, J. Zhang, X. Song, H. Zarrin, X. Tian, J. Qiao, L. Rasen, K. Li, Z. Chen, A flexible solid-state electrolyte for wide-scale integration of rechargeable zinc-air batteries, Energy Environ. Sci. 2016, **9**, 663-670

222. H. Ma, C. Li, Y. Su, J. Chen, Studies on the vapour-transport synthesis and electrochemical properties of zinc micro-, meso-, and nanoscale structures, J. Mater. Chem. 2007, **17**, 684-691

223. C.W. Lee, K. Sathiyanarayanan, S.W. Eom, M.S. Yun, Novel alloys to improve the electrochemical behavior of zinc anodes for zinc/air battery, J. Power Sources, 2006, **160**, 1436-1441

224. S.J. Banik, R. Akolkar, Suppressing dendrite growth during zinc electrodeposition by PEG-200 additive, J. Electrochem. Soc. 2013, **160,** D519-D523

225. Y. Ein-Eli, M. Auinat, D. Starosvetsky, Electrochemical and surface studies of zinc in alkaline solutions containing organic corrosion inhibitors, J. Power Sources, 2003, **114**, 330-337

View Article Online
DOI: 10.1039/C8EE01419A

226. S.-M. Lee, Y.-J. Kim, S.-W. Eom, N.-S. Choi, K.-W. Kim, S.-B. Cho, Improvement in self-discharge of Zn anode by applying surface modification of Zn-air batteries with high energy density, J. Power Sources, 2013, **227**, 177-184

227. G. Fu, Z. Cui, Y. Chen, L. Xu, Y. Tang, J.B. Goodenough, Hierarchically mesoporous nickel-iron nitride as a cost-efficient and highly durable electrocatalyst for Zn-air battery, Nano Energy, 2017, **39,** 77-85

228. D.U. Lee, J.-Y. Choi, K. Feng, H.W. Park, Z. Chen, Advanced extremely durable 3D bifunctional air electrodes for rechargeable zinc-air batteries, Adv. Energy Mater. 2014, **4**, 1301389 -1-5

229. Y. Li, M. Gong, Y. Liang, J. Feng, J.-E. Kim, H. Wang, G. Hong, B. Zhang, H. Dai, Advanced zinc-air batteries based on high-performance hybrid electrocatalysts, Nature Commun. 2013, **4**, 1805 -1-7

230. M. L. Perry, A. Z. Weber, Advanced redox-flow batteries: A perspective, J. Electrochem. Soc. 2016, **163**, A5064-5067

231. W. Wang, Q. Luo, B.Li, X. Wei, L. Li, Z. Yang, Recent progress in redox flow battery research and development, Adv. Funct. Mater.2013, **23**, 970-986

232. A.Z. Weber, M.M. Mench, J.P. Meyers, P.N. Ross, J.T. Gostick, Q. Liu, Redox flow batteries: A review, J. Appl. Electrochem. 2011, **41**, 1137-1164

233. M. Skyllas-Kazacos, M. H. Chakrabarti, S. A. Hajimolana, F. S. Mjalli, M. Saleem, Progress in flow battery research and development, J. Electrochem. Soc. 2011, **158**, R55-R79

234. P. Alotto, M. Guarnieri, F. Moro, Redox flow batteries for the storage of renewable energy: A review, Renew. Sustain. Energy Rev., 2014, **29**, 325-335

235. R. Ye, D. Henkensmeier, S.J. Yoon, Z. Haung, D.Y. Kim, Z. Chang, S. Kim, R. Chen, Redox flow batteries for energy storage: A technology review, J. Electrochem. Energy Conversion Storage, 2018, **15**, 010801 -1-21

236. JES Focus Issue on Redox Flow Batteries – Reversible Fuel Cells, J. Electrochem. Soc. 2016, **163**(1)

237. X. Wei, W. Pan, W. Duan, A. Hollas, Z. Yang, B. Li, Z. Nie, J. Liu, D. Reed, W. Wang, V. Sprenkle, Materials and systems for organic redox flow batteries: Status and challenges, ACS Energy Lett. 2017, **2**, 2187-2204

238. K. Lin, Q. Chen, M.R. Gerhardt, L. Tong, S.B. Kim, L. Eisenach, A.W. Valle, D. Hardee, R.G. Gordon, M.J. Aziz, M.P. Marshak, Alkaline quinone flow battery, Science 2015, **349**, 1529-1532

239. Q. Chen, M. R. Gerhardt, L. Hartle, M. J. Aziz, A quinone-bromine flow battery with 1 W/cm^2 power density, J. Electrochem. Soc. 2016, **163**, A5010-A5103

240. R.M. Darling, K.G. Gallagher, J.A. Kowalski, S. Ha, F.R.Brushett, Pathways to low-cost electrochemical energy storage: A comparison of aqueous and nonaqueous flow batteries, Energy Environ. Sci. 2014, **7**, 3459-3477

View Article Online
DOI: 10.1039/C8EE01419A

241. Grid-Scale Rampable Intermittent Dispatchable Storage (GRIDS), U.S. Department of Energy, Advanced Research Projects Agency – Energy (ARPA-E) Funding Opportunity Announcement DE-FOA-0000290 CFDA# 81,135, Washington D.C., March 2, 2010, https://arpa-e-foa.energy.gov/Default.aspx?Archive=1#FoaId85e239bb-8908-4d2c-ab10-dd02d85e7d78 (accessed April 6, 2018)

242. C. Ding, H. Zhang, X. Li, T. Liu, F. Xing, Vanadium flow battery for energy storage: prospects and challenges, J. Phys. Chem. Lett. 2013, **4**, 1281-1294

243. A. Parasuraman, T. M. Lim, C. Menictas, M. Skyllas-Kazacos, Review of material research and development for vanadium redox flow battery applications, Electrochim. Acta, 2013, **101**, 27-40

244. A. Cunha, J. Martins, N. Rodrigues, F. B. Brito, Vanadium redox flow batteries: A technology review, Intern. J. Energy Res. 2015, **39**, 889-918

245. G. Kear, A. A. Shah, F. C. Walsh, Development of the all-vanadium redox flow battery for energy storage: A review of technological, financial, and policy aspects, Intern. J. Energy Res. 2012, **36**, 1105-1120

246. A.A. Shinkle, A.E. S.Sleightholeme, L.T. Thompson, C.W. Monroe, Electrode kinetics in non-aqueous vanadium acetylacetonate redox flow batteries, J. Appl. Electrochem. 2011, **41**, 1191-1199

247. S. Suresh, T. Kevasan, Y. Munaiah, I. Arulraj, S. Dheenadayalan, P. Ragupathy, Zinc-bromine hybrid flow battery: Effect of zinc utilization and performance characteristics, RSC Adv. 2014, **4**, 37947-37953

248. S. Biswas, A. Senju, R. Mohr, T. Hudson, N. Karthikeyan, K.W. Knehr, A.G. Hsieh, X. Yang, B.E. Koel, D.A. Steingart, Minimal architecture zinc-bromine battery for low cost electrochemical energy storage, Energy Environ. Sci. 2017, **10**, 114-120

249. G. Wang, L.Zhang, J. Zhang, A review of electrode materials for electrochemical supercapacitors, Chem. Soc. Rev. 2012, **41**, 797-828

250. A. Gonzalez, E. Goikolea, J.A. Barrena, R. Mysyk, Review of supercapacitors: technologies and materials, Renew. Sustain. Energy Rev. 2016, **58,** 1189-1206

251. L.L. Zhang, X.S. Zhao, Carbon-based materials as supercapacitor electrodes, Chem. Soc. Rev. 2009, **38**, 2520-2531

252. P. Simon, Y. Gogotsi, Materials for electrochemical capacitors, Nature Mater. 2008, **7**, 845-854

253. A. Burke, R&D considerations for the performance and application of electrochemical capacitors, Electrochim. Acta, 2007, **53**, 1083-1091

254. M. Zhi, C. Xiang, J. Li, M. Li, N. Wu, Nanostructured carbon-metal oxide composite electrodes for supercapacitors: A review, Nanoscale, 2013, **5,** 72-88

View Article Online
DOI: 10.1039/C8EE01419A

255. C. Zhong, Y. Deng, W. Hu, J. Qiao, L. Zhang, J. Zhang, A review of electrolyte materials and compositions for electrochemical supercapacitors, Chem. Soc. Rev. 2015, **44**, 7484-7539

256. A. Burke, Ultracapacitors: Why, how, and where is the technology, J. Power Sources, 2000, **91**, 37-50

257. P. Simon, Y. Gogotsi, B. Dunn, Where do batteries end supercapacitors begin?, Science, 2014, **343**, 1210-1211

258. A. Burke, Batteries and ultracapacitors for electric, hybrid, and fuel cell vehicles, Proceed. IEEE, 2007, **95**, 806-820

259. B.E. Conway, Electrochemical Supercapacitors: Scientific Fundamentals and Technological Applications, Kluwer Academics/Plenum Publisher, New York (1999)

260. M. Ye, Z. Zhang, Y. Zhao, L. Qu, Graphene platforms for smart energy generation and storage, Joule, 2018, **2**, 245-268

261. Y. Huang, J. Liang, Y. Chen, An overview of the applications of grapheme-based materials in supercapacitors, Small, 2012, **8**, 1805-1834

262. B.E. Conway, W.G. Bell, Power limitations of supercapacitor operation associated with resistance and capacitance distribution in porous electrode devices, J. Power Sources, 2002, **105**, 169-181

263. M. Mastragostino, F. Soavi, Strategies for high-performance supercapacitors for HEV, J. Power Sources, 2007, **174**, 89-93

264. G.G. Amatucci, F. Badway, A. Du Pasquir, T. Zheng, An asymmetric hybrid nonaqueous energy storage cell, J. Electrochem. Soc. 2001, **148**, A930-A939

265. Y.P. Lin, N.L. Wu, Characterization of $MnFe_2O_4/LiMn_2O_4$ aqueous asymmetric supercapacitor, J. Power Sources, 2011, **196**, 851-854

266. V. Augustyn, J. Come, M.A. Lowe, J.W. Kim, P.-L. Taberna, S.H.Tolbert, H.D. Abruna, P. Simon, B. Dunn, High-rate electrochemical storage through Li+ intercalation pseudocapacitance, Nature Mater. 2013, **12**, 518-522

267. A.B. Stambouli, E. Traversa, Renew. Sustain. Energy Reviews, 2002, **6**, 433-455

268. M. Lo Faro, V. Antonucci, P.L. Antonucci, A.S. Arico, Fuel flexibility: A key challenge for SOFC technology, Fuel, 2012, **102**, 554-559

269. Z. Shao , S.M. Haile, J. Ahn, P.D. Ronney, Z. Zhan, S.A. Barnett, A thermally self-sustained micro solid-oxide fuel-cell stack with high power density, Nature, 2005, **435**, 795-798

270. Z. Zhan, S.A. Barnett, Use of a catalyst layer for propane partial oxidation in solid oxide fuel cells, Solid State Ionics, 2005, **176**, 871-879

271. S. Park, R.J. Gorte, J.M. Vohs, Applications of heterogeneous catalysis in the direct oxidation of hydrocarbons in a solid-oxide fuel cell, Appl. Catal. A: General, 2000, **200**, 55-61

View Article Online
DOI: 10.1039/C8EE01419A

272.. O. Costa-Nunes, J.M. Vohs, R.J. Gorte, A study of direct-conversion SOFC with n-butane at higher fuel utilization, J. Electrochem. Soc. 2003, **150**, A858-A863

273. E.P. Murray, S.J. Harris, H. Jen, Solid oxide fuel cells utilizing dimethyl ether fuel, J. Electrochem. Soc. 2002, **149**, A1127-A113

274. M. Liu, Y. Choi, L. Yang, K. Blinn, W. Qin, P. Liu, M. Liu, Direct octane fuel cells: A promising power for transportation, Nano Energy, 2012, **1**, 448-455

275. H. Kim, S. Park, J.M. Vohs, R.J. Gorte, Direct oxidation of liquid fuels in a solid oxide fuel cell, J. Electrochem. Soc. 2001, **148**, A693-A695

276. T.M. Gür, R.A. Huggins, Direct electrochemical conversion of carbon to electrical energy in a high temperature fuel cell, J. Electrochem. Soc. 1992, **132**, L95-L97

277. T.M. Gür, Mechanistic modes for solid carbon conversion in high temperature fuel cells, J. Electrochem. Soc. 2010, **157**, B571-B759

278. A.C. Lee, S. Li, R.E. Mitchell, T.M. Gür, Conversion of solid carbonaceous fuels in a fluidized bed fuel cell, Electrochem. Solid State Lett. 2008, **11**, B20-B23

279. B.R. Alexander, R.E. Mitchell, T.M. Gür, Experimental and modeling study of biomass conversion in a solid carbon fuel cell, J. Electrochem. Soc. 2012, **159**, B347-B354

280. T.M. Gür, M. Homel, A.V. Virkar, High performance solid oxide fuel cell operating on dry gasified coal, J. Power Sources, 2010, **195,** 1085-1090

281. M. Homel, T.M. Gür, J.H. Koh, A.V. Virkar, Carbon Monoxide-Fueled Solid Oxide Fuel Cell, J. Power Sources 2010, **195**, 6367

282. Y. Wang, D.Y.C. Leung, J. Xuan, H. Wang, A review of unitized regenerative fuel cell technologies, part B: Unitized regenerative alkaline fuel cell, solid oxide fuel cell, and microfluidic fuel cell, Renew. Sustain. Energy Rev. 2017, **75**, 775-795

283. J. Pettersson, B. Ramsey, D. Harrison, A review of the latest developments in electrodes for unitized regenerative polymer electrolyte fuel cells, J. Power Sources, 2006, **157**, 28-34

284. S.S. Dihrab, K. Sopian, M.A. Alghoul, M.Y. Sulaiman, Review of the membrane and bipolar plates materials for conventional and unitized regenerative fuel cells, Renew. Sustain. Energy Rev. 2009, **13**, 1663-1668

285. T. Sadhasivam, K. Dhanabalan, S.-H. Roh, T.-H. Kim, K.-W. Park, S. Jung, M.D. Kurkuri, H.-Y. Jung, A comprehensive review on unitized regenerative fuel cells, Crucial challenges and developments, Intern. J. Hydrogen Energy, 2017, **42**, 4415-4433

286. H.A. Gasteiger, S.S. Kocha, B. Sompalli, F.T. Wagner, Activity benchmarks and requirements for Pt, Pt-alloy, and non-Pt oxygen reduction catalysts for PEMFCs, Appl. Catal. B: Environ. 2005, **56**, 9-35

View Article Online
DOI: 10.1039/C8EE01419A

287. F.D. Kong, S. Zhang, G.P. Yin, N. Zhang, Z.B. Wang, C.Y. Du, Pt/porous-IrO_2 nanocomposite as promising electrolcatalyst for unitized regenerative fuel cell, Electrochem. Commun. 2012, **14**, 63-66

288. W. Sheng, H.A. Gasteiger, Y. Shao-Horn, Hydrogen oxidation and evolution reaction kineticson platinum: acid and alkaline electrolytes, J. Electrochem. Soc. 2010, **157**, B1529-B1536

289. J. Durst, A. Sibel, C. Simon, F. Hasche, J. Herranz, H.A. Gasteiger, New insights into the electrochemical hydrogen oxidation and evolution reaction mechanism, Energy Environ. Sci. 2014, **7**, 2255-2260

290. W.-K. Hu, D. Noreus, Metal hydrides as bi-functional catalysts for hydrogen generation and oxidation in reversible MH-air fuel cells, Electrochem. Commun. 2009, **11**, 2212-2215

291. Y. Wang, D.Y.C. Leung, J. Xuan, H. Wang, A review of unitized regenerative fuel cell technologies, part A: Unitized regenerative proton exchange membrane fuel cells, Renew. Sustain. Energy Rev. 2016, **65,** 961-977

292. K.R. Sridhar, J. McElroy, F. Mitlitsky, V. Venkataraman, M.C. Williams, Applications and markets for solid oxide regenerative fuel cells, Electrochem. Soc. Proceedings 2005, **2005-07**, 295-305

293. D.M. Bastidas, S. Tao, J.T.S. Irvine, A symmetrical solid oxide fuel cell demonstrating redox stable perovskite electrodes, J. Mater. Chem. 2006, **16**, 1603-1605

294. S.Y. Gomez, D. Hotza, Current developments in reversible solid oxide fuel cells, Renew. Sustain. Energy Rev., 2016, **61**, 155-174

295. J.C. Ruiz-Morales, D. Marrero-Lopez, J. Canales-Vazquez, J.T.S. Irvine, Symmetric and reversible solid oxide fuel cells, RSC Adv. 2011, **1**, 1403-1414

296. C.H. Wendel, R.J. Braun, Design and techno-economic analysis of high efficiency reversible solid oxide cell systems for distributed energy storage, Appl. Energy, 2016, **172**, 118-131

297. Meeting the needs of the future warriors, The National Academic Press (2004), http://www.nap.edu/openbook/0309092612/html/89.html

298. K. Eguchi, T. Hatagishi, H. Arai, Power generation and steam electrolysis characteristics of an electrochemical cell with a zirconia- or ceria-based electrolyte, Solid State Ionics, 1996, **86-88**, 1245-1249

299. S.D. Ebbesen, S.H. Jensen, A. Hauch, M.B. Mogensen, High temperature electrolysis in alkaline cells, solid proton conducting cells, and solid oxide cells, Chem. Rev. 2014, **114**, 10697-10734

300. M.A. Laguna-Bercero, Recent advances in high temperature electrolysis using solid oxide fuel cells: A review, J. Power Sources, 2012, **203**, 4-16

View Article Online
DOI: 10.1039/C8EE01419A

301. C. Graves, S.D. Ebbesen, S.H. Jensen, S.B. Simonsen, M.B. Mogensen, Eliminating degradation in solid oxide electrochemical cells by reversible operation, Nature Mater. 2015, 14, 239-244

302. J. Hong, H.-J. Kim, S.-Y. Park, J.-H. Lee, S.-B. Park, J.-H. Lee, B.-K. Kim, H.-J. Je, J.Y. Kim, K.J. Yoon, Electrochemical performance and long-term durability of a 200 W-class solid oxide regenerative fuel cell stack, Intern. J. Hydrogen Energy, 2014, **39**, 20819-20828

303. L. Bi, S. Boulfrad, E. Traversa, Steam electrolysis by solid oxide electrolysis cells (SOECs) with proton-conducting oxides, Chem. Soc. Rev. 2014, **43**, 8255-8270

304. J.H. Shim, J.S. Park, J. An, T.M. Gür, S. Kang, and F.B. Prinz, Intermediate-Temperature Ceramic Fuel Cells with Thin Film Yttrium-doped Barium Zirconate Electrolytes, Chem. Mater. 2009, **21**, 3290-3296

305. C. Duan, J. Tong, M. Shang, S. Nikodemski, M. Sanders, S. Ricote, A. Almansoori, R. O'Hayre, Readily processed protonic ceramic fuel cells with high performance at low temperatures, Science, 2015, **349**, 1321-1326

306. S. Tao, J. T. S. Irvine, A redox-stable efficient anode for solid-oxide fuel cells, Nature Mater. 2003, **2**, 320-323

307. S.H. Jensen, C. Graves, M. Mogensen, C. Wendel, R. Braun, G. Hughes, Z. Gao, S.A. Barnett, Large-scale electricity storage utilizing reversible solid oxide cells combined with underground storage of CO_2 and CH_4, Energy Environ. Sci. 2015, **5**, 2471-2479

308. Z. Zhan, D. M. Bierschenk, J. S. Cronin,, S. A. Barnett, A reduced temperature solid oxide fuel cell with nanostructured anodes, Energy Environ. Sci. 2011, **4**, 3951-3954

309. Z. Zhan, D. Han, T. Wu, X. Ye, S. Wang, T. We, S. Cho, S. A. Barnett, A solid oxide cell yielding high power density below 600^{o}C, RSC Adv. 2012, **2**, 4075-4078

310. J. An, J.H. Shim, Y.-B. Kim, J.S. Park, W. Lee, T.M. Gür, F.B. Prinz, MEMS-based thin-film solid-oxide fuel cells, MRS Bull. 2014, **39**, 798-804

311. P. Macoteguy, A. Brisse, A review and comprehensive analysis of degradation mechanisms of solid oxide electrolysis cells, Intern. J. Hydrogen Energy, 2013, **38**, 15887-15902

312. J.T.S. Irvine, D. Neagu, M.C. Verbraeken, C. Chatzichristodoulou, C. Graves, M.B. Mogensen, Evolution of the electrochemical interface in high-temperature fuel cells and electrolyzers, Nature Energy, 2016, **1**, 1-13

313. J.M. Ogden, Prospects for building a hydrogen energy infrastructure, Ann. Rev. Energy Environ. 1999, **24**, 227-279

314. C.-J. Winter, Hydrogen energy – Abundant, efficient, clean: A debate over the energy-system-of-change, Intern. J. Hydrogen Energy, 2009, **34**, S1-S52

315. H. Barthelemy, M. Weber, F. Barbier, Hydrogen storage: Recent developments and industrial perspectives, Intern. J. Hydrogen Energy, 2017, **42**, 7254-7262

View Article Online
DOI: 10.1039/C8EE01419A

316. D.J. Durbin, C. Malardier-Jugroot, Review of hydrogen storage techniques for on board vehicle applications, Intern. J. Hydrogen Energy, 2013, **38**, 14595-14617

317. H.W. Langmi, J. Ren, B. North, M. Mathe, D. Bessarabov, Hydrogen storage in metal-organic frameworks: A review, Electrochim. Acta, 2014, **128**, 368-392

318. P.E. de Jonghe, P. Adelhelm, Nanosizing and nanoconfinement: New strategies towards meeting hydrogen storage goals, Chem. Sus. Chem. 2010, **3**, 1332-1348

319. NREL Technology Brief: Analysis of current-day commercial electrolyzers, NREL/FS-840-36705 (2004) http://www.nrel.gov/docs/fy04osti/36705.pdf

320. Hydrogen Production Cost Analysis, National Renewable Energy Laboratory, https://www.nrel.gov/hydrogen/production-cost-analysis.html

321. G. Saur, C. Ainscough, U.S. Geographic Analysis of the Cost of Hydrogen from Electrolysis, National Renewable Energy Laboratory (NREL, Technical report: NREL/TP-5600-52640 (Dec. 2011) https://www.nrel.gov/docs/fy12osti/52640.pdf (accessed April 3, 2018)

322. U.S. DOE Office of Energy Efficiency & Renewable Energy (EERE), Section 3.1. Hydrogen Production, https://www.energy.gov/sites/prod/files/2015/06/f23/fcto_myrdd_production.pdf at https://www.energy.gov/eere/fuelcells/downloads/fuel-cell-technologies-office-multi-year-research-development-and-22 and (accessed April 2, 2018)],

323. A. Urus, L. M. Gandia, P. Sanchis, Hydrogen production from water electrolysis: Current status and future trends, Proceed. IEEC, 2012, **100,** 410-426

324. M. Carmo, D.L. Fritz, J. Mergel, D. Stolten, A comprehensive review on PEM water electrolysis, Intern. J. Hydrogen Energy, 2013, **38**, 4901-4934

325. K. Zeng, D. Zhang, Recent progress in alkaline water electrolysis for hydrogen production and applications, Progress Energy Combust. Sci. 2010, **36,** 307-326

326. S. Marini, P. Salvi, P. Nelli, R. Pesenti, M. Villa, M. Berrettoni, G. Zangari, Y. Kiros, Advanced alkaline water electrolysis, Electrochim. Acta, 2012, **82**, 384-391

327. U. Babic, M. Suermann, F.N. Buchi, L. Gubler, T.J. Schmidt, Review-Identifying critical gaps for polymer electrolyte water electrolysis development, J. Electrochem. Soc. 2017, **164**, F387-F399

328. Solar-Hydrogen Energy Systems: An Authoritative Review of Water-Splitting Systems by Solar Beam and Solar Heat: Hydrogen Production, Storage and Utilization, T. Ohta (ed.), Pergamon Press (Oct. 22, 2013)].

329. http://energy.gov/eere/fuelcells/hydrogen-production-electrolysis

330. A. Allebrod, C. Chatzichristodoulou, M.B. Mogensen, Alkaline electrolysis at high temperature and pressure of 250°C and 42 bar, J. Power Sources, 2013, **229**, 22-31

View Article Online
DOI: 10.1039/C8EE01419A

331. N.-T. Suen, S.-F. Hung, Q. Quan, N. Zhang, Y.-J. Xu, H.M. Chen, Electrocatalysis for the oxygen evolution reaction: recent developments and future perspectives, Chem. Soc. Rev. 2017, **46**, 337-365,

332. P.C.K. Vesborg, B. Seger, I. Chorkendorff., Recent developments in hydrogen evolution reaction catalysts and their practical implementation, J. Phys. Chem. Lett. 2015, **6**, 951-957

333. T.M. Gür, S.F. Bent, F.B. Prinz, Nanostructuring materials for solar-to-hydrogen conversion, J. Phys. Chem. C. 2014, **118**, 21301-21315

334. K.L. Pickrahn, S.W. Park, Y. Gorlin, H.-B.-R. Lee, T.F. Jaramillo, S.F. Bent,, Active MnO_x electrocatalysts prepared by atomic layer deposition of oxygen evolution and oxygen reduction reactions, Adv. Energy Mater. 2012, **2**, 1269-1277

335. Y. Lei, J. Lu, X. Luo, T. Wu, P. Du, X. Zhang, Y. Ren, J. Wen, D.J. Miller, J.T. Miller, Y.-K. Sun, J.W. Elam, K. Amine,, Synthesis of porous carbon supported palladium nanoparticle catalysts by atomic layer deposition: Application to rechargeable lithium-O_2 battery, Nano Lett. 2013, **13**, 4182-4189

336. X. Jiang, T.M. Gür, F.B. Prinz, S.F. Bent, Atomic layer deposition (ALD) co-deposited Pt-Ru binary and Pt skin catalysts for concentrated methanol oxidation, Chem. Mater. 2010, **22**, 3024-3032

337. Z.W. She, J. Kibsgaard, C.F. Dickens, I. Chorkendorff, J.K. Norskov, T.F. Jaramillo, Combining theory and experiments in electrocatalysis: Insights into materials design, Science, 2017, **355**, 1-12

338. T.F. Jaramillo, K.P. Jorgensen, J. Bonde, J.H. Nielsen, S. Horch, I. Chorkendorff, Identification of active edge sites for electrochemical H_2 evolution from MoS_2 nanocrystals, Science, 2007, **317**, 100-102

339. J. Kibsgaard, Z. Chen, B.N. Reinecke, T.F. Jaramillo, Engineering the surface structure of MoS_2 to preferentially expose active edge sites for electroctalysis, Nature Mater. 2012, **11**, 963-969

340. M. Ni, M.K.H. Leung, D.Y.C. Leung, Energy and exergy analysis of hydrogen production by solid oxide electrolyzer plant, Intern J. Hydrogen Energy, 2007, **32**, 4648-4660

341. H. Iwahara, Y. Asakura, K. Katahira, M. Tanaka, Prospect of hydrogen technology using proton-conducting ceramics, Solid State Ionics, 2004, **168**, 299-310

342. T.M. Gür, A. Duskin, Steam-Carbon Cell for Hydrogen Production, US patent application US2008/0022593 A1 (Jan. 31, 2008)]

343. B. Alexander, R. E. Mitchell, T. M. Gür, A New Steam-Carbon Fuel Cell Concept for Cogeneration of Hydrogen and Electrical Power, J. Electrochem. Soc. 2011, **158**, B505-B513

344. A.C. Lee, R. E. Mitchell, T. M. Gür, Feasibility of Hydrogen Production in a Steam-Carbon Electrochemical Cell, Solid State Ionics, 2011, **192**, 607-610

View Article Online
DOI: 10.1039/C8EE01419A

345. T.M. Gür, B. Alexander, R.E. Mitchell, Steam-Carbon Fuel Cell for Simultaneous Production of Hydrogen and Electric Power, invited talk # 121 presented at the 243rd American Chemical Society Annual Meeting, San, San Diego, CA, March 25-29, 2012

346. W. Wang, J. H. Vohs, R. J. Gorte, Hydrogen production via CH_4 and CO assisted steam electrolysis, Top. Catal. 2007, **46**, 380-385

347. C.J.M. van der Ham, M.T.M. Koper, D.G.H. Hetterscheid, Challenges in reduction of dinitrogen by proton and electron transfer, Chem. Soc. Rev. 2014, **43**, 5183-5191

348. F. Köleli, D.B. Kayan, Low overpotential reduction of dinitrogen to ammonia in aqueous media. J. Electroanal. Chem., 2010, **638**, 119-122

349. V. Kordali, G. Kyriacou, C. Lambrou, Electrochemical synthesis of ammonia at atmospheric pressure and low temperature in a solid polymer electrolyte cell. Chemical Communications, 2000, **17,** 1673-1674

350. R. Lan, J. T. S. Irvine, S. Tao, Synthesis of ammonia directly from air and water at ambient temperature and pressure, Sci. Reports, 2013, **3**, 1145 1-7

351. G. Marnellos, M. Stoukides, Ammonia synthesis of ammonia at atmospheric pressure, Science, 1998, **282**, 98-100

352. G. Marnellos, S. Zisekas, M. Stoukides, Synthesis of ammonia at atmospheric pressure with the use of solid state proton conductors, J. Catal. 2000, **193**, 80-87

353. V. Kyriakou, I. Garagounis, E. Vasileiou, A. Vourros, M. Stoukides, Progress in the electrochemical synthesis of ammonia, Catal. Today, 2017, 2**86**, 2-13

354. S. Kishira, G. Qing, S. Suzu, R. Kikuchi, A. Takagaki, S.T. Oyama, Ammonia synthesis at intermediate temperatures in solid-state electrochemical cells using cesium hydrogen phosphate based solid electrolytes and noble metal catalysts, Inter. J. Hydrogen Energy, 2017, **42**, 26843-26854

355. E. Vasileiou, V. Kyriakou, I. Garagounis, A. Vourros, M. Stoukides, Ammonia synthesis at atmospheric pressure in a $BaZr_{0.7}Ce_{0.2}Y_{0.1}O_{2.9}$ solid electrolyte cell, Solid State Ionics, 2015, **275**, 110-116

356. E. Vasileiou, V. Kyriakou, I. Garagounis, A. Vourros, A. Manerbino, W.G. Coors, M. Stoukides, Reaction rate enhancement during the electrocatalytic synthesis of ammonia in a $BaZr_{0.7}Ce_{0.2}Y_{0.1}O_{2.9}$ solid electrolyte cell, Topics Catal. 2015, **58**, 1193-1201

357. S. Licht, B. Cui, B. Wang, F.-F. Li, J. Lau, S. Liu, Ammonia synthesis by N2 and steam electrolysis in molten hydroxide suspensions of nanoscale Fe_2O_3, Science, 2014, 3**45**, 637-640

358. Y. Bicer, I. Dincer, Electrochemical synthesis of ammonia in molten salt electrolyte using hydrogen and nitrogen at ambient pressure, J. Electrochem. Soc. 2017, **164**, H5036-H5042

View Article Online
DOI: 10.1039/C8EE01419A

359. S. Mukherjee, D.A. Cullen, S. Karakalos, K. Liu, H. Zhang, S. Zhao, H. Xu, K.L. More, G. Wang, G. Wu, Metal-organic framework-derived nitrogen-doped highly disordered carbon for electrochemical ammonia synthesis using N_2 and H_2O in alkaline electrolytes, Nano Energy, 2018, DOI: 10.1016/j.nanoen.2018.03.059

360. S. Back, Y. Jung, On the mechanism of electrochemical ammonia synthesis on the Ru catalyst, Phys. Chem. Chem. Phys. 2016, **18,** 9161-9166

361. I. Matanaovic, F.H. Garzon, N.J. Henson, Electro-reduction of nitrogen on molybdenum nitride: Structure, energetics, and vibrational spectra from DFT, Phys. Chem. Chem. Phys. 2014, **16**, 3014-3026

362. I. Matanaovic, F.H. Garzon, Nitrogen electro-reduction and hydrogen evolution on cubic molybdenum carbide: A density functional study, Phys. Chem. Chem. Phys. 2018, **20**, 14679-14687

363. J. Zhao, J. Zhao, Q. Cai, Single transition metal atom embedded into a MoS_2 nanosheet as a promising catalyst for electrochemical ammonia synthesis, Phys. Chem. Chem. Phys. 2018, DOI: 10.1039/C7CP08626A

364. J. Montoya, C. Tsai, A. Vojvodic, J.K. Norskov, The challenge of electrochemical ammonia synthesis: A new perspective on the role of nitrogen scaling relations, ChemSusChem, 2015, **8**, 2180-2186

365. R.S. Diesselkamp, Energy storage using aqueous hydrogen peroxide, Energy Fuels, 2008, **22**, 2771-2774

366. S. Hasegawa, K. Shimotani, K. Kishi, H. Watanabe, Electricity generation from decomposition of hydrogen peroxide, Electrochem. Solid State Lett. 2005, **8**, A119-A121

367. S. Fukuzumi, Y. Yamada, K.D. Karlin, Hydrogen peroxide as a sustainable energy carrier: electrocatalytic production of hydrogen peroxide and the fuel cell, Electrochim. Acta, 2012, **82**, 493-511

368. Y. Yamada, Y. Fukunishi, S.-I. Yamazaki, S. Fukuzumi, Hydrogen peroxide as sustainable fuel: electrocatalysts for production with a solar cell and decomposition with a fuel cell, Chem. Commun. 2010, **46**, 7334-7336

369. A.E. Sanli, A. Aytac, Direct peroxide/peroxide fuel cell as a novel type fuel cell, Intern. J. Hydrogen Energy, 2011, **36**, 865-875

370. L. An, T. Zhao, X. Yan, X. Zhou, P. Tan, The dual role of hydrogen peroxide in fuel cell, Sci. Bulletin, 2015, **60**, 55-64

371. C. Hahn, T. Hatsukade, Y.-G. Kim, A. Vailionis, J.H. Baricuatro, D.C. Higgins, S.A. Nitopi, M.P. Soriaga, T.F. Jaramillo, Engineering Cu surfaces for the electrocatalytic conversion of CO_2; Controlling selectivity towards oxygenates and hydrocarbons, Proceed. National Acad. Sci. 2017, **114**, 5918-5923

View Article Online
DOI: 10.1039/C8EE01419A

372. R. Kotrlever, J. Shen, K.J.P. Schouten, F. Calle-Vallejo, M.T.M. Koper, Catalysts and reaction pathways for the electrochemical reduction of carbon dioxide, J. Phys. Chem. Lett.2015, **6**, 4073-4082

373. A.A. Peterson, J.K. Norskov, Activity descriptors for CO2 electroreduction to methane on transition-metal catalysts, J. Phys. Chem. Lett. 2012, **3**, 251-258

374. T.M. Gür, R.A. Huggins, Methane synthesis on nickel by a solid state ionic method, Science, 1983, **219**, 967-969

375. W. Li, H. Wang, Y. Shi, N. Cai, Performance and methane production characteristics of H_2O-CO_2 co-electrolysis in solid oxide electrolysis cells, Intern. J. Hydrogen Energy, 2013, **38**, 11104-11109

376. S.H. Jensen, P.H. Larsen, M. Mogensen, Hydrogen and synthetic fuel production from renewable energy sources, Intern. J. Hydrogen Energy, 2007, **32**, 3253-3257

377. S.D. Ebbesen, R. Knibbe, M. Mogensen, Co-electrolysis of steam and carbon dioxide in solid oxide cells, J. Electrochem. Soc. 2012, **159**, F482-F489

378. H. Jahangiri, J. Bennett, P. Mahjoubi, K. Wilson, S. Gu, A review of advanced catalyst development for Fischer-Tropsch synthesis of hydrocarbons from biomass derived syn-gas, Catal. Sci. Technol. 2014, **4**, 2210-2229

379. B. Kumar, M. Llorente, J. Froehlich, T. Dang, A. Sathrum, C.P. Kubiak, Photochemical and photoelectrochemical reduction of CO_2, Annu. Rev. Phys. Chem. 2012, **63**, 541-569

380. S.C. Roy, O.K. Varghese, M. Paulose, C.A. Grimes, Towards solar fuels: Photocatalytic conversion of carbon dioxide to hydrocarbons, ACS Nano, 2010, **4**, 1259-1278

381. S. Styring, Artificial photosynthesis for solar fuels, Faraday Discuss. 2012, **155**, 357-376

382. W.C. Chueh, C. Falter, M. Abbott, D. Scipio, P. Furler, S.M. Haile, High-flux solar-driven thermochemical dissociation of CO_2 and H_2O using nonstoichiometric ceria, Science, 2010, **330**, 1797-1801

383. E.V. Kondratenko, G. Mul, J. Baltrusiatis, G.O. Larrazabal, J. Perez-Ramirez, Status and perspectives of CO_2 conversion into fuels and chemicals by catalytic, photocatalytic and electrolytic processes, Energy Environ. Sci. 2013, **6**, 3112-3135

384. J.B. Greenblatt, D.J. Miller, J.W. Ager, F.A. Houle, A.D. Sharp, The technical and energetic challenges of separating (photo)electrochemical carbon dioxide reaction products, Joule, 2018, **2**, 381-420

385. Y. Hori, Electrochemical CO_2 reduction on metal electrodes, in "Modern Aspects of Electrochemistry",
C.G. Vayenas, R.E. White, M.E. Gamboa-Aldeco (eds.), Springer, New York, 2008, **42**, 89-189

View Article Online
DOI: 10.1039/C8EE01419A

386. M. Kiehnel, K.L. Orchard, K.E. Dalle, E. Resiner, Selective photocatalytic CO_2 reduction in water through anchoring of a molecular Ni catalyst on CdS nanocrystal, J. Am. Chem. Soc. 2017, **139**, 7217-7223

387. H. Wang,, J. Jia, P. Song, Q. Wang, D. Li, S. Min, C. Qian, L. Wang, Y.F. Li, C. Ma, T. Wu, J. Yuan, M. Antonietti, G.A. Ozin, Efficient electrocatalytic reduction of CO_2 by nitrogen doped nanoporous carbon/carbon nanotube membranes: A step towards the electrochemical CO_2 refinery, Angew. Chem. 2017, **129**, 7955-7960

388. C.S. Diercks, Y. Liu, K.E. Coroda, O.M. Yaghi, The role of reticular chemistry in the design of CO_2 reduction catalysts, Nature Mater. 2018, **17**, 301-307

389. T.M. Gür, H. Wise, R.A. Huggins, Electrocatalytic conversion of carbon dioxide to methane and oxygen with an oxide ion-conducting electrolyte, J. Catal. 1991, **129**, 216-224

390. C. Graves, S.D. Ebbesen, M. Mogensen, K.S. Lackner, Sustainable hydrocarbon fuels by recycling CO_2 and H_2O with renewable or nuclear energy, Renewable Sustain. Energy Rev. 2011, **15**, 1-23

391. S.D. Ebbesen, M. Mogensen, Electrolysis of carbon dioxide in solid oxide electrolysis cells, J. Power Sources, 2009, 193, 349-358

392. R. Sebastian, R. Pena Alzola, Flywheel energy storage systems: Review and simulation for an isolated wind power system, Renewable and Sustainable Energy Reviews, 2012, **16**, 6803-6813

393. S.M. Mousavi, G.F. Faraji, A. Majazi, K. Al-Haddad, A comprehensive review of flywheel energy storage systems technology, Renew. Sustain. Energy Rev. 2017, **67**, 477-490

394. A.A.K. Arani, H. Karami, G.B. Gharehpetian, M.S.A. Hejazi, Review of Flywheel energy storage systems structures and applications in power systems and microgrids, Renew. Sustain. Energy Rev., 2017, **69**, 9-18 (2017),

395. B. Bolund, H. Bernhoff, M. Leijon, Flywheel energy and power storage systems, Renew. Sustain. Energy Reviews, 11, 235-258

396. G. Cimuca, S. Breban, M.M. Radulescu, C. Saudemont, B. Robyns, Design and control strategies of an induction-machine based flywheel energy storage system associated to a variable-speed wind generator, IIEEE Transactions on Energy Conversion, 2010, **25**, 526-534

397. M. Strasik, J.R. Hull, J.A. Mittleider, J.F. Gonder, P.E. Johnson, K.E. McCrary, C.R. McIver, An overview of Being flywheel energy storage systems with high-temperature superconducting bearings, Superconductor Science and Technology, 2010, **23**, 034021

398. K.G. Vosburgh, Compressed air energy storage, J. Energy, 1978, **2**, 106-112

399. M. Budt, D. Wolf, R. Pan, J. Yan, A review on compressed air energy storage: Basic principles, past milestones and recent developments, Appl. Energy, 2016, **170**, 250-268

View Article Online
DOI: 10.1039/C8EE01419A

400. G. Venkataramani, P. Parankusam, V. Ramalingam, J. Wang, A review on compressed air energy storage – A pathway for smart grid and polygeneration, Renew. Sustain. Energy Rev., 2016, **62**, 895-907

401. H. Lund, G. Salgi, The role of compressed air energy storage (CAES) in future sustainable energy systems, Energy Conversion and Management, 2009, **50**, 1172-1179

402. A. Bagdanavicius, N. Jenkins, Exergy and exergoeconomic analysis of compressed air energy storage combined with a district energy system, Energy Conversion and Management, 2014, **77**, 432-440

403. Hydropower, Renewable Energy Technologies: Cost Analysis Series, Vol. 1: Power Sector, issue 3/5, International Renewable Energy Agency (IRENA), June 2012

404. I.E.A. Technology Roadmap: Hydropower © OECD/IEA; 2012, https://www.iea.org/publications/freepublications/publication/2012_Hydropower_Roadmap.pdf

405. International Renewable Energy Agency, Renewable Energy Technologies: Cost Analysis Series, Volume 1: Power Sector, issue 3/5, Hydropower (June 2012). http://www.irena.org/documentdownloads/publications/re_technologies_cost_analysis-hydropower.pdf].

406. S. Rehman, L.M. Al-Hadhrami, Md.M. Alam, Pumped hydro energy storage system: A technological review, Renew. Sustain. Energy Revi., 2015, **44**, 586-598

407. E. Barbour, I.A.G. Wilson, J. Radcliffe, Y. Ding, Y. Li, A review of pumped hydro energy storage development in significant international electricity markets, Renew. Sustain. Energy Rev. 2016, **61**, 421-432

408. J.I. Perez-Diaz, M. Chazarra, J. Garcia-Gonzalez, G. Cavazzini, A Stoppato, Trends and challenges in the operation of pumped-storage hydropower plants, Renew. Sustain. Energy Rev., 2015, **44**, 767-784

409. G. Ardizzon, G. Cavazzini, G. Pavesi, A new generation of small hydro and pumped-hydro power plants: Advances and future challenges, Renew. Sustain. Energy Rev., 2014, **31**, 746-761

410. J.P. Deane, B.P. O Galachoir, E.J. McKeogh, Techno-economic review of existing and new pumped hydro energy storage plant, Renew. Sustain. Energy Rev., 2010, **14**, 1293-1302

411. International Energy Agency, Energy Technology Perspectives 2015. www.iea.org/newsroomandevents/graphics/2015-06-30-installed-global-capacity-for-grid-connected-storage.html

412. I. Hadjipaschalis, A. Poullikkas, V. Efthimiou, Overview of current and future energy storage technologies for electric power applications, Renew. Sustain. Energy Rev., 2009, **13**, 1513-1522

View Article Online
DOI: 10.1039/C8EE01419A

413. J.K. Kaldellis, M. Kapsali, K.A. Kavadias, Energy balance analysis of wind-based pumped hydro storage systems in remote island electrical networks, Applied Energy, 2010, **87**, 2427-2437

414. X. Luo, J. Wang, M. Dooner, J. Clarke, Overview of current development in electrical energy storage technologies and the application potential in power system operation, Appl. Energy, 2015, **137**, 511-536

415. F. Agyenim, N. Hewitt, P. Eames, M. Smyth, A review of materials, heat transfer and phase change problem formulation for latent heat thermal energy storage systems (LHTESS), Renew. Sustain. Energy Rev., 2010, **14**, 615-628

416. A. Sharma, V.V. Tyagi, C.R. Chen, D. Buddhi, Review on thermal energy storage with phase change materials and applications, Renew. Sustain. Energy Rev., 2009, **13**, 318-345

417. B. Zalba, J. M. Marin, L.F. Cabeza, H. Mehling, Review on thermal energy storage with phase change: materials, heat transfer analysis and applications, Applied Thermal Engineering, 2003, **23**, 251-283

418. S.M. Hasnain, Review of sustainable thermal energy storage technologies, Part I: heat storage materials and techniques, Energy Conversion and Management, 1998, **39**, 1127-1138

419. M. Liu, W. Saman, F. Bruno, Review on storage materials and thermal performance enhancement techniques for high temperature phase change thermal storage systems, Renew. Sustain. Energy Rev., 2012, **16**, 2118-2132

420. R. G. Reddy, Novel Molten Salts Thermal Energy Storage for Concentrating Solar Power Generation, DOE-Solar Energy Technologies Program review, Oct 6, 2012 see http://www1.eere.energy.gov/solar/sunshot/pdfs/csp_review_meeting_042413_reddy.pdf

421. R. A. Huggins, Energy Storage: Fundamentals, Materials and Applications, 2nd edition, Springer (2016)

422. Economic Benefits of Increasing Electric Grid Resilience to Weather Outages, Executive Office of the President, The White House, August 2013, https://www.energy.gov/sites/prod/files/2013/08/f2/Grid%20Resiliency%20Report_FINAL.pdf

423. K. Eber, D. Corbus, Hawaii Solar Integration Study: Executive Summary, U.S. National Renewable Energy Laboratory (NREL), NREL/TP-5500-57215 (2013), see https://www.nrel.gov/docs/fy13osti/57215.pdf

424. National Assessment of Energy Storage for Grid Balancing and Arbitrage, Phase II: WECC, ERCOT, EIC, Vol. 1: Technical Analysis, (Sept. 2013), PNNL-21388 Phase II/Vol.1, https://energyenvironment.pnnl.gov/pdf/National_Assessment_Storage_PHASE_II_vol_1_final.pdf (accessed April 3, 2018)]

View Article Online
DOI: 10.1039/C8EE01419A

425. S. Chu, A. Majumdar, Opportunities and challenges for a sustainable energy future, Nature, 2012, **488**, 294-303

426. C. Curry, Lithium-ion Battery Costs and Market, July 5, 2017, Bloomberg New Energy Finance, https://data.bloomberglp.com/bnef/sites/14/2017/07/BNEF-Lithium-ion-battery-costs-and-market.pdf (accessed April 6, 2018)].

427. Technology Roadmap: Energy Storage, International Energy Agency 2014 report (OECD/IEA, 2014), available at https://www.iea.org/publications/freepublications/publication/TechnologyRoadmapEnergystorage.pdf (accessed July 9, 2018)

428. M.Z. Jacobson, M.A. Delucchi, M.A. Cameron, B.A. Frew, Low-cost solution to the grid reliability problem with 100% penetration of intermittent wind, water, and solar for all purposes, Proceed. National Acad. Sci. 2015, **112**, 15060-10565

429. M.Z. Jacobson, M.A. Delucchi, Z.A.F. Bauer, S.C. Goodman, W.E. Chapman, M.A. Cameron, C. Bozonnat, L. Chobadi, H.A. Clonts, P. Enevoldsen, J.R. Erwin, S.N. Fobi, O.K. Goldstrom, E.M. Hennesy, J. Liu, J. Lo, C.B. Meyer, S.B. Morris, K.R. Moy, P.L. O'Neill, I. Petkov, S. Redfern, R. Schucker, M.A. Sontag, J. Wang, E. Weiner, A.S. Yachanin, 100% clean and renewable wind, water, and sunlight all-sector energy roadmaps for 139 countries of the world, Joule, 2017, **1**, 108-121

430. C.T.M. Clack, S.A.Qvist, J. Apt, M. Bazilian, A.R. Brandt, K. Cladeira, S.J. Davis, V. Diakov, M.A. Handschy, P.D.H. Hines, P. Jaramillo, D.M. Kammen, J.C.S. Long, M.G. Morgan, A. Reed, V. Sivaram, J. Sweeney, G.R. Tynan, D.G. Victor, J.P. Weyant, J.F. Whitacre, Evaluation of a proposal for reliable low-cost grid power with 100% wind, water, and solar, Proceed. National Acad. Sci. 2017, **114**, 6722-6727

431. World Energy Resources: E-Storage 2016, World Energy Council, available at https://www.worldenergy.org/wp-content/uploads/2017/03/WEResources_E-storage_2016.pdf (accessed July 6, 2018)

432. W.-W. Yin, Z.-W. Fu, The potential of Na-air batteries, ChemCatChem, 2017, **9**, 1545-1553

433. D. Larcher, J.-M. Tarascon, Towards greener and more sustainable batteries for electrical energy storage, Nature Chem. 2015, **7**, 19-29

434. M.S. Whittingham, C. Su, J. Ding, Can multielectron intercalation reactions be the basis of next generation batteries?, Accnt. Chem. Res. 2018, **51**, 258-264

View Article Online
DOI: 10.1039/C8EE01419A

Broader Context Box
Gür – EE-REV-05-2018-001419.R1

200 words

Electricity is a ubiquitous, indispensible and effective energy carrier. But nearly 2/3rd of it is produced from fossil fuels resulting in copious CO_2 emissions to the environment. Rapid decarbonization of global electricity infrastructure necessitates shifting from fossil fuels to renewable sources such as solar and wind. Due to their intermittency, however, this is difficult to realize without building sufficient storage capacities to assure grid reliability, quality, availability and security. Indeed, overbuilding solar and wind without adequate storage capacity has recently resulted in discarding electricity with negative pricing in China, Germany and California. Storage also helps reduce reliance on the central grid, while allowing distributed generation and storage for local microgrids. This article presents a comprehensive review of a wide variety of electrochemical, chemical, mechanical, and thermal energy storage systems, materials and technologies. It critically assesses their advantages and shortcomings, and discusses the challenges yet to be overcome. As storage requirements of the electric grid vary widely depending on application specifications and often do not fully match the performance characteristics of any one particular storage system, the article highlights this mismatch and emphasizes the need to advance multitude of cost effective, efficient and scalable storage technologies compatible with grid storage requirements.

Gür Table 1

Power Technology	Installed capacity (2016)		Realized electricity generation (2016)		Expected electricity generation (2040)	
	Capacity *(GW)*	% of World	Generation *(billion kWh)*	% of World	Generation *(billion kWh)*	% of World
World Total	**6,637.8**	**100**	**23,735.2**	**100**	**34,049.0**	**100**
Renewables	2,112.4	31.82	5,593.8	23.57	10,702.3	31.43
Hydro	*1,081.5*	*16.29*	*3,910.0*	*16.47*	*5,677.9*	*16.68*
Solar	*278.3*	*4.19*	*275.6*	*1.16*	*1,390.3*	*4.08*
Wind	*459.8*	*6.92*	*826.2*	*3.48*	*2,524.5*	*7.41*
Geothermal	*13.8*	*0.21*	*77.1*	*0.32*	*353.4*	*1.04*
Other	*279.1*	*4.20*	*504.9*	*2.12*	*756.3*	*2.22*
Nuclear	352.0	5.30	2,510.1	10.58	3,657.3	9.79
Fossil fuels	4,173.4	62.88	15,631.3	65.86	19,689.4	57.83

Gür Table 2

Storage Technology	Installed Capacity *(GW)*	% Share
2016 World Total	**168.6**	**100**
Pumped-hydro	162.2	96.2
Electrochemical	1.6	0.95
Thermal	3.2	1.9
Mechanical	1.6	0.95
New projects under construction		
2016	*2*	
2017	*5*	
2018	*6*	

Gür Table 3

Cathode chemistry	Battery size	Theor. Wh/l	Actual Wh/l	% Realized	Theor. Wh/kg	Actual Wh/kg	% Realized
$LiFePO_4$	54 208	1980	292	14.8	587	156	26.6
$LiFePO_4$	16 650	1980	223	11.3	587	113	19.3
$LiMn_2O_4$	26 700	2060	296	14.4	500	109	21.8
$LiCoO_4$	18 650	2950	570	19.3	1000	250	25.0
Sr-$LiMO_4$ Panasonic	18 650	2950	919	31.2	1000	252	25.2

Note: Theoretical values include only active components

Gür Table 4

Battery systems	Li-air	K-air	Na-air	Mg-air	Zn-air	Fe-air	Al-air
Cost of metal ($/kg)[a]	68	20	1.7	2.75	1.85	0.4	1.75
Theoretical voltage (V)	**2.96**	**2.48**	**2.27**	**3.09**	**1.65**	**1.28**	**2.71**
Practical voltage (V)	**2.6**	**2.4**	**2.2**	**1.2-1.4**	**1.0-1.2**	**1.0**	**1.1-1.4**
Theoretical energy density (Wh/kg)[b]	**3458**	**935**	**1106**	**2840**	**1086**	**763**	**2796**
Practical energy density (Wh/kg)	Not known[c]	Not known[c]	Not known[c]	**400-700**	**350-500**	**60-80**	**300-500**
Electrolyte	Aprotic	Aprotic	Aprotic	Saline	Alkaline	Alkaline	Alkaline, or saline
Primary(P), or rechargeable (R)	R	R	R	P	R	R	P
Year invented	1996	2013	2012	1966	1878	1968	1962

Notes: (a) 2014 prices, (b) includes oxygen, © Literature values are normalized to mass of catalyst

Gür Table 5

Battery system and net cell reaction	Cell voltage (V)	Theoretical specific energy (Wh/kg)	Theoretical energy density (Wh/L)
Li-O_2 battery *(nonaqueous)*	**3.0**	**3505**	**3436[a]**
$2Li + O_2 = Li_2O_2$			
Li-O_2 battery *(aqueous)*	**3.2**	**3582**	**2234[b]**
$2Li + ½\ O_2 + H_2O = 2LiOH$			
Li-ion battery	**3.8**	**387**	**1015**
$½\ C_6Li + Li_{0.5}CoO_2 = 3C + LiCoO_2$			
Li-S battery	**2.2**	**2567**	**2199[c]**
$2Li + S = Li_2S$			

Note: (a) based on the sum of initial volume of Li and the final volume of Li_2O_2 after discharge, (b) based on the sum of initial volume of ($Li+H_2O$) consumed and the final volume of LiOH after discharge, (c) based on the sum of initial volume of Li and the final volume of Li_2S after discharge,

Gür Table 6

Fuel	Gravimetric Energy Density (Wh/kg)	Volumetric Energy Density (Wh/L)
Gasoline	12,330	9.060
Diesel	12,700	10,700
Propane	12,870	7,490
Butane	12,700	7,190
Ethanol	7,490	5,890
Methanol	5,620	4,470
Liq. Hydrogen	33,570	2,200
Liq. Ammonia	5,170	3,750
Batteries:		
*Li-ion battery**	*150-210*	*450*
*Ni-metal hydride**	*70*	*220*
*Zn-air battery**	*300*	*240*
* Practical values		

Gür Table 7

	Alkaline	Acid	PEM	SOEC
Electrolyte	NaOH KOH	H_2SO_4 H_3PO_3	Polymer (Nafion™)	Ceramic (YSZ, BYZ)
Carrier ion	OH^-	H^+	H^+	O^{2-} (YSZ) H^+ (BYZ)
Electrodes	Ni	Pt/C, IrO_2	Pt/C, IrO_2	Ni, ceramic
Operating temperature	80°C	150°C	80°C	600-900°C
Strengths	Cheap materials Commercial technology	High activity electrodes	High activity electrodes Commercial technology	Cheap materials Lower barrier to split H2O Higher efficiency
Short-comings	High barrier to split H2O Lower efficiency	High barrier to split H2O Expensive electrodes Cell durability Developing technology	High barrier to split H2O Expensive electrodes Hydrogen crossover Cell durability	High operating temperature Materials stability Fabrication costs Developing technology

Gür Table 8

Material	Density	Tensile Strength	Max. Energy Density		Cost
	(kg/m³)	*(Mpa)*	*(MJ/kg)*	*(kWh/kg)*	*($/kg)*
4340 Stainless Steel	**7700**	**1520**	**0.19**	**0.05**	**1**
Composites:					
E-glass	**2000**	**100**	**0.05**	**0.014**	**11.0**
S2-glass	**1920**	**1470**	**0.76**	**0.21**	**24.6**
Carbon T1000	**1520**	**1950**	**1.28**	**0.35**	**101.8**
Carbon AS4C	**1510**	**1650**	**1.1**	**0.30**	**31.3**

Gür Table 9

Country	Installed Capacity (GW)	Hydro Electricity Production (TWh)	Share of Electricity Generation (%)
China	210	694	14.8
Brazil	84	403	80.2
Canada	74	379	62.0
United States	79	328	7.6
Russia	50	165	15.7
India	38	132	13.1
Norway	30	122	95.3
Japan	28	85	7.8
Venezuela		84	68
Sweden		67	42.2
World Total	*936*	*3300*	*16*

Gür Table 10

Materials	Melting Point (°C)	Thermal Conductivity (W/m.K)	Density (kg/m³)	Specific Heat, Cp (J/kg.K)	Vol. Energy Density (kJ/m³)
Solids					
Aluminum	**660**	**205**	**2700**	**920**	**2484**
Iron (cast)	**1150**	**58**	**7200**	**540**	**3890**
Glass	**N/A**		**2710**	**837**	**2272**
Brick	**>1500**	**1.3**	**1970**	**921**	**1813**
Concrete	**N/A**	**1.0-1.8**	**2000**	**880**	**1760**
Granite	**1215-1260**	**1.7-4.0**	**2400**	**790**	**1896**
Liquids					
Water	**100**	**0.58**	**1000**	**4190**	**4190**
Molten sodium	**98**		**750**	**1260**	**945**
50:50 ethylene glycol -water mix			**1075**	**3480**	**3740**
Molten salts					
50 wt% KNO_3 -40% $NaNO_2$ - 7% $NaNO_3$	**149**		**1680**	**1560**	**2620**
$LiNO_3$-$NaNO_3$-KNO_3	**117**		**1710**	**1540**	**1056**
$NaNO_3$-KNO_3	**222**		**1750**	**1530**	**756**

Gür Table 11

Material	Transition Temperature *(°C)*	Enthalpy of Fusion *(MJ/kg)*
Water	0	0.335
Paraffin	20-60	0.14 – 0.28
$LiNO_3$	250	0.37
NH_4NO_3	170	0.12
$NaNO_3$	307	0.13
NaOH	318	0.15
$Ca(NO_3)_2$	561	0.12
LiCl	614	0.31
$FeCl_2$	670	0.34
$MgCl_2$	708	0.45
KCl	776	0.34
NaCl	801	0.50
$LiNO_3.2H_2O$	30	0.296
$FeCl_3.6H_2O$	37	0.223
$Na_2PHO_4.12H_2O$	40	0.279

Gür Table 12

Application	Output (e,t)	Size (MW)	Discharge duration	Cycles (typical)	Response time
Seasonal storage	e,t	500 - 2,000	Days to months	1 – 5 per year	day
Arbitrage	e	100 - 2,000	8 – 20 hours	0.25 – 1 per day	> 1 hour
Frequency regulation	e	1 – 2,000	1 – 15 minutes	20 – 40 per day	1 minute
Load following	e,t	1 – 2,000	15 minutes to 1 day	1 – 29 per day	< 15 min
Voltage support	e	1 - 40	1 second to 1 minute	10 – 100 per day	millisecond to second
Black start	e	0.1 - 400	1 – 4 hours	< 1 per year	< 1 hour
Transmission & distribution (T&D) congestion relief	e,t	10 - 500	2 – 4 hours	0.14 – 1.25 per day	> 1 hour
T&D infrastructure investment deferral	e,t	1 - 500	2 – 5 hours	0.75 – 1.25 per day	> 1 hour
Demand shifting and peak reduction	e,t	0.001 - 1	Minutes to hours	1 – 29 per day	< 15 minutes
Off-grid	e,t	0.001 – 0.01	3 – 5 hours	0.75 – 1.5 per day	< 1 hour
Variable supply resource integration	e,t	1 - 400	1 minute to hours	0.5 – 2 per day	< 15 minutes
Waste heat utilization	t	1 - 10	1 hour to 1 day	1 – 20 per day	< 10 minutes
Combined heat and power	t	1 - 5	Minutes to hours	1 – 10 per day	< 15 minutes
Spinning reserve	e	10 – 2,000	15 minutes to 2 hours	0.5 – 2 per day	< 15 minutes
Non-spinning	e	10 – 2,000	15 minutes to	0.5 – 2 per	< 15 minutes

Gur Table 13

	Power Rating (MW)	Discharge Time	Cycles or Lifetime	Self-discharge (%)	Energy Density (Wh/l)	Power Density (W/l)	Efficiency (%)	Response Time
Pumped-hydro	100-2,500	4 -16 h	30 - 60 yr	~ 0	0.2 - 2	0.1 – 0.2	70 - 85	10 s - min
Compressed Air	100-1,000	2 - 30 h	20 - 40 yr	~ 0	2 - 6	0.2 – 0.6	40 - 70	min
Flywheel	0.001-20	sec - min	20,000 – 100,000	1.3 - 100	20 - 80	5,000	70 - 95	< sec
Li-ion Battery	0.05-100	1 min - 8 h		0.1 – 0.3	200 - 400	1,300 – 10,000	85 - 95	< sec
Lead-acid Battery	0.001-100	1 min - 8 h	6 – 40 yr	0.1 – 0.3	50 80	90 - 700	80 - 90	< sec
Na-S Battery	10-100	1 min – 8 h	2,500 – 4,500	0.05 - 20	150 - 300	120 - 160	70 - 90	< sec
Flow Battery	0.1-100	hours	12,000 – 14,000	0.2	20 - 70	0.5 - 2	60 - 85	< sec
Supercon. Magnet	0.1-1	ms - sec	100,000	10 - 15	~ 6	~ 2,600	80 - 95	< sec
Super-capacitor	0.01-1	ms - min	10,000 – 100,000	20 - 40	10 - 20	40,000 – 120,000	80 - 95	< sec
Hydrogen	0.01-100	min - week	5 - 30 yr	0 - 4	600 (200 bar)	0.2 - 20	25 - 45	sec - min
Synthetic Natural Gas	1-100	hour - week	30 yr	~ 0	1800 (200 bar)	0.2 - 2	25 - 50	sec - min
Molten Salt (Latent thermal)	1-150	hours	30 yr	N/A	70 - 210	N/A	80 - 90	min

Gür Table 14

System	Calculated energy density (Wh/kg)	Real energy density (Wh/kg)	Utilization (%)
Pb-acid	171	25-55	15-32
Na-S	792	80-150	10-19
Ni-MH	240	50-70	20-29
Li-ion	360	150-210	42-58
Li-S	2654	250-350	9-13
Li-O_2	5217	-	-
Zn-O_2	1094	150-200	14-18
H_2-O_2	3525	120-800	3-23

Gür Table 15

Country	Electro-chemical unspecified	Electro-chemical capacitor	Li-ion battery	Flow battery	Vanadium redox flow battery	Pb-acid battery	Metal-air battery	Na-based battery	Total capacity (kW)
United States	500,398		61,959	3,030	20,250	21,500	14,250		621,397
Australia	122,010		9,400						131,410
Germany	30,000		92,000	210					122,210
India	110,000		125						110,125
Rep. of Korea			48,500						48,500
Canada	12,150		12,010	4,000	5,000				33,160
Egypt			30,000						30,000
Italy		1,920	20,000	1,950				4,000	27,870
Kazakhstan				25,000					25,000
United Kingdom	1,000		20,300	140					21,440
Top 10	775,558	1,920	294,304	34,330	25,250	21,500	14,250	4,000	1,171,112
World	784,258	2,920	333,404	34,965	25,250	21,500	5,650	4,800	1,212,747